Geochemistry and isotopic composition of sediment cores to understand the lithological and anthropogenic controls on eutrophication in the New River Estuary, Southland, New Zealand

by

Danielle J. Brown

A thesis submitted in partial fulfillment
of the requirements for the degree of
Master of Science (MSc) in Geology

The Faculty of Graduate Studies
Laurentian University
Sudbury, Ontario, Canada

THESIS DEFENCE COMMITTEE/COMITÉ DE SOUTENANCE DE THÈSE
Laurentian Université/Université Laurentienne
Faculty of Graduate Studies/Faculté des études supérieures

Title of Thesis Titre de la thèse	GEOCHEMISTRY AND ISOTOPIC COMPOSITION OF SEDIMENT CORES TO UNDERSTAND THE LITHOLOGICAL AND ANTHROPOGENIC CONTROLS ON EUTROPHICATION IN NEW RIVER ESTUARY, SOUTHLAND, NEW ZEALAND
Name of Candidate Nom du candidat	Brown, Danielle
Degree Diplôme	Master of Science
Department/Program Département/Programme	Geology
Date of Defence Date de la soutenance	March 22, 2019

APPROVED/APPROUVÉ

Thesis Examiners/Examinateurs de thèse:

Dr. Matthew Leybourne
(Supervisor/Directeur de thèse)

Dr. Graeme Spiers
(Committee member/Membre du comité)

Dr. Clinton Rissmann
(Committee member/Membre du comité)

Dr. Ian Clark
(External Examiner/Examinateur externe)

Approved for the Faculty of Graduate Studies
Approuvé pour la Faculté des études supérieures
Dr. David Lesbarrères
Monsieur David Lesbarrères
Dean, Faculty of Graduate Studies
Doyen, Faculté des études supérieures

ACCESSIBILITY CLAUSE AND PERMISSION TO USE

Abstract

The New River Estuary (NRE) in Southland, New Zealand is highly eutrophic and has rapidly declining ecosystem health. Historic estuarine reclamation, extensive catchment drainage, and waterway modification have increased the susceptibility of the estuary to degradation. In addition, more recent (post-1984) agricultural intensification and a shift in primary land use from sheep to dairy farming have increased the fine-sediment and associated pollutant loss to the catchment. Extensive macroalgae cover in the NRE reflects the ecosystem's response to eutrophication, where opportunistic species outcompete native plants in the nutrient-enriched environment. Three sediment cores from the primary depositional areas in the NRE, the Waihopai Arm and Daffodil Bay, were geochemically characterized, including stable and radiogenic isotopes, to assess changes in the rate of sediment, nutrient, and heavy metal accumulation. The sedimentation rate in the upper Waihopai Arm has increased from 7.3-13 mm yr^{-1} before 1935 to a very high rate of 20-22 mm yr^{-1} from 2009-2017. The lower Waihopai Arm and Daffodil Bay have increased to a high rate of sedimentation in the last decade from 5.9 to 17.5 mm yr^{-1} and 5.5-7 to 10.3 mm yr^{-1}, respectively. Phosphorus and trace metal concentrations in the bioavailable sediment fraction, which includes Fe- and Mn-oxides, sulfide, organic, or surface-adsorbed phases, have increased up to three and eight times higher than geogenic levels, respectively, which heightens their vulnerability to mobilization in response to changes in salinity and redox state. Increasing heavy metals and decreasing calcium loads, coupled with carbon- and nitrogen-isotopic values trending toward a terrestrial signature ($\delta^{13}C$ = -28‰, $\delta^{15}N$ = 8‰), delineates a transition in sediment source from marine-dominated (pre-1935) to terrestrial-dominated (post-1985). The composition of fallout radionuclides also indicates a

change in the delivery of terrestrial sediment from channel bank collapse and subsoil erosion (pre-1965) to sheet erosion of surface, likely pasture, soils (post-1997). This study highlights the importance of differentiating the natural sediment signatures from the anthropogenic sources of pollutants to assess the proportion of low-quality sediment (i.e., high nutrient and/or metal concentration) for which a targeted mitigation approach should be applied.

Keywords: Eutrophication, Sedimentation, Sediment Cores, Geochemistry, Stable Isotopes

Co-Authorship

The thesis, and the manuscript herein, contain work prepared by Danielle J. Brown. The manuscript in Chapter 2 is co-authored by Dr. Matt Leybourne (thesis supervisor), Dr. Clint Rissmann, and Nick Ward who provided scientific, logistical, and editorial support for the research in the New River Estuary catchment. The manuscript will be submitted to Chemical Geology for publication.

Acknowledgements

Firstly, I would like to thank my supervisor and co-author, Dr. Matt Leybourne for giving me the opportunity to take on this project. Thank you for your guidance, scientific discussion, and friendship throughout this study; your sense of humour was always appreciated. Thanks as well to Dr. Graeme Spiers for his constructive suggestions, questions, and editorial support. This research would not have been possible without the funding of Environment Southland, the regional council of Southland, New Zealand, and the Ontario Graduate Scholarship (OGS-M). Many thanks to Tim Ellis, Dr. Clint Rissmann, Nick Ward, Rachael Millar, and Graham Sevicke-Jones for their enthusiasm in setting up and supporting this project, for organizing peer seminars and workshops, and for accepting a Canadian into the Environment Southland family. Special thanks to Dr. Clint Rissmann and Nick Ward for their endless scientific and logistical support, and for Nick's help with sample collection and preparation. Thanks to the entire Environment Southland team, especially James Dare, Lisa Pearson, Darren May, Jane McMecking, Matt Couldrey, Monique Beyer, Ewen Rodway, Lawrence Kees, Jeremy Kidd, and Alice Woodward, for their assistance with field training and sample collection, preparation, and logistics. Thanks as well to Chris Owens, with Southern Waterways, for his logistics and in-field support during deep-core sample collection, and to Adam Martin and Rose Turnbull, with the Institute of Geological and Nuclear Sciences Limited (GNS), for their enthusiasm and for their contribution of the Geochemical Atlas of Southern New Zealand and their radiometric survey.

I would like to thank William Zhe from Laurentian University for his assistance and expertise with XRD analysis; Craig Radford and the team at Hill Laboratories in Christchurch, New Zealand, for their stormwater analyses and sample preparations; the Geoscience

Laboratories of the Ministry of Northern Development and Mines for allowing me to use their facilities for sample preparation and centrifugation; Bureau Veritas in Vancouver for their geochemical analysis of the core material; the National Centre for Radiation Science in Christchurch, New Zealand, for their radioisotopic analyses; the team at Queen's Facility for Isotope Research at Queen's University, especially April Vuletich and Evelyne Leduc, for their stable isotopic (C, N, S) and concentration analyses; Watercare Laboratory Services in Invercargill, New Zealand, for providing me with equipment and assisting with sample preparations; and the ALS Geochemistry Analytical Lab in Vancouver for their analyses of supplementary estuarine and storm-event sediment.

Lastly, I would like to thank all my family and friends for their unconditional support throughout my thesis, especially my parents, Karrie and Norm Brown, for keeping me grounded and for their endless curiosity with my project. Thanks to Shannon Gill for recommending the project to me and making the introductions, as well as to the graduate student group from Laurentian University for their support, interest, and questions, for endless laughs and adventures, and for making the whole process a lot more enjoyable!

Table of Contents

List of Figures

List of Tables

List of Abbreviations

GNS – Institute of Geological and Nuclear Sciences Limited

NRE – New River Estuary

OGS-M – Ontario Graduate Scholarship (Masters level)

XRD – X-ray diffraction

ANZECC – Australian and New Zealand Environment and Conservation Council

ARMCANZ – Agriculture and Resource Management Council of Australia and New Zealand

C3 (plant) – plants whose first product of carbon fixation is a 3-carbon compound ("normal")

C4 (plant) – plants whose first product of carbon fixation is a 4-carbon compound

CLUES – Catchment Land Use and Environmental Sustainability

C-org – Organic carbon (organic-C)

CSSI – Compound-specific stable isotope

DE – East Daffodil Bay (sample name)

EF – Enrichment factor

GIS – Geographic Information Systems

HREE – Heavy rare earth elements (Tb-Lu)

ICP-MS – Inductively coupled plasma mass spectrometry

IRMS – Isotope ratio mass spectrometer

LREE – Light rare earth elements (La-Gd)

LW – Lower Waihopai Arm (sample name)

mC_d – Modified degree of contamination

NZTM – New Zealand Transverse Mercator (map projection)

PVC – Polyvinyl chloride

Q1-10 (soils) – names of Quaternary geological formations: deposits are coded by "Q" followed by their assessed oxygen isotope stage (i.e., 1-10)

REY – Rare earth elements (La-Lu) and yttrium (Y)

SN (subscript) – shale-normalized, referring to normalization to the Post-Archean Australian Shale international standard

TN – Total nitrogen

TP – Total phosphorus

UNA – Upper North Arm (sample name)

VPDB – Vienna Pee Dee Belemnite (international standard for carbon stable-isotopes)

Chapter 1. General Introduction

1.1. Overview

A key trend in modern society is to employ more natural methods of production in the agricultural industry. The adverse side-effects on local and regional ecosystems, however, are often overlooked. For example, repurposing land in Southland, the second largest region in New Zealand, to accommodate the growth of dairy farming and its perennial pasture-feeding practices has had serious environmental implications. Southland supports an agriculturally-based economy with approximately 40% of its landmass occupied by farmland (Fig. 1-1). The recent shift in agricultural focus from sheep to more intensive dairy farming, along with the subsequent increased demand for water, parallels a significant decline in regional water quality in terms of nutrient enrichment and significant fine-sediment (<2 mm) accumulation.

Similar trends of anthropogenic influence exacerbating sediment loss and pollutant (i.e., nutrients and heavy metals) loading are evident worldwide. In the lower Great Lakes of Canada and the United States, for example, ecological effects of nutrient-loading associated with early settlement and forest clearance are recorded by a peak in diatom production, silica depletion, and a subsequent shift toward algae production (Schelske et al., 1983). Sediment cores show maximum diatom production between 1820 and 1850 in Lake Ontario, around 1880 in Lake Erie, but not until 1970 in Lake Michigan after increases in phosphorus loading from human wastes and detergents (Schelske et al., 1983). Load reductions had to be implemented in the Lake Erie catchment in 1972 to reduce the degradation of ecology and water quality associated with phosphorus loading (DePinto et al., 1986). However, phosphorus levels in Lake Erie have risen

since the mid-1990s, partially in response to changes in agricultural practices, leading to its re-eutrophication with subsequent cyanobacteria blooms, benthic algae growth, and extensive bottom-water hypoxia (Scavia et al., 2014). Similarly, eroding pasture soils in the United Kingdom (Collins et al., 2012, 1997) and erosion from livestock grazing in Australia (Wilkinson et al., 2013) have resulted in excessive loss of terrestrial sediment, commonly nutrient-rich, to river basins and marine habitats, which has been detrimental to water quality and the ecology.

1.1.1. Historic land use influencing sedimentation in Southland, New Zealand

The effects of sedimentation in Southland were already prominent by the early 20th century. For example, in the New River Estuary (NRE) catchment, a once well-developed trade port, significant channel depth was lost after a 12.2 km^2 section was reclaimed between 1910-1920 (Thoms, 1981). Reclamation accommodated municipal and agricultural expansion and increased the accumulation of sediment, primarily marine in origin, a natural response to the 25% reduction in the estuary's tidal compartment (Thoms, 1981; van Maren et al., 2016). Agricultural development from the late 19th century has also had an impact on sediment loss in Southland (Fig. 1-2). In the 1860's significant expanses of native bush were cleared, and wetlands were drained, to accommodate colonization and agricultural growth; today, wetlands and native forest occupy <10% of their original coverage in the region, with the majority replaced by exotic species. Sheep farming in particular was a major development, where stock units increased from approximately 1 to 3.5 million from 1870-1950 (Pearson and Couldrey, 2016). River channelization and agricultural intensification occurred through 1950-1980, which led to a significant increase in sheep numbers to a peak of 9.5 million in 1984 (Ledgard, 2013). Beef

farming also grew in the industry during this time. After 1985, the industry was no longer expanding into undeveloped areas and the total number of stock units stabilized at 10-11 million. Concurrently, there was a major transition from sheep and beef pastoral and arable land to dairy and dairy support land (Ledgard, 2013). By 2015, the number of sheep had decreased to 4.1 million whereas dairy cows had increased from about 0.05 to 0.73 million cattle (Pearson and Couldrey, 2016). Over the last two decades (1996-2015), dairy farming and support properties have taken over approximately 30% of the lowland areas (by hectare) previously used to farm sheep, beef and deer (Pearson and Couldrey, 2016). In the NRE catchment, for example, dairying coverage doubled from 87,109 Ha to 195,500 Ha between 2000 and 2011 (Fig. 1-2), with 54% of that being on soils with high risk for nutrient and heavy metal contaminant loss due to artificial drainage and coarse soil structure (Houlbrooke et al., 2004; Ledgard, 2013). This agricultural shift is linked to changes in land management, including the introduction of winter cropping, which refers to the strip-grazing of cattle, sheep and deer on resilient forage crops when there is minimal pasture growth instead of using feedlots. Coupled with seasonally high rainfall and minimal pasture uptake due to strip-grazing, winter cropping locally increases soil erosion, resulting in excessive sediment, nutrient and contaminant losses to riverways. Dairying is more intensive, commonly requiring irrigation to maintain production, and has higher nitrate and phosphorus loading from waste compared to other stock, which contributes to poor water quality (Ledgard, 2013; Monaghan et al., 2010, 2007, 2005, 2002). Further, due to technological advancements in farming practices, including mole drains, land previously classified as unsuitable for intensive agriculture (i.e., coarse soil or poor drainage) is increasingly being developed, which increases the stress on Southland's natural resources (Pearson and Couldrey, 2016). These changes to the indigenous land cover have impacted the biodiversity, soil stability,

and water quality in the region, and have increased the ecosystem's vulnerability to pressures from land use (Ledgard, 2013). The *Water and Land 2020 & Beyond* (Environment Southland, 2018) project was developed in response to increased pressure on water quantity and quality (i.e., increases in nitrogen, phosphorus, microbial activity, sedimentation) in the region of Southland. The project includes water and land management strategies designed to halt the deterioration of water quality and implement limits to prevent further declines, with the intent to prioritize the most significantly contaminated (i.e., nutrient and sediment loads) areas in the region, including New River Estuary's Makarewa River and lowland Oreti River catchments (Snelder et al., 2014).

1.1.2. Influence of sedimentation in New River Estuary

New River Estuary is the most contaminated (heavy metals) and the second most nutrient- and sediment-enriched catchment in the region (Robertson et al., 2017). The catchment primarily drains the Oreti River and its tributaries, which originates in the Eyre Mountains, and, to a lesser degree, the lowland catchments, which includes the Waihopai River, Otepuni Creek, Duck Creek, and Mokotua Stream. Whereas much of the northern catchment retains high water quality, anthropogenic influence in the middle to lower reaches highlights the need for a robust understanding of the interaction between land use and water quality. Anthropogenic land use, development and modification, coupled with increased annual rainfall associated with climate change, has exacerbated erosion in the catchment. The addition of greater volumes of fine-sediment (<2 mm), most of which deposits in the NRE, parallels a decline in water quality, impacting the agricultural, industrial and municipal fresh water supply and degrading ecological wellbeing both in-stream and within the estuary. The transport of sediment into and through river

systems is a key component of fluvial hydrogeomorphological function. However, the movement of excessive fine-sediment can be physically detrimental to aquatic ecology by smothering habitats, damaging fish gills, reducing the capacity to predate, and decreasing substrate porosity and permeability in the nutrient-rich hyporheic zone, which is an important ecosystem for fish, plants, and other organisms (Collins et al., 2012). Suspended fine-sediment also plays an important role in water quality as it is a mechanism for pollutant transport, especially heavy metals and nutrients, which increases the potential for catchment contamination and eutrophication (Horowitz, 2008). Excess nutrients favour the growth of opportunistic, nuisance plant and algal species that not only inhibit recreational use and aesthetic appeal but can degrade habitats by reducing water clarity and consuming dissolved oxygen. Evidence of eutrophication in the NRE, especially over the past two decades, includes opportunistic macroalgal (i.e., *Gracilaria* and *Ulva*) dominance in intertidal zones associated with the loss of indigenous seagrass, a reduction in sediment oxygenation, and an increase in fine-sediment and pollutant accumulation (Robertson et al., 2017; Robertson and Stevens, 2007, 2001; Stevens and Robertson, 2012). The eutrophic condition in the upper estuary, where sulfide levels and anoxia are elevated, is more advanced because macroalgal growth is eliminated by the proliferation of cyanobacteria (Robertson et al., 2017).

1.2. Techniques used to assess eutrophication and contamination

The eutrophication of the NRE, along with significant increases in the rate of sedimentation, especially over the last two decades, presents two important questions: 1) Where does the bulk of the fine-sediment load originate, and 2) Is this sediment transporting a significant portion of the

pollutants deposited in the estuary? Answering these questions will provide useful information on the provenance and quality of sediment migrating through the catchment.

Sediment source is a key control on the physical and chemical properties of the suspended load, which governs its ability to act as a means of natural attenuation or as a transport mechanism in different hydrochemical environments (Chapman and Wang, 2001; Horowitz, 1991). Southland was subdivided into distinct physiographic zones to differentiate how sediment, microbes, and pollutants (nutrients and heavy metals) will build up and move through the soil, groundwater, and into surface water systems in the region's variable landscape (Fig. 1-3; Rissmann et al., 2016b). The zones are classified based on a combination of biogeochemical and hydrological controls, including primary transport pathways: overland flow/surface runoff, artificial drainage (i.e., mole pipe and tile drains), deep drainage/leaching into groundwater, natural bypass flow, or lateral drainage through soil (Hughes et al., 2016; Rissmann et al., 2016a, 2016b; Snelder et al., 2016). For example, in Bedrock/Hill Country landscapes, as opposed to Alpine zones, soil strongly influences hydrochemistry and water quality in both the steeper regions where overland flow is a major pathway and in lower elevations where sediment and pollutants from land use activities are primarily mobilized through lateral or artificial drainage (Hughes et al., 2016; Rissmann et al., 2016b). Physiographic discrimination helps assess how different land areas and uses will impact Southland's water chemistry and quality and provides a spatial framework to assist with targeting management strategies to minimize the impacts of nutrient-loading in the waterways.

To help determine the sources of sediment accumulating in New River Estuary, a study in 2015 used the compound-specific stable isotope (CSSI) technique on bulked samples of estuarine and surface riverine sediment compared against reference soils from different land uses in the

catchment (Gibbs et al., 2015). The CSSI technique involves using plant-specific biomarkers that are strongly bound to soil particles as a tracer of terrestrial sources. The CSSI results showed that recently deposited estuary sediment (top 20 cm) was dominated by terrestrial material from surface soil erosion of sheep, deer, and dairy pastures, and suggested that elevation and slope play an important role in catchment sediment loss (Gibbs et al., 2015).

For an indication of ecological pressure, total nitrogen (TN) concentrations in the NRE were predicted using the GIS-based Catchment Land Use and Environmental Sustainability (CLUES) modeling tool (Elliott et al., 2016; Plew, 2017). The model provides time- and volume-averaged potential TN concentrations based on land use inputs and the dilution between fluvial and seawater for given tidal prisms and freshwater inflow, not including biological uptake and denitrification processes (Elliott et al., 2016). Predictions showed a seasonality to TN loads in the NRE where decreased total concentrations paralleled increases in the tidal prism due to greater dilution and flushing. Further, due to greater fluvial and marine inputs, winter loads (~534 mg m^{-3}) are higher than summer (~154 mg m^{-3}), although both are high enough to initiate macroalgal growth (i.e., *Ulva*) (Plew, 2017). Wastewater treatment effluent, the only point source (non-fluvial) of nitrogen considered, was found to contribute 6.5% of the current annual TN load (Plew, 2017). It is important to characterize temporal changes in the sediment load associated with seasonal variability; for example, in dry, summer seasons, sediment is accumulated and temporarily stored in the substrate, whereas, in the early stages of the wet, autumn-winter seasons high-flow events flush fluvial systems and move significant quantities of sediment (Horowitz, 2008). It has been widely accepted that flow velocity is an important control on the suspended sediment concentration of fluvial systems (Salomons and Forstner, 1984). As flow increases, sediment in the substrate becomes remobilized through bank/channel erosion and

overland flow. Therefore, although high-flow events occur over a relatively short duration in a small portion of time per annum, they are typically the main driver of the annual fluxes of suspended sediment and sediment-associated chemical constituents (Horowitz, 2008, 1991).

In this study, cores of NRE sediment from major depositional areas are used to assess historical changes in sediment texture and accumulation rate, as well as pollutant concentrations, especially within the last century. Physical and chemical characteristics of the sediment reflects the composition and quality (based on nutrient and heavy metal compositions) of its sources (i.e., high Ca may correlate to a greater marine input). Similarly, enrichment of trace metals beyond background (geogenic) levels can indicate the magnitude of anthropogenic impact on the sediment load over time (Birch, 2017; Birch and Olmos, 2008). Metal enrichment is commonly assessed by normalizing concentrations to a reference, conservative element like aluminum to eliminate correlation with grain size (Schropp et al., 1990; Windom et al., 1989). Concentrations of heavy metals in both bioavailable and resistant (silicate) phases are evaluated by pre-defined levels ("trigger values") for sediment and water quality that, when exceeded, signify contamination and potential for ecological degradation (ANZECC and ARMCANZ, 2000). Combined carbon and nitrogen stable isotopic signatures are used to qualitatively apportion the allochthonous (terrestrial soil and plant debris) and autochthonous (marine phytoplankton and algae) contributions to the historical sediment load (Middelburg and Nieuwenhuize, 1998). Terrestrial sources range in $\delta^{13}C$ from -26 to -30.9‰ (av. -28‰) and in $\delta^{15}N$ from 2 to 6.3‰ (Kendall et al., 2001; Lehmann et al., 2002; Middelburg and Nieuwenhuize, 1998; Peters et al., 1978; Peterson and Fry, 1987). Anthropogenic influence on terrestrial nitrogen isotopic signatures is evident where unpolluted signatures (0‰) trend towards anthropogenic (polluted) nitrogen (8‰) as eutrophication intensifies (Fry, 2002). Marine sources range in $\delta^{13}C$ from -18

to -22‰ (av. -21.5‰) and in $\delta^{15}N$ from 5 to 9‰ (av. 5‰) (Alling et al., 2008; Fry, 2002; Kendall et al., 2001; Peters et al., 1978; Peterson and Fry, 1987; Tan and Strain, 1979). Due to their short half-lives, radionuclides (^{210}Pb, ^{226}Ra, ^{137}Cs, ^{7}Be) can be used not only to date sediment horizons but to trace the physical processes that release sediment into riverways. The presence and concentration of radionuclides in soils represents direct exposure to atmospheric fallout and discriminates between sheet erosion of surface soils, in-channel resuspension, and gully erosion of subsoils and other subsoil erosional processes, including channel bank erosion (Hancock and Caitcheon, 2010; Walling et al., 1999; Walling and Woodward, 1992; Wilkinson et al., 2013). Determining the dominant erosional process controlling sediment loss in the catchment can help define how anthropogenic influence has changed over time because different land uses will control how the soil is susceptible to erosion (Hancock and Caitcheon, 2010).

1.3. Thesis objective and rationale

Previous studies in Southland focused on recent nutrient and sediment mobility in surface and groundwater systems (Measures, 2016; Plew, 2017; Rissmann, 2012), controls on fluvial hydrochemistry (Hughes et al., 2016; Rissmann et al., 2016a, 2016b), specific nutrient, heavy metal and sediment losses from land uses (esp. dairy farming) (Elliott et al., 2016; Gibbs et al., 2015; Hamill and McBride, 2003; Hicks et al., 2000; Hicks and Basher, 2008; Houlbrooke et al., 2004; Houlbrooke and Laurenson, 2013; Martin et al., 2017; McDowell et al., 2013, 2003; McDowell and Wilcock, 2004; Monaghan et al., 2010, 2007, 2005, 2002; Pearson and Couldrey, 2016), and the current water and ecological states of affected catchments in the region (Cavanagh and Ward, 2014; Morgenstern and Daughney, 2012; Robertson et al., 2017;

Robertson and Stevens, 2012a, 2012b, 2007, 2001; Snelder et al., 2014; Sparling and Schipper, 2002; Stevens and Robertson, 2012). The primary aim of this study is to support the *Water and Land 2020 & Beyond* (Environment Southland, 2018) project by providing a historical record of textural and geochemical changes in the NRE sediment to be used as a proxy for estuary health in the last century. Characteristics of the sediment load from radioisotopically-dated horizons are correlated to known anthropogenic changes (i.e., agricultural and urban) to highlight when there was significant contribution of fine-sediment, nutrients, and heavy metals to the NRE, and from which practices and erosional processes they primarily originate. Improved understanding of anthropogenic influence on the sediment load, primary methods of sediment mobilization, and the subsequent effects on estuary health, allows for targeted policies and management strategies to be developed and implemented in high risk areas to minimize future sediment and pollutant loss and focus estuary remediation. Collecting estuarine cores in affected zones is an effective technique to accomplish these objectives and is easily transferable across New Zealand and in other catchments worldwide.

1.4. Thesis structure

Chapter 2 is presented as a manuscript and contains the main research of this study, focusing on the geochemical and isotopic characterization of sediment cores from New River Estuary. Chapter 2 includes downcore variability in sediment texture, elemental concentration, and stable- (^{13}C, ^{15}N) and radiogenic-isotope (^{7}Be, ^{137}Cs, $^{210}Pb_{ex.}$) signatures against the radiogenic ($^{210}Pb_{ex.}$) age of deposition. Chapter 3 is a general conclusion that includes an overall discussion of this study's findings as well as recommendations for future work.

References

Alling, V., Humborg, C., Morth, C., Rahm, L., Pollehne, F., 2008. Tracing terrestrial organic matter by delta-S-34 and delta-C-13 signatures in a subarctic estuary. Am. Soc. Limnol. Oceanogr. Inc 53, 2594–2602.

ANZECC, ARMCANZ, 2000. Australian and New Zealand Guidelines for Fresh and Marine Water Quality (No. 4), National Water Quality Management Strategy.

Birch, G.F., 2017. Determination of sediment metal background concentrations and enrichment in marine environments - A critical review. Sci. Total Environ. 580, 813–831.

Birch, G.F., Olmos, M.A., 2008. Sediment-bound heavy metals as indicators of human influence and biological risk in coastal water bodies. ICES J. Mar. Sci. 65, 1407–1413.

Cavanagh, J.E., Ward, N., 2014. Contaminants in estuarine and riverine sediments and biota in Southland (Landcare Research Report for Environment Southland No. LC1789). Landcare Research New Zealand Ltd., Lincoln, New Zealand.

Chapman, P.M., Wang, F., 2001. Assessing sediment contamination in estuaries. Environ. Toxicol. Chem. 20, 3–22.

Collins, A.L., Walling, D.E., Leeks, G.J.L., 1997. Fingerprinting the origin of fluvial suspended sediment in larger river basins: Combining assessment of spatial provenance and source type. Geogr. Ann. 79 A, 239–254.

Collins, A.L., Zhang, Y., Walling, D.E., Grenfell, S.E., Smith, P., Grischeff, J., Locke, A., Sweetapple, A., Brogden, D., 2012. Quantifying fine-grained sediment sources in the River Axe catchment, southwest England: application of a Monte Carlo numerical modelling framework incorporating local and genetic algorithm optimisation. Hydrol. Process. 26, 1962–1983. https://doi.org/10.1002/hyp.8283

DePinto, J.V., Young, T.C., McIlroy, L.M., 1986. Impact of phosphorus control measures on water quality of the Great Lakes. Environ. Sci. Technol. 20, 752–759.

Elliott, A.H., Semadeni-Davies, A.F., Shankar, U., Zeldis, J.R., Wheeler, D.M., Plew, D.R., Rys, G.J., Harris, S.R., 2016. A national-scale GIS-based system for modelling impacts of land use on water quality. Environ. Model. Softw. 86, 131–144.

Environment Southland, 2018. Water and Land 2020 & Beyond: Proposed Southland Water and Land Plan Part A.

Fry, B., 2002. Conservative mixing of stable isotopes across estuarine salinity gradients: A conceptual framework for monitoring watershed influences on downstream fisheries production. Estuaries 25, 264–271.

Gibbs, M., Olsen, G., Stewart, M., 2015. New River Estuary sediment sources tracking pilot study (NIWA Client Report for Southland Regional Council No. HAM2014-002). National Institute of Water and Atmospheric Research Ltd., Hamilton, New Zealand.

Hamill, K.D., McBride, G.B., 2003. River water quality trends and increased dairying in Southland, New Zealand. N. Z. J. Mar. Freshw. Res. 37, 323–332.

Hancock, G., Caitcheon, G., 2010. Sediment sources and transport to the Logan-Albert River estuary during the January 2008 flood event (No. 1835-095X), CSIRO: Water for a Healthy Country National Research Flagship.

Hicks, D.M., Basher, L.R., 2008. The signature of an extreme erosion event on suspended sediment loads: Motueka River catchment, South Island, New Zealand, in: Sediment Dynamics in Changing Environments. International Association of Hydrological Sciences, Christchurch, New Zealand, pp. 184–191.

Hicks, D.M., Gomez, B., Trustrum, N.A., 2000. Erosion thresholds and suspended sediment

yields, Waipaoa River Basin, New Zealand. Water Resour. Res. 36, 1129–1142.

Horowitz, A.J., 2008. Determining annual suspended sediment and sediment-associated trace element and nutrient fluxes. Sci. Total Environ. 400, 315–343.

Horowitz, A.J., 1991. A Primer on Sediment-Trace Element Chemistry, Second Edition (Open-File No. 91-76). United States Geological Survey.

Houlbrooke, D.J., Horne, D.J., Hedley, M.J., Hanly, J.A., Snow, V.O., 2004. A review of literature on the land treatment of farm-dairy effluent in New Zealand and its impact on water quality. N. Z. J. Agric. Res. 47, 499–511.

Houlbrooke, D.J., Laurenson, S., 2013. Effect of sheep and cattle treading damage on soil microporosity and soil water holding capacity. Agric. Water Manag. 121, 81–84. https://doi.org/10.1016/j.agwat.2013.01.010

Hughes, B., Wilson, K., Rissmann, C.W., Rodway, E., 2016. Physiographics of Southland: Development and application of a classification system for managing land use effects on water quality in Southland (Technical Report No. 2016/11). Environment Southland, Invercargill, NZ.

Kendall, C., Silva, S.R., Kelly, V.J., 2001. Carbon and nitrogen isotopic compositions of particulate organic matter in four large river systems across the United States. Hydrol. Process. 15, 1301–1346.

Ledgard, G., 2013. Land use change in the Southland region (Technical Report No. 2013-13). Environment Southland, Invercargill, NZ.

Lehmann, M.F., Bernasconi, S.M., Barbieri, A., McKenzie, J.A., 2002. Preservation of organic matter and alteration of its carbon and nitrogen isotope composition during simulated and in situ early sedimentary diagenesis. Geochim. Cosmochim. Acta 66, 3573–3584.

Martin, A.P., Turnbull, R.E., Rissmann, C.W., Rieger, P., 2017. Heavy metal and metalloid concentrations in soils under pasture of southern New Zealand. Geoderma Reg. 11, 18–27.

McDowell, R.W., Monaghan, R.M., Morton, J., 2003. Soil phosphorus concentrations to minimise potential P loss to surface waters in Southland. N. Z. J. Agric. Res. 46, 239–253.

McDowell, R.W., Norris, M., Cox, N., 2013. Waituna Sediment Fingerprinting Study (Technical Report for Environment Southland No. RE500/2013/136). AgResearch Ltd., Christchurch, New Zealand.

McDowell, R.W., Wilcock, R.J., 2004. Particulate phosphorus transport within stream flow of an agricultural catchment. J. Environ. Qual. 33, 2111–2121.

Measures, R., 2016. New River Estuary hydrodynamic modelling: Model build, calibration, and tracer simulations (NIWA Client Report for Environment Southland No. 2016077CH). National Institute of Water and Atmospheric Research Ltd., Christchurch, New Zealand.

Middelburg, J.J., Nieuwenhuize, J., 1998. Carbon and nitrogen stable isotopes in suspended matter and sediments from the Schelde Estuary. Mar. Chem. 60, 217–225.

Monaghan, R.M., Paton, R.J., Drewry, J.J., 2002. Nitrogen and phosphorus losses in mole and tile drainage from a cattle-grazed pasture in eastern Southland. N. Z. J. Agric. Res. 45, 197–205.

Monaghan, R.M., Paton, R.J., Smith, L.C., Drewry, J.J., Littlejohn, R.P., 2005. The impacts of nitrogen fertilisation and increased stocking rate on pasture yield, soil physical condition and nutrient losses in drainage from a cattle-grazed pasture. N. Z. J. Agric. Res. 48, 227–240.

Monaghan, R.M., Semadeni-Davies, A., Muirhead, R., Elliott, S., Shankar, U., 2010. Land use and land management risks to water quality in Southland. Report prepared for Environment Southland. AgResearch.

Monaghan, R.M., Wilcock, R.J., Smith, L.C., Tikkisetty, B., Thorrold, B.S., Costall, D., 2007. Linkages between land management activities and water quality in an intensively farmed catchment in southern New Zealand. Agric. Ecosyst. Environ. 118, 211–222. https://doi.org/10.1016/j.agee.2006.05.016

Morgenstern, U., Daughney, C.J., 2012. Groundwater age for identification of baseline groundwater quality and impacts of land-use intensification - The National Groundwater Monitoring Programme of New Zealand. J. Hydrol. 456, 79–93.

Pearson, L.K., Couldrey, M., 2016. Methodology for GIS-based land use maps for Southland (Technical Report No. 2016-10). Environment Southland, Invercargill, NZ.

Peters, K.E., Sweeney, R.E., Kaplan, I.R., 1978. Correlation of carbon and nitrogen stable isotope ratios in sedimentary organic matter. Limnol. Oceanogr. 23, 598–604.

Peterson, B.J., Fry, B., 1987. Stable Isotopes in Ecosystem Studies. Annu. Rev. Ecol. Syst. 18, 293–320. https://doi.org/10.1146/annurev.ecolsys.18.1.293

Plew, D.R., 2017. New River Estuary: CLUES estuary analysis (NIWA Client Report for Environment Southland No. 2016004CH). National Institute of Water and Atmospheric Research Ltd., Christchurch, New Zealand.

Rissmann, C., 2012. The Extent of Nitrate in Southland Groundwaters - Regional 5 Year Median (2007-2012) (Technical Report No. 2012-09). Environment Southland, Invercargill.

Rissmann, C.W., Pearson, L.K., Killick, M., Rodway, E., Beyer, M., Marapara, T.R., Hodgetts, J., 2016a. An assessment of the drivers of soil chemical variation across the Southland

region (Technical Report No. 3/8), Physiographics of Southland.

Rissmann, C.W., Rodway, E., Beyer, M., Hodgetts, J., Snelder, T., Pearson, L.K., Killick, M., Marapara, T.R., Akbaripasand, A., Hodson, R., Dare, J., Millar, R., Ellis, T., Lawton, M., Ward, N., Hughes, B., Wilson, K., McMecking, J., Horton, T., May, D., Kees, L., 2016b. Physiographics of Southland: Delineation of key drivers of regional hydrochemistry and water quality (Technical Report No. 2016/3). Environment Southland, Invercargill, NZ.

Robertson, B.M., Stevens, L., 2001. Southland Estuaries State of Environment Report 2001 (Report prepared by Wriggle Coastal Management for Environment Southland).

Robertson, B.M., Stevens, L.M., 2007. New River Estuary 2007: Broad Scale Habitat Mapping and Sedimentation Rate (Report prepared by Wriggle Coastal Management for Environment Southland). Nelson, New Zealand.

Robertson, B.M., Stevens, L., 2012a. Tasman Coast: Waimea Inlet to Kahurangi Point. Habitat Mapping, Ecological Risk Assessment and Monitoring Recommendations. (State of the Environment Report).

Robertson, B.M., Stevens, L.M., 2012b. New River Estuary: Fine Scale Monitoring of Highly Eutrophic Arms 2011/2012 (Report prepared by Wriggle Coastal Management for Environment Southland). Nelson, New Zealand.

Robertson, B.M., Stevens, L.M., Robertson, B.P., 2017. Condition of Southland's shallow, intertidal dominated estuaries in relation to eutrophication and sedimentation: Output 1: Data analysis and technical assessment - Habitat mapping, vulnerability assessment and monitoring recommendations related to issues of eutrophication and sedimentation (Report prepared by Wriggle Coastal Management for Environment Southland). Nelson, New Zealand.

Salomons, W., Forstner, U., 1984. Metals in the hydrocycle. Springer, Berlin Heidelberg Tokyo.

Scavia, D., Allan, J.D., Arend, K.K., Bartell, S., Beletsky, D., Bosch, N.S., Brandt, S.B., Briland, R.D., Daloglu, I., DePinto, J.V., Dolan, D.M., Evans, M.A., Farmer, T.M., Goto, D., Han, H., Hook, T.O., Knight, R., Ludsin, S.A., Mason, D., Michalak, A.M., Richards, R.P., Roberts, J.J., Rucinski, D.K., Rutherford, E., Schwab, D.J., Sesterhenn, T.M., Zhang, H., Zhou, Y., 2014. Assessing and addressing the re-eutrophication of Lake Erie: Central basin hypoxia. J. Gt. Lakes Res. 40, 226–246.

Schelske, C.L., Stoermer, E.F., Conley, D.J., Robbins, J.A., Glover, R.M., 1983. Early eutrophication in the lower Great Lakes: New evidence from biogenic silica in sediments. Science 222, 320–322.

Schropp, S.J., Lewis, F.G., Windom, H.L., Ryan, J.D., Calder, F.D., Burney, L.C., 1990. Interpretation of metal concentrations in estuarine sediments of Florida using aluminum as a reference element. Estuaries 13, 227–235. https://doi.org/10.2307/1351913

Snelder, T., Fraser, C., Hodson, R., Ward, N., Rissmann, C., Hicks, A., 2014. Regional Scale Stratification of Southland's Water Quality - Guidance for Water and Land Management (No. C13055/02). Aqualinc Research Ltd.

Snelder, T., Hughes, B., Wilson, K., Dey, K., 2016. Physiographic zones for the Southland region (Technical Report). Lyttelton, NZ, Land Water People Ltd.

Sparling, G.P., Schipper, L.A., 2002. Soil quality at a national scale in New Zealand. J. Environ. Qual. 31, 1848–1857.

Stevens, L.M., Robertson, B.M., 2012. New River Estuary 2012: Broad Scale Habitat Mapping (Report prepared by Wriggle Coastal Management for Environment Southland). Nelson, New Zealand.

Tan, F.C., Strain, P.M., 1979. Organic carbon isotope ratios in recent sediments in the St Lawrence Estuary and the Gulf of St Lawrence. Estuar. Coast. Mar. Sci. 8, 213–225.

Thoms, M.C., 1981. Sedimentation in the New River Estuary, Southland (Master of Science in Geography). University of Canterbury, Christchurch, New Zealand.

van Maren, D.S., Oost, A.P., Wang, Z.B., Vos, P.C., 2016. The effect of land reclamations and sediment extraction on the suspended sediment concentration in the Ems Estuary. Mar. Geol. 376, 147–157.

Walling, D.E., Owens, P.N., Leeks, G.J.L., 1999. Fingerprinting suspended sediment sources in the catchment of the River Ouse, Yorkshire, UK. Hydrol. Process. 13, 955–975.

Walling, D.E., Woodward, J.C., 1992. Use of radiometric fingerprints to derive information on suspended sediment sources. Eros. Sediment Transp. Monit. Programme River Basins, Proceedings of the Oslo Symposium, August 1992.

Wilkinson, S.N., Hancock, G.J., Bartley, R., Hawdon, A.A., Keen, R.J., 2013. Using sediment tracing to assess processes and spatial patterns of erosion in grazed rangelands, Burdekin River basin, Australia. Catchments Reef Contin. Minimising Impacts Agric. Gt. Barrier Reef 180, 90–102. https://doi.org/10.1016/j.agee.2012.02.002

Windom, H.L., Schropp, S.J., Calder, F.D., Ryan, J.D., Smith, R.G., Burney, L.C., Lewis, F.G., Rawlinson, C.H., 1989. Natural trace metal concentrations in estuarine and coastal marine sediments of the southeastern United States. Environ. Sci. Technol. 23, 314–320. https://doi.org/10.1021/es00180a008

Figures

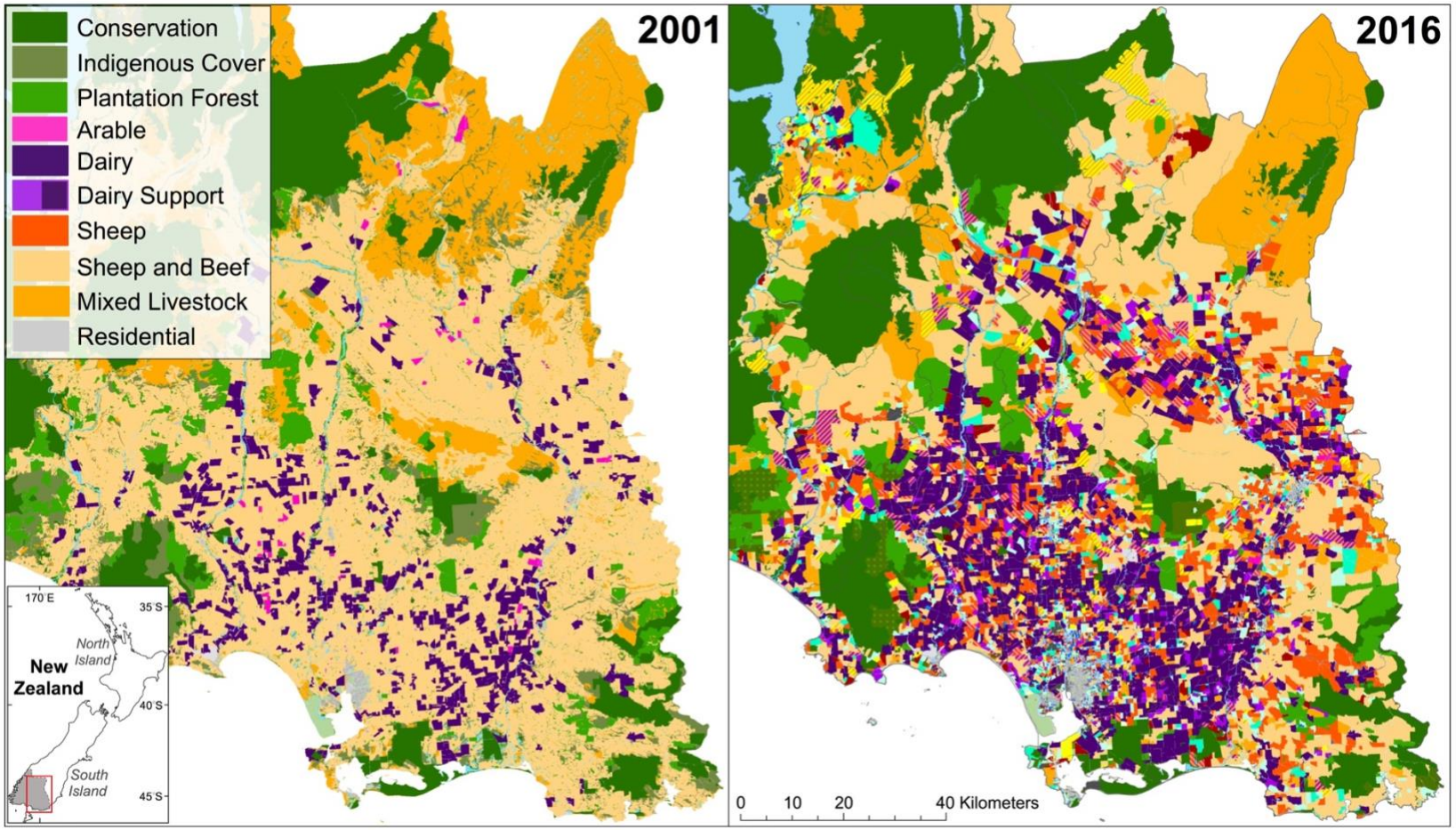

Figure 1-1. Map of land use cover in Southland from 2001 and 2016 (after Pearson and Couldrey, 2016).

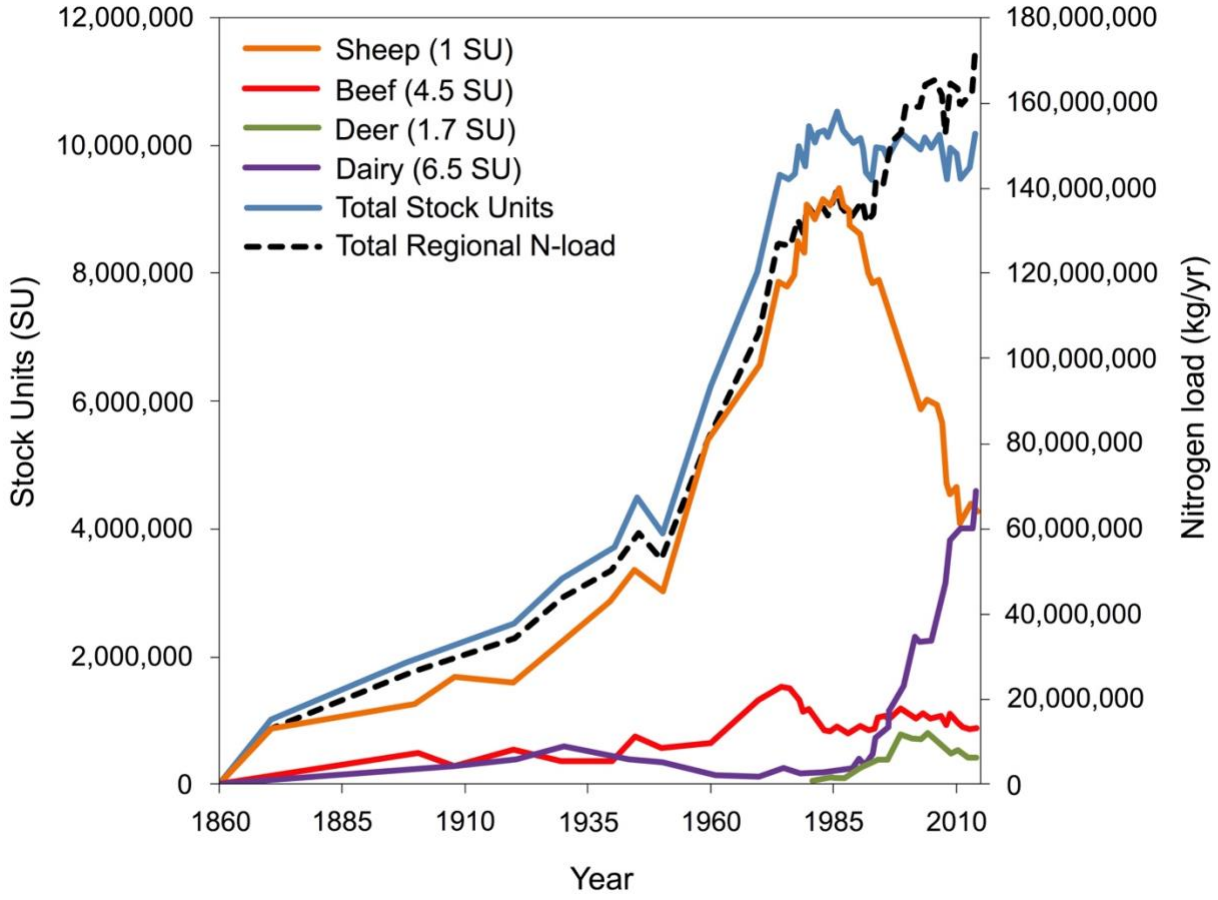

Figure 1-2. Number of stock units of sheep, beef, deer, and dairy cattle, as well as the regional nitrogen load in Southland from 1860-2015 (after Ledgard, 2013; Pearson and Couldrey, 2016; Statistics New Zealand, 1960).

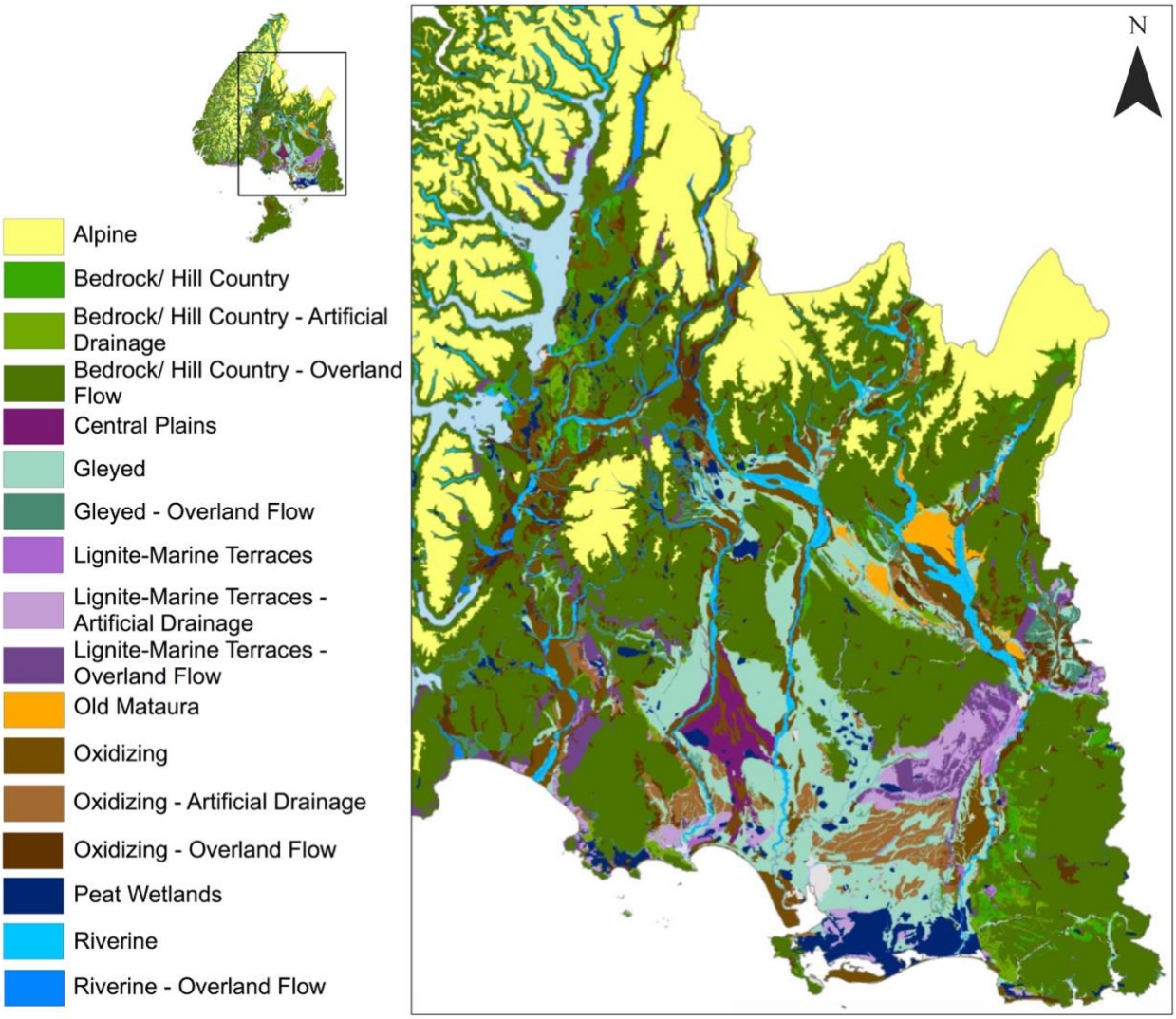

Figure 1-3. Map of the physiographic zones in Southland (after Pearson and Couldrey, 2016; Rissmann et al., 2016).

Chapter 2. Using estuarine cores to assess changes in terrestrial-sediment loss and eutrophication in New River Estuary, Southland, New Zealand

Danielle J. Brown[1], Clint W.F. Rissmann[2,3], Nick Ward[4], and Matthew I. Leybourne[*5]

[1] Harquail School of Earth Sciences, Mineral Exploration Research Centre, Laurentian University, Sudbury, Ontario, Canada P3E 2C6

[2] Land and Water Science Ltd., Invercargill 9810, Southland, New Zealand

[3] Waterways Centre, University of Canterbury, Christchurch 8041, New Zealand

[4] Environment Southland, Waikiwi, Invercargill 9810, Southland, New Zealand

[5] Queen's Facility for Isotope Research, Department of Geological Sciences and Geological Engineering, Queen's University, Kingston, Ontario, Canada K7L 3N6

*Corresponding author: m.leybourne@queensu.ca

2.1. Introduction

Delineating the impact of anthropogenic activity on the degradation of water quality and ecological health is a major concern in land management. Sediment loss, a natural response to water- or wind-driven erosional processes, is exacerbated by land clearance and intensive human activity, becoming a threat to aquatic ecosystems when the volume of mobilized sediment exceeds what can be attenuated by the receiving environment. Increases in fine-sediment (<2 mm) accumulation, a widespread, global issue in developed landscapes, has long been linked to declines in ecosystem health and, as a result, cultural, soil and economic wellbeing. Increased sediment deposition in several United Kingdom river basins (i.e., Rivers Axe, Exe, and Severn), which is degrading habitat quality, was shown to be majorly sourced from eroding pasture soils (38%, 71.7%, and 65.3%, respectively; Collins et al., 2012, 1997). The increase of terrestrial sediment to the Burdekin River basin in Australia is primarily derived from livestock grazing areas (~75%) and has been detrimental to coral reef communities in the adjacent Great Barrier Reef (Wilkinson et al., 2013). Transformation from primarily pastoral activity to an extensively urbanized and industrial landscape, particularly in the last 60 years, has had negative ecological impacts in the Tamaki Estuary catchment in Auckland, New Zealand (Abrahim, 2005; Abrahim and Parker, 2008). In fact, many estuarine and delta systems in New Zealand have experienced an increase in ecological vulnerability due to accelerated sedimentation exacerbated by human activity (Halliday et al., 2006; Hicks et al., 2000; Hicks and Basher, 2008; Horrocks et al., 2007; McDowell and Wilcock, 2004; Monaghan et al., 2010, 2007; Quinn and Cooper, 1997; Roddy, 2010).

The New River Estuary (NRE), in Southland, New Zealand (Fig. 2-1), is the most heavy-metal contaminated, and second most nutrient- and sediment-enriched receiving environment in the region (Robertson et al., 2017). It is a 34 km^2 mesotidal lagoon that primarily drains the Oreti River and its tributaries (inflow of 44 $m^3 s^{-1}$), which comprise 88.9% of the 4314 km^2 catchment, and the Waihopai River (inflow of 2.8 $m^3 s^{-1}$) into the Foveaux Strait. The climate of the catchment is cool and temperate with a moderately high mean annual rainfall (750-1500 mm) (Martin et al., 2015). Land use is dominated by intensive pasture (55%), which includes dairy and beef cattle, sheep, and deer, followed by native forest (20%), low-producing pasture (14%), and exotic forest (9%). Adjacent to the NRE, the region's capital city, Invercargill, releases treated wastewater, stormwater discharge, and historic landfill leachate into the estuary (Robertson et al., 2017). Non-point sources (fluvial) account for 80%, 68%, and 99.9% of the total nitrogen, phosphorus, and sediment loads, respectively, and are, therefore, considered more important contributors in the catchment than point sources (i.e., factories, municipal waste, etc.) (Robertson et al., 2017; Snelder et al., 2014).

Development within the NRE catchment has affected the hydrological balance and sediment yield in the estuary. Extensive clearing of native bush and draining of wetlands to accommodate urbanization and agricultural growth in the late 19th century exacerbated catchment sediment loss. The reclamation of a 12.2 km^2 section of the NRE from 1910-1920, a 25% reduction in the estuary's tidal compartment, accelerated sediment accumulation, a common estuarine response (van Maren et al., 2016). Textural analysis of the deposited sediment determined the medium-fine sand was primarily marine in origin, with up to 47% of fine-fluvial material transferred out onto the continental shelf (Thoms, 1981). Agricultural intensification, sheep farming was the major development, through 1950-1984 led to the channelization of riverways and expansion of

farmland onto previously undeveloped areas (Ledgard, 2013; Pearson and Couldrey, 2016). By 1984 the industry was no longer expanding into undeveloped terrain and the number of stock units in the region stabilized. The level of nitrate in the riverine waters, however, continued to rise due to the shift from sheep and beef farming to dairying and dairy support, which began in 1985 (Ledgard, 2013). The expansion of dairying onto unsuitable soils (coarse structure or artificial drainage), linked with irrigation, tile drainage, and wintering practices, results in excessive sediment, nutrient, and contaminant (heavy metals) losses to riverways (Monaghan et al., 2010, 2007). Instead of using feedlots, dairy farming in New Zealand allows cattle to range freely year-round on either grassland or wintering paddocks. Wintering, which involves the strip-grazing of cattle, sheep, and deer on resilient crops when there can be little to no pasture growth, especially localizes soil erosion. Dairy cattle also contribute higher nitrate and phosphorus loads than the other stock (Monaghan et al., 2005, 2002). Anthropogenic exacerbation of sediment loss drives estuarine contamination and nutrient loading as fine-sediment acts as a mechanism to transport the increased volume of pollutants, especially phosphorus and heavy metals, in the catchment (Chapman and Wang, 2001). Modifications to land use and management, especially since 1985, have led to the deterioration of biodiversity, soil stability, and water quality in the catchment, which has increased the pressure on the ecosystem and reduced its ability to respond to land use changes (Ledgard, 2013).

The effects of eutrophication in the NRE have been monitored over the last two decades (Robertson et al., 2017; Robertson and Stevens, 2007, 2001; Stevens and Robertson, 2012). Increased macroalgal growth (i.e., *Gracilaria* and *Ulva*), which currently cover ~8% of the estuary, a 60% increase in areas with fine-sediment accumulation (Fig. 2-1), an average loss of seagrass cover by 40% since 2001, and a reduction in sediment oxygenation indicates that the

NRE ecosystem is highly vulnerable as the result of nutrient enrichment and fine-sediment accumulation (Corbett et al., 2005; Robertson et al., 2017). The proliferation of opportunistic plants and algae, which will outcompete other native species in the nutrient-enriched environment, degrades ecological health and further accelerates fine-sediment accumulation as it acts as an effective sediment trap. The upper section of the Waihopai Arm is even further developed in its eutrophic state, transitioning from macroalgal dominance to prolific sulfur-oxidizing bacterial mats (i.e., *Beggiatoa*) as a result of increased sediment anoxia and sulfide concentrations (Robertson et al., 2017).

This study focuses on the physiochemical characterization of cores from areas in the NRE accumulating fine-sediment (Fig. 2-1) to identify historical changes to the catchment's sediment load. A geochemical assessment of deposited sediment is a cost-effective, reliable, and globally-analogous approach that can provide insight to the composition and quality of sediment source materials. For example, the enrichment of trace metals above regional background (geogenic) levels and pre-determined "trigger values" defines sediment quality and can indicate the magnitude of anthropogenic influence (ANZECC and ARMCANZ, 2000; Birch, 2017; Birch and Olmos, 2008). Similarly, using stable carbon and nitrogen isotope signatures in a dual-isotopic approach can qualitatively apportion the allochthonous (terrestrial soil and plant debris) and autochthonous (marine phytoplankton and algae) contributions to the sediment load. Terrestrial sources range in $\delta^{13}C$ from -26 to -30.9‰ (av. -28‰) and trend from unpolluted $\delta^{15}N$ signatures (0‰) to anthropogenic (polluted) nitrogen (8‰) as eutrophication intensifies, whereas marine sources range in $\delta^{13}C$ from -18 to -22‰ (av. -21.5‰) and have an average $\delta^{15}N$ of 5‰ (Alling et al., 2008; Fry, 2002; Kendall et al., 2001; Lehmann et al., 2002; Middelburg and Nieuwenhuize, 1998; Peterson and Fry, 1987; Tan and Strain, 1979). In contrast, terrestrial soils that host plant

material, C4 (i.e., corn, prairie grass, etc.) and C3 (i.e., deciduous and coniferous trees, etc.), will reflect the isotopic signature of the plants: $\delta^{13}C$ of -13 to -14‰ and -26 to -27‰, respectively (Kendall et al., 2001). These chemical and isotopic changes, when correlated to the sediment's radioisotopic age, can help delineate a timeline of anthropogenic influence on the rate of delivery and quality of the sediment load. As well, radionuclide concentrations (^{210}Pb, ^{226}Ra, ^{137}Cs, ^{7}Be) denote the physical processes that release sediment into riverways: sheet erosion of surface soils, gully erosion of subsoils, including channel bank collapse, and in-channel resuspension (Hancock and Caitcheon, 2010; Walling et al., 1999; Walling and Woodward, 1992; Wilkinson et al., 2013). Determining the dominant erosional process further defines the anthropogenic influence on the sediment load because different land uses affect soil susceptibility to erosion. Understanding human impacts is critical for the development of targeted mitigation and land management strategies that will help alleviate the pressure on the ecosystem from an excess of sediment, nutrients, and contaminants.

2.2. Geological context

The New River Estuary catchment encompasses diverse geological units of the Austral Superprovince, including the Caples, Dun Mountain-Maitai, Murihiku, and Brook Street Terranes (Turnbull and Allibone, 2003). The alluvial gravels, unconsolidated sand and silt, and glacial till of the Pakihi Supergroup dominate the Quaternary cover in most of the lowland areas of the catchment, including the Southland and Waimea Plains (Martin et al., 2015; Turnbull and Allibone, 2003). The Caples Terrane of the Eyre Mountains, the northernmost reach of the catchment, is comprised of low-grade metamorphic greywacke grading to schist toward the

north. The Caples Terrane is fault-bound to the southwest against the Dun Mountain-Maitai Terrane, which underlies and skirts the gravel outwash on the Waimea Plains. The Dun-Mountain-Maitai Terrane contains variably serpentinized mafic volcanic and ultramafic rocks that are distinguished by elevated Cu, Fe, Ni, and Cr concentrations (Robinson et al., 1996). The Dun-Mountain-Maitai Terrane is fault-bound along the northeastern limb of the Southland Syncline against the Murihiku Terrane of the Hokonui Hills, the headland of the Makarewa River catchment. The Murihiku Terrane, which underlies much of the catchment, is comprised of calc-alkaline arc-derived volcaniclastic sedimentary rocks that transition from marine shelf and slope units in the north to shallow, near-shore environment units in the south (Turnbull and Allibone, 2003). Well-bedded siltstone and fine sandstone with vitric and lithic tuff (North Range Group) dominates the northern rim of the east and west Murihiku blocks. Tuffaceous sandstones and conglomerates of the Taringatura Group dominate the rest of the east block and the northern and easternmost extent of the west block. Further south on the west block, and up stratigraphy, are coarse, arkosic, tuffaceous sandstones and fossiliferous mudstones (Diamond Peak Group), followed by cross-bedded, plant-rich sandstones and mudstones from the Ferndale Group (Ledgard, 2013; Martin et al., 2015; Turnbull and Allibone, 2003).

Southland has a complex and dynamic history of fluvial and glacial erosion through the Quaternary, which led to the formation of extensive gravel deposits in the Waimea and Southland Plains (Herman and Braun, 2008; Turnbull and Allibone, 2003). There have been nine documented glacial periods in the South Island in the past 0.7 Ma, with four of them occurring in the last 0.35 Ma (Herman and Braun, 2008). The last period of glaciation (Otira) had three major advances with successive glacial retreats that are inferred to be in association with global sea level and temperature rise (Herman and Braun, 2008). Radiocarbon dating places the end of the

Otira Glaciation at 14 ka, after which began the interglacial (post-glacial) Aranuian Stage of sustained glacial retreat (Fitzsimons, 1997). Marine bench deposits spanning from the modern-day Waiau and Mataura Rivers represent marine sedimentation in the Southland Plain resulting from the fluctuations in sea level and tectonic uplift during the interglacial periods (Turnbull and Allibone, 2003). Middle Quaternary deposits of loess underlain by variably weathered sandstone-dominated gravel make up the Kamahi Terrace in the Southland Plain, an alluvial fan created by a proto-Mataura River with inferred drainage towards present-day Invercargill City. Loess over weathered greywacke gravel deposits in the upper Mataura catchment (Waimea Plain) are attributed to an ancestral "Lumsden River" that drained eastward where the modern Oreti River flows to the south. Conversely, the upper Oreti catchment historically drained south at Mossburn instead of east and joined the Aparima River, forming a wide plain of alluvial gravel and fan deposits between the two present-day river channels. The eventual diversion of the upper Oreti River to the east was likely the result of fault movement near Mossburn. These examples of channel switching in response to tectonism, as well as aggradation and stream capture, combined with glacial evolution resulted in a complex paleodrainage system in the region that is reflected in Southland's fluvioglacial stratigraphy (Turnbull and Allibone, 2003).

Due to the region's diverse lithologies and dynamic tectonic and glacial history, soil chemistry and physical characteristics in Southland are highly variable (Hewitt, 2010; Ledgard, 2013; Martin et al., 2017, 2015; Rissmann et al., 2016a). Across the NRE catchment, especially the Southland Plain and Eyre Mountains, Brown and Gley soils dominate with lesser Pallic, Melanic, and Organic soils (Hewitt, 2010). The New Zealand Soil Classification (Hewitt, 2010) can be correlated to the US Soil Taxonomy (Soil Survey Staff, 1999; Appendix F), which is closely related to the Canadian system of soil taxonomy (Soil Classification Working Group,

1998). The soils in the NRE catchment increase in age moving inland with Alpine soils > Hill Country > Lowland areas, which reflects the control that elevation, slope, and the most recent Otira Glaciation ice extent has on geomorphic surface age (Rissmann et al., 2016a). The lowland plain ranges in age from Recent (Q1) soils in the modern-day floodplains to deeply weathered Brown with minor Ultic soils associated with Q8-10 outwash surfaces. Older soils (>Q2-4) are formed from mixed alluvium and loess derived from successive glacial-interglacial cycles. Recent (Q1) soils are often coarse textured and define the river margins of the upper Oreti River and its tributaries in the Eyre Mountains, whereas Gley soils define the margins of the lower Oreti, Makarewa, and Waihopai River catchments (Q2-8). The coastal lowlands, the southern Southland Plain, is dominated by imperfectly drained Gley, Podzolic, and Organic soils (Hewitt, 2010; Rissmann et al., 2016a). Geomorphic surface age (degree of weathering) and parent material composition are the dominant drivers of chemical variability in Southland's soils, followed, to a lesser degree, by geomorphic position (i.e., elevated terrace vs. lowland landscape) and marine aerosol loading (Martin et al., 2017; Rissmann et al., 2016a). The chemical signatures in the upper soil profile (0-30 cm) are also significantly influenced by anthropogenic activity, where deeper soil levels are dominated by geogenic controls (Martin et al., 2017).

2.3. Methods

At each sample site the date and time collected and time of low/high tide, as well as the northing, easting, and elevation in NZTM, the flora and fauna present and any other comments were recorded. Samples were labeled after the depositional area in NRE or after previous studies (i.e., Upper North Arm; Robertson and Stevens, 2007), refer to Figure 2-1.

2.3.1. Sample location

Areas with fine-sediment accumulation, defined by Wriggle Coastal Management's broad-scale habitat mapping (Robertson et al., 2017; Stevens and Robertson, 2012), which followed the National Estuary Monitoring Protocol (Robertson et al., 2002), were targeted for core collection. This substrate mapping identified three regions of significant sedimentation in the NRE: the western Waihopai Arm, Daffodil Bay, and Bushy Point, which decrease in intensity of fine-grained sedimentation, respectively. Shallow and deep sediment cores were collected in March 2017 from these depositional sites to determine historical variations in sediment physiochemistry. The Upper North Arm (UNA) site was chosen as a repeat site from a previous study (Robertson and Stevens, 2007).

2.3.2. Field methods

Shallow cores (top 25 cm of sediment) were collected at low tide to capture the surface material relatively undisturbed by tidal mobilization. A 25 cm-long, 5 cm-diameter PVC pipe was inserted into the sediment by hand, leaving a 0.5 cm gap to ensure surrounding sediment and water could not infiltrate the top of the core. The top of the pipe was capped, a cleaned plastic trowel was used to dig around the sides, and then the bottom was capped prior to complete extraction from the substrate. The caps were sealed with tape and the cores were transported and stored upright in a refrigerator. Deep cores, up to 1.5 m of sediment, were collected by boat at high tide by inserting a pre-measured, 5 cm-diameter PVC pipe, into the sediment until it could

no longer be inserted. The length from the top of the pipe to the top of the sediment horizon was measured and recorded to estimate the amount of compaction during core collection (refer to Section 2.3.4 for more detail). The pipe was cut using a hand saw at the sediment-water interface and the difference between the actual sediment-water interface in the pipe to this cut surface was measured. The pipe was subsequently cut again to just above the actual interface, capped, sealed with tape, and kept upright to limit sediment mobility and leaking during transport and storage. Replicate shallow and deep cores were collected at each sampling location within 25 m of the original sample to assess the representativeness of sediment stratigraphy within the cores at each location.

2.3.3. Analytical methods

The cores were extruded using a sterilised wedge, measured, photographed and sliced in half length-wise using clean fishing line. The stratigraphy was described in detail and the core was cut into 2-cm slices that were individually bagged and labelled; care was taken to not collect the outer edge that could have been smeared during collection and extrusion.

Samples from one length at representative depths, based on visual characteristics such as colour, grain size, and biota, were sent to the National Radiation Laboratory with the Institute of Environmental Science and Research Limited in Christchurch, New Zealand, for radioisotope analysis (^{7}Be, ^{137}Cs, ^{210}Pb, ^{226}Ra, and ^{228}Ra). The samples were embedded in an epoxy resin and stored for 30 days to retain ^{222}Rn. The concentration of ^{226}Ra is determined with higher sensitivity and accuracy by measuring the decay isotopes of ^{222}Rn (^{214}Bi and ^{214}Pb), which are in equilibrium with ^{226}Ra after the 30-day interval. The samples were then counted on high-purity

germanium detectors for 23 hours. Detection limits were calculated based on the baseline of individual spectrum at the peak energy of each sample, determined by the sample's radioactivity. The measured concentrations of the radionuclides are reported at the 95% level of confidence above the background baseline. Rates of sedimentation and the age of the sediment at the representative depths were calculated using ^{210}Pb isotope concentrations following the methodology of (Robertson and Stevens, 2007) (see Section 2.3.5).

The 2-cm subsections of the remaining length of the deep cores were collected in 50 mL Thermo-brand conical centrifuge tubes. These samples were preserved in nitrogen gas using a glove bag and N_2 gas to flush oxygen from the tubes before capping and sealing them with tape. Samples were idle for 4 months before being shipped to Canada for analysis. A portion of these subsections were sent to Bureau Veritas Commodities Canada Ltd., Vancouver, British Columbia, for geochemical analysis of a suite of 65 elements, including the rare earth elements. The samples were dried at 60°C then sieved to <180 μm (80 mesh). One split was analyzed for low to ultra-trace elemental determination by inductively coupled plasma mass spectrometry (ICP-MS) after a modified aqua regia digestion (1:1:1 of HCl, HNO_3, and water). The second split was analyzed by ultra-trace ICP-MS after a multi-acid digestion to give near total values for all elements. In the multi-acid digestion, the split is heated to fuming in HNO_3-$HClO_4$-HF, and the dried residue is then dissolved in hydrochloric acid.

Another portion of the deep core subsections were analyzed for carbon (organic), nitrogen (total), and sulfur (total) concentrations and stable isotopes at Queen's Facility for Isotope Research at Queen's University, Kingston, Ontario. The samples were weighed into tin capsules and the carbon and nitrogen isotopic compositions were measured using a Costech ECS 4010 Elemental Analyzer coupled to a Thermo-Finnigan DeltaPlus XP Continuous Flow Isotope Ratio

Mass Spectrometer (IRMS). The sulfur isotopic composition was measured using a MAT 253 Stable IRMS coupled to a Costech ECS 4010 Elemental Analyzer. The $\delta^{13}C$ and $\delta^{15}N$ values are reported using the delta (δ) notation in units of permil (‰) relative to the international standards Vienna Pee Dee Belemnite (VPDB) and Air ($\delta^{15}N$=0‰), respectively, with 0.2‰ precision. The delta value is expressed as:

$$\delta^{15}N\ (‰) = (R_{sample}-R_{reference})\ (1000/R_{reference}) \qquad (1)$$

where R is the ratio of the heavy isotope to the light, i.e., $^{15}N/^{14}N$, measured in both the sample and standard reference material (Peterson and Fry, 1987).

2.3.4. Compaction

The amount of compaction as a result of cohesive (fine-grained and wet) material being cored is calculated following Skilbeck et al., (2017):

$$X = (D-E)\ (100/D) \qquad (2)$$

$$Y = (E-F)\ (100/E) \qquad (3)$$

$$Z = [(X+Y)/100] + 1 \qquad (4)$$

where: X = the average amount of compaction from sample collection (%); Y = the average amount of compaction from sample extrusion from core (%); Z = the compaction factor; A = the initial length of pipe; B = the length of the pipe exposed above the sediment-water interface after

insertion; C = the length of the pipe from B to the actual sediment-water interface within the pipe; D = the length of pipe submerged below the natural sediment-water interface after insertion; E = the actual length of sediment collected within the pipe; and, F = the total length of sediment extruded from the pipe during analysis.

The amount of compaction at any one location in the core may vary depending on the grain size and initial porosity of the sediment. Similarly, physical packing of coarser grains and adhesion of cohesive finer-grains to the outside of the core barrel can further impact the rate of compaction within the pipe. For simplicity, the compaction factor is calculated assuming homogeneous sediment collection with minimal impact from physical packing or adhesion. The amount of autocompaction, which refers to the increase in bulk density of sediment through compaction during sediment accretion, including subsurface organic processes such as bioturbation, is also not considered in the above calculation.

2.3.5. Sediment age and rate of accumulation

^{210}Pb is a naturally occurring radionuclide derived from the decay of ^{238}U, which is eroded from rocks and incorporated into sediments. In the ^{238}U series, ^{226}Ra and ^{222}Rn are successive daughter products. ^{226}Ra (half-life of 1622 years) decays within the estuary sediments to ^{222}Rn and then to ^{210}Pb ("supported"). The loss of supported ^{210}Pb by radioactive decay in the estuary sediment is equal to the gain of ^{210}Pb by the in-situ decay of ^{226}Ra, thus the concentration of ^{226}Ra measured in the sediment is considered equivalent to the concentration of supported ^{210}Pb. Gaseous ^{222}Rn (half-life of 3.83 days) can also escape into the atmosphere and decay to ^{210}Pb ("unsupported"), which rapidly precipitates out of the atmosphere and is deposited in the

sediment. This unsupported ^{210}Pb is not replaced as it decays (half-life of 22.23 years) as it is not in radioactive equilibrium with its source. Therefore, unsupported ^{210}Pb can be used as a viable geochronometer in recent sediments (<100-150 years) (Appleby et al., 1992; Appleby and Oldfield, 1978). The total concentration of ^{210}Pb measured in the sediments less the measured concentration of ^{226}Ra (supported ^{210}Pb) represents the concentration of unsupported (or "excess") ^{210}Pb sourced from the atmosphere (Appleby et al., 1992).

Assuming a constant flux of atmospheric ^{210}Pb (unsupported) that is not redistributed through post-depositional processes, and with a reasonably constant rate of sediment accumulation, the age in years (t) since the sediment at depth x was deposited can be calculated using the following equation from the constant rate of supply (CRS) model (Appleby et al., 1979):

$$t = (1/\lambda) \ln (C_0/C_x) \qquad (5)$$

where: C_0 = the unsupported concentration of ^{210}Pb in the modern surface sediments; C_x = the unsupported concentration of ^{210}Pb at the (uncompacted) depth x; and λ = the ^{210}Pb decay constant (0.03114 y^{-1}).

Using the ^{210}Pb dates and the uncompacted depths an average rate of sedimentation (s) can be calculated (Eq. 6) between the representative sediment depths measured for radioisotope concentrations:

$$s_{x-0} = (d_x - d_0) / t_{x-0} \qquad (6)$$

where: d_x = the maximum (uncompacted) depth of the ^{210}Pb-dated horizon; d_0 = zero or the (uncompacted) depth from the previous ^{210}Pb-dated horizon; and t = the time duration (in years) between the deposition of d_x and d_0.

2.4. Results

2.4.1. Core descriptions

The shallow cores (and replicates) were visually, texturally, and radioisotopically equivalent in stratigraphy to the top 25 cm of the deep cores, thus the following stratigraphic descriptions are given collectively (full descriptions in Appendix A).

2.4.1.1. Age determination

Where the calculated unsupported ^{210}Pb concentrations of the sampled horizons are negative values, the sediment age cannot be calculated directly (refer to Section 2.3.5). In these cases, the age is reported as "<date", which is calculated using the maximum and minimum range of unsupported ^{210}Pb concentrations determined from the total ^{210}Pb and ^{226}Ra concentrations plus and minus their given standard deviations, respectively (Table 2-1).

Peak atmospheric fallout of ^{137}Cs occurred in 1964 in New Zealand, with elevated levels from 1959-1964 (Robertson and Stevens, 2007). Continual down-core measurements of radionuclide concentrations were not obtained, therefore there are depth disparities between the

measured peak concentrations and the lower limit of detection of ^{137}Cs in the cores. This means that ^{137}Cs can only be used to highlight a range of sediment depths dated to 1959-1964.

Where present, peak-maximums in down-core Pb concentration can be used to infer the relative age of sediment in the estuary based on industrial- and urban-sourced lead, predominantly from petroleum additives in New Zealand (Pearson et al., 2010). Lead concentrations were negligible prior to 1950, increased to a peak between 1975 and 1986, and subsequently declined as New Zealand transitioned from leaded to unleaded petroleum between 1987 and 1996, notably eliminating airborne lead (Ministry of Commerce, 1996; Statistics New Zealand, 1960; Wilson and Horrocks, 2008).

2.4.1.2. Compaction

The UNA short core had a recorded depth of 20 cm when extruded. The expected length of the core was 24 cm; thus, the core was compacted at a factor of 1.17 (refer to Section 2.3.4). The UNA deep core was 85 cm long upon extrusion. The expected length of the core was 166 cm yielding an average compaction factor of 1.49. The replicate deep core was measured at 73 cm in length with a compaction factor of 1.56. These factors are used to calculate the uncompacted depth of sampled horizons (Table 2-1).

The LW short core was recorded to be 18 cm long upon extrusion, where it was expected to be 24 cm long. This gives the LW short core an average compaction factor of 1.25. The LW deep core was 33 cm in length upon extrusion, but it was expected to be 61.5 cm long, yielding an average compaction factor of 1.49. The replicate deep core was measured at 31.8 cm long with a compaction factor of 1.53.

The DE short core was measured to be 20.5 cm long whereas it was expected to be 24 cm in length, yielding an average compaction factor of 1.15. The DE deep core was 99 cm in length after extrusion, but was expected to be 171.5 cm long, giving an average compaction factor of 1.48. The replicate deep core was 78 cm long with a compaction factor of 1.57.

2.4.1.3. Upper North Arm (UNA)

The top 2 cm of the cores, dated at 2017 (^{210}Pb), is comprised of dark greyish brown (2.5Y 4/2) silty mud containing rare *Gracilaria* fronds (Figs. 2-3, A-1). From 2-8 cm depth the cores are dominated by bioturbation, shown by black silty mud mottled with dark greyish brown mud, some of which outline vertical burrow traces, and interspersed with pockets of rusty brown silty mud. Bioturbation in the recent sediment is confirmed by the high concentration of ^{7}Be (10-14 Bq kg^{-1}) in the top 2 cm of both cores, dropping to the lower limit of detection (<10 Bq kg^{-1}) by 10 cm depth in the deep core (Table 2-1). There was also a live blood worm present in the sediment at 5 cm depth in the deep core. The bioturbated layer is marked at its base by an undulating and irregular boundary at 8 cm depth. From 8-48 cm depth the sediment darkens to black silty mud with sporadic patches of dark greyish brown throughout. The sediment in this section decreases in moisture and mud content with depth and is dated to 2009 (^{210}Pb) at 12 cm and to 2008 (^{210}Pb) at 16 cm depth. There are two traces of the dark greyish brown sediment at 33-34 cm depth, which have the appearance of vertical burrows. Based on the peak concentration of ^{137}Cs (1.1-1.81 Bq kg^{-1}) in the deep core, the sediment can be dated to 1959-1964 between the depths of 16-46 cm. The concentration of Pb increases up-core from 11-19 ppm, with a peak of 22-23 ppm occurring between 30-38 cm. This Pb peak indicates an age range of 1975-1986,

where lead emissions from leaded petroleum use was at its highest (Fig. 2-3). At 48 cm, dated to <1935 (^{210}Pb), there is an undulating and gradational boundary between the overlying black muddy silt and very dark grey (5Y 3/1) muddy silt with coarser, visible grains (sand-sized) and shell fragments. The very dark grey muddy silt becomes a coarser muddy sand at a textural boundary at 60-62 cm depth, which is dated to <1933 (^{210}Pb). The sand content continually increases to a depth of 80 cm with 10% small (<1 mm) fragments of shells present from 70-80 cm depth. The base of this muddy sand layer, at 78 cm, is dated to <1915 (^{210}Pb). The bottom of the core, from 80-86 cm depth, is a lighter grey sand with low moisture content and 20% small shell fragments (<1 mm) of unidentified species.

2.4.1.4. Lower Waihopai Arm (LW)

The top 2 cm of the cores, dated to 2017 (^{210}Pb), are comprised of very dark greyish brown (2.5Y 3/2) silty mud with smaller pockets of rusty brown silty mud (Figs. 2-4, A-2). Bioturbation in the recent sediment is confirmed by the high concentration of ^{7}Be (11-19 Bq kg^{-1}) in the top 2 cm of the shallow core dropping to the lower limit of detection by 10 cm depth in the shallow core (Table 2-1). After an irregular and undulating boundary, the sediment from 2-4 cm depth is a grey silty mud mottled with black silty mud and pockets of very dark greyish brown silty mud that resembles horizontal and burrow traces. The base of this layer is marked by an undulating boundary, followed by black silty mud mottled with grey silty mud with pockets of very dark greyish brown silty mud burrow traces from 4-20 cm depth. At 10 cm in the deep core a live blood worm was present. This unit is dated to 2007 (^{210}Pb) at 14 cm depth. The concentration of Pb increases up-core from 13-16 ppm, with a peak of 17-18 ppm at 16-20 cm, similar to the Pb

peak in the UNA core, which gives an age range of 1975-1986 at this depth. However, there is also a peak in Pb concentration (17-19 ppm) from 4-10 cm depth, potentially the result of sediment reworking and bioturbation. At the base of the black silty mud unit, 20-22 cm, is a gradational boundary into very dark grey (5Y 4/1) silty sand mottled with darker and lighter grey patches, which is dated to 1956 (^{210}Pb) at 24 cm depth. Concentrations of ^{137}Cs are at the lower limit of detection throughout the core, so it cannot be used to determine the sediment horizon dated at 1959-1964. At 31 cm depth there is a sharp boundary into a layer of the same sediment but with greater than 50% shells (1-20 mm in diameter) and increased moisture content down to the base of the core at 33 cm. The layer contains large whole shells and fragments of cockle (*Austrovenus stutchburyi*) and trough (*Mactra sp.*) shells.

2.4.1.5. East Daffodil Bay (DE)

There is a thin layer of fresh yellow-brown fine mud at the top of both cores to about 1 cm depth, dated to 2017 (^{210}Pb) (Figs. 2-5, A-3). Bioturbation in the recent sediment is confirmed by the high concentration of ^{7}Be (6 Bq kg^{-1}) in the top 1 cm of the deep core dropping to the lower limit of detection by 12 cm depth in the deep core (Table 2-1). From 1-40 cm depth the sediment is black muddy silt mottled with patches of grey muddy silt and pockets of yellow-brown muddy silt that resemble vertical burrow traces. The sediment in this layer is dated to 1997 (^{210}Pb) at 14 cm depth in the deep core and to 1982 (^{210}Pb) at 14 cm in the shallow core. The high concentration of ^{137}Cs (0.86-0.94 Bq kg^{-1}) in the deep core down to a depth of 14 cm dates the sediment between 14-24 cm depth to 1959-1964. The ^{137}Cs dates correlate to the ^{210}Pb age of 1965 at 26 cm depth in the deep core. At 28-32 cm depth in the deep core there is a shelly layer

with a mud-flat whelk (*Cominella glandiformis*) and non-articulated cockle (*A. stutchburyi*) shell. From 40-44 cm depth there is an irregular and gradational boundary into black muddy sand, which dates to <1923 (^{210}Pb). At 46-48 cm there is a layer dense with plant material, potentially indigenous seagrass or *Spartina* ("cord grass") that was introduced between 1930-1955 in an attempt to reclaim "waste land" in New River Estuary (Thoms, 1981), as well as shell material, including an articulated cockle shell (*A. stutchburyi*). The base of this layer, at 52 cm depth, is dated to 1906 (^{210}Pb). There are also fragments of cockle (*A. stutchburyi*) and trough (*Mactra sp.*) shells from 54-56 cm (1-2 mm), below which the sediment becomes coarser as a black silty sand with 10% shell fragments. From 62-65 cm depth the amount of shell fragments continually increases to a peak (20%) at 66-70 depth, with black sandy silt being dense with shell fragments and whole cockle (*A. stutchburyi*) and trough (*Mactra sp.*) shells. At 70 cm the sediment gradually transitions into a grey-brown sand with minimal moisture retention, visible sand-sized grains, and fine (1-2 mm) shell fragments (20%) from 70-76 cm depth. This grey-brown sand layer is dated to <1927 (^{210}Pb) at 74 cm depth. The grey-brown sand becomes mottled with dark grey sand at 88 cm to the bottom of the core at 99 cm depth.

2.4.2. Sedimentation

The UNA shallow core has an average rate of sedimentation of 20.7 mm yr^{-1} from 2008 (14-16 cm) to 2017 (top of core) (Table 2-1). The UNA deep core has an average sedimentation rate of 22.4 mm yr^{-1} from 2009 (10-12 cm) to 2017 (top of core). The rate of sedimentation in the deep core decreases to 7.3 mm yr^{-1} from <1935 (46-48 cm) to 2009, assuming the sediment is

dated to its maximum age (1935), to 104.5 mm yr^{-1} from <1933 (60-62 cm) to <1935, and to 13.3 mm yr^{-1} from <1915 (76-78 cm) to <1933.

The LW shallow core has an average rate of sedimentation of 17.5 mm yr^{-1} from 2007 (10-14 cm) to 2017 (top). The LW deep core has an average sedimentation rate of 5.9 mm yr^{-1} from 1956 (22-24 cm) to 2017 (top of core).

The DE shallow core has an average rate of sedimentation of 4.6 mm yr^{-1} from 1982 (10-14 cm) to 2017 (top of core). The DE deep core has an average sedimentation rate of 10.3 mm yr^{-1} from 1997 (12-14 cm) to 2017 (top of core). The rate of sedimentation in the deep core decreases to 5.5 mm yr^{-1} from 1965 (24-26 cm) to 1997, to 6.3 mm yr^{-1} from <1923 (42-44 cm) to 1965, assuming the sediment is dated to 1923, and to 7.0 mm yr^{-1} from 1906 (50-52 cm) to <1923.

2.4.3. Core geochemistry

2.4.3.1. Grain size effect

In an estuary, contaminants (heavy metals) can undergo transformations, including adsorption/desorption, coagulation, flocculation, and precipitation, due in part to the change in water composition (Chapman and Wang, 2001). Hydrophobic metals are commonly desorbed from sediments and then flocculate from the water column making estuaries an effective heavy metal and nutrient trap and increasing the susceptibility of estuaries to contamination and eutrophication (Li et al., 1984). The concentration of contaminants is partially controlled by grain size distribution, where decrease in grain size correlates to an increase in metal concentrations due to greater reactive surface area (Horowitz, 1991). Fine-grained sediment

generally correlates to higher Al concentrations, therefore, to correct for the grain size effect on composition, elemental concentrations are normalized to the conservative element aluminum (Schropp et al., 1990; Windom et al., 1989). Total aluminum concentrations (after a multi-acid digestion) increase up-core from 5.1-7.0 wt.% in the UNA core, from 5.9-6.9 wt.% in the LW core, and from 4.6-6.2 wt.% in the DE core (Fig. 2-2). This up-core increase in Al correlates to a general trend of upward fining in grain size. Therefore, normalizing elemental concentrations to aluminum (Fig. 2-2) presents true down-core elemental trends, independent of grain size variability (Chapman and Wang, 2001).

2.4.3.2. Lithologic changes through time

Total zirconium concentrations decrease from approximately 40 to 20 ppm in all three cores (Fig. 2-2). The down-core trend is a "step-like" decrease; UNA has an average Zr concentration of 42 ppm from 0-38 cm (2017 to 1975-1986), 28 ppm from 40-58 cm (<1986 to <1935), and 18 ppm from 60-85 cm (<1933) at the bottom of the core. The steps are not as well defined in LW, which has an average Zr concentration of 40 ppm from 0-18 cm (2017 to 1975-1986) and 25 ppm from 18-30 cm depth (1975-1986 to <1956) at the bottom of the core. The DE core has the least developed steps, with an average Zr concentration of 27 ppm from 2-34 cm (<2017 to <1965), with 37 ppm at the top (2017), and 16 ppm from 48-95 cm (<1923 to <1906) at the bottom of the core. The normalized Zr profiles demonstrate that the decrease in Zr concentrations cannot solely be explained by down-core coarsening. In addition, peaks of Zr at particular horizons (UNA: 32 cm, 48 cm, and 70 cm; DE: 30-38 cm) are accentuated in the normalized profiles and the step-like trend is preserved to a degree in all three cores (Fig. 2-2).

Calcium concentrations increase down-core, a trend that is further emphasized in the three normalized profiles (Fig. 2-2). UNA has an average Ca concentration of 1.4 wt.% from 0-34 cm (2017 to 1975-1986), which increases from 34 cm to a peak of 2.3 wt.% at 66 cm (<1933) as the sediment transitions texturally from silty mud to muddy sand with a higher proportion of shell fragments. The bottom of the UNA core has a constant concentration of 2.1-2.2 wt.% from 66-82 cm. The DE core follows a similar trend with an average of 50% higher Ca concentrations than UNA. DE has 2.2 wt.% from 2-34 cm depth (2017 to <1965), which increases from 34 cm to a peak of 3.6 wt.% at 66 cm (<1906) where there is a highly concentrated shelly bed at the base of a transition from muddy silt to silty sand. The bottom of the DE core, comprised of sand with fine shell fragments, has an average Ca content of 3.0 wt.% from 66-92 cm. The LW upper core is 25% greater in Ca than UNA with a concentration of 1.75 wt.% from 0-16 cm depth, this increases to an average of 2.8 wt.% from 18-26 cm as the sediment changes from silty mud to silty sand. The bottom of the LW core continues to increase in Ca concentration to 4.0 wt.% from 26-30 cm where the sediment coarsens and has a higher amount of shell fragments.

Sodium and K have comparable down-core trends of fairly constant concentrations. However, normalized to Al, both Na and K increase down-core in the UNA and DE cores. In the UNA and DE cores normalized Na and K increase in concentration at 38-46 cm (1975-1986 to <1935) and 30-78 cm (<1965 to <1906) depth, respectively. The lower UNA and DE cores have peak lows in the Na and K normalized profiles from 48-56 cm (UNA) and 60-66 cm depth (DE), which corresponds to the transition from mud to silt/sand and an increase in shell fragments in the UNA core and to the start of the shell-enriched horizon in the DE core. The normalized Na and K profiles from the LW core remain fairly constant down-core.

The UNA and DE plots have constant Ti and La concentrations in the upper core that decrease and include Ti and La peak concentrations in the lower cores (Fig. 2-2). The LW core has the opposite trend, where the Ti and La concentrations increase in the lower core, however, there is still a peak in Ti and La concentrations. These trends are accentuated in the Al-normalized profiles, except that the decrease in Ti and La concentrations in the lower UNA core, including the Ti and La peaks, are not as well defined as in the DE core. The UNA core has constant concentrations of 0.46 wt.% (Ti) and 13 ppm (La) from 0-38 cm (2017 to 1975-1986), which decrease to 0.33 wt.% at 38 cm (Ti) and 8 ppm at 44 cm (La) to the bottom of the core. Both Ti and La increase to a slight peak of 0.4 wt.% from 46-58 cm (Ti) and 10 ppm from 48-56 cm (La) in the lower UNA core. The DE core has Ti concentrations that drop from 0.47 wt.% to 0.33 wt.% at 48 cm depth (<1923) with a defined peak of 0.72 wt.% Ti at 64-66 cm and La concentrations that drop from 14.5 ppm to 8 ppm at 46 cm depth (<1923) with a defined peak of 20 ppm La at 62-66 cm. In the lower DE core, peaks highs of Ti, La, Fe, and Cr correspond to peak lows in Na and K (Figs. 2-2, 2-5). Alternatively, the LW core increases down-core with an upper Ti concentration of 0.43 wt.% from 0-14 cm (2017 to 1986-2007), which increases to 0.72 wt.% at the bottom of the core, with a peak of 0.88 wt.% Ti from 20-24 cm depth. The La concentrations in the LW core increases from 22 ppm La in the upper core (0-16 cm) to 30 ppm at the bottom of the core, with a peak of 43 ppm La at 22-24 cm depth.

The Fe concentration in the cores (Figs. 2-3 to 2-5) is constant at 4.0 wt.% from 0-38 cm (UNA), 4.1 wt.% from 0-18 cm (LW), and 3.6 wt.% from 2-40 cm, with 4.3 wt.% in the top 2 cm (DE). At 38 cm to the bottom of the UNA core the Fe concentration decreases to 3.0 wt.% (38-46 cm) and to 2.5 wt.% (60-86 cm), with a peak to 3.6 wt.% at 54-56 cm. From 18-24 cm in the LW core the Fe concentration increases to a peak of 4.6 wt.%. The DE core decreases at 40

cm down to 2.5 wt.%, with a peak in Fe concentration at 64-66 cm of 3.7 wt.%. When normalized to Al, there is a slight increase in the upper core Fe concentration starting at 38 cm in the UNA core and at 48 cm in the DE core, with lower core peaks in Fe, as seen in the raw data, preserved. The peak in Fe in the lower LW core is also preserved in the normalized plot, however, there is a trend of down-core increasing Fe concentration from 0-6 cm and at 18 cm depth.

Higher sulfur concentrations recorded in the partial sediment split (after modified aqua regia digestion) than the total fraction (after multi-acid digestion) is considered the result of analytical error, thus the partial fraction concentrations are presented as total values. The S content in the UNA core (Fig. 2-3) is fairly constant down-core to 48 cm (av. 0.54 wt.%), with the exception of a peak high of 0.7 wt.% at 6-10 cm. There is another peak in S up to 1.1 wt.% (55 cm) from 46-60 cm depth. The bottom of the UNA core has a slightly lower S content (av. 0.45 wt.%) from 62 cm to the bottom of the core. The upper LW core has an S content (Fig. 2-4) of av. 0.53 wt.% from 0-16 cm depth, with a broad peak up to 0.76 wt.% from 4-12 cm. The lower LW core increases from av. 0.53 wt.% at 16 cm to 0.95 wt.% at the bottom of the core (30 cm). The S content in the DE core (Fig. 2-5) decreases from 1.2 wt.% in the top 2 cm to an average of 0.14 wt.% reached by 50 cm to the bottom (80 cm).

2.4.3.3. Pollutant changes through time

Total phosphorus (TP), nitrogen (TN), and organic-carbon concentrations increase up-core in the sediment of all three cores, irrespective of grain size variability, from a background of 0.03-0.05 wt.% (TP), 0.05-0.1 wt.% (TN), and 0.2-0.5 wt.% (organic-C) (Fig. 2-8). In all three

cores the organic-C concentrations variably increase up-core to a concentration of 2-2.5 wt.%, with significant increases starting at 38 cm in UNA, 24 cm in LW, and 52 cm and 4 cm in DE. The TP concentrations increase to 0.074 wt.% at 38 cm and, sharply, to 0.1-0.14 wt.% from 10 cm to the top of the UNA core. TN in the UNA core increases most significantly at 38 cm depth from about 0.1 wt.% to 0.2-0.3 wt.%. In the LW core, P and N have steadily increased in concentration starting at 22-24 cm up to 0.1 wt.% (TP) and 0.4-0.5 wt.% (TN) at the top of the core. TP in the DE core is slightly but constantly increasing up-core and only rises significantly in the upper 4 cm (recent sediment) from 0.058 wt.% up to 0.072 wt.%, and TN increases from 0.1-0.3 wt.% starting at 50 cm depth and, more significantly, from 0.3-0.7 wt.% at 6 cm to the top of the core. The surficial (recent) sediment of the cores are inversely enriched with the highest TP and lowest TN concentrations in the UNA core (1.4 and 2 times greater P than LW and DE) and the lowest TP and highest TN values in the DE core (3 and 1.4 times greater N in DE than UNA and LW). This is likely due to the hydrodynamics in the NRE, where fluval input (Oreti and Waihopai River catchments) is a more significant contributor of nutrients to the Waihopai Arm than Daffodil Bay (Measures, 2016). The inverse in nitrogen could be representative of increased biotic activity (opportunistic algae and bacteria) due to the higher eutrophic condition in the Waihopai Arm compared to Daffodil Bay, where nitrogen is most likely the limiting nutrient.

Heavy metal concentrations increase up-core, independent of grain size, in the UNA, LW, and DE cores (Figs. 2-3 to 2-5). In the UNA and DE cores, the Cr concentration increases from 40 ppm in the lower cores (40 cm to the bottom of the cores) to 60 cm in the upper cores (0-40 cm). There is a peak in the lower cores of 53 ppm Cr from 46-58 cm (UNA) and 77 ppm Cr from 60-64 cm (DE). The LW core has an average Cr concentration of 63 ppm down-core, with a peak

of up to 88 ppm Cr from 18-24 cm depth. Copper and Zn increase from initial concentrations of 7.5-9.7 ppm (Cu) and 38-47 ppm (Zn). The UNA core has a Cu concentration of 7.6 ppm from 64-86 cm, which increases to 17 ppm at 38-60 cm (<1975) and increases to 25 ppm from 0-38 cm depth (2017 to 1975-1986). The LW core increases from 9.7 ppm Cu at the bottom of the core (24-30 cm) to 23 ppm Cu from 0-18 cm depth (2017 to 1975-1986). The DE core increases from 7.5 ppm Cu in the lower core (50-96 cm) to 16 ppm Cu in the upper core (4-24 cm; <2017-1965) and again to 25 ppm Cu at the top of the core (0-2 cm; 2017). Zinc concentrations in the UNA core increase from 38 ppm in the lower core (62-86 cm; <1933) to an average of 75 ppm from 38-58 cm depth (1975-1986 to <1935) and further increases to an average of 136 ppm in the upper core (0-38 cm; 2017 to 1975-1986). The LW core increases in Zn concentration from 47 ppm at 26-30 cm (<1956) to an average of 105 ppm in the upper core (0-18 cm; 2017 to 1975-1986). Zinc in the DE core starts to increase at 38 cm depth (<1965) from 40 ppm in the lower core (38-96 cm) up to 81 ppm at the top of the core. Though all three cores have similar initial Zn concentrations, the upper UNA core has a 1.3 times higher Zn concentration than the upper LW core and 1.9 times higher than the upper DE core. The UNA core has Ni concentrations (Fig. 2-3) of 15 ppm in the lower core (64-86 cm; <1933), which increases to an average of 28 ppm (with a peak of 37 ppm at 58 cm) from 38-60 cm (1975-1986 to <1933) and to 37 ppm in the upper core (0-38 cm; 2017 to 1975-1986). The LW core has a Ni concentration that increases from 20 ppm at the bottom of the core (<1956) to 36 ppm in the upper core (0-12 cm; 2017-2007). The DE core starts to increase in Ni concentration at 48 cm depth (<1923 to >1906) from 15 ppm Ni in the lower core (48-96 cm) to up to 28 ppm in the upper core (2-48 cm), which jumps to 34 ppm Ni from 0-2 cm (2017). Lead concentrations also increase up-core (Figs. 2-3 to 2-5), and UNA has 1.2 times higher Pb concentrations in the upper core than the upper LW and

DE cores. UNA increases from 11 ppm Pb in the lower core (62-86 cm; <1933) up to 19 ppm in the upper core (0-38 cm; 2017 to 1975-1986). There is a peak in Pb concentration in the UNA core of 22-23 ppm at 30-34 cm depth (1975-1986). In the LW core Pb increases from 13 ppm in the lower core (22-30 cm; <1956) to 17 ppm in the upper core (0-20 cm; 2017 to 1975-1986). There is also a broad peak in Pb concentration up to 18 ppm at 16-20 cm (1975-1986), however, it is less prominent than the UNA peak. The DE core has Pb concentrations of 11-13 ppm from the base of the core to 6 cm depth where it increases to a maximum of 16 ppm at the core top.

2.4.3.4. Pollutant impact

Reference "baseline" values are established assuming pre-anthropogenic concentrations occur at the bottom portion of the cores (Abrahim and Parker, 2008). The LW core does not appear to extend deep enough to reach background levels of all the pollutants. In this case, the baseline UNA or DE values were used where the down-core elemental trend in the LW core is similar to the UNA core (Al, C-org, Cu, Ni, Pb, Cr, As, Ag, Sb) or the DE core (N, Cd), respectively. Calculating baseline values from the cores instead of using standard material ensures that natural geochemical variability is taken into account (Abrahim and Parker, 2008). The baseline pollutant concentrations are normalized to aluminum to eliminate the effect of grain size distribution or down-core coarsening.

The enrichment factor (EF) estimates pollutant impact by quantifying the increase of pollutants (P, N, C-org, Ni, Cu, Pb, Zn, Cd, Cr, As, Ag, Sb) in the estuarine sediment. The EF is calculated with the following equation (Abrahim and Parker, 2008; Birch and Olmos, 2008; Salomons and Forstner, 1984):

$$EF = (C/Al)_x / (C/Al)_b \quad (7)$$

where (C/Al) is the ratio of the concentrations of the pollutant (C) to aluminum (Al) from the sample horizon (x) and the unpolluted baseline (b). The EF values can be categorized as little to no enrichment (EF < 2), moderate enrichment (2 < EF < 5), moderate to severe enrichment (5 < EF < 10), severe enrichment (10 < EF < 25) and very severe enrichment (25 < EF < 50) (Birch and Olmos, 2008). The UNA core is moderately enriched in Ag (2.1-4.6) from 48-64 cm and at 74 cm, and is moderately to severely enriched (7.3-10) from 0-48 cm depth, with severe enrichment (10-16) at 8-12 cm, 16 cm, 18-38 cm, and 46 cm. UNA is moderately to severely enriched in TN (5.0-6.7) at 0-8 cm, 12, 16, and 32 cm, with moderate enrichment (2.3-4.9) down to 34 cm and at 42, 48-52, and 54-66 cm. UNA is moderately enriched in organic-C (2.2-4.9) at 20 cm and from 24-60 cm, with moderate to severe enrichment (5.1-6.8) at 0-18 cm and 24 cm. UNA is moderately to severely enriched in Cd (5.2-8.6) from 0-16 cm, and at 20, 28, 38, and 48 cm, with moderate enrichment (2.3-4.9) at 18, 22-26, 30-34, 38-46, 48-58, 60-66, and 74 cm depth. UNA is also moderately enriched in: TP (2.0-3.1) from 0-12 cm and at 18 cm depth, Cu (2.2-2.7) from 0-38 cm and at 48 cm depth, Ni (2.0-2.2) at 10, 30-34, 48, and 58 cm depth, Zn (2.1-3.2) from 0-38 cm and 44-48 cm depth, and Sb (2.0-2.3) from 0-14, 16-24, and 34 cm depth. The LW core has little to moderate enrichment in TN (1.9-5.0) from 16-30 cm and is moderately to severely enriched (7.1-10) from 0-16 cm, with severe enrichment (10-13) from 20-80 cm depth. LW has moderate enrichment from 22-30 cm and is moderately to severely enriched in Ag (5.0-8.2) from 0-22 cm, with severe enrichment (11) at 18 cm depth. LW is moderately to severely enriched in organic-C (5.0-7.0) from 0-14 cm and is moderately enriched (2.9-4.2) from

14-22 cm depth. LW is also moderately enriched in TP (2.1) at 0-2 cm, Cu (2.2-2.5) from 0-14 and 18 cm, Cr (2.1) at 20 and 24 cm, Cd (2.3-3.6) from 6-12 and 16-22 cm, and Sb (2.0-2.1) from 4-10 cm and at 14 cm depth. The DE core is severely enriched in TN (12-16) from 0-4 cm, moderately to severely enriched from 4-22 cm and at 30 cm, and moderately enriched (3.0-4.9) from 22-28, 30-38, 42, and 46-50 cm depth. DE has moderate to severe enrichment in organic-C (6.5) at 0-2 cm and is moderately enriched from 2-24, 26-36, and 48 cm depth. DE is moderately to severely enriched in Ag (6.3-8.5) at 60 and 62-66 cm and has moderate enrichment (2.1-3.8) from 0-14, 16-24, 28-34, and 78 cm depth. DE is also moderately enriched in Cu (2.3-2.4) from 0-4 cm, Ni (2.0-2.1) from 0-4 cm, Cr (2.0) at 38 cm, and Cd (2.0-3.1) from 0-6, 10, 14, 20, 24, 40, 48, 60, and 64-70 cm depth.

The modified degree of contamination (mC_d) provides an indicator of sediment contamination based on the contamination factors (C_f) of a number (n) of pollutants (Abrahim and Parker, 2008). The mC_d is calculated using the following equations, with the assumption that the pollutant concentration (C_x) is the average of at least three impacted subsamples (upper core), and the baseline concentration (C_b) is the mean of unpolluted samples (lower core) (Abrahim, 2005):

$$C_f = C_x / C_b, \text{ and} \quad (8)$$

$$mC_d = (\sum C_f^i) / n, \text{ where } i = 1\text{-}n. \quad (9)$$

The degree of contamination is classified as very low (<1.5), low (1.5-2), moderate (2-4), high (4-8), very high (8-16), extremely high (16-32), and ultra-high (>32). Eleven pollutants (TP, TN, Cu, Ni, Pb, Zn, Cr, Cd, As, Ag, and Sb) were used to characterize sediment contamination. The

UNA core has a high degree of contamination (mC_d = 4.4, n=11). The LW core has a moderate degree of contamination (mC_d = 3.9, n=11) on the verge of high contamination. The DE core also has a moderate degree of contamination (mC_d = 3.0, n=11). The highest pollutant concentrations, baseline values, contamination factors, and the overall degree of contamination for each core are presented in Table 2-2.

2.4.3.5. Rare earth element and yttrium changes through time

Yttrium anomalies are quantified by the decoupling of the geochemical twins Y and Ho: $Y_{SN}/Ho_{SN}>1$ (positive) and $Y_{SN}/Ho_{SN}<1$ (negative) (Bau et al., 1996), where the subscript "SN" means the values are "shale-normalized" to Post-Archean Australian Shale (McLennan, 1989). Europium anomalies are quantified by $(Eu/Eu^*)_{SN}>1$ (positive) and $(Eu/Eu^*)_{SN}<1$ (negative), where $Eu^* = (Sm_{SN} \times 0.67) + (Tb_{SN} \times 0.33)$ (Bau et al., 1996). The REY normalized total sediment fraction (multi-acid digestion) in all three cores (Fig. 2-6) is defined by an increase in light rare earth element (LREE) concentrations from La to Gd with a positive Eu anomaly (1.24-1.31) and constant heavy REE (HREE) concentrations with a negative Y anomaly (0.74-0.82). The normalized REY concentrations of the total fractions in the LW core are 1.6 (Sm-Lu) to 2.2 (La-Nd) times higher than in the UNA and DE core. The normalized partial fraction (modified aqua regia) of the three cores is characterized by an increase in LREE with a positive Eu anomaly (1.26-1.30) and a decrease in HREE with a negative Y anomaly (0.85-0.89). The partial fractions in the UNA and LW cores are 1.5 times higher in REY concentrations than the DE core. Overall, the total fraction of sediment is 1.2 times more concentrated in REY than the

partial fraction in the UNA core, 1.7 times in the LW core, and 2 times more concentrated in the DE core.

In the UNA core, the total fractions in the upper core (0-38 cm) are up to 2 times more concentrated in REY than the lower core (38-86 cm) and the partial fractions are 1.3-3 times more concentrated in REY in the upper core. In both partial and total sediment fractions of UNA, the upper core REY traces plot above and the lower core plots below the average discriminant line. In the LW core, the total fractions in the upper core (0-18 cm) are 0.75-1 times as concentrated in REY as the lower core (18-30 cm) and the partial fractions are 1.2-1.8 times more concentrated in the upper than the lower UNA core. In the total plots the upper core REY traces plot above and the lower core traces plot below the average discriminant line, whereas, the opposite is true for the partial REY plot. In the DE core, the total fractions in the upper core (0-48 cm) are 0.75-2.4 times as concentrated in REY as the lower core (48-96 cm) and the partial fractions are 1.2-3 times more concentrated in the upper than the lower DE core. In the total plot the upper core REY traces plot above the average discriminant line and the lower DE core plots both above and below the line, whereas, in the partial plot the upper core traces mainly plot above and the lower core plots below the discriminant averages.

2.4.4. Element concentrations in total and partial fractions

The partial digestion of sediment (after modified aqua regia) accounts for the composition of surface adsorbed, organic, oxide, and sulfide fractions, and the total digestion (multi-acid) includes the more resistant, whole rock components, mainly silicates. Some resistant minerals,

including zircon and monazite, may not be quantitatively broken down during the multi-acid digestion.

Iron in the UNA core and the upper LW (0-18 cm) and DE (0-48 cm) cores (Fig. 2-7) has a constant proportion from partial sediment fractions of 75-85% (UNA) and 60-70% (LW, DE), irrespective of the upward increase in overall Fe concentrations. The lower LW (18-30 cm) and DE (48-96 cm) cores have variable Fe concentrations from silicate fractions with a constant input from partial sediment fractions (2.2 wt.% in LW, 1.5 wt.% in DE). Phosphorus in all three cores has a constant proportion from the partial sediment fraction (85-100%) with the up-core increase in total P concentrations, however, there is a slight increase in the silicate fraction proportion of 0-15% to 10-20% starting at 18 cm in UNA and 4 cm in LW to the tops of the cores. The three cores have a constant input of K from partial fractions of 0.1-0.3 wt.% (10-15%) with slight variability in the overall K concentration (1.1-1.6 wt.%). Sodium in the cores has a similar trend, though with greater variability in the Na input from partial fractions of 0.2-0.8 wt.%, which increases up-core and changes in proportion from 10-30% in UNA and DE, and 15-20% in LW. The UNA core and the upper LW (0-18 cm and 20-26 cm) and DE (0-64 cm) cores have a constant partial fraction input of Ca of 0.6 wt.% with the overall Ca concentration increasing down-core. The proportion of Ca from partial fractions also decreases from 50% to 25% in the UNA core and from 45% to 15% in the LW and DE cores. At the bottom of the LW (18-20 cm and 26-30 cm) and DE (64-96 cm) cores the total Ca concentrations increase to 4 wt.% in LW with 40% from partial fractions, and to 3.2-3.6 wt.% in DE with 30-50% from partial sediment fractions. The three cores have uniform inputs of Ti and Zr from partial sediment fractions of 0.1 wt.% (Ti) and 5 ppm (Zr). The total Zr concentrations and proportion of Zr sourced from silicate

fractions increase up-core (16-56 ppm; 75-90%), with boundaries between the upper and lower core clear at 38 cm in UNA, 18 cm in LW, and 2 cm in the DE core.

In all three cores, Ni, Cu, Zn, and As have constant proportions from partial and total fractions, irrespective of the general increase in total concentration up-core (Fig. 2-7). The proportion of heavy metals attained from the partial fraction of sediment is 80-85% for Ni, 95-100% for Cu and Zn, and 85-100% for As. Chromium in the DE core has a constant ratio of Cr from partial and total fractions in the upper core (60% partial: 0-2 cm, 40% partial: 2-48 cm) and a constant concentration of Cr from partial fractions (15 ppm) in the lower core (48-96 cm) with varying total Cr concentrations (34-77 ppm). The LW core has a similar constant ratio of Cr from both partial and total fraction sources (55% partial: 0-18 cm and 24-30 cm), except from 18-24 cm there is an increase in proportion of Cr from the silicate fraction of 45% to 70% with an unchanged concentration of Cr from partial fractions (26 ppm). In the UNA core, however, the Cr proportion from partial and total fractions (50-55% partial) remains constant with the overall increase in concentration up-core. In all three cores there is an up-core trend towards an average total Cr concentration of 60 ppm with 60% sourced from partial sediment fractions (~35 ppm). Cobalt also has a fairly constant proportion from partial and total digestions with a slight up-core increase in the partial fraction of the UNA (65 to 85%) and LW (55 to 75%) cores. The DE core has a similar trend in the upper core with an increase from partial fractions of 55% to 85% Co starting at 48 cm to the top of the core. The lower DE core (48-96 cm), however, has a constant proportion of Co from partial fractions (4-5 ppm) with an increase in the total Co concentration (8-12 ppm). The proportion of Pb in the three cores sourced from partial fractions increases up-core with an upward increase in total Pb concentration. The lower sections of the cores have a Pb concentration that is 15-25% sourced from partial fractions, whereas the upper

cores are 80% (LW and DE) and 80-95% (UNA) sourced from partial fractions. The primary shift to increasing Pb from partial fractions is apparent in UNA at 38 cm, LW at 18 cm, and DE at 2 cm depth.

The sum of the light and heavy rare earth elements (LREE: La-Gd, HREE: Tb-Lu) increases upward in all three cores (Fig. 2-7). The LREE increase from an average of 32 ppm at 60-86 cm in UNA and 34-96 cm in DE, to 52 ppm at 38-60 cm in UNA, 18-30 cm in LW, and 2-34 cm in DE, and to 76 ppm at 0-38 cm in UNA, 0-18 cm in LW, and 0-2 cm in DE. The HREE increase at the same depth boundaries in all three cores from averages of 3 ppm to 5 ppm to 7 ppm. The input of REE from partial fractions in the UNA core is constant at 90-100% (LREE) and 80-90% (HREE), regardless of the overall increase in concentration. The input of REE from partial fractions in the LW core, however, increases from 30% (LREE, HREE) at the bottom of the core up to 75% (LREE) and 70% (HREE) at the top. Also, the REE input from partial fractions to the DE core fluctuates in the lower core (34-96 cm) from 30-100% (LREE) and 25-60% (HREE). The upper DE core (2-34 cm) has a more constant input from partial fractions of 55-85% (LREE) and 50-60% (HREE), with 75% (LREE) and 70% (HREE) in the top 2 cm.

2.4.5. Stable isotopes

The $\delta^{15}N$ signature in the three cores decreases down-core with an overall decrease in TN content (Fig. 2-8). The UNA core decreases from 7‰ at the top (0-8 cm) to 4.5‰ at the bottom (66-86 cm), with TN content decreasing from 0.24 wt.% (0-8 cm) to 0.15 wt.% (26-36 cm) and to an average of 0.07 wt.% (38-86 cm). There is a peak low in $\delta^{15}N$ and TN content of 5.4‰ and 0.13 wt.% at 8-10 cm and a peak high of 7.4‰ and 0.26 wt.% at 28-32 cm in the UNA core. The

LW core decreases in average $\delta^{15}N$ signature from 8.1‰ (0-14 cm) to 5.3‰ (20-30 cm), with a decrease in average TN content from 0.45 wt.% (0-12 cm) to 0.09 wt.% (22-30 cm). The DE core decreases in average $\delta^{15}N$ from 6.8‰ (0-18 cm) to 4.8‰ (36-46 cm) and 2.7‰ (70-80 cm), with major peak increases to 8.5‰ at 47 cm (*Spartina* layer) and to 5.1‰ at 69 cm (shell-rich layer), and peak lows to -0.8‰ at 58-62 cm and to 0.9‰ at 75 cm. The TN content in the DE core decreases from 0.67-0.27 wt.% from 0-6 cm, where the concentration drops to an average of 0.03 wt.% in the lower core (50-80 cm).

The $\delta^{13}C$ signature in all three cores increases down-core with a decrease in organic-C content (Fig. 2-8). From 0-36 cm in the UNA core $\delta^{13}C$ is constant at an average of -27‰, with the organic-C content dropping from 2.3 wt.% at the top to an average of 1.4 wt.% at 24-36 cm depth. From 36-86 cm, $\delta^{13}C$ in the lower UNA core drops from -26‰ to an average of -23‰ at the bottom, with a peak signature of -16.5‰ at 48-50 cm depth where there is a textural boundary between silty mud and muddy silt, ^{210}Pb dated to <1935. The organic-C content in the lower UNA core drops to 0.3 wt.% at the bottom, with a peak in concentration up to 1.2 wt.% (53 cm) from 44-52 cm depth. The LW core increases in $\delta^{13}C$ from an average of -26.5‰ (0-20 cm) to -24.8‰ (20-30 cm), with a decrease in organic-C content from 2.2 wt.% (0-8 cm) to 0.5 wt.% (22-30 cm) at the bottom of the core. The DE core increases from an average $\delta^{13}C$ of -25.5‰ (0-44 cm) to -22‰ (44-64 cm) and to -12‰ at the bottom of the core (72-80 cm). There is a peak in $\delta^{13}C$ in the lower DE core of -14.9‰ at 50-52 cm, which is directly below a sediment layer at 46-50 cm that has a high concentration of plant material and cockle shells, and a slight peak in organic-C content of 0.6 wt.%. The organic-C content in the DE core decreases from 2.4 wt.% in the upper 2 cm to 0.1 wt.% at 56-64 cm and increases slightly to an average of 0.4 wt.% at the bottom of the core (64-80 cm).

The plot of $\delta^{15}N$ versus $\delta^{13}C$ signatures (Fig. 2-8) emphasizes the down-core variability in sediment chemistry. In the upper UNA core (0-36 cm) the sediment samples have a fairly constant $\delta^{13}C$ signature of about -27‰ but the $\delta^{15}N$ signature in these samples increases up-core from about 5.5‰ to 7.5‰. The mid-UNA core (36-62 cm) has a fairly constant $\delta^{15}N$ signature of 5-6‰ but a down-core decrease in $\delta^{13}C$ signature from -27‰ to -22‰. The lower UNA core (62-85 cm) has $\delta^{15}N$ signatures below 6‰ and $\delta^{13}C$ signatures above -24‰. The DE core follows a similar trend, with the upper core (0-36 cm) having less constant $\delta^{13}C$ signatures ranging from -27‰ to -25‰ and $\delta^{15}N$ signatures that increase up-core from 5.5‰ to 7.5‰. The mid-DE core (36-58 cm) has a fairly constant $\delta^{15}N$ concentration of 4-6‰ with variability in the $\delta^{13}C$ signatures from -26‰ to -22.5‰. The lower DE core (58-80 cm) has $\delta^{15}N$ signatures below 5‰ and $\delta^{13}C$ signatures ranging from -24‰ to -12‰. The LW core shows a more linear up-core trend of increasing $\delta^{15}N$ (5-6‰ from 22-30 cm, 6-7‰ from 14-22 cm, and 7.5-8.5‰ from 0-14 cm) and decreasing $\delta^{13}C$ signatures (-25‰ from 22-30 cm, -26 to -27‰ from 14-22 cm, and -27 to -28‰ from 0-14 cm).

2.5. Discussion

2.5.1. Changes in sediment sources

2.5.1.1. Historical sediment characteristics (early 1900's)

The effects of sedimentation in the NRE, a once well-developed trade port, were already prominent in the early 20th century. Significant channel depth was lost after a 12.2 km^2 section was reclaimed beginning in 1910, resulting in a 25% reduction in estuary surface area. The reclamation was undertaken to accommodate municipal and agricultural expansion and with it the reported number of vessel groundings in the channel increased from 1-3 in 1910-1915 to 5-9 between 1920-1930 (Thoms, 1981). Increased sedimentation in the estuary was considered the response to the 25% reduction in the estuary's tidal compartment, however, the supply of sediment was determined to primarily originate from a marine source (Thoms, 1981). This is particularly evident in the lower cores collected in 2017 from the upper Waihopai Arm and Daffodil Bay. The bottom of the UNA core has a consistent Ca concentration of 2.2 wt.% from 62-85 cm depth in sediment classified as muddy sand to sand. At 62 cm, dated at <1933, is the boundary between sand, with higher contents of shells and fragments, and muddy silt. At this boundary, the Ca concentration starts to decrease and the Zr, P, Cr, Zn, and Cr concentrations begin to increase. The bottom of the DE core also has a consistent Ca concentration of 3.0 wt.% from 58-95 cm, which is 1.36 times more concentrated than UNA because it is closer in proximity to the mouth of the estuary and, therefore, has a greater influence from marine than fluvial sources. At 58 cm in the DE core, dated to <1906, is the boundary between sediment classified as (silty) sand and muddy sand, and where Ca begins to decrease in concentration. Zirconium, La, Ti, Cu, and Cr show a more important change in sediment chemistry at 46-50 cm in the DE core where these elements increase in concentration. From 46-50 cm depth in the DE core is a sediment horizon that is dominated by shells and plant material, above which is a textural transition from (muddy/silty) sand to muddy silt. The plant material in this layer is most likely indigenous seagrass that has since been eliminated from the area due to increased nutrient

loading and sedimentation (Stafford-Bell, 2016). *Spartina*, or "cord grass", was introduced at a later date than this plant-rich horizon (1930-1955) to help trap the increased flux of fine-sediment associated with the estuary reclamation and later agricultural growth. Important textural boundaries, where fine-sediment begins to accumulate in higher quantities and heavy metal and nutrient concentrations increase (referred to as Transition A), are then recorded at 62 cm in the upper Waihopai Arm (UNA; Fig. 2-3) and at 46 cm in Daffodil Bay (DE; Fig. 2-5). The timing of this transition is fairly similar in the two cores, <1933 in UNA and between 1906-1923 in DE. The boundaries also mark a transition in sediment source around the time of estuary reclamation (1910-1920) from a marine-dominated load (high Ca) to increased input from terrestrial sources due to anthropogenic land development and modification. Land use impacting sediment loss in the catchment includes agricultural development from the late 19th century and urbanization (Cavanagh and Ward, 2014; Ledgard, 2013). For example, in the 1860's significant expanses of native bush were cleared, and wetlands were drained, to accommodate colonization and agricultural growth; today, wetlands and forest occupy <10% of their original coverage in the region, with the majority replaced by exotic pasture species. Sheep farming in particular was a major development, where stock units increased from approximately 1 to 3.5 million from 1870-1950 (Pearson and Couldrey, 2016).

Marine dominance in the historical sediment load of the NRE is also apparent in the stable isotopic signatures (Fig. 2-8). The upper Waihopai Arm (UNA) has a constant average $\delta^{13}C$ signature of -23.1‰ before the textural boundary at 62 cm (<1933), which is consistent with a primary marine source (-21.5‰; Peterson and Fry, 1987) that contributes 75% of organic material to the sediment load. The proportion of organic matter sourced from terrestrial material ($\%OC_{ter}$) is determined by:

$$\%OC_{ter} = (\delta^{13}C_x - \delta^{13}C_{mar}) / (\delta^{13}C_{ter} - \delta^{13}C_{mar}) * 100, \quad (10)$$

where the subscripts "x", "mar", and "ter" represent the carbon isotopic signatures in the sample, marine (-21.5‰), and terrestrial (-28%) sources, respectively (Alling et al., 2008; Peterson and Fry, 1987). The $\delta^{15}N$ signature in the bottom of the UNA core (<60 cm) is on average 4.8‰, which suggests a marine source (5‰; Fry, 2002) contributing 95% of the organic matter load over the relatively unpolluted fluvial sediment (0‰; Fry, 2002) from that time. The DE core has a similar relationship with a consistent average $\delta^{13}C$ of -22.7‰ from 64 cm up to the transitional boundary (46 cm), which is equivalent to having 81% of the organic load sourced from marine material. Overall the $\delta^{13}C$ signature is slightly higher in the DE core than UNA due to its proximity to the sea and thus greater influence of marine material. The lower DE core (64-80 cm), before 1906, differs from UNA as it has $\delta^{13}C$ values ranging from -19 to -12‰, which could represent the remnant isotopic signatures of native terrestrial plants being cleared from the land in the late 19th century to accommodate agricultural development (C4 plants, including *Spartina* and saltmarsh, have $\delta^{13}C$ of -13 to -14‰; Kendall et al., 2001, and seagrass has an average $\delta^{13}C$ of -10 to -11‰; Hemminga and Mateo, 1996). The higher isotopic range in the lower DE core could also be relic shell material (i.e., cockles have an average $\delta^{13}C$ of -18‰ (adults) to -15‰ (juveniles) and $\delta^{15}N$ of 8‰; Sauriau and Kang, 2000). To validate the relationship of plant and shell material signatures in the early sediment, the lower UNA core is expected to show the same isotopic signatures at the bottom of the core, however, radioisotopic dating of the 2017 UNA core does not confirm whether pre-1906 sediment was collected at the UNA site. The DE core also has a peak in $\delta^{13}C$ of -14.9‰ at 50-52 cm (1906) that is likely

recording the mixed signature of plant material (likely seagrass: $\delta^{13}C$ = -10 to -11‰) and shells ($\delta^{13}C$ = -15 to -18‰) that are dominating the sediment horizon, which occurs below the textural transition (A) marking the onset of increased terrestrially-derived muddy sediment and the associated pollutants. The $\delta^{15}N$ signature in DE below transitional boundary A (46 cm) is not uniform like in the UNA core, however, separating the distinct $\delta^{15}N$ peaks illustrates that below 50 cm the sediment has a predominantly marine source of organic material (74%) with an average signature of 3.7‰. Peak lows of $\delta^{15}N$ down to 0.9‰ at 75 cm and -0.8‰ at 58-62 cm could highlight sediment horizons with an unpolluted terrestrial source contributing 82-100% of the organic matter. At the DE textural boundary (46 cm) the $\delta^{15}N$ signature increases to a peak of 8.5‰, which is consistent with anthropogenically-polluted riverine sediment (8‰), however, the peak also aligns with the plant and shell-rich sediment layer and so could potentially be recording the $\delta^{15}N$ signature of shell material ($\delta^{15}N$ = 8‰) in that horizon.

2.5.1.2. Sediment characteristics during agricultural expansion

Sediment in the UNA core continually decreases in Ca concentration from an average of 2.2 wt.% below the textural boundary at 62 cm to an average constant of 1.4 wt.% reached by 34 cm depth (Fig. 2-3). Increases in the Zr, Ti, La, heavy metal, and nutrient concentrations at or up to 38 cm in the UNA core similarly highlights this horizon as an important transition in sediment chemistry. The sediment at this boundary (34-38 cm: referred to as Transition B) is dated to between 1975-1986, which shows that prior to this time period the sediment is dynamically changing as terrestrial contributions to the sediment load are becoming increasingly more important. The LW core also records this transitional period (B) with Zr, K, Cu, Zn, and Ni

increasing and Ti, La, Ca, and Cr decreasing up-core towards a fairly constant concentration that is reached around 18 cm depth (Fig. 2-4). This boundary in the LW core is also dated to 1975-1986, which shows that terrestrial material input to the NRE is increasing in dominance in both the upper and lower stretches of the Waihopai Arm. Similarly, the sediment chemistry in the DE core changes above the textural boundary (46 cm) with Zr, La, Zn, Ni, and Pb increasing and Ca continually decreasing in concentration, however, uniform chemistry in the upper core is not achieved (Fig. 2-5). Normalized profiles of these elements confirm that these periods of change in sediment chemistry occur irrespective of down-core grain size variability. River channelization and agricultural intensification through 1950-1980 are probable contributors to these chemical changes because both processes increase sediment loss, with higher levels of associated heavy metals and nutrients. During the period of expansion there was a significant increase in sheep numbers to a peak of 9.5 million in 1984 (Ledgard, 2013); to accommodate for this growth, agriculture expanded into undeveloped areas up until 1984 (Pearson and Couldrey, 2016). Contaminants (i.e., Ni, Cu, Zn, and As) are also supplied, often more importantly, by urbanization, which includes stormwater runoff, discharge from the wastewater treatment plant, and landfill leachate (now closed) (Cavanagh and Ward, 2014). The dynamic chemical change is shown to reflect urban and agricultural expansion because uniform sediment chemistry attained in the Waihopai Arm between 1975-1986 (34-38 cm in UNA and 16-18 cm in LW), likely when agricultural expansion was at a maximum (1984). Isotopic signatures support this (Fig. 2-8) as $\delta^{13}C$ in the UNA core increases from -23.1‰ at the textural boundary (62 cm) to a constant of -27‰ by 36 cm depth, an increase from 25% to 84% of organic matter sourced from terrestrial material. At 48-50 cm in the UNA core the $\delta^{13}C$ signature peaks to -16.5‰, which marks another textural boundary between silt-sand and mud. The high $\delta^{13}C$ signature is identical to the peak in

$\delta^{13}C$ seen in the DE core at 50 cm and could, therefore, be recording the mixed signature of remnant plant material (seagrass: -10 to -11‰) and shells (cockles: -15 to -18‰) that have mostly decomposed or broken down due to an increase in microbial activity associated with eutrophication. If this is the case then the high $\delta^{13}C$ peaks could be representative of a "healthy" estuarine state with prolific indigenous flora and fauna (pre-1935 in UNA, pre-1923 in DE), which are eliminated with the onset of significant fine-sediment accumulation (terrestrially-derived) associated with agricultural growth, including land clearing and river channelization, and urbanization after estuarine reclamation. The $\delta^{13}C$ signature in the LW core increases from an average of -24.8‰ at the bottom of the core (20-30 cm) to an average of -26.4‰ by 16 cm depth, an increase from 52% to 75% of organic material from terrestrial sources. The $\delta^{13}C$ signature in the upper LW core is 1.2 times lighter than in the UNA core because it is closer to the mouth of the estuary and, therefore, has 10% more marine contribution to its organic load. Similarly, the $\delta^{15}N$ signature in the UNA core is constant at 5.6‰ from 60 cm up to 22 cm and is increasing from 5.3‰ in the lower LW core up to an average of 8.1‰ by 14 cm depth. In the UNA core, the $\delta^{15}N$ values signify a change from 5% contribution from unpolluted terrestrial sediment (0‰) at 60 cm to 20% contribution from polluted terrestrial sediment (8‰) at 22 cm, with marine contribution subsequently decreasing from 95% to 80%. In the LW core, the $\delta^{15}N$ values signify an increase from only 10% of organic matter from terrestrial sources at the bottom (22-30 cm) to 100% contribution by 14 cm depth.

2.5.1.3. Modern sediment characteristics (post-1984)

After the period of chemical transitioning during agricultural expansion, where terrestrial sources are contributing greater quantities of sediment, the sediment in the Waihopai Arm becomes fairly uniform in chemistry by 34-38 cm in the UNA core (Fig. 2-3: Transition B) and 14-18 cm in the LW core (Fig. 2-4: Transition B). The consistency in the upper UNA and LW cores does not represent a constant supply of sediment transported to and deposited in the NRE because radiogenic-Pb shows that the rate of sedimentation has been increasing beyond those depths (Table 2-1). The attained uniform chemistry, therefore, represents an equilibrium between the contributions of terrestrial and marine sources of sediment. This is supported by the constant $\delta^{13}C$ signatures in the upper UNA (-27‰) and LW (-26.4‰) cores, which give a ratio of terrestrial- to marine-sourced material of 84:16 and 75:25, respectively (LW has higher marine influence due to greater proximity to the estuary mouth). As well as by the $\delta^{15}N$ signatures of the upper LW (8.1‰: 100% terrestrial-sourced) and UNA core, which increases from an average of 5.6‰ (22-34 cm) to 7.0‰ (0-22 cm) and records a change in the organic load from 20% to 65% terrestrial-sourced material. Daffodil Bay hasn't reached this uniformity in sediment chemistry likely because it receives a greater input from marine sources than the Waihopai Arm as it is closer to the Foveaux Strait; the upper DE core is 1.39 and 1.17 times more concentrated in Ca than the UNA and LW cores, respectively. However, the isotopic signatures of the upper DE core have become fairly stable: an average $\delta^{13}C$ signature of -25.5‰ from 0-44 cm (62% terrestrial) and an average $\delta^{15}N$ of 5.8‰ from 18-36 cm (26% terrestrial) increasing to 6.8‰ from 0-18 cm (59% terrestrial). Therefore, although the upper DE core is not chemically consistent, isotope signatures suggest that an equilibrium between terrestrial- and marine-sourced sediment has been reached, especially by 18 cm depth (Fig. 2-5: potentially Transition B).

Sediment uniformity is reached between 1975 and 1986 in the UNA (34-38 cm) and LW (14-18 cm) cores and isotopically in the DE core between 1965 and 1997 (18 cm), which is consistent in timing with the end of agricultural expansion onto undeveloped land and the peak sheep farming (1984). After 1985, there was a major transition from sheep and beef pastoral and arable land to dairy and dairy support land (Ledgard, 2013). By 2015, the number of sheep had decreased to 4.1 million while dairy cows had increased from about 0.05-0.73 million cattle (Pearson and Couldrey, 2016). Within the last two decades (1996-2015), dairy farming and support properties have taken over approximately 30% of the lowland area (by hectare) used to farm sheep, beef and deer (Pearson and Couldrey, 2016). From 2000 to 2011 dairying coverage doubled from 87,109 Ha to 195,500 Ha, with 54% of that being on soils with high risk for nutrient and contaminant loss due to artificial drainage and coarse soil structure (Houlbrooke et al., 2004; Ledgard, 2013). This agricultural shift is also linked to changes in land management, including irrigation, tile drainage, and the introduction of winter cropping, which refers to the strip-grazing of cattle, sheep and deer on resilient forage crops when there is little to no pasture growth. When coupled with seasonally high rainfall and minimal pasture uptake due to strip-grazing, winter cropping locally increases soil erosion, resulting in excessive sediment, nutrient and contaminant losses to riverways. Dairying is more intensive on the land, often requiring irrigation to maintain production, and has higher nitrate and phosphorus loading from waste compared to other stock, which contributes to poor water quality (Ledgard, 2013; Monaghan et al., 2010, 2007, 2005, 2002). Additionally, due to technological advancements in farming practices, including mole drains, land previously classified as unsuitable for intensive agriculture is developed, which increases the stress on natural resources in the region (Pearson and Couldrey, 2016). These changes impact the biodiversity, soil stability, and water quality in the

region and increase ecosystem vulnerability to pressures from land use (Ledgard, 2013). For example, although the total regional number of stock units has been stable at 10-11 million since 1984 (Transition B), the nutrient load is estimated to continue rising in response to these shifts in agricultural practice (Ledgard, 2013; Pearson and Couldrey, 2016). This relationship is supported by the continual increase in TN, TP, and organic-C concentrations in the upper UNA, LW, and DE cores (Fig. 2-8) when an equilibrium in proportion of sediment delivered from terrestrial and marine sources has been reached (constant $\delta^{13}C$ and $\delta^{15}N$: post-Transition B).

Non-point source discharges (fluvial) to the NRE are estimated to contribute 99.9% of the total suspended sediment load (76% from Oreti River, 21% from Makarewa, 1% from Waihopai River). By contrast, point source discharges are estimated to contribute only 0.1% of the total suspended sediment load, with the majority from Alliance Lorneville (meat processor), when calculated from a high load year (2009/2010) (Robertson et al., 2017). Urban supplies of particulate matter, such as stormwater runoff, discharge from the wastewater treatment plant, and historic landfill leachate, also presumably contribute to the sediment load, and especially the associated heavy metal load (Williamson and Morrisey, 2000). The estimations support that the majority of fine-sediment delivered to the NRE is fluvial in origin, where the proportion of fine-grained, nutrient- and metal-rich agricultural soil has increased in the fluvial sediment load through the aforementioned land usage.

2.5.1.4. Changes in primary erosional process

Fallout radionuclides can be used to determine the primary erosional processes that mobilize sediment into the waterway, which includes sheet erosion of surface soil and subsoil erosional

processes that includes channel bank collapse. Due to differences in their half-lives, the presence and amount present of each radioisotope can identify the dominant erosional process (Hancock and Caitcheon, 2010). Because it tends to be concentrated in the upper 10 cm of soil, high activities of ^{137}Cs (>0.8 Bq kg^{-1}) indicates surface soil sources of sediment, and low or no concentrations signify channel bank collapse or other subsoil erosion origins, respectively. Unsupported "excess" ^{210}Pb is typically low in concentration or not detectable in channel bank and other subsoil erosion derived sediment, therefore, high concentrations (>10 Bq kg^{-1}) also indicate surface soil origins. Due to its short half-life, ^{7}Be tends to be concentrated in the top few millimetres of soil, such that high concentrations (>10 Bq kg^{-1}) indicate surface soil sources. However, ^{7}Be is created through the interaction of cosmic rays and atmospheric nitrogen and oxygen and can, therefore, also be deposited with heavy rainfall in exposed soils, including surface soil, gullies and recently cultivated soils. Excess ^{210}Pb and ^{137}Cs will be low in concentration or not detected in the exposed subsoils, including channel banks, distinguishing them from surface soil signatures. Sediment sourced from sheet erosion of surface soils that is deposited in the riverways and remobilized will retain its high excess ^{210}Pb and ^{137}Cs concentrations while its ^{7}Be signature will be reduced (Hancock and Caitcheon, 2010).

Sediment in the shallow and deep UNA cores are dominantly sourced by surface soil erosion from 0-2 cm, and down to 16 cm in the shallow core and 12 cm in the deep core the source is either in-channel sediment resuspension, due to the decrease in ^{7}Be concentration, or surface soil erosion (Fig. 2-9, Table 2-1). The lower UNA deep core (46-78 cm) is dominantly sourced by a mix of channel bank collapse and other subsoil erosional processes. The LW shallow core is dominantly sourced by surface soil erosion (0-14 cm). The LW deep core has a mainly channel bank and subsoil erosion source from 0-2 cm and 22-24 cm, and either in-channel sediment

resuspension or surface soil erosion from 6-8 cm. The shallow DE core, from 0-14 cm, is mainly sourced from channel bank collapse and other subsoil erosional processes, though potentially from in-channel resuspension or surface soil erosion from 0-1 cm. The upper DE deep core, from 0-14 cm, is dominantly sourced by in-channel sediment resuspension or surface soil erosion and the lower deep core, from 24-74 cm, is predominantly sourced by channel bank collapse and other subsoil exposures. Based on the radionuclide concentrations in the sampled reference horizons we determined that the dominant process active in the modern sediments at the NRE depositional sites (esp. the Waihopai Arm) is surface soil erosion (± in-channel resuspension), most likely from pasture soil (Hancock and Caitcheon, 2010), and the dominant process in the historical sediment from these areas is channel bank collapse and other subsoil erosion processes. The down-core change where surface soil dominated erosion transitions to channel bank and subsoil dominated erosion occurs between 2009 and 1935 in the UNA deep core and between 1997 and 1965 in the DE deep core. It is apparent that agricultural development and river channelization between 1950-1980 and the shift towards dairying have altered the primary mechanism of sediment loss to riverways, increasing the pressure from contaminated surface soils (esp. pasture soils), which has a negative ecological impact both in stream and in the estuary.

A study using the compound-specific-stable-isotope (CSSI) technique similarly showed that terrestrial sources in the bulked upper 20 cm of NRE sediment were dominated by surface soil erosion (56-74% from sheep, 17-25% from deer, and 3-18% from dairy pasture), with minimal input from subsoil and bank erosion (0-1%) (Gibbs et al., 2015). The study also found that there was a decrease in terrestrial influence with increased proximity to the estuarine mouth: 30-40% from terrestrial sources in the upper estuary (i.e., Waihopai Arm) and only 0-10% in the lower

estuary (Gibbs et al., 2015). However, their conclusions that sheep and deer pasture, which are majorly within Alpine and Hill Country landscapes in the region, provide the majority of terrestrial sourced sediment suggests that elevation and slope are important factors that contribute to sediment loss.

2.5.2. Increased sedimentation, metal contamination, nutrient loading

2.5.2.1. Sedimentation

Sedimentation in New River Estuary has variably increased over time, with fine-sediment accumulating in increasing intensity, particularly within the last two decades. By 1981 it was evident that the surface sediment in the Waihopai Arm underwent a textural change from sand in the lower reaches to a dominance of mud in the upper section (Thoms, 1981). Between 2001 and 2016, the surface substrate of the NRE was mapped four times to monitor the most significant progression of sedimentation in the estuary (Robertson et al., 2017, 2002; Robertson and Stevens, 2007, 2001; Stevens and Robertson, 2012). The total area in the estuary dominated by soft muds, defined as >25% mud-sized grains, increased from 548 Ha in 2001 to 569 Ha in 2007, an increase of 15% of the total area. By 2007, the accumulation of very soft mud spanned the entire western margin and the northeastern side of the channel in the Waihopai Arm, as well as on the southern flank of the Oreti confluence and in Daffodil Bay (Fig. 2-1). The soft mud coverage increased to 669 Ha in 2012, a 36% increase from 2001, with the growth of developed depositional areas and new accumulation at Bushy Point. By 2016, the soft mud area had increased to 747 Ha, a 52% increase from 2001, with expansion towards Whalers Bay. The rapid

growth of these areas can be partially attributed to the increase in opportunistic macroalgal beds (*Gracilaria* or *Ulva*), which outcompete native species in highly eutrophic environments and are effective traps for fine-sediment (Robertson et al., 2017; Robertson and Stevens, 2012). From 2001-2016 the area of the estuary that is covered in >50% macroalgae increased from 43-364 Ha, which is linked to increased nutrient-loading, high sulfide content, and declining sediment oxygenation. These factors demonstrate the eutrophic condition of the depositional areas in the NRE, to which current agricultural practices, including winter cropping and intensive dairying, contribute through their high sediment, nutrient, and contaminant loss (Houlbrooke et al., 2004; Ledgard, 2013; Robertson et al., 2017).

In a core collected in 2007 (UNA), the rate of sedimentation was calculated at 3 mm yr^{-1} from 1906-1967, 12.4 mm yr^{-1} from 1967-1982, 10.4 mm yr^{-1} from 1982-1990, 7 mm yr^{-1} 1990-2001, and 28 mm yr^{-1} from 2001-2007 (Robertson and Stevens, 2007). The general trend of increasing sedimentation rate at UNA is confirmed in the 2017 core with 13.3 mm yr^{-1} from 1915-1933, 7.3 mm yr^{-1} from 1935-2009, and 22.4 mm yr^{-1} from 2009-2017. A similar trend of increasing sedimentation rate, though lower in intensity, is apparent at the southern extent of the western Waihopai Arm (LW) and the relatively sheltered Daffodil Bay (DE) areas. The LW site increases from 5.9 mm yr^{-1} over 1956-2017 to 17.5 mm yr^{-1} from 2007-2017 and the DE site increases from 5.5-7.0 mm yr^{-1} in 1906-1965 to 10.3 mm yr^{-1} from 1997-2017. Rates of 10-20 mm yr^{-1} are considered high and >20 mm yr^{-1} signifies a very high sedimentation rate that is likely to lead to major changes in the estuary that are detrimental to the ecology and difficult to reverse (Robertson and Stevens, 2007). The calculated rates suggest that sedimentation is not uniform in the depositional areas of New River Estuary; the upper Waihopai Arm (UNA), being the most developed with fine-sediment accumulating prior to 1981 (Thoms, 1981), has reached

the highest rate of sedimentation followed by the lower Waihopai Arm (LW) and Daffodil Bay (DE), which began to significantly accumulate very-fine sediment by 2001 and 2007, respectively (Ledgard, 2013; Robertson and Stevens, 2007, 2001). Although sediment was already accumulating in the estuary due to agricultural expansion, river channelization, urbanization, and estuary reclamation throughout the 20th century, it is evident from this study that the rate of fine-sedimentation increased most significantly from the 1990's to present day, as also suggested elsewhere (Pearson and Couldrey, 2016; Robertson et al., 2017). Agricultural development, especially on sloped landscapes, as well as the shift to dairying contribute to this increase as farming expansion onto unsuitable land, irrigation, tile drains, and wintering practices enhance the sediment loss to the catchment (Ledgard, 2013; Monaghan et al., 2010). Additionally, macroalgal growth in the estuary allows for greater quantities of fine-sediment to be retained in the depositional areas (Robertson et al., 2017). This manifests as up-core fining with increasing concentrations of pollutants, where the dominant grain size transitions from (silty) sand in the lower cores to soft silty mud (>50% mud) in the upper 60 cm (esp. top 48 cm) of the UNA core, 18 cm of the LW core, and 44 cm of the DE core.

2.5.2.2. Contamination and eutrophication

The agriculturally-sourced fine-sediment can be enriched in nutrients and certain heavy metals, which contributes to eutrophication and sedimentation when these loads are transported to and deposited in a receiving environment (Ledgard, 2013; Monaghan et al., 2010, 2007, 2005). Fine-, nutrient-rich sediment accumulation can cause ecological degradation by smothering habitats, reducing water clarity, decreasing pore water exchange, consumption of

dissolved oxygen through microbial decomposition, increasing organic matter, and elevating sulfide concentrations. Broad- and fine-scale mapping of the physical and chemical health of the NRE shows evidence of eutrophication in the estuary (Robertson et al., 2017, 2002; Robertson and Stevens, 2012, 2007, 2001; Stevens and Robertson, 2012). Indicators of eutrophication include an approximate 800% increase in high-density macroalgal cover (mainly *Gracilaria* and *Ulva*) since 2001 (about 100% increase since 2007), which currently cover about 8% of the total estuary surface area; a 60% increase in areas of soft mud, with the 17% of the estuary classified as soft mud in 2001 increasing to 27% in 2016; reduced sediment oxygenation from an estimated 1-2% of the estuary classified as a low sediment-oxygen zone in 2001-2007 to 15% in 2016; and an average of 40% loss of seagrass cover, with >80% losses in the Waihopai Arm (Robertson et al., 2017). Nuisance, opportunistic species that thrive in nutrient-rich environments are very effective at trapping fine-sediment and accelerating accumulation, which, in turn, accelerates nutrient-loading and the effects of eutrophication. Eutrophication has intensified since 2013 such that the macroalgal biomass has been significantly reduced in the Waihopai Arm with the proliferation of cyanobacteria (i.e., *Beggiatoa*), likely the result of increased anoxia and sulfide levels in the sediment (Robertson et al., 2017).

The highly eutrophic conditions in the NRE are defined by elevated concentrations of organic matter (org-C >1.2 wt.%), nutrients (TP >0.05 wt.%; TN >0.1 wt.%) and sulfides (Fig. 2-8), which results in limited to no subsurface macrofaunal communities (Robertson et al., 2017). Up-core changes in the UNA core indicate a major increase in the nutrient and organic-C load received at the upper Waihopai Arm between 1975-1986 (38 cm), when agricultural expansion was reaching its peak and the industry shifted to dairying (Ledgard, 2013). Further increases in the TP load around 2008 (18 cm) in the UNA core can be linked to the intensified accumulation

of fine-sediment, which transports P from fertilizers and animal excreta, in the upper Waihopai Arm due to the spread of macroalgal communities. The UNA core has moderate to severe enrichment of TN and organic-C, with moderate enrichment of TP (see Section 2.4.3.4), that induced a high degree of contamination in the upper Waihopai Arm (Table 2-2). Changes in the LW core at 22-24 cm record an increase in the nutrient and organic matter loads received at the lower Waihopai Arm depositional site from 1956 to present day, which is linked to agricultural intensification. The LW core is also moderately to severely enriched in TN and organic-C, with moderate enrichment in TP, giving the lower Waihopai Arm a slightly lower degree of contamination (moderate to high) than in the upper section. The increase in organic matter and nitrogen at 50 cm in the DE core shows that nutrients and organic-C loads received at the Daffodil Bay depositional site have been increasing marginally since 1906 due to the growth of agriculture and land development that enhanced nutrient-rich sediment loss. The most significant increase at Daffodil Bay, however, occurred between 1997 and 2017 (0-6 cm), when the effects of contaminated fine-sediment loss from agricultural intensification and the shift to dairy farming became apparent (Hamill and McBride, 2003; Ledgard, 2013; Pearson and Couldrey, 2016). Moderate to severe enrichment of TN and organic-C in the DE core emphasizes the moderate degree of contamination in Daffodil Bay, lowest of the three depositional sites.

Current non-point source discharges (fluvial) to New River Estuary are estimated to contribute 80% of the total nitrogen load and 68% of the total phosphorus load, with 41% (N) and 38% (P) from the Oreti River, 22% (N) and 19% (P) from the Makarewa River, 8% (N) and 5% (P) from the Waihopai River, and 6% (N) and 4% (P) from Mokotua Stream (Robertson et al., 2017). By contrast, point source discharges are estimated to contribute only 20% of the total nitrogen load and 32% of the total phosphorus load, with 8% (N) and 11% (P) from Blue Sky

Meats (distributor), 6% (N) and 8% (P) from Alliance Lorneville (meat processor), and 4% (N) and 11% (P) from ICC Clifton (wastewater plant) (Robertson et al., 2017). These estimates demonstrate that the majority of the nutrient and organic matter loads that are deposited with the fine-sediment in the estuary are fluvial in origin and sourced from agricultural inputs. Winter foraging, which primarily supports dairying in the region, is considered a key source of N and P to the river network, especially in hill country landscapes (Monaghan et al., 2010). Furthermore, in terms of pastoral land use, dairy farming is considered to have the highest loss of N, P and sediment, comparable only, in P and sediment, to deer farming, which is significantly less prominent in the catchment (Ledgard, 2013; Monaghan et al., 2010). Over 60% of dairy farms in Southland are on land with high leaching vulnerability, which increases the risk for N loss (Ledgard, 2013).

Contamination in the NRE is shown by up-core increases in heavy metal concentrations (Figs. 2-3 to 2-5) in the bioavailable (i.e., oxides, sulfides, organic compounds, and adsorbed phases; after a modified aqua regia digestion) and/or non-available (silicates; after total, multi-acid digestion) fractions. Down-core profiles of these contaminants normalized to Al indicates that the increase in contaminants is independent of grain size variability, and thus, is associated with the rise in fine-sediment accumulation. Sediment can act as a source or sink for heavy metals and as a result, can negatively influence water quality and ecological health when predetermined, non-toxic levels of these contaminants ("trigger values") are exceeded (ANZECC and ARMCANZ, 2000). Although heavy metal concentrations increase up-core above background values in all three cores, only Ni exceeds the trigger value (Figs. 2-3 to 2-5). Background concentrations are defined by the lower core values of each heavy metal when there is a constant concentration that can be considered pre-agricultural expansion (i.e., when marine

sources of sediment were greater than terrestrial/anthropogenic). The input of Ni in non-available forms remains constant up-core (total fraction), which shows that Ni concentrations are increasing in the bioavailable sediment fractions. This increase in bioavailable Ni is a risk to water quality and ecological health as Ni in these phases are most readily exchangeable within the water column and ecosystem, especially with changes in redox potential and pH as sediment in the NRE becomes anoxic when buried. Organic matter can transport Ni in its bioavailable phase and the increase in organic carbon losses to the catchment from increased dairying and winter grazing likely contributes, along with urban sources, to the up-core increase in total nickel concentration (Cavanagh and Ward, 2014). In high concentrations, Ni can have adverse effects on the ecology and human health, especially as toxins become biomagnified up the food chain (Das et al., 2008; Freedman, 1995; Svobodova et al., 1993).

Down-core concentration profiles of Cu, Ni, and Zn accentuate a period of contaminant increase above background values in the UNA core at 62-64 cm to 38 cm, which is dated to <1933-1975 (Fig. 2-3). These increases can be partially attributed to the increase in fine-sediment losses from land use changes, catchment modifications, and estuary reclamation, though urban sources (i.e., stormwater runoff, wastewater treatment plant discharge, historic landfill leachate) are potentially more significant heavy metal contributors (Cavanagh and Ward, 2014). The metal concentration in the UNA core remains unchanged from 38 cm to the top of the core, which suggests that from between 1975-1986 to present day the sources of bioavailable heavy metals have provided a constant supply. The LW core shows a similar relationship, with an increase from <1956 to 1975 (18-30 cm), and a near-constant concentration reached between 1975-1986 (18 cm) to present day (Fig. 2-4). The DE core also has a transitional period of increasing heavy metal concentrations, however, it spans from 60-62 cm depth up to the top of

the core, which suggests that equilibrium of fine-sediment and transported heavy metals has not yet been attained in this part of the estuary (Fig. 2-5). This variability between the depositional sites is accentuated in the Zn and TP profiles, which show that UNA, with the longest period of sediment and pollutant accumulation, is 1.3 and 1.9 times more concentrated in Zn and 1.4 and 2.0 times more concentrated in TP than the upper LW and DE cores, respectively. The inverse relationship is present in the TN concentrations (Fig. 2-8), likely because more N is used where there is greater (or different types of) macroalgal growth as N may be the rate-limiting nutrient. The increases in these pollutants is partially attributed to enhanced sediment loss from more intensive agricultural practices (i.e., dairying on vulnerable land, winter foraging, tile drainage), which provide heavy metals and nutrients. Phosphorus in its bioavailable fraction is primarily sourced from phosphatic fertilizers, which are used to improve pasture productivity (Longhurst et al., 2004). Heavy metals are present, to some degree, in these fertilizers depending on the source of rock used in their manufacturing, however, elements such as Cu, Ni, Pb, Zn, and As are considered to be mainly pedogenic in origin (Martin et al., 2017). Alternative sources of these metals include the application of copper-sulfate fertilizers or pesticides (Cu) (Longhurst et al., 2004), the historic usage of leaded gasoline (Pb), especially between 1975-1986 (Pearson et al., 2010), and municipal, industrial, and agricultural wastes (Cd, Co, Cr, Cu, Hg, Ni, Pb, Zn) (Huisingh, 1974). Unlike other heavy metals that may accumulate in the sediment (i.e., Cd in correlation to phosphate fertilizers), Cu and Zn can be taken up by plants and animals as essential nutrients and excess will then be contained in their waste and can accumulate in the environment. Urbanization also contributes to catchment contamination with heavy metals derived from stormwater runoff, wastewater discharge, and landfill leachate (Cavanagh and Ward, 2014; Williamson and Morrisey, 2000).

2.5.3. Global perspective

Estuarine eutrophication and heavy metal contamination due to anthropogenic influence and increased sediment loss is a world-wide issue (Chapman and Wang, 2001; Foster et al., 2007; Jin et al., 2010; Kendall et al., 2001; Owens et al., 1999; Peters et al., 1978; Reimann et al., 2009; Walling et al., 1999; Walling and Woodward, 1995). Heavy metals are sequestered in the Great Lakes of Canada and the United States (i.e., Lake Michigan and Lake Erie) as the proportion of anthropogenic components surpass natural background levels (Robbins and Edgington, 1975; Schelske and Hodell, 1995). The St. Lawrence Estuary is a sink for terrestrially-derived material, which comprises almost the entire organic load (Tan and Strain, 1979). Metal contamination in Florida's estuaries is shown to be the result of anthropogenic activity (Schropp et al., 1990; Windom et al., 1989). Apportioning sources of fine-sediment in United Kingdom river basins helps to focus remediation against correlated ecological impacts (Collins et al., 2012, 1997). Urban industrial regions, fishing, and nutrient input from fluvial systems add significant pressure to the northwest European continental shelf and can be detrimental to the marine ecosystem (Wakelin et al., 2015). Deposited sediment in the Schelde Estuary is primarily sourced from the polluted river catchment of a dense urban and industrial zone in western Europe (Middelburg and Nieuwenhuize, 1998). Increased nutrient loading in the Oder River, the largest freshwater source to the western Baltic Sea, is the result of catchment urbanization, industrialization, and agricultural development (Voss and Struck, 1997). Increased sedimentation in the Lower Jordan Valley, where water is scarce, has a negative impact on water quality and reservoir capacity (Kraushaar et al., 2015). Almost half the suspended matter delivered to the Godavari estuary in India is terrestrial in origin (Sarma et al., 2012). The terrestrially-derived suspended sediment

load delivered to the Great Barrier Reef is estimated to have increased five-fold over pre-European levels and is detrimental to the ecology, especially coral reef communities (Wilkinson et al., 2013). The commonality is that human influence exacerbates low-quality (pollutant-enriched) sediment loss, which has detrimental impacts to water quality and aquatic ecology that require targeted remedial action. Reliable and practical assessment tools are necessary to identify significant pressures and minimize sediment and pollutant loss to riverways (Schropp et al., 1990). This study provided geochemical and isotopic evidence of physical and chemical changes to the deposited sediment load in the New River Estuary that correlate in time to major modifications in land use (i.e., estuary reclamation, urbanization, agricultural development, and the switch to dairying). This geochemical database can be used in sediment source fingerprinting analyses using multivariate mixing models to qualitatively determine sediment origin based on a catalogue of distinct source signatures (Collins et al., 2017; Haddadchi et al., 2014; Kraushaar et al., 2015; Martinez-Carreras et al., 2008; Walling et al., 1993; Walling and Woodward, 1992). As well, the database can be linked to other catchments in the region of Southland, and the rest of New Zealand, using the same methodology to assess the level of eutrophication and contamination in each receiving environment regarding the aforementioned changes in land use. The methodology, using dated sediment cores to assess the change in human activity that result in the increased rate of organic matter supply (Bottcher et al., 2010; King et al., 2008; Owens et al., 1999) can also be used as a comparative assessment tool in international settings.

2.6. Conclusions

The current rates of sedimentation in New River Estuary vary in classification from 'high' (10-20 mm yr^{-1}) in the lower Waihopai Arm and Daffodil Bay to 'very high' (>20 mm yr^{-1}) in the upper Waihopai Arm (Robertson and Stevens, 2007). The rate of fine-sediment accumulation, along with concentrations of heavy metals, nutrients, and organic carbon, has increased most significantly between 1975 and 1986 in the Waihopai Arm and between 1965 and 1997 in Daffodil Bay. The timing of this transition in the three depositional areas correlates to the peak of agricultural expansion onto undeveloped land (1984) and the onset of the switch from sheep farming to dairying (1985) with the application of irrigation, tile drainage, and wintering practices. These agricultural practices increase the sediment, nutrient, and contaminant losses to the riverways, which has contributed to estuarine eutrophication. Opportunistic species that thrive in eutrophic conditions (i.e., *Gracilaria*) have outcompeted native plants, changing the ecological landscape and exacerbating sedimentation by effectively trapping sediment. The sources of sediment have changed over time. In the early 20th century (i.e., before 1935), 75-80% of sediment was marine in origin, deposited in response to estuary reclamation, with the 20-25% of terrestrial sediment sourced primarily from channel bank collapse and gully erosion of subsoil. Through the mid-20th century, especially after 1975-1986, the sediment contribution increased to 75-84% (Waihopai Arm) and 55-65% (Daffodil Bay) from terrestrial sources by the erosion of surface soil (likely pasture soil).

Sedimentation and eutrophication, critical issues world-wide, have a negative impact on water quality and degrade ecological wellbeing. Understanding the sources of pollutants and sediment, as well as how these factors vary with respect to seasonal, climatic, and land-use changes, helps to identify high risk areas where a targeted mitigation approach should be applied.

References

Abrahim, G.M.S., 2005. Holocene sediments of Tamaki Estuary: Characterisation and impact of recent human activity on an urban estuary in Auckland, New Zealand (PhD Thesis). University of Auckland, Auckland, New Zealand.

Abrahim, G.M.S., Parker, R.J., 2008. Assessment of heavy metal enrichment factors and the degree of contamination in marine sediments from Tamaki Estuary, Auckland, New Zealand. Environ. Monit. Assess. 136, 227–238.

Alling, V., Humborg, C., Morth, C., Rahm, L., Pollehne, F., 2008. Tracing terrestrial organic matter by delta-S-34 and delta-C-13 signatures in a subarctic estuary. Am. Soc. Limnol. Oceanogr. Inc 53, 2594–2602.

ANZECC, ARMCANZ, 2000. Australian and New Zealand Guidelines for Fresh and Marine Water Quality (No. 4), National Water Quality Management Strategy.

Appleby, P.G., Oldfield, F., 1978. The calculation of Pb-210 dates assuming a constant rate of supply of unsupported Pb-210 to the sediment. Catena 5, 1–8.

Appleby, P.G., Oldfield, F., Ivanovich, M. (Ed)., Harmon, R.S. (Ed)., 1992. Applications of 210Pb to sedimentation studies, in: Uranium-Series Disequilibrium: Applications to Earth, Marine, and Environmental Sciences. Oxford University Press, Oxford, pp. 731–778.

Appleby, P.G., Oldfield, F., Thompson, R., Huttunen, P., Tolonen, K., 1979. Pb-210 dating of annually laminated lake sediments from Finland. Nature 280, 53–55.

Bau, M., Koschinsky, A., Dulski, P., Hein, J.R., 1996. Comparison of the partitioning behaviours of yttrium, rare earth elements, and titanium between hydrogenetic marine

ferromanganese crusts and seawater. Geochim. Cosmochim. Acta 60, 1709–1725. https://doi.org/10.1016/0016-7037(96)00063-4

Birch, G.F., 2017. Determination of sediment metal background concentrations and enrichment in marine environments - A critical review. Sci. Total Environ. 580, 813–831.

Birch, G.F., Olmos, M.A., 2008. Sediment-bound heavy metals as indicators of human influence and biological risk in coastal water bodies. ICES J. Mar. Sci. 65, 1407–1413.

Bottcher, M.E., Voss, M., Schulz-Bull, D., Schneider, R., Leipe, T., Knoller, K., 2010. Environmental changes in the Pearl River Estuary (China) as reflected by light stable isotopes and organic contaminants. J. Mar. Syst. 82, 543–553.

Carmichael, R.H., Hattenrath, T., Valiela, I., Michener, R.H., 2008. Nitrogen stable isotopes in the shell of Mercenaria mercenaria trace wastewater inputs from watersheds to estuarine ecosystems. Aquat. Biol. 4, 99–111.

Chapman, P.M., Wang, F., 2001. Assessing sediment contamination in estuaries. Environ. Toxicol. Chem. 20, 3–22.

Collins, A.L., Pulley, S., Gellis, A., Porto, P., Horowitz, A.J., 2017. Sediment source fingerprinting as an aid to catchment management: A review of the current state of knowledge and a methodological decision-tree for end-users. J. Environ. Manag. 86–108. https://doi.org/http://dx.doi.org/10.1016/j.jenvman.2016.09.075

Collins, A.L., Walling, D.E., Leeks, G.J.L., 1997. Fingerprinting the origin of fluvial suspended sediment in larger river basins: Combining assessment of spatial provenance and source type. Geogr. Ann. 79 A, 239–254.

Collins, A.L., Zhang, Y., Walling, D.E., Grenfell, S.E., Smith, P., Grischeff, J., Locke, A., Sweetapple, A., Brogden, D., 2012. Quantifying fine-grained sediment sources in the

River Axe catchment, southwest England: application of a Monte Carlo numerical modelling framework incorporating local and genetic algorithm optimisation. Hydrol. Process. 26, 1962–1983. https://doi.org/10.1002/hyp.8283

Corbett, C.A., Doering, P.H., Madley, K.A., Ott, J.A., Tomasko, D.A., 2005. Chapter 15. Using Seagrass Coverage as an Indicator of Ecosystem Condition, in: Environment Indicators. CRC Press.

Craine, J.M., Brookshire, E.N.J., Cramer, M.D., Hasselquist, N.J., Koba, K., Marin-Spiotta, E., Wang, L., 2015. Ecological interpretations of nitrogen isotope ratios of terrestrial plants and soils. Plant Soil 396, 1–26.

Das, K.K., Das, S.N., Dhundasi, S.A., 2008. Nickel, its adverse health effects and oxidative stress. Indian J. Med. Res. 128, 412–425.

Foster, I.D.L., Boardman, J., Keay-Bright, J., 2007. Sediment tracing and environmental history for two small catchments, Karoo Uplands, South Africa. Geomorphology 90, 126–143. https://doi.org/10.1016/j.geomorph.2007.01.011

Freedman, B., 1995. Toxic Elements, in: Environmental Ecology: The Ecological Effects of Pollution, Disturbance, and Other Stresses. Academic Press, Inc., pp. 62–93.

Fry, B., 2002. Conservative mixing of stable isotopes across estuarine salinity gradients: A conceptual framework for monitoring watershed influences on downstream fisheries production. Estuaries 25, 264–271.

Haddadchi, A., Olley, J., Laceby, P., 2014. Accuracy of mixing models in predicting sediment source contributions. Sci. Total Environ. 497-498, 139–152.

Hamill, K.D., McBride, G.B., 2003. River water quality trends and increased dairying in Southland, New Zealand. N. Z. J. Mar. Freshw. Res. 37, 323–332.

Hancock, G., Caitcheon, G., 2010. Sediment sources and transport to the Logan-Albert River estuary during the January 2008 flood event (No. 1835-095X), CSIRO: Water for a Healthy Country National Research Flagship.

Hewitt, A.E., 2010. New Zealand Soil Classification, 3rd ed, Landcare Research Science Series. Manaaki Whenua Press.

Horowitz, A.J., 1991. A Primer on Sediment-Trace Element Chemistry, Second Edition (Open-File No. 91-76). United States Geological Survey.

Houlbrooke, D.J., Horne, D.J., Hedley, M.J., Hanly, J.A., Snow, V.O., 2004. A review of literature on the land treatment of farm-dairy effluent in New Zealand and its impact on water quality. N. Z. J. Agric. Res. 47, 499–511.

Huisingh, D., 1974. Heavy metals: Implications for agriculture. Annu. Rev. Phytopathol. 12, 375–388.

Jin, Z., You, C.-F., Yu, T.-L., Wang, B.-S., 2010. Sources and flux of trace elements in river water collected from the Lake Qinghai catchment, NE Tibetan Plateau. Appl. Geochem. 25, 1536–1546. https://doi.org/10.1016/j.apgeochem.2010.08.004

Kendall, C., Silva, S.R., Kelly, V.J., 2001. Carbon and nitrogen isotopic compositions of particulate organic matter in four large river systems across the United States. Hydrol. Process. 15, 1301–1346.

King, J.W., Hubeny, J.B., Gibson, C.L., Laliberte, E., Ford, K.H., Cantwell, M., McKinney, R., Appleby, P.G., Desbonnet, A. (Ed. ., Costa-Pierce, A. (Ed. ., 2008. Chapter 7. Anthropogenic Eutrophication of Narragansett Bay: Evidence from Dated Sediment Cores, in: Science for Ecosystem-Based Management. Springer, pp. 211–232.

Kraushaar, S., Schumann, T., Ollesch, G., Schubert, M., Vogel, H.-J., Siebert, C., 2015.

Sediment fingerprinting in northern Jordan: element-specific correction factors in a carbonatic setting. J. Soils Sediments 15, 2155–2173. https://doi.org/10.1007/s11368-015-1179-2

Ledgard, G., 2013. Land use change in the Southland region (Technical Report No. 2013-13). Environment Southland, Invercargill, NZ.

Lehmann, M.F., Bernasconi, S.M., Barbieri, A., McKenzie, J.A., 2002. Preservation of organic matter and alteration of its carbon and nitrogen isotope composition during simulated and in situ early sedimentary diagenesis. Geochim. Cosmochim. Acta 66, 3573–3584.

Li, Y.H., Burkhardt, L., Teraoka, H., 1984. Desorption and coagulation of trace elements during estuarine mixing. Geochim. Cosmochim. Acta 48, 1659–1664.

Longhurst, R.D., Roberts, A.H.C., Waller, J.E., 2004. Concentrations of arsenic, cadmium, copper, lead, and zinc in New Zealand pastoral topsoils and herbage. N. Z. J. Agric. Res. 47, 23–32. https://doi.org/10.1080/00288233.2004.9513567

Martin, A.P., Turnbull, R.E., Rattenbury, M.S., Baisden, W.T., Christie, A.B., Cohen, D.., Hoogewerff, J., Rogers, K.M., 2015. Geochemical Atlas of Southern New Zealand (GNS Science Report No. 2015/26).

Martinez-Carreras, N., Gallart, F., Iffly, J.F., Pfister, L., Walling, D.E., Krein, A., 2008. Uncertainty assessment in suspended sediment fingerprinting based on tracer mixing models: A case study from Luxembourg. Sediment Dyn. Chang. Environ. IAHS Publ. no. 325, 94–105.

McLennan, S.M., 1989. Rare earth elements in sedimentary rocks: Influence of provenance and sedimentary processes. Rev. Mineral. Geochem. 21, 169–200.

Middelburg, J.J., Nieuwenhuize, J., 1998. Carbon and nitrogen stable isotopes in suspended

matter and sediments from the Schelde Estuary. Mar. Chem. 60, 217–225.

Ministry of Commerce, 1996. Premium unleaded petrol: detailed report on investigations into reported fuel system failures following the introduction of premium unleaded petrol. Ministry of Commerce, Wellington, New Zealand.

Monaghan, R.M., Paton, R.J., Drewry, J.J., 2002. Nitrogen and phosphorus losses in mole and tile drainage from a cattle-grazed pasture in eastern Southland. N. Z. J. Agric. Res. 45, 197–205.

Monaghan, R.M., Paton, R.J., Smith, L.C., Drewry, J.J., Littlejohn, R.P., 2005. The impacts of nitrogen fertilisation and increased stocking rate on pasture yield, soil physical condition and nutrient losses in drainage from a cattle-grazed pasture. N. Z. J. Agric. Res. 48, 227–240.

Monaghan, R.M., Semadeni-Davies, A., Muirhead, R., Elliott, S., Shankar, U., 2010. Land use and land management risks to water quality in Southland. Report prepared for Environment Southland. AgResearch.

Monaghan, R.M., Wilcock, R.J., Smith, L.C., Tikkisetty, B., Thorrold, B.S., Costall, D., 2007. Linkages between land management activities and water quality in an intensively farmed catchment in southern New Zealand. Agric. Ecosyst. Environ. 118, 211–222. https://doi.org/10.1016/j.agee.2006.05.016

Owens, P.N., Walling, D.E., Leeks, G.J.L., 1999. Use of floodplain sediment cores to investigate recent historical changes in overbank sedimentation rates and sediment sources in the catchment of the River Ouse, Yorkshire, UK. Catena 36, 21–47.

Pearson, L.K., Couldrey, M., 2016. Methodology for GIS-based land use maps for Southland (Technical Report No. 2016-10). Environment Southland, Invercargill, NZ.

Pearson, L.K., Hendy, C.H., Hamilton, D.P., Pickett, R.C., 2010. Natural and anthropogenic lead in sediments of the Rotorua lakes, New Zealand. Earth Planet. Sci. Lett. 297, 536–544.

Peters, K.E., Sweeney, R.E., Kaplan, I.R., 1978. Correlation of carbon and nitrogen stable isotope ratios in sedimentary organic matter. Limnol. Oceanogr. 23, 598–604.

Peterson, B.J., Fry, B., 1987. Stable Isotopes in Ecosystem Studies. Annu. Rev. Ecol. Syst. 18, 293–320. https://doi.org/10.1146/annurev.ecolsys.18.1.293

Reimann, C., Finne, T.E., Nordgulen, O., Saether, O.M., Arnoldussen, A., Banks, D., 2009. The influence of geology and land-use on inorganic stream water quality in the Oslo region, Norway. Appl. Geochem. 24, 1862–1874. https://doi.org/10.1016/j.apgeochem.2009.06.007

Robbins, J.A., Edgington, D.N., 1975. Determination of recent sedimentation rates in Lake Michigan using Pb-210 and Cs-137. Geochim. Cosmochim. Acta 39, 285–304.

Robertson, B.M., Gillespie, P.A., Asher, R.A., Frisk, S., Keeley, N.B., Hopkins, G.A., Thompson, S.J., Tuckey, B.J., 2002. Estuarine Environmental Assessment and Monitoring: A National Protocol (Prepared for supporting Councils and the Ministry for the Environment No. Sustainable Management Fund Contract No. 5096).

Robertson, B.M., Stevens, L.M., 2001. Southland Estuaries State of Environment Report 2001 (Report prepared by Wriggle Coastal Management for Environment Southland).

Robertson, B.M., Stevens, L.M., 2007. New River Estuary 2007: Broad Scale Habitat Mapping and Sedimentation Rate (Report prepared by Wriggle Coastal Management for Environment Southland). Nelson, NZ.

Robertson, B.M., Stevens, L.M., 2012. New River Estuary: Fine Scale Monitoring of Highly Eutrophic Arms 2011/2012 (Report prepared by Wriggle Coastal Management for

Environment Southland). Nelson, NZ.

Robertson, B.M., Stevens, L.M., Robertson, B.P., 2017. Condition of Southland's shallow, intertidal dominated estuaries in relation to eutrophication and sedimentation: Output 1: Data analysis and technical assessment - Habitat mapping, vulnerability assessment and monitoring recommendations related to issues of eutrophication and sedimentation (Report prepared by Wriggle Coastal Management for Environment Southland). Nelson, NZ.

Robinson, B.H., Brooks, R.R., Kirkman, J.H., Gregg, P.E.H., Gremigni, P., 1996. Plant-available elements in soils and their influence on the vegetation over ultramafic ("serpentine") rocks in New Zealand. J. R. Soc. N. Z. 26, 457–468.

Salomons, W., Forstner, U., 1984. Metals in the hydrocycle. Springer, Berlin Heidelberg Tokyo.

Sarma, V.V.S.S., Arya, J., Subbaiah, C.V., 2012. Stable isotopes of carbon and nitrogen in suspended matter and sediments from the Godavari estuary. Oceanogr. Soc. Fo Jpn. 68, 307–319.

Schelske, C.L., Hodell, D.A., 1995. Using carbon isotopes of bulk sedimentary organic matter to reconstruct the history of nutrient loading and eutrophication of Lake Erie. Limnol. Oceanogr. 40, 918–929.

Schropp, S.J., Lewis, F.G., Windom, H.L., Ryan, J.D., Calder, F.D., Burney, L.C., 1990. Interpretation of metal concentrations in estuarine sediments of Florida using aluminum as a reference element. Estuaries 13, 227–235. https://doi.org/10.2307/1351913

Soil Classification Working Group, 1998. The Canadian System of Soil Classification. Research Branch Agriculture and Agri-Food Canada Publication No. 1646. Third Edition. NRC Canada. Ottawa, ON. 187 p.

Soil Survey Staff, 1999. Soil Taxonomy: A Basic System of Soil Classification for Making and Interpreting Soil Surveys. USDA Agriculture Handbook No. 436. Second Edition. U.S. Department of Agriculture. Washington, DC. 754 p.

Snelder, T., Fraser, C., Hodson, R., Ward, N., Rissmann, C., Hicks, A., 2014. Regional Scale Stratification of Southland's Water Quality - Guidance for Water and Land Management (No. C13055/02). Aqualinc Research Ltd.

Statistics New Zealand, 1960. New Zealand Official Yearbook, 1960. Department of Statistics, R.E. Owen, Government Printer, Wellington, New Zealand.

Stevens, L.M., Robertson, B.M., 2012. New River Estuary 2012: Broad Scale Habitat Mapping (Report prepared by Wriggle Coastal Management for Environment Southland). Nelson, NZ.

Svobodova, Z., Lloyd, R., Machova, J., Vykusova, B., 1993. Water quality and fish health (EIFAC Technical Paper No. 54). FAO, Rome.

Tan, F.C., Strain, P.M., 1979. Organic carbon isotope ratios in recent sediments in the St Lawrence Estuary and the Gulf of St Lawrence. Estuar. Coast. Mar. Sci. 8, 213–225.

Thoms, M.C., 1981. Sedimentation in the New River Estuary, Southland (Master of Science in Geography). University of Canterbury, Christchurch, New Zealand.

Turnbull, I.M., Allibone, A.H. (compilers), 2003. Geology of the Murihiku area. Institute of Geological & Nuclear Sciences Limited.

van Maren, D.S., Oost, A.P., Wang, Z.B., Vos, P.C., 2016. The effect of land reclamations and sediment extraction on the suspended sediment concentration in the Ems Estuary. Mar. Geol. 376, 147–157.

Voss, M., Struck, U., 1997. Stable nitrogen and carbon isotopes as indicators of eutrophication of

the Oder river (Baltic sea). Mar. Chem. 59, 35–49.

Wakelin, S.L., Artioli, Y., Butenschoen, M., Allen, J.I., Holt, J.T., 2015. Modelling the combined impacts of climate change and direct anthropogenic drivers on the ecosystem of the northwest European continental shelf. J. Mar. Syst. 152, 51–63. https://doi.org/10.1016/j.jmarsys.2015.07.006

Walling, D.E., Owens, P.N., Leeks, G.J.L., 1999. Fingerprinting suspended sediment sources in the catchment of the River Ouse, Yorkshire, UK. Hydrol. Process. 13, 955–975.

Walling, D.E., Woodward, J.C., 1995. Tracing sources of suspended sediment in river basins: A case study of the River Culm, Devon, UK. Mar. Freshw. Res. 327–336.

Walling, D.E., Woodward, J.C., 1992. Use of radiometric fingerprints to derive information on suspended sediment sources. Eros. Sediment Transp. Monit. Programme River Basins, Proceedings of the Oslo Symposium, August 1992.

Walling, D.E., Woodward, J.C., Nicholas, A.P., 1993. A Multi-Parameter Approach to Fingerprinting Suspended-Sediment Sources. Tracers Hydrol. IAHS Publ. no. 215.

Wilkinson, S.N., Hancock, G.J., Bartley, R., Hawdon, A.A., Keen, R.J., 2013. Using sediment tracing to assess processes and spatial patterns of erosion in grazed rangelands, Burdekin River basin, Australia. Catchments Reef Contin. Minimising Impacts Agric. Gt. Barrier Reef 180, 90–102. https://doi.org/10.1016/j.agee.2012.02.002

Williamson, R.B., Morrisey, D.J., 2000. Stormwater contamination of urban estuaries: 1. Predicting the build-up of heavy metals in sediments. Estuaries 23, 56–66.

Wilson, N., Horrocks, J., 2008. Lessons from the removal of lead from gasoline for controlling other environmental pollutants: A case study from New Zealand. Environ. Health 7, 1–10.

Windom, H.L., Schropp, S.J., Calder, F.D., Ryan, J.D., Smith, R.G., Burney, L.C., Lewis, F.G., Rawlinson, C.H., 1989. Natural trace metal concentrations in estuarine and coastal marine sediments of the southeastern United States. Environ. Sci. Technol. 23, 314–320. https://doi.org/10.1021/es00180a008

Figures

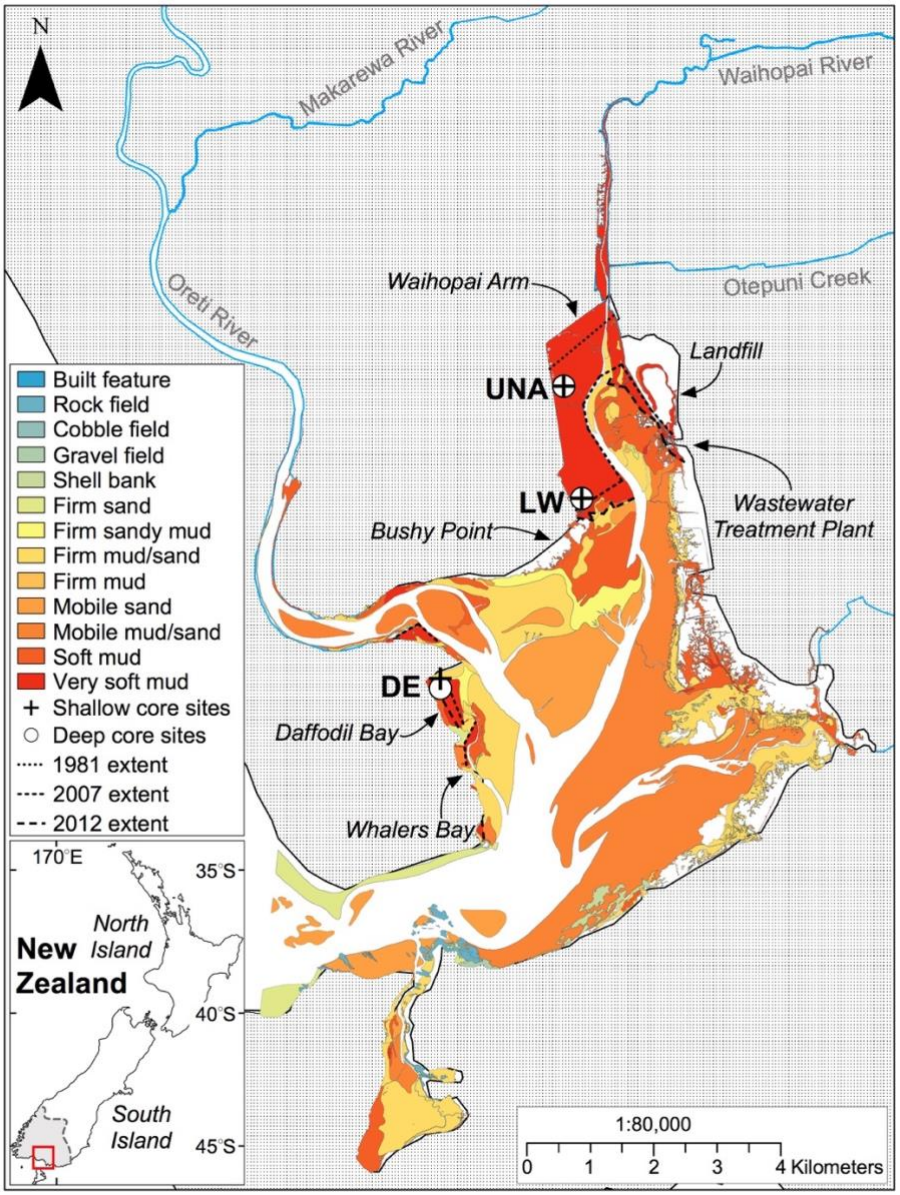

Figure 2-1. Map of New River Estuary (red box in insert) in the region of Southland, New Zealand (shaded grey in insert). Sampling locations of shallow (low tide) and deep (high tide) sediment cores are shown on a colour-coded map of the estuary, which shows the different substrate textures (Robertson et al., 2017). The extent of very soft mud in 1981, 2007 and 2012 is shown with progressive dashed lines in the Waihopai Arm, Daffodil Bay, and Whalers Bay (Robertson and Stevens, 2012b, 2007; Thoms, 1981). Sample site abbreviations from top down: UNA-Upper North Arm (from previous study (Robertson and Stevens, 2007)), LW-Lower Waihopai Arm, and DE-East Daffodil Bay.

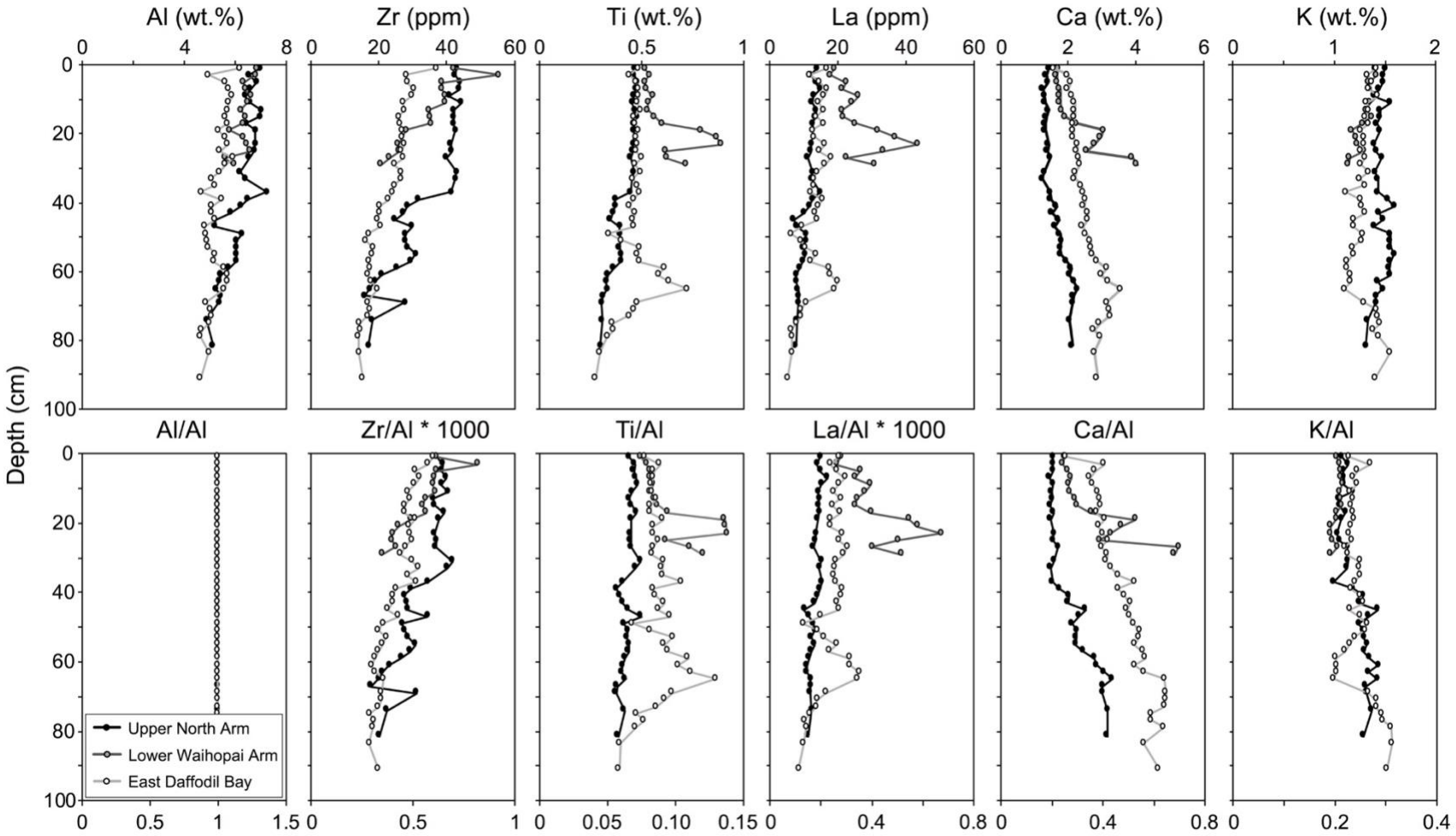

Figure 2-2. Total (after a multi-acid digestion) elemental concentrations from the Upper North Arm, Lower Waihopai Arm, and East Daffodil Bay deep cores are shown in the top row, with the concentrations normalized to the conservative element aluminum in the bottom row.

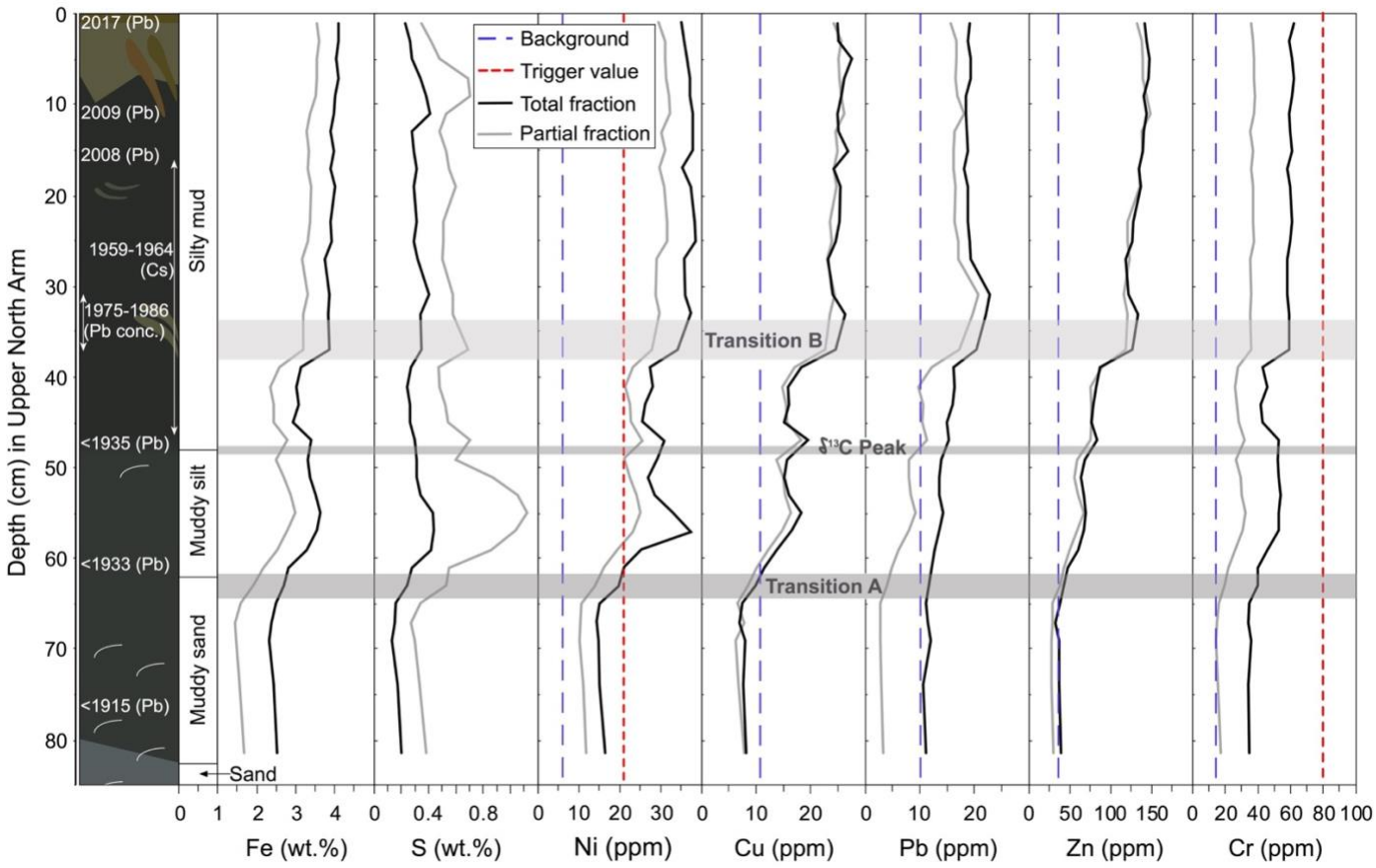

Figure 2-3. Total (after multi-acid digestion) and partial (after modified aqua regia digestion) iron, sulfur, and heavy metal concentrations from the Upper North Arm deep core with background concentrations of Ni, Cu, Pb, Zn, and Cr averaged from medians of rock units present in Southland (n>10) (Cavanagh et al., 2015). Trigger values, which signify contaminated sediment when exceeded, of Ni and Cr are determined by ANZECC and ARMCANZ (2000). Transition "A" (dark-grey shaded area) signifies the onset of terrestrial sediment accumulation (post-1920); the $\delta^{13}C$ Peak marks the plant/shell-rich layer; and transition "B" (light-grey shaded area) signifies increased terrestrial sediment (and pollutant) loads after agricultural intensification and the transition to dairying (post-1984). Plots are shown next to downcore illustrations that signify changes in colour, texture (grain size), material present (whole shells or fragments, plant matter, burrow traces), and calculated ages (based on ^{210}Pb and ^{137}Cs radioisotopes or Pb concentrations).

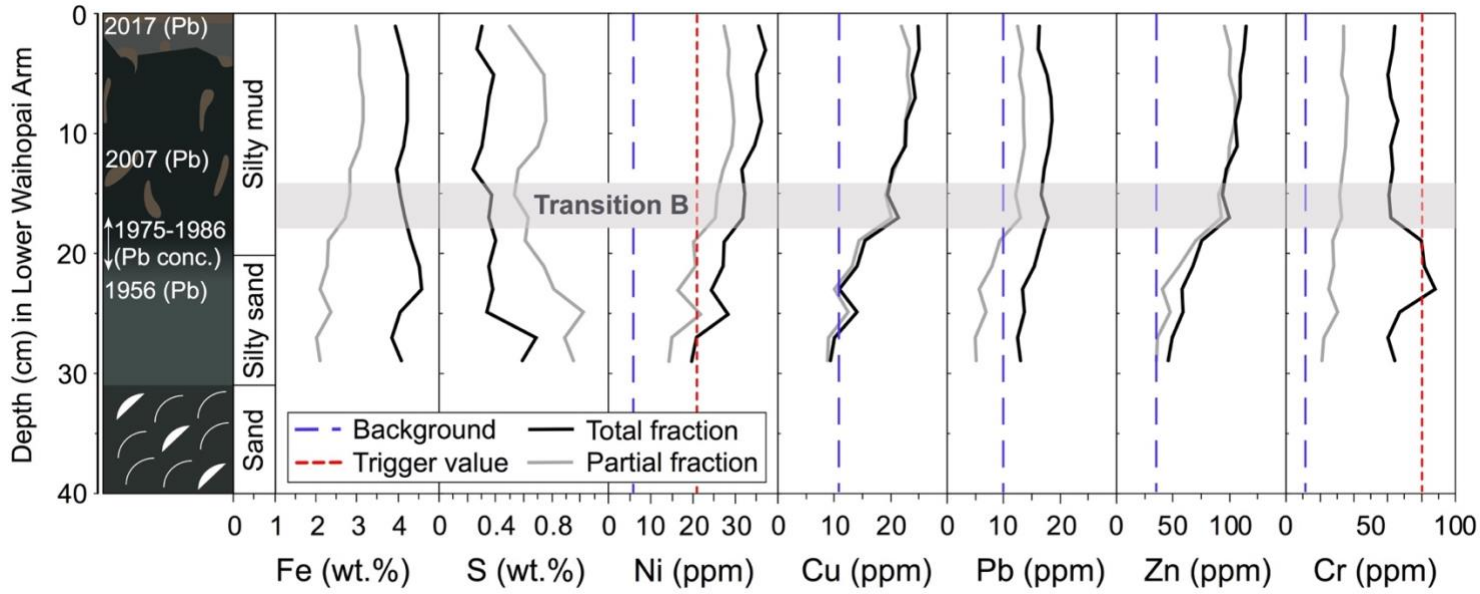

Figure 2-4. Total (after multi-acid digestion) and partial (after modified aqua regia digestion) iron, sulfur, and heavy metal concentrations from the Lower Waihopai Arm deep core with background concentrations of Ni, Cu, Pb, Zn, and Cr averaged from medians of rock units present in Southland (n>10) (Cavanagh et al., 2015). Trigger values of Ni and Cr, where exceeded denotes contamination, are determined by ANZECC and ARMCANZ (2000). The major physiochemical transition ("B") is highlighted by a shaded light-grey box and signifies the increase in the fine-sediment and pollutant loads after agricultural intensification and the switch to dairying (post-1984). The plots are shown next to downcore illustrations that signify changes in colour, texture (grain size), material present (whole shells or fragments, plant matter, burrow traces), and calculated ages (based on ^{210}Pb radioisotopes or Pb concentrations).

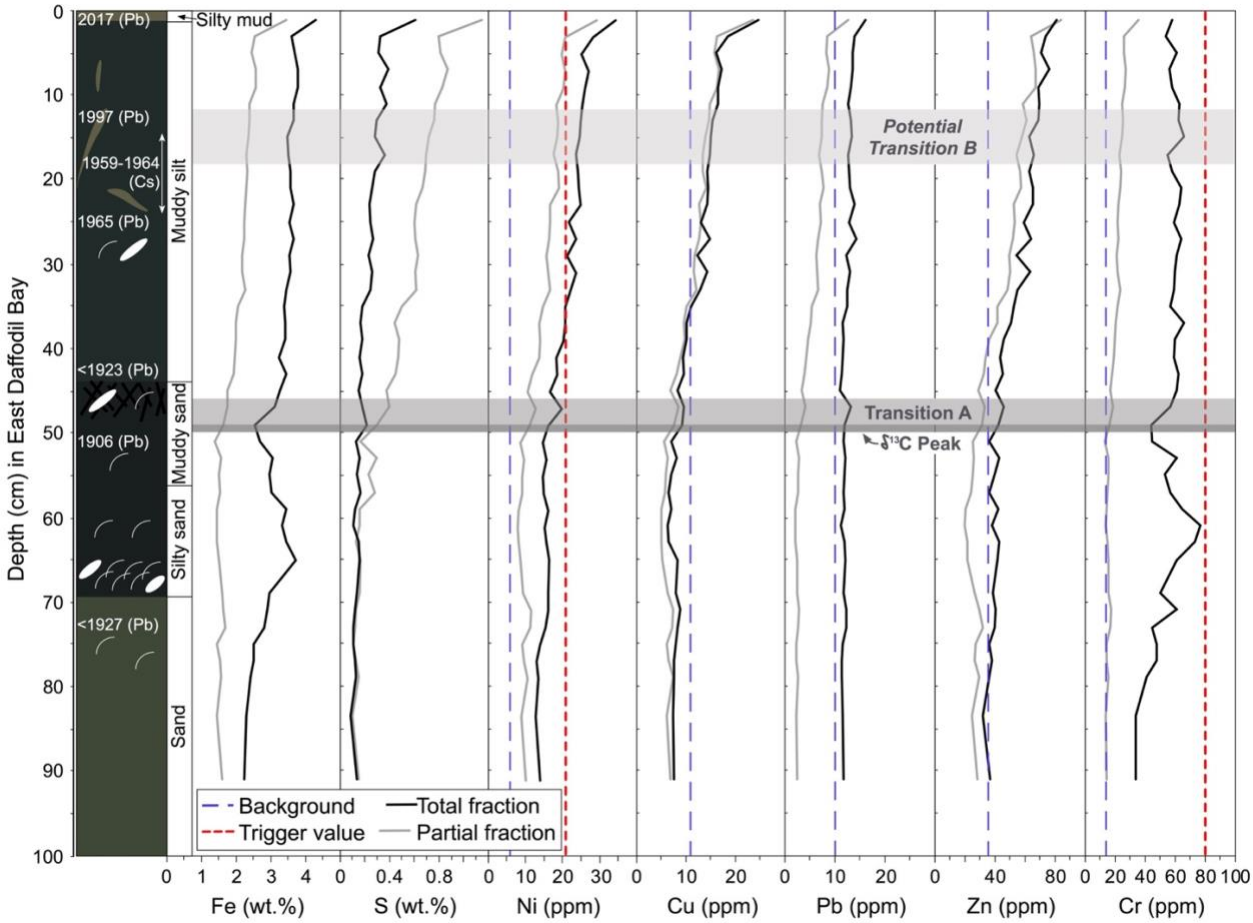

Figure 2-5. Total (after multi-acid digestion) and partial (after modified aqua regia digestion) iron, sulfur, and heavy metal concentrations from the East Daffodil Bay deep core with averaged background concentrations of Ni, Cu, Pb, Zn, and Cr (Cavanagh et al., 2015) and trigger values of Ni and Cr, which denote contamination when exceeded (ANZECC and ARMCANZ, 2000). Transition "A" (dark-grey shaded area) signifies the onset of increased sediment deposition after estuary reclamation (post-1920); the $\delta^{13}C$ Peak marks the plant/shell-rich layer; and (potential) transition "B" (light-grey shaded area) signifies increased terrestrial sediment (and pollutant) loads after agricultural intensification and the transition to dairying (post-1984). Plots are next to a downcore illustration showing changes in colour, texture (grain size), material present (whole shells or fragments, plant matter, burrow traces), and calculated ages (based on ^{210}Pb and ^{137}Cs radioisotopes or Pb concentrations).

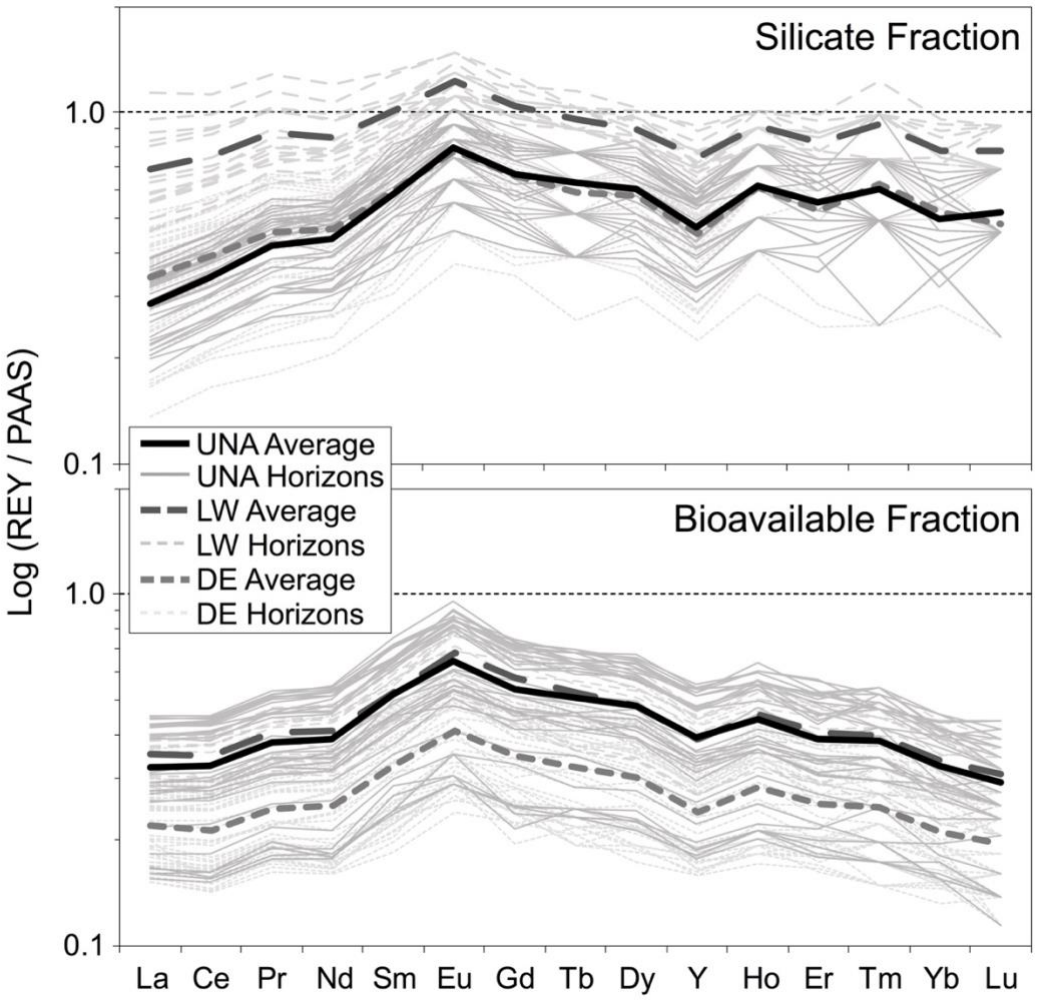

Figure 2-6. Rare earth element and yttrium (REY) concentrations of total (silicate fraction; after a multi-acid digestion) and partial (bioavailable fraction; after a modified aqua regia digestion) sediment fraction samples from the Upper North Arm (UNA), Lower Waihopai Arm (LW), and East Daffodil Bay (DE) deep core sampled horizons are plotted log-normalized to Post-Archean Australian Shale (McLennan, 1989). Average log-normalized REY traces are bolded.

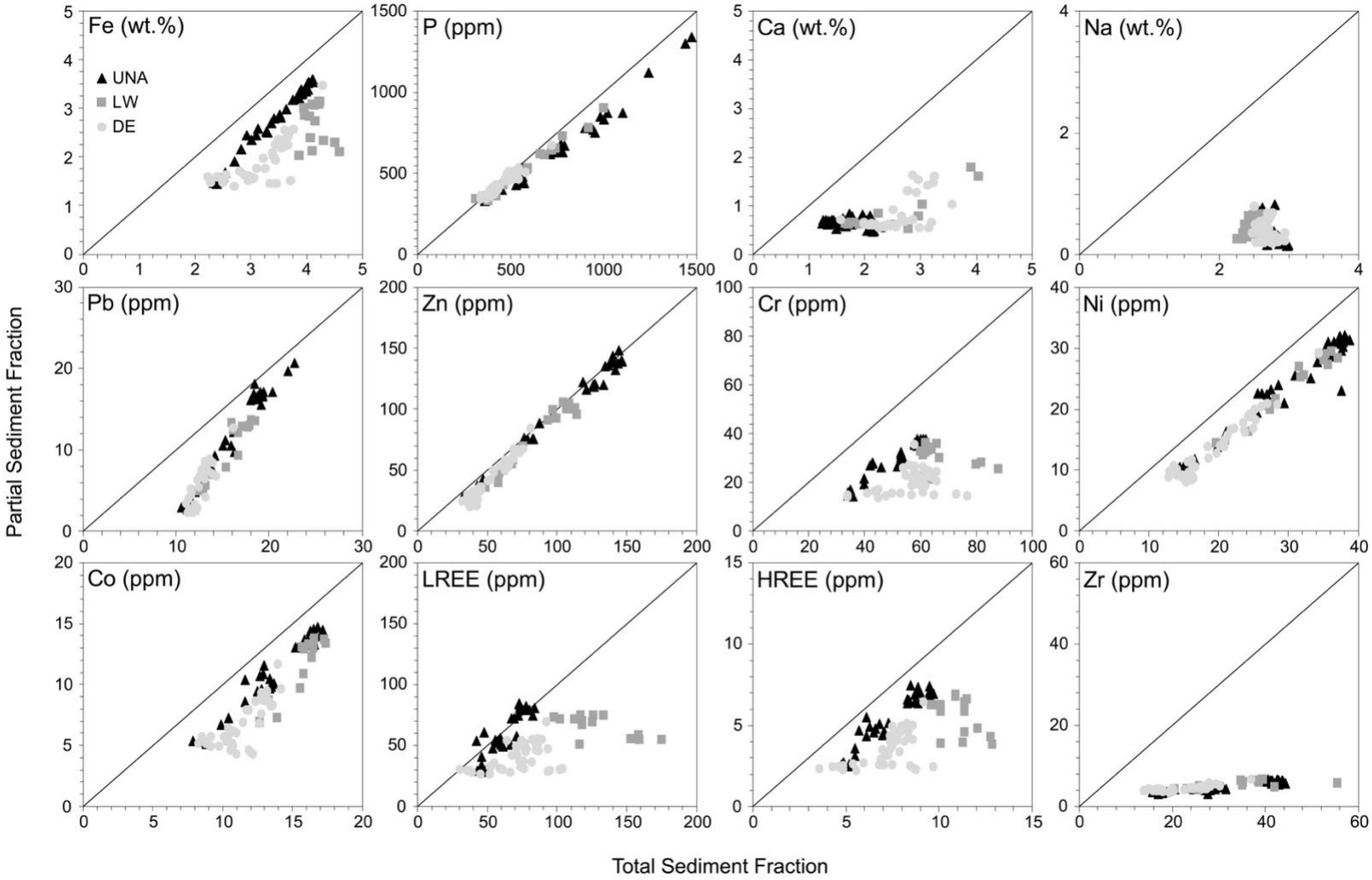

Figure 2-7. Total (silicate; after a multi-acid digestion) versus partial (bioavailable; after a modified aqua regia digestion) sediment fraction concentrations of Fe, P, Ca, Na, Pb, Zn, Cr, Ni, Co, light (LREE) and heavy (HREE) rare earth elements, and Zr.

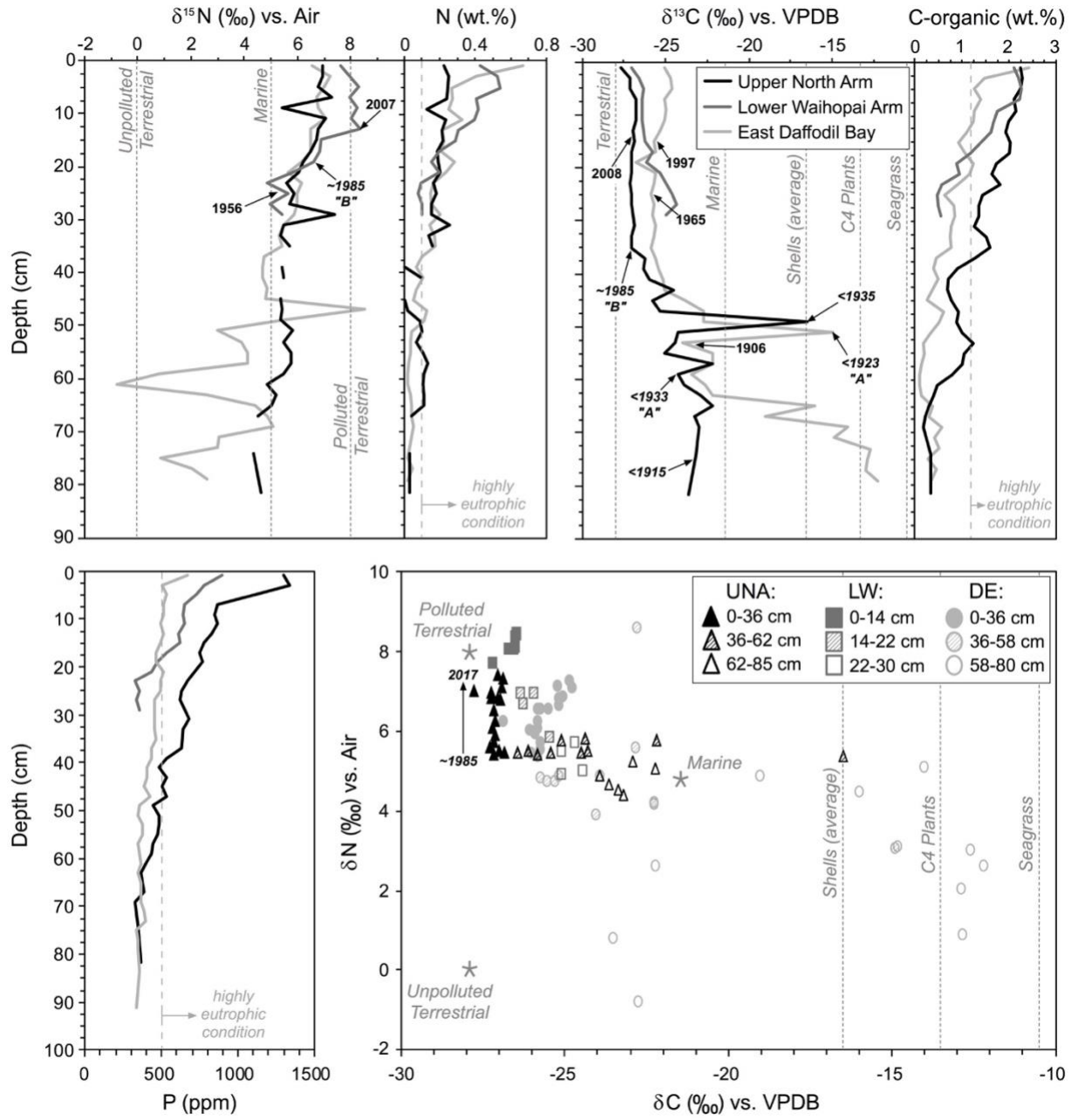

Figure 2-8. Down-core nitrogen and carbon stable isotope signatures and nitrogen, organic carbon, and phosphorus concentrations from the Upper North Arm (UNA), Lower Waihopai Arm (LW), and East Daffodil Bay (DE) deep cores, with the age (^{210}Pb) of specific sediment horizons in each core highlighted. Unpolluted terrestrial δ^{15}N (0‰), polluted terrestrial δ^{15}N (8‰), and marine δ^{15}N (av. 5‰) signatures (Fry, 2002), as well as terrestrial δ^{13}C (av. -28‰), marine δ^{13}C (av. -21.5‰), shell δ^{13}C (av. -16.5‰), C4 plant δ^{13}C (av. -13.5‰), and seagrass δ^{13}C (av. -10.5‰) signatures (Hemminga and Mateo, 1996; Kendall et al., 2001; Peterson and Fry, 1987; Sauriau and Kang, 2000) are plotted to emphasize the variability in sediment source.

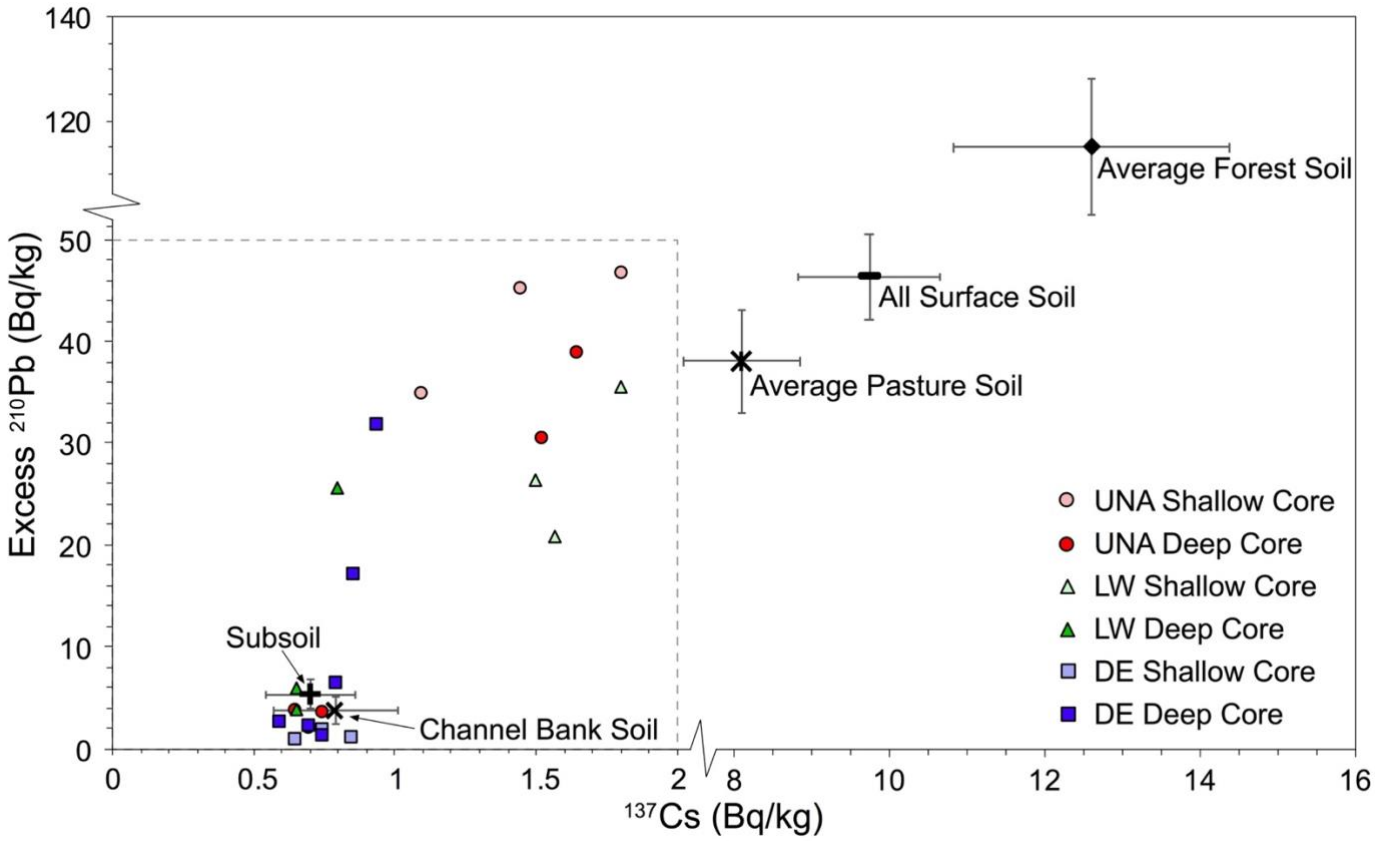

Figure 2-9. Radiogenic excess ^{210}Pb concentrations of Upper North Arm (UNA), Lower Waihopai Arm (LW), and East Daffodil Bay (DE) shallow and deep core samples plotted against radiogenic ^{137}Cs concentrations to discriminate between primary processes that initiate catchment sediment loss, including sheet erosion of surface soil, channel bank collapse, and other subsoil erosion (Hancock and Caitcheon, 2010).

Tables

Table 2-1. Radioisotope concentrations of shallow and deep cores from the Upper North Arm (UNA), Lower Waihopai Arm (LW), and East Daffodil Bay (DE) sites. Uncompacted depths were calculated following Section 2.3.4. Unsupported ^{210}Pb is the difference between the total ^{210}Pb and ^{226}Ra; when the unsupported ^{210}Pb value is negative, the maximum and minimum concentrations are calculated using total ^{210}Pb and ^{226}Ra plus or minus their standard deviation, respectively. Age is calculated using Eq. 5 in Section 2.3.5 and is reported as "<date" where the maximum unsupported ^{210}Pb was used instead of a negative value. Sedimentation rate is calculated using Eq. 6 in Section 2.3.5. *Concentrations at the lower limit of detection are reported as LLD/2 for plotting.

Site	Core	Depth (cm)	Uncompacted Depth (cm)	^{7}Be (Bq/kg)	^{137}Cs (Bq/kg)	Total ^{210}Pb (Bq/kg)	^{226}Ra (Bq/kg) (Supported ^{210}Pb)	Unsupported ^{210}Pb (Bq/kg)	Age
UNA	Shallow	0-1	1.17	12 ± 7.1	1.45*	68 ± 12	23.1 ± 2.8	44.9	
UNA	Shallow	1-2	2.33	14 ± 6.3	1.81 ± 0.91	67 ± 11	20.5 ± 2.4	46.5	2017
UNA	Shallow	14-16	18.67	6*	1.1 ± 0.69	53.9 ± 8.7	19.2 ± 2.5	34.7	2008
UNA	Deep	0-2	2.99	10.1 ± 4.7	1.65*	57 ± 8.8	18.3 ± 1.9	38.7	2017
UNA	Deep	10-12	17.92	4.9*	1.53 ± 0.6	46.6 ± 7.4	16.4 ± 1.7	30.2	2009
UNA	Deep	46-48	71.69	4.45*	0.65*	13.2 ± 5.1	13.3 ± 1.5	-3.7 to 3.5	<1935
UNA	Deep	60-62	92.60	4.7*	0.75*	16.4 ± 4.5	16.8 ± 0.8	-4.1 to 3.3	<1933
UNA	Deep	76-78	116.50	4.5*	0.7*	12.8 ± 5	14.4 ± 1.5	-5.1 to 1.9	<1915
LW	Shallow	0-1	1.25	11.4 ± 4.1	1.57 ± 0.59	40.8 ± 7.7	20 ± 1.8	20.8	
LW	Shallow	1-2	2.50	19.4 ± 5.6	1.8*	56.1 ± 9	20.7 ± 2.1	35.4	2017
LW	Shallow	10-14	17.50	10*	1.5*	46 ± 10	19.8 ± 2.6	26.2	2007
LW	Deep	0-2	2.99	4.55*	0.65*	31.1 ± 15.9	25.2 ± 2.1	5.9	
LW	Deep	6-8	11.95	5*	0.8*	46.1 ± 7.2	20.6 ± 2	25.5	2017
LW	Deep	22-24	35.84	4.75*	0.65*	30 ± 17	26.2 ± 2.2	3.8	1956
DE	Shallow	0-1	1.15	5.5*	0.85*	22.5 ± 5.4	17.6 ± 1.9	4.9	
DE	Shallow	1-2	2.29	4.95*	0.65*	21 ± 6	14.7 ± 1.6	6.3	2017
DE	Shallow	10-14	16.04	4.8*	0.75*	18.7 ± 5.7	16.6 ± 1.6	2.1	1982
DE	Deep	0-1	1.48	5.8 ± 3.7	0.94 ± 0.6	47.7 ± 7.6	16.1 ± 1.7	31.6	2017
DE	Deep	12-14	20.70	5.5*	0.86 ± 0.57	39.2 ± 7	22.3 ± 2.2	16.9	1997
DE	Deep	24-26	38.44	5*	0.8*	25.7 ± 5.6	19.5 ± 2	6.2	1965
DE	Deep	42-44	65.05	4.2*	0.7*	17.8 ± 4.7	18.4 ± 2.1	-3.2 to 2	<1923
DE	Deep	50-52	76.88	4.9*	0.75*	19.8 ± 4.8	18.8 ± 1.9	1	1906
DE	Deep	72-74	109.40	4.45*	0.6*	12.7± 4.8	13.8 ± 1.4	-4.5 to 2.3	<1927

Table 2-2. Summary of the baseline concentrations (C_b), maximum concentrations (C_X), contamination factors (C_f), and overall degree of contamination (mC_d) of 12 toxicants in the Upper North Arm, Lower Waihopai Arm, and East Daffodil bay deep cores. The degree of contamination in the three cores fall in the moderate (2-4) and high (4-8) ranges (Abrahim, 2005; Abrahim and Parker, 2008).

	Upper North Arm			Lower Waihopai Arm			East Daffodil Bay	
	C_b (ppm)	C_x (ppm)	C_f	C_b (ppm)	C_x (ppm)	C_f	C_b (ppm)	C_x (ppm)
Organic C[a]	2707	22553	8.3	2707	21996	8.1	2924	17155
P	380	1383	3.6	365	900	2.5	380	613
N[b]	324	2400	7.4	334	4617	14	334	4464
Cu[a]	8.0	25.2	3.2	8.0	23.9	3.0	8.0	18.3
Ni[a]	15.2	36.8	2.4	15.2	35.6	2.3	13.4	28.7
Pb[a]	11.3	18.9	1.7	11.3	17.4	1.5	11.6	14.6
Zn	36.8	143.0	3.9	47.5	109.6	2.3	37.5	75.4
Cr[a]	34.8	59.9	1.7	34.8	62.6	1.8	34.0	60.1
Cd[b]	0.02	0.13	8.8	0.04	0.09	2.4	0.04	0.11
As[a]	6.7	11.3	1.7	6.7	10.7	1.6	7.8	10.3
Ag[a]	0.01	0.15	11	0.01	0.12	8.9	0.02	0.07
Sb[a]	0.18	0.47	2.7	0.18	0.42	2.4	0.24	0.35
mC_d			**4.4**			**3.9**		

[a] UNA baseline values are used for the LW core baseline

[b] DE baseline values are used for the LW core baseline

Chapter 3. General Conclusion

3.1. Discussion and implications

New River Estuary has been classified as highly eutrophic over the last two decades, which is linked to the rapid decline of its ecosystem's health (Robertson et al., 2017, 2002; Robertson and Stevens, 2012b, 2007, 2001). Excessive fine-sediment and nutrient loading has resulted in nuisance macroalgae (i.e., *Gracilaria* and *Ulva*) outcompeting other native species in the highly eutrophic environment. Historically, a marine-dominated sediment load accumulated in the NRE in response to estuary reclamation (Thoms, 1981). The majority of the terrestrial fine-sediment load at that time, sourced from land clearance and agricultural and urban development, was tidally redistributed to the continental shelf (Ledgard, 2013; Pearson and Couldrey, 2016; Thoms, 1981). Sediment cores from the NRE record the onset of fine-sediment accumulation and increasing terrestrial dominance between 1906-1935 (post-reclamation) by a shell- and/or plant-rich layer with a distinct $\delta^{13}C$ signature that approaches a mixed seagrass (-10 to -11‰; Hemminga and Mateo, 1996) and cockle shell (-18 to -15‰; Sauriau and Kang, 2000) endmember. It is evident that reclamation reduced the estuary's ability to process sediment influx due to the reduction in surface area, resulting in increased sedimentation and a subsequent change in the ecological hierarchy. Furthermore, urbanization and agricultural expansion through the mid- to late-1900s, including river channelization, artificial drainage, and the removal of riparian structures and wetlands, has exacerbated terrestrial sediment loss, particularly after 1985 with the transition to more intensive dairy farming (Ledgard, 2013; Pearson and Couldrey, 2016). This sediment transports an increased volume of nutrients and heavy metals from

fertilizers, animal excreta, and urban discharges (i.e., stormwater runoff, wastewater discharge, landfill leachate, etc.), which contributes to the eutrophication and contamination of New River Estuary. With the majority of the estuary's sediment and nutrient load originating from fluvial (terrestrial) sources (Robertson et al., 2017) and with much of the heavy metal load originating from urban sources (Williamson and Morrisey, 2000), targeted limits and regulations to the NRE catchment need to be implemented and enforced to minimize future sediment (and pollutant) losses. Continued fine-sediment accumulation and nutrient enrichment has been shown to advance ecological degradation in the upper Waihopai Arm where nuisance macroalgae are eliminated as bacterial species (i.e., *Beggiatoa*) flourish in the increasingly anoxic and sulfide-rich sediment (Robertson et al., 2017). Similar processes impacting ecological degradation are apparent in catchments in Southland (i.e., Cavanagh and Ward, 2014; Robertson et al., 2017, 2002), in other regions of New Zealand (Augustinus et al., 2006; Chapman, 1996; Halliday et al., 2006; Marsden and Bressington, 2009; McDowell et al., 2013; Robertson and Stevens, 2012a), and in systems world-wide (Cooper and Brush, 1993; King et al., 2008; Schelske and Hodell, 1995; Smith et al., 2006; Vaalgamaa and Conley, 2008). Therefore, assessing the state of an environment, especially based on its historical condition, is becoming increasingly important as a first step toward effecting change and improving water quality and ecological well-being.

3.2. Conclusion

This study provides a historical record of the textural and geochemical changes in the NRE sediment, a proxy of estuary health in the last century. The primary aim was to improve our understanding of anthropogenic influence on estuary (and consequently ecological) dynamics, to

help target areas of the catchment with a greater risk for low-quality (pollutant-rich) sediment loss (i.e., based on land uses, slope/elevation, soil type and drainage, etc.). The *Water and Land 2020 & Beyond* (Environment Southland, 2018) project can use this evidence to focus policy-making decisions and facilitate remedial actions in Southland's catchments to prevent further decline in ecological health.

3.3. Future research

3.3.1. Sediment fingerprinting

Understanding the provenance (where the load originates) and quality (level of pollutant enrichment) of sediment in a fluvial network allows for a pathway of migration to be developed to assess catchment sediment fluxes, including remobilization and sequestration. Sediment source tracking is a direct approach that uses chemical properties as "fingerprints" to discriminate potential source material and qualitatively apportion their contribution to a sediment load. A combination of distinct signatures (i.e., major and trace element concentrations, stable and radiogenic isotope signatures, or magnetic properties) distinguish between potential source (reference) material that are representative of variations in catchment lithology, soil, and land use practices. This method has been successfully used to apportion sediment sources in smaller, farm-scale catchments (Collins et al., 2012; Collins and Walling, 2007; Foster et al., 2007; Jalowska et al., 2017; Walling et al., 1999; Walling and Woodward, 1995). A challenge for applying this technique to the NRE catchment is discriminating between the diverse range of reference materials that are both intra- and intervariable in their geochemical signatures. Instead

of predetermined tracers, statistical tests, such as the Kruskal-Wallis test and cluster analysis, can be used to identify the optimal suite of chemical constituents that characterize each source (Collins et al., 2017; Pulley et al., 2017).

In an extension of this thesis project, agitated surface water was collected in-stream using an isolation core to represent the suspended sediment load during low- and mid-flow periods. Sites for these sample collections were determined based on accessibility, flow rate, and tributary sub-catchment size. Collecting sufficient, and representative, material for analysis in low-flow settings can be problematic. In these cases, time-integrated sediment traps are commonly used, especially for detecting relative changes along or between proximal sites (Phillips et al., 2000). However, due to the scale of the catchment and its relatively unstable flow regime (McDowell et al., 2013), and that these shuttles may preferentially select coarse particles, this technique was deemed impractical for a fine-sediment investigation in the NRE catchment. High-flow storm events have been proven to be important drivers of annual sediment loads because increases in flow velocity positively correlate to greater suspended-sediment concentrations in fluvial systems (Horowitz, 2008; Salomons and Forstner, 1984). Automatic samplers (i.e., Teledyne Isco portable samplers; Perks et al., 2014) were used for material collection at high-flow when waters were turbid, fast-flowing, and contained debris, making them unsafe to enter. To represent the bulk of material that is transported to, and deposited in, the NRE, fresh, surficial sediment deposited within a few tidal cycles of a high-flow event was collected, with sites determined based on accessibility and rate of deposition. In-stream (low- and high-flow) and estuarine samples were analysed for trace and major ion concentrations, including nutrient fractions and organic carbon, using ICP-MS following partial (sequential, aqua regia) and near-total (multi-acid) digestions at ALS Global's Geochemistry Analytical Lab in Vancouver,

Canada. Surficial (0-30 cm) and subsurface (50-70 cm) soil horizons were sampled by GNS Science in an 8-km grid as an unbiased and cost-effective approach to collecting soil and will be used in this investigation as a catalogue of potential source material (Martin et al., 2015).

To apply the sediment fingerprinting technique to this NRE dataset, a correction factor will be applied to account for the variation in particle size composition between the riverine and estuarine sediment loads and the source material (Collins et al., 2017). Using the statistically-determined group of discriminators, a quantitative mixing model will be created to estimate the contributions of each source to the sediment load at a specific site (Collins et al., 2017; Haddadchi et al., 2014; Martinez-Carreras et al., 2008; Yu and Oldfield, 1989). Bayesian, Monte Carlo, and other statistical uncertainty approaches can be applied to overcome the fact that several combinations of source material could potentially produce the same outcome (Martinez-Carreras et al., 2008; Small et al., 2002). The sediment fingerprinting results, combined with physiographic zonation (Hughes et al., 2016; Rissmann et al., 2016b) and land use maps (Pearson and Couldrey, 2016), can be useful in the identification of specific areas in the NRE catchment, and eventually in the region of Southland, with higher potential for low-quality sediment loss.

3.3.2. Additional recommendations

Further research includes designing a more specific regional-scale reference material library, that includes a representative number of samples from different soil types, parent material, and land uses. This library would use a precise methodology (i.e., collecting the top 10 cm to avoid

signature dilution, and collecting the subsurface material from the B-horizon specific to each soil profile) that would be easily transferable to other systems world-wide.

Furthermore, research could be expanded by applying the same techniques to additional receiving environments in Southland that are sensitive to the greater inputs of sediment and pollutants exacerbated by human influence, including Jacobs River Estuary (Robertson et al., 2017). Sediment cores could be collected from the primary depositional areas to determine, and compare, the historical changes in each catchment and to delineate a plan-of-action to improve Southland's water quality and ecological health.

References

Augustinus, P., Reid, M., Andersson, S., Deng, Y., Horrocks, M., 2006. Biological and geochemical record of anthropogenic impacts in recent sediments from Lake Pupuke, Auckland City, New Zealand. J. Paleolimnol. 35, 789–805.

Cavanagh, J.E., Ward, N., 2014. Contaminants in estuarine and riverine sediments and biota in Southland (Landcare Research Report for Environment Southland No. LC1789). Landcare Research New Zealand Ltd., Lincoln, New Zealand.

Chapman, M.A., 1996. Human impacts on the Waikato River system, New Zealand. GeoJournal 40, 85–99.

Collins, A.L., Pulley, S., Gellis, A., Porto, P., Horowitz, A.J., 2017. Sediment source fingerprinting as an aid to catchment management: A review of the current state of

knowledge and a methodological decision-tree for end-users. J. Environ. Manag. 86–108. https://doi.org/http://dx.doi.org/10.1016/j.jenvman.2016.09.075

Collins, A.L., Walling, D.E., 2007. The storage and provenance of fine sediment on the channel bed of two contrasting lowland permeable catchments, UK. River Res. Appl. 23, 429–450. https://doi.org/10.1002/rra.992

Collins, A.L., Zhang, Y., Walling, D.E., Grenfell, S.E., Smith, P., Grischeff, J., Locke, A., Sweetapple, A., Brogden, D., 2012. Quantifying fine-grained sediment sources in the River Axe catchment, southwest England: application of a Monte Carlo numerical modelling framework incorporating local and genetic algorithm optimisation. Hydrol. Process. 26, 1962–1983. https://doi.org/10.1002/hyp.8283

Cooper, S.R., Brush, G.S., 1993. A 2,500-year history of anoxia and eutrophication in Chesapeake Bay. Estuaries 16, 617–626.

Environment Southland, 2018. Water and Land 2020 & Beyond: Proposed Southland Water and Land Plan Part A.

Foster, I.D.L., Boardman, J., Keay-Bright, J., 2007. Sediment tracing and environmental history for two small catchments, Karoo Uplands, South Africa. Geomorphology 90, 126–143. https://doi.org/10.1016/j.geomorph.2007.01.011

Haddadchi, A., Olley, J., Laceby, P., 2014. Accuracy of mixing models in predicting sediment source contributions. Sci. Total Environ. 497-498, 139–152.

Halliday, J., Thrush, S.F., Hewitt, J., 2006. Ecological monitoring for potential effects of forestry activity on the intertidal habitats of Whangapoua Harbour (NIWA Client Report No. HAM2006-113).

Hemminga, M.A., Mateo, M.A., 1996. Stable carbon isotopes in seagrasses: variability in ratios and use in ecological studies. Mar. Ecol. Prog. Ser. 140, 285–298.

Horowitz, A.J., 2008. Determining annual suspended sediment and sediment-associated trace element and nutrient fluxes. Sci. Total Environ. 400, 315–343.

Hughes, B., Wilson, K., Rissmann, C.W., Rodway, E., 2016. Physiographics of Southland: Development and application of a classification system for managing land use effects on water quality in Southland (Technical Report No. 2016/11). Environment Southland, Invercargill, NZ.

Jalowska, A.M., McKee, B.A., Laceby, J.P., Rodriguez, A.B., 2017. Tracing the sources, fate, and recycling of fine sediments across a river-delta interface. Catena 154, 95–106.

King, J.W., Hubeny, J.B., Gibson, C.L., Laliberte, E., Ford, K.H., Cantwell, M., McKinney, R., Appleby, P.G., Desbonnet, A. (Ed. ., Costa-Pierce, A. (Ed. ., 2008. Chapter 7. Anthropogenic Eutrophication of Narragansett Bay: Evidence from Dated Sediment Cores, in: Science for Ecosystem-Based Management. Springer, pp. 211–232.

Ledgard, G., 2013. Land use change in the Southland region (Technical Report No. 2013-13). Environment Southland, Invercargill, NZ.

Marsden, I.D., Bressington, M.J., 2009. Effects of macroalgal mats and hypoxia on burrowing depth of the New Zealand cockle (Austrovenus stutchburyi). Estuar. Coast. Shelf Sci. 81, 438–444.

Martin, A.P., Turnbull, R.E., Rattenbury, M.S., Baisden, W.T., Christie, A.B., Cohen, D.., Hoogewerff, J., Rogers, K.M., 2015. Geochemical Atlas of Southern New Zealand (GNS Science Report No. 2015/26).

Martinez-Carreras, N., Gallart, F., Iffly, J.F., Pfister, L., Walling, D.E., Krein, A., 2008. Uncertainty assessment in suspended sediment fingerprinting based on tracer mixing models: A case study from Luxembourg. Sediment Dyn. Chang. Environ. IAHS Publ. no. 325, 94–105.

McDowell, R.W., Norris, M., Cox, N., 2013. Waituna Sediment Fingerprinting Study (Technical Report for Environment Southland No. RE500/2013/136). AgResearch Ltd., Christchurch, New Zealand.

Pearson, L.K., Couldrey, M., 2016. Methodology for GIS-based land use maps for Southland (Technical Report No. 2016-10). Environment Southland, Invercargill, NZ.

Perks, M.T., Warburton, J., Bracken, L., 2014. Critical assessment and validation of a time-integrating fluvial suspended sediment sampler. Hydrol. Process. 28, 4795–4807. https://doi.org/10.1002/hyp.9985

Phillips, J.M., Russell, M.A., Walling, D.E., 2000. Time-integrated sampling of fluvial suspended sediment: A simple method for small catchments. Hydrol. Process. 14, 2589–2602.

Pulley, S., Foster, I.D.L., Collins, A.L., 2017. The impact of catchment source group classification on the accuracy of sediment fingerprinting outputs. J. Environ. Manage. 194, 16–26.

Rissmann, C.W., Rodway, E., Beyer, M., Hodgetts, J., Snelder, T., Pearson, L.K., Killick, M., Marapara, T.R., Akbaripasand, A., Hodson, R., Dare, J., Millar, R., Ellis, T., Lawton, M., Ward, N., Hughes, B., Wilson, K., McMecking, J., Horton, T., May, D., Kees, L., 2016. Physiographics of Southland: Delineation of key drivers of regional hydrochemistry and water quality (Technical Report No. 2016/3). Environment Southland, Invercargill, NZ.

Robertson, B.M., Gillespie, P.A., Asher, R.A., Frisk, S., Keeley, N.B., Hopkins, G.A., Thompson, S.J., Tuckey, B.J., 2002. Estuarine Environmental Assessment and Monitoring: A National Protocol (Prepared for supporting Councils and the Ministry for the Environment No. Sustainable Management Fund Contract No. 5096).

Robertson, B.M., Stevens, L., 2012a. Tasman Coast: Waimea Inlet to Kahurangi Point. Habitat mapping, ecological risk assessment and monitoring recommendations (State of the Environment Report).

Robertson, B.M., Stevens, L.M., 2012b. New River Estuary: Fine Scale Monitoring of Highly Eutrophic Arms 2011/2012 (Report prepared by Wriggle Coastal Management for Environment Southland). Nelson, NZ.

Robertson, B.M., Stevens, L.M., 2007. New River Estuary 2007: Broad Scale Habitat Mapping and Sedimentation Rate (Report prepared by Wriggle Coastal Management for Environment Southland). Nelson, NZ.

Robertson, B.M., Stevens, L.M., Robertson, B.P., 2017. Condition of Southland's shallow, intertidal dominated estuaries in relation to eutrophication and sedimentation: Output 1: Data analysis and technical assessment - Habitat mapping, vulnerability assessment and monitoring recommendations related to issues of eutrophication and sedimentation (Report prepared by Wriggle Coastal Management for Environment Southland). Nelson, NZ.

Robertson, B., Stevens, L., 2001. Southland Estuaries State of Environment Report 2001 (Report prepared by Wriggle Coastal Management for Environment Southland).

Salomons, W., Forstner, U., 1984. Metals in the hydrocycle. Springer, Berlin Heidelberg Tokyo.

Sauriau, P.-G., Kang, C.-K., 2000. Stable isotope evidence of benthic microalgae-based growth and secondary production in the suspension feeder Cerastoderma edule (Mollusca, Bivalvia) in the Marennes-Oleron Bay. Hydrobiologia, Island, Ocean and Deep-Sea Biology 440, 317–329.

Schelske, C.L., Hodell, D.A., 1995. Using carbon isotopes of bulk sedimentary organic matter to reconstruct the history of nutrient loading and eutrophication of Lake Erie. Limnol. Oceanogr. 40, 918–929.

Small, I.F., Rowan, J.S., Franks, S.W., 2002. Quantitative sediment fingerprinting using a Bayesian uncertainty estimation framework. Struct. Funct. Manag. Implic. Fluv. Sediment. Syst. IAHS Publ. no. 276, 443–450.

Smith, V.H., Joye, S.B., Howarth, R.W., 2006. Eutrophication of freshwater and marine ecosystems. Limnol. Oceanogr. 51, 351–355.

Thoms, M.C., 1981. Sedimentation in the New River Estuary, Southland (Master of Science in Geography). University of Canterbury, Christchurch, New Zealand.

Vaalgamaa, S., Conley, D.J., 2008. Detecting environmental change in estuaries: Nutrient and heavy metal distributions in sediment cores in estuaries from the Gulf of Finland, Baltic Sea. Estuar. Coast. Shelf Sci. 76, 45–56.

Walling, D.E., Owens, P.N., Leeks, G.J.L., 1999. Fingerprinting suspended sediment sources in the catchment of the River Ouse, Yorkshire, UK. Hydrol. Process. 13, 955–975.

Walling, D.E., Woodward, J.C., 1995. Tracing sources of suspended sediment in river basins: A case study of the River Culm, Devon, UK. Mar. Freshw. Res. 327–336.

Williamson, R.B., Morrisey, D.J., 2000. Stormwater contamination of urban estuaries: 1. Predicting the build-up of heavy metals in sediments. Estuaries 23, 56–66.

Yu, L., Oldfield, F., 1989. A Multivariate Mixing Model for Identifying Sediment Source from Magnetic Measurements. Quat. Res. 168–181.

Appendix A – Core Descriptions

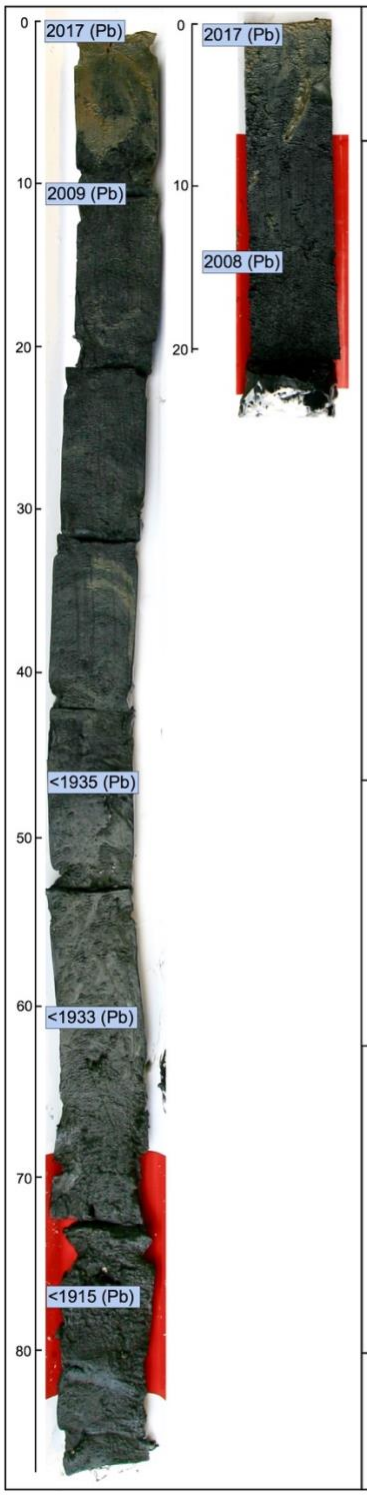

0 - 2 cm 2 - 8 cm 5 cm 7 - 8 cm	Dark greyish brown (2.5Y 4/2) silty mud with few Gracilaria fronds Dark greyish brown (some in burrow traces) mottled with black silty mud, small amount of rustier brown pockets Live blood worm Undulating boundary
8 - 48 cm 33 - 34 cm	Black silty mud with mottled dark greyish brown, decreasing in moisture and mud content with depth Two potential burrow traces of dark greyish brown
48 - 62 cm 60 - 62 cm	Undulating and gradational boundary as sediment becomes very dark grey (5Y 3/1) muddy silt with visible grains and shell fragments Textural boundary as sediment becomes muddy sand
62 - 80 cm 70 - 80 cm	Very dark grey (5Y 3/1) muddy sand with increasing sand content with depth Smalll shell fragments
80 - 85 cm	Lighter grey sand with small shell fragments, unidentified species

Figure A-1. Description of the Upper North Arm (UNA) deep and shallow cores, including photographs of the core splits with the specific sampled horizons showing its radioisotopic age.

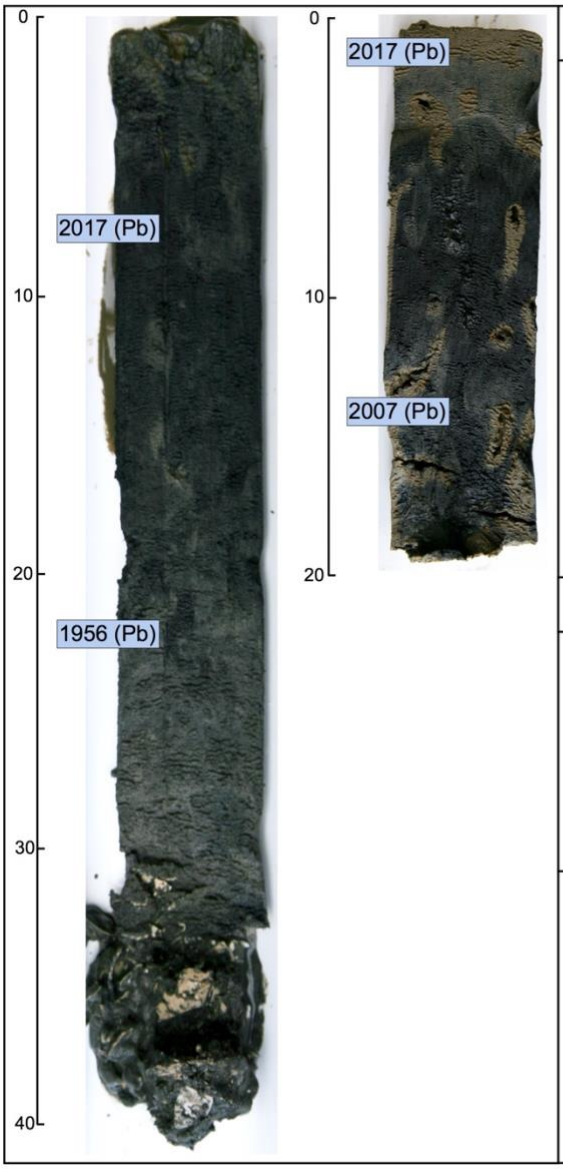

0 - 2 cm	Fresh, very dark greyish brown (2.5Y 3/2) silty mud with small pockets of a rustier brown
2 - 4 cm	Grey silty mud with patches of black and burrows of very dark greyish brown (2.5Y 3/2) silty mud
4 - 20 cm	Black silty mud with patches of grey and burrows of very dark greyish brown (2.5Y 3/2) silty mud
10 cm	Live blood worm in deep core
20 - 22 cm	Gradational boundary
22 - 31 cm	Very dark grey (5Y 4/1) silty sand, mottled with darker and lighter patches
31 - 39 cm	Very dark grey (5Y 4/1) silty sand, wet with lots of water retained, and large whole shells and fragments of cockle (*Austrovenus stutchburyi*) and trough shells (*Mactra sp.*)

Figure A-2. Description of the Lower Waihopai Arm (LW) deep and shallow cores, including photographs of the core splits with the specific sampled horizons showing its radioisotopic age.

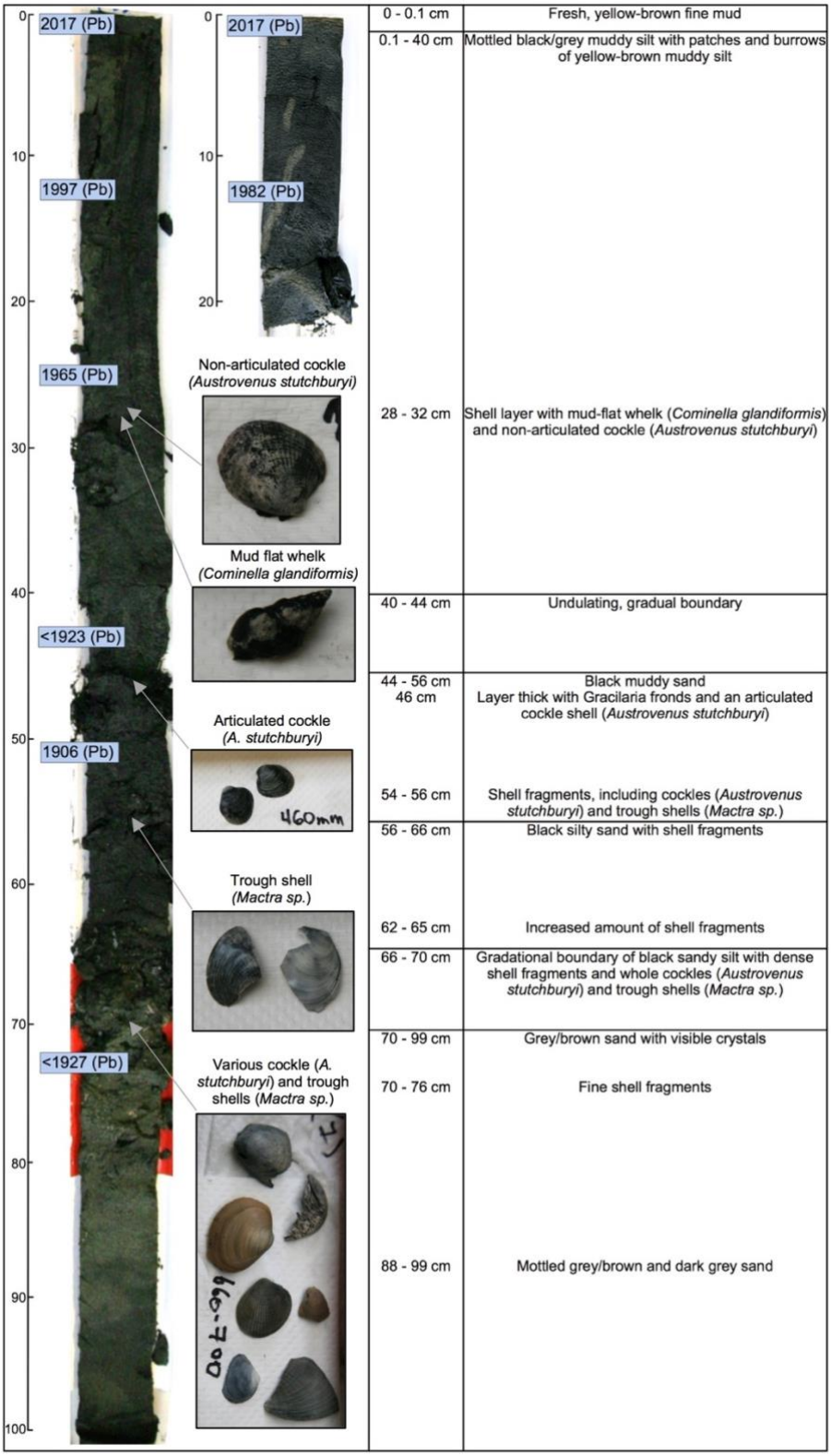

Figure A-3. Description of the East Daffodil Bay (DE) deep and shallow cores, including photographs of the core splits with shell species identified and the specific sampled horizons showing its radioisotopic age.

Appendix B – Total Geochemistry

Table B-1. Total elemental concentrations by ICP-MS after a multi-acid digestion in the Upper North Arm (UNA) deep core.

Upper North Arm (UNA)		Maximum Sampled Depth (cm)									
Element	Detection Limit	2	4	6	8	10	12	14	16	18	20
Al (%)	0.01	7.01	6.56	6.85	6.61	6.39	6.61	7.03	6.97	6.45	6.81
Na (%)	0.001	2.793	2.546	2.56	2.622	2.543	2.513	2.561	2.578	2.569	2.604
K (%)	0.01	1.5	1.48	1.48	1.44	1.39	1.55	1.45	1.45	1.42	1.45
Ca (%)	0.01	1.44	1.35	1.4	1.26	1.31	1.32	1.42	1.35	1.33	1.33
Mg (%)	0.02	1.21	1.17	1.2	1.16	1.14	1.17	1.19	1.17	1.1	1.14
Fe (%)	0.01	4.11	4.11	4.04	4.09	4.02	3.98	3.9	3.98	3.88	4.02
Mn (ppm)	1	588	595	574	535	540	568	580	568	570	571
Ti (%)	0.001	0.464	0.463	0.478	0.472	0.462	0.453	0.465	0.475	0.463	0.463
P (%)	0.001	0.144	0.147	0.124	0.11	0.098	0.102	0.1	0.09	0.095	0.094
S (%)	0.04	0.23	0.26	0.28	0.34	0.38	0.41	0.28	0.29	0.31	0.29
Ni (ppm)	0.1	35	35.7	36.5	37.3	37.3	38	37.8	37.8	35.4	37.5
Cu (ppm)	0.1	24.9	25.1	27.6	26.1	25.7	24.9	25.1	26.8	24.2	25.4
Pb (ppm)	0.02	19.21	18.82	19.36	19.38	18.4	18.47	18.61	18.75	18.06	18.77
Zn (ppm)	0.2	142	143.6	147.1	146.3	140.4	144.3	140.6	139.9	134.7	137.3
Cr (ppm)	1	62	59	61	62	61	59	60	61	58	60
Co (ppm)	0.2	15.2	15.8	15.9	16.3	16.8	16.5	17	17.2	16.5	17.2
Cd (ppm)	0.02	0.12	0.16	0.13	0.13	0.15	0.12	0.11	0.14	0.09	0.1
As (ppm)	0.2	11.5	11.1	11	11.4	11.4	10.6	9.7	10.2	10.9	11.5
Ag (ppb)	20	154	137	124	134	165	169	143	210	159	177
Li (ppm)	0.1	50.2	51.8	55.9	53.9	51.9	52.6	49.3	51.2	51.4	52
Be (ppm)	1	1	1	1	2	1	1	1	1	1	2
Rb (ppm)	0.1	31.9	25.7	30	31.2	27.6	27.2	27.9	26.7	25	26.3
Sr (ppm)	1	257	237	255	247	232	239	245	247	239	254
Cs (ppm)	0.1	2.4	2.1	2.5	1.8	1.8	2	2	2	1.8	2
Ba (ppm)	1	337	307	329	316	300	306	317	319	292	313
Mo (ppm)	0.05	0.64	0.63	0.85	1.31	0.99	0.94	0.92	1.1	1.03	1.01
W (ppm)	0.1	1.1	1	1.1	1.1	1.1	1.1	0.9	0.9	1.1	1
Re (ppm)	0.002	<0.002	<0.002	<0.002	0.003	<0.002	<0.002	<0.002	<0.002	<0.002	<0.002
Ga (ppm)	0.02	18.29	16.96	17.74	16.99	17.37	17.59	17.65	17.75	16.97	18
In (ppm)	0.01	0.08	0.06	0.05	0.06	0.05	0.05	0.03	0.06	0.03	0.05
Sn (ppm)	0.1	2.1	2.2	2.1	2	2	2.3	2.2	2	2	2
Sb (ppm)	0.02	0.49	0.45	0.5	0.49	0.46	0.46	0.47	0.45	0.46	0.48
Bi (ppm)	0.04	0.27	0.26	0.26	0.26	0.24	0.24	0.24	0.25	0.24	0.23
Se (ppm)	0.3	<0.3	<0.3	<0.3	<0.3	<0.3	<0.3	<0.3	<0.3	<0.3	<0.3
Te (ppm)	0.05	0.06	<0.05	<0.05	0.07	<0.05	<0.05	<0.05	<0.05	<0.05	0.05
U (ppm)	0.1	1.7	1.8	1.8	1.9	1.8	1.7	1.8	1.9	1.8	1.7
Th (ppm)	0.1	5.2	4.7	5	5.3	4.7	4.7	5	5	4.7	4.5
Tl (ppm)	0.05	0.36	0.47	0.46	0.38	0.53	0.9	0.58	0.37	0.34	0.4
Zr (ppm)	0.2	43	42.4	43.9	43.7	40.7	44.4	42.1	42.1	42	42.6
Hf (ppm)	0.02	1.4	1.47	1.5	1.4	1.38	1.4	1.36	1.38	1.45	1.39
V (ppm)	1	130	129	129	132	129	131	128	132	129	130
Nb (ppm)	0.04	6.25	6.26	6.4	6.3	6.15	5.95	6.04	6.28	6	6.21
Ta (ppm)	0.1	0.5	0.4	0.4	0.5	0.4	0.4	0.4	0.4	0.4	0.4
Sc (ppm)	0.1	15.4	14.5	15.3	15.4	13.8	14.4	15.7	15.8	14.5	14.3
La (ppm)	0.1	13.8	12.1	13.5	14.8	12.9	12.4	13.6	13.3	12.5	12.7
Ce (ppm)	0.02	34.26	30.83	32.3	35.76	30.24	30.87	32.96	32.96	32.02	30.85
Pr (ppm)	0.1	4.7	4.1	4.5	5	4.3	4.4	4.8	4.4	4.4	4.2
Nd (ppm)	0.1	18.8	17.8	17.9	19	17.5	16.8	18.1	17.4	17.5	17.2
Sm (ppm)	0.1	3.9	3.8	4.5	4.2	4	4	4.1	4.3	3.9	3.6
Eu (ppm)	0.1	1	1	1	1	1	1	1.1	1.1	1.1	1
Gd (ppm)	0.1	3.7	3.4	3.9	3.8	3.4	3.6	3.7	4.2	3.7	3.6
Tb (ppm)	0.1	0.6	0.6	0.6	0.6	0.6	0.6	0.6	0.6	0.6	0.6
Dy (ppm)	0.1	3.7	3.4	3.5	3.9	3.3	3.4	3.7	3.5	3.1	3.5
Y (ppm)	0.1	15.3	15	16	16.9	14.9	15.9	16.4	16.4	14.9	15.8
Ho (ppm)	0.1	0.8	0.7	0.8	0.8	0.7	0.8	0.8	0.7	0.7	0.7
Er (ppm)	0.1	2	1.9	2.1	2.1	1.8	1.8	2	1.9	2	1.7
Tm (ppm)	0.1	0.3	0.4	0.3	0.3	0.2	0.3	0.3	0.3	0.3	0.3
Yb (ppm)	0.1	1.8	1.6	1.9	1.7	1.6	1.7	1.8	1.7	1.7	1.8
Lu (ppm)	0.1	0.3	0.3	0.3	0.3	0.3	0.3	0.3	0.3	0.3	0.3

Upper North Arm (UNA)		Maximum Sampled Depth (cm)									
Element	Detection Limit	24	26	28	32	34	38	40	42	44	46
Al (%)	0.01	6.81	6.76	6.56	6.2	6.39	7.24	6.49	6.21	5.82	5.21
Na (%)	0.001	2.573	2.605	2.61	2.561	2.55	2.645	2.645	2.718	2.737	2.638
K (%)	0.01	1.39	1.41	1.47	1.4	1.43	1.43	1.53	1.59	1.44	1.48
Ca (%)	0.01	1.42	1.39	1.48	1.3	1.24	1.47	1.49	1.66	1.53	1.73
Mg (%)	0.02	1.12	1.11	1.07	1.08	1.1	1.14	0.92	0.88	0.84	0.78
Fe (%)	0.01	3.9	3.92	3.75	3.87	3.84	3.86	3.13	3.01	3.09	2.92
Mn (ppm)	1	579	578	575	550	542	572	510	494	516	506
Ti (%)	0.001	0.459	0.456	0.446	0.463	0.454	0.447	0.37	0.369	0.358	0.344
P (%)	0.001	0.079	0.078	0.071	0.077	0.076	0.074	0.058	0.056	0.056	0.052
S (%)	0.04	0.31	0.29	0.32	0.4	0.34	0.35	0.27	0.24	0.26	0.26
Ni (ppm)	0.1	38.4	38.7	35.8	36	37.5	34.1	27.5	28.2	26.2	25.6
Cu (ppm)	0.1	25.3	24.5	23.2	24.1	26.4	24.5	18.2	15.9	16	15.1
Pb (ppm)	0.02	18.82	19.09	19.42	22.77	22.09	20.39	16.18	16.3	15.94	15.05
Zn (ppm)	0.2	127.3	126.4	118.8	121.5	133.5	126.6	87.3	82.7	78.9	76.5
Cr (ppm)	1	61	60	58	58	59	59	43	46	42	43
Co (ppm)	0.2	16.1	16.6	15.4	15.9	16.5	16.5	13	13.7	12.7	11.6
Cd (ppm)	0.02	0.07	0.08	0.12	0.06	0.09	0.12	0.09	0.05	0.06	0.05
As (ppm)	0.2	10.2	11	9.6	10.3	10.7	11.1	9.4	10.1	10.2	8.9
Ag (ppb)	20	197	205	205	249	185	213	140	123	133	137
Li (ppm)	0.1	50.3	49.7	48	50.2	49.9	50.2	38.3	36.7	35.8	31.8
Be (ppm)	1	1	<1	1	2	1	2	1	1	2	2
Rb (ppm)	0.1	27.1	27.9	24.3	33.7	32.1	34.9	32.3	30.5	23.4	20
Sr (ppm)	1	247	244	259	263	239	270	320	344	323	316
Cs (ppm)	0.1	2.2	2.3	2.1	2.2	2.1	2.6	2	1.8	1.6	1.3
Ba (ppm)	1	319	311	301	311	295	324	393	422	376	351
Mo (ppm)	0.05	0.75	0.82	0.89	0.91	1.11	0.99	0.82	0.9	1	0.82
W (ppm)	0.1	0.9	0.9	0.9	1	1.1	1	0.7	0.6	0.7	0.6
Re (ppm)	0.002	<0.002	<0.002	<0.002	<0.002	<0.002	<0.002	<0.002	<0.002	<0.002	<0.002
Ga (ppm)	0.02	17.17	17.64	16.44	16.97	17.68	17.26	14.99	15.45	15.14	15.52
In (ppm)	0.01	0.06	0.06	0.06	0.04	0.04	0.05	0.06	0.06	0.06	0.05
Sn (ppm)	0.1	2.1	2	2.1	2.1	2	2.1	1.7	1.5	1.6	1.5
Sb (ppm)	0.02	0.49	0.43	0.42	0.4	0.49	0.43	0.31	0.36	0.34	0.29
Bi (ppm)	0.04	0.23	0.22	0.22	0.23	0.25	0.25	0.23	0.25	0.24	0.2
Se (ppm)	0.3	<0.3	<0.3	0.3	<0.3	<0.3	<0.3	<0.3	<0.3	<0.3	<0.3
Te (ppm)	0.05	0.07	<0.05	<0.05	<0.05	<0.05	<0.05	0.06	0.05	0.06	<0.05
U (ppm)	0.1	1.6	1.6	1.7	1.7	1.9	1.6	1.3	1.5	1.3	0.9
Th (ppm)	0.1	4.4	4.5	4	4.7	4.6	4.8	4	4	3.1	2.6
Tl (ppm)	0.05	0.38	0.46	0.33	0.36	0.4	0.34	0.36	0.35	0.35	0.33
Zr (ppm)	0.2	41.2	41.6	40	43	42.6	41.4	31.7	28.3	27.2	24.7
Hf (ppm)	0.02	1.41	1.36	1.33	1.44	1.37	1.32	1.03	0.91	0.94	0.74
V (ppm)	1	128	128	126	126	128	122	105	100	101	99
Nb (ppm)	0.04	6	5.93	5.55	6.03	5.8	5.64	4.69	4.84	4.37	4.4
Ta (ppm)	0.1	0.4	0.4	0.4	0.4	0.4	0.4	0.3	0.4	0.3	0.3
Sc (ppm)	0.1	14.4	15.4	13.4	14.4	14.1	14.5	11.4	11.5	10.1	9.8
La (ppm)	0.1	12.2	12.1	11.1	12.5	12.3	14.7	12.6	11.6	10.1	7
Ce (ppm)	0.02	29.94	29.43	27.87	30.68	30.6	35.5	30.15	28.38	23.99	18.22
Pr (ppm)	0.1	4.1	3.9	3.9	4.3	4.4	4.6	4	3.7	3.2	2.3
Nd (ppm)	0.1	17.2	16.4	16	16.7	16.2	19	16.8	15.8	12.2	9.3
Sm (ppm)	0.1	3.9	3.3	3.7	3.6	3.6	4	3.4	3.3	2.8	2.4
Eu (ppm)	0.1	1	0.9	1.1	1	0.9	0.9	0.9	0.8	0.7	0.6
Gd (ppm)	0.1	3.5	3.4	3.5	3.6	3.6	3.7	3.4	3.1	2.7	2.2
Tb (ppm)	0.1	0.6	0.6	0.6	0.6	0.6	0.6	0.5	0.5	0.4	0.3
Dy (ppm)	0.1	3.4	3.1	3	3.3	3	3.4	2.9	2.7	2.4	2.3
Y (ppm)	0.1	15.1	14.7	14.3	15.2	14.8	15.9	13.3	12.9	11	9.5
Ho (ppm)	0.1	0.8	0.6	0.7	0.7	0.7	0.8	0.6	0.6	0.5	0.5
Er (ppm)	0.1	1.7	1.8	1.9	1.7	1.9	1.9	1.6	1.6	1.3	1.2
Tm (ppm)	0.1	0.3	0.3	0.3	0.3	0.2	0.3	0.2	0.2	0.2	0.2
Yb (ppm)	0.1	1.7	1.7	1.6	1.6	1.6	1.7	1.3	1.3	1.3	1
Lu (ppm)	0.1	0.2	0.2	0.2	0.2	0.3	0.2	0.2	0.2	0.2	0.2

Upper North Arm (UNA)		Maximum Sampled Depth (cm)									
Element	Detection Limit	48	50	52	54	56	58	60	62	64	66
Al (%)	0.01	5.22	6.28	6.06	6.03	6.06	6.04	5.74	5.43	5.38	5.23
Na (%)	0.001	2.653	2.728	2.656	2.752	2.654	2.779	2.835	2.875	2.872	2.894
K (%)	0.01	1.39	1.55	1.55	1.55	1.59	1.55	1.54	1.55	1.43	1.48
Ca (%)	0.01	1.6	1.75	1.81	1.78	1.78	1.96	2.1	2.04	2.18	2.28
Mg (%)	0.02	0.93	0.94	0.92	0.95	1.02	0.97	0.88	0.78	0.73	0.66
Fe (%)	0.01	3.41	3.3	3.36	3.52	3.64	3.54	3.28	2.82	2.7	2.5
Mn (ppm)	1	562	585	592	594	602	585	581	533	542	557
Ti (%)	0.001	0.393	0.393	0.398	0.39	0.402	0.399	0.363	0.334	0.327	0.332
P (%)	0.001	0.055	0.057	0.05	0.056	0.055	0.056	0.053	0.045	0.041	0.039
S (%)	0.04	0.3	0.31	0.31	0.34	0.43	0.44	0.42	0.28	0.24	0.16
Ni (ppm)	0.1	30.9	29.3	26.9	28.5	33.1	37.5	25.4	21.1	19.8	15.1
Cu (ppm)	0.1	19.5	15.7	15.1	16	18.3	16.6	13.7	11.4	9.9	7.5
Pb (ppm)	0.02	15.33	13.85	13.62	13.52	14.22	13.55	12.65	12.09	11.64	11.19
Zn (ppm)	0.2	83.4	68.1	63.9	67.5	70	67.6	60.7	47.3	42.6	38.1
Cr (ppm)	1	53	52	53	54	53	53	46	40	40	35
Co (ppm)	0.2	12.9	12.8	12.5	13.5	13.4	13.4	11.6	10.4	9.9	8.9
Cd (ppm)	0.02	0.11	0.06	0.04	0.07	0.04	0.06	<0.02	0.05	0.04	0.04
As (ppm)	0.2	10.6	10	11.4	11.3	11.6	12.7	10.9	7.9	7.5	5.9
Ag (ppb)	20	110	72	57	54	51	51	47	47	28	<20
Li (ppm)	0.1	40.4	36.6	37.9	38	41.9	38.5	33.8	26.6	23.7	17.9
Be (ppm)	1	1	1	2	1	1	2	2	1	1	1
Rb (ppm)	0.1	21.3	24.5	23.6	20.7	27.2	20.9	18.9	18.2	15.8	17.2
Sr (ppm)	1	292	336	329	322	319	344	357	344	362	375
Cs (ppm)	0.1	1.4	1.6	1.6	1.4	1.6	1.6	1.2	1.1	0.9	0.8
Ba (ppm)	1	336	372	371	364	366	378	400	400	410	430
Mo (ppm)	0.05	0.88	0.91	1.03	1.27	1.34	1.02	0.77	0.46	0.39	0.38
W (ppm)	0.1	0.7	0.7	0.6	0.6	0.7	0.6	0.5	0.4	0.4	0.3
Re (ppm)	0.002	<0.002	<0.002	<0.002	<0.002	<0.002	<0.002	<0.002	<0.002	<0.002	<0.002
Ga (ppm)	0.02	16.16	15.75	15.66	16.26	16.07	16.76	15.07	14.44	14.52	14.74
In (ppm)	0.01	0.06	0.06	0.06	0.04	0.05	0.04	0.05	0.05	0.04	0.03
Sn (ppm)	0.1	1.6	1.5	1.6	1.6	1.6	1.5	1.3	1.1	1	0.9
Sb (ppm)	0.02	0.33	0.32	0.32	0.31	0.29	0.31	0.26	0.18	0.19	0.16
Bi (ppm)	0.04	0.19	0.15	0.15	0.14	0.16	0.14	0.12	0.1	0.07	0.07
Se (ppm)	0.3	<0.3	<0.3	<0.3	<0.3	<0.3	<0.3	<0.3	<0.3	<0.3	<0.3
Te (ppm)	0.05	0.07	<0.05	<0.05	<0.05	<0.05	<0.05	0.07	<0.05	0.08	0.05
U (ppm)	0.1	1.2	1.3	1.5	1.3	1.3	1.2	1.1	0.9	0.8	0.8
Th (ppm)	0.1	2.8	3.6	3.9	3.1	3.6	3.1	2.7	2.4	2.7	2.6
Tl (ppm)	0.05	0.34	0.35	0.35	0.38	0.35	0.37	0.36	0.36	0.37	0.33
Zr (ppm)	0.2	29.8	27.9	27.7	28.5	30.9	29.3	25.2	20.7	18.8	17.3
Hf (ppm)	0.02	0.95	0.92	0.94	0.89	1	0.92	0.78	0.8	0.75	0.64
V (ppm)	1	112	106	109	111	114	109	101	93	90	86
Nb (ppm)	0.04	4.94	4.8	5.2	4.95	5.28	5	4.46	4.3	4.04	3.89
Ta (ppm)	0.1	0.4	0.4	0.4	0.3	0.4	0.3	0.3	0.3	0.3	0.3
Sc (ppm)	0.1	10.7	11.5	11.5	10.3	12.1	11.5	9.3	8.8	8.4	7.8
La (ppm)	0.1	8	10.6	10.6	9.7	10.5	9.7	8.8	7.8	7.8	8.3
Ce (ppm)	0.02	20.36	26.53	25.68	24.34	25.33	23.85	22.51	19.51	19.48	20.79
Pr (ppm)	0.1	2.7	3.8	3.4	3.4	3.4	3.4	3.1	2.7	2.7	2.8
Nd (ppm)	0.1	10.7	13.5	13.5	13.1	13.6	13.1	13.2	10.4	10.6	11.8
Sm (ppm)	0.1	2.5	2.9	3	2.9	3	3.1	2.9	2.2	2.4	2.4
Eu (ppm)	0.1	0.7	0.8	0.9	0.8	0.8	0.9	0.7	0.7	0.7	0.6
Gd (ppm)	0.1	2.5	2.9	3	2.6	2.7	3.4	2.8	2.4	2.3	2.2
Tb (ppm)	0.1	0.4	0.5	0.4	0.5	0.5	0.5	0.4	0.4	0.4	0.3
Dy (ppm)	0.1	2.3	2.9	2.7	2.7	2.6	2.4	2.2	2	2.1	1.9
Y (ppm)	0.1	10.3	11.5	12.1	11.2	12	11.7	10.6	9.2	8.5	8.6
Ho (ppm)	0.1	0.5	0.6	0.6	0.5	0.6	0.6	0.5	0.4	0.4	0.4
Er (ppm)	0.1	1.3	1.4	1.5	1.2	1.5	1.4	1.4	1.2	1.2	1.2
Tm (ppm)	0.1	0.2	0.2	0.3	0.2	0.2	0.2	0.2	0.2	0.2	0.2
Yb (ppm)	0.1	1.2	1.2	1.3	1.3	1.2	1.2	1.2	1.1	1	1
Lu (ppm)	0.1	0.2	0.2	0.2	0.2	0.2	0.2	0.2	0.2	0.2	0.2

Upper North Arm (UNA)		Maximum Sampled Depth (cm)			
Element	Detection Limit	68	70	78	85
Al (%)	0.01	5.43	5.38	4.89	5.12
Na (%)	0.001	2.994	2.982	2.694	2.86
K (%)	0.01	1.41	1.41	1.33	1.31
Ca (%)	0.01	2.16	2.14	2.05	2.13
Mg (%)	0.02	0.65	0.63	0.63	0.65
Fe (%)	0.01	2.38	2.33	2.45	2.53
Mn (ppm)	1	531	511	490	504
Ti (%)	0.001	0.312	0.304	0.307	0.298
P (%)	0.001	0.039	0.036	0.036	0.04
S (%)	0.04	0.15	0.13	0.17	0.2
Ni (ppm)	0.1	14.4	14.8	15.1	16.5
Cu (ppm)	0.1	6.9	8	7.7	8.1
Pb (ppm)	0.02	11.48	11.96	10.63	11.16
Zn (ppm)	0.2	32.2	37.1	37.3	39.2
Cr (ppm)	1	34	36	34	35
Co (ppm)	0.2	8.6	8.8	7.9	8.4
Cd (ppm)	0.02	<0.02	<0.02	0.03	<0.02
As (ppm)	0.2	6	5.9	6.6	7.1
Ag (ppb)	20	<20	<20	25	<20
Li (ppm)	0.1	16.2	18	18	20
Be (ppm)	1	1	1	1	1
Rb (ppm)	0.1	19.7	17.4	14.4	14.9
Sr (ppm)	1	387	377	355	350
Cs (ppm)	0.1	0.8	0.8	0.7	0.8
Ba (ppm)	1	464	470	393	398
Mo (ppm)	0.05	0.33	0.44	0.64	0.61
W (ppm)	0.1	0.3	0.4	0.3	0.3
Re (ppm)	0.002	<0.002	<0.002	<0.002	<0.002
Ga (ppm)	0.02	14.16	14.36	13.04	13.35
In (ppm)	0.01	0.03	0.03	0.03	0.03
Sn (ppm)	0.1	0.9	1	0.9	0.8
Sb (ppm)	0.02	0.17	0.19	0.15	0.19
Bi (ppm)	0.04	0.06	0.07	0.07	0.07
Se (ppm)	0.3	<0.3	<0.3	<0.3	<0.3
Te (ppm)	0.05	0.1	<0.05	0.05	<0.05
U (ppm)	0.1	0.7	0.9	0.8	0.9
Th (ppm)	0.1	2.9	2.7	2.4	2.4
Tl (ppm)	0.05	0.32	0.33	0.29	0.32
Zr (ppm)	0.2	15.8	27.7	18	17
Hf (ppm)	0.02	0.56	0.96	0.59	0.62
V (ppm)	1	82	81	83	84
Nb (ppm)	0.04	3.69	3.89	3.52	3.5
Ta (ppm)	0.1	0.3	0.3	0.3	0.3
Sc (ppm)	0.1	7.5	7.1	7.1	7.4
La (ppm)	0.1	8.6	8.4	8	7.6
Ce (ppm)	0.02	20.6	20.83	19.96	17.94
Pr (ppm)	0.1	2.8	2.7	2.8	2.4
Nd (ppm)	0.1	11.4	11.3	10.6	10.2
Sm (ppm)	0.1	2.4	2.8	2.2	2
Eu (ppm)	0.1	0.6	0.6	0.5	0.6
Gd (ppm)	0.1	2.3	2.4	1.9	2.1
Tb (ppm)	0.1	0.3	0.3	0.3	0.3
Dy (ppm)	0.1	2.1	1.8	1.8	1.8
Y (ppm)	0.1	8.5	8.5	8.3	7.8
Ho (ppm)	0.1	0.4	0.4	0.4	0.4
Er (ppm)	0.1	1	1.1	1.1	1.1
Tm (ppm)	0.1	0.2	0.2	0.1	0.2
Yb (ppm)	0.1	1.1	1	1	0.9
Lu (ppm)	0.1	0.2	0.1	0.1	0.2

Table B-2. Total elemental concentrations by ICP-MS after a multi-acid digestion in the Lower Waihopai Arm (LW) deep core.

Lower Waihopai Arm (LW)		Maximum Sampled Depth (cm)									
Element	Detection Limit	2	4	6	8	10	12	14	16	18	20
Al (%)	0.01	6.87	6.8	6.33	6.4	6.62	6.49	6.22	6.43	6.31	5.77
Na (%)	0.001	2.547	2.594	2.43	2.476	2.517	2.497	2.439	2.409	2.375	2.346
K (%)	0.01	1.4	1.42	1.34	1.35	1.42	1.35	1.31	1.37	1.28	1.17
Ca (%)	0.01	1.71	1.65	1.67	1.76	1.76	1.75	1.81	1.91	2.24	3.04
Mg (%)	0.02	1.16	1.17	1.08	1.08	1.11	1.08	1.03	1.02	0.99	0.9
Fe (%)	0.01	3.95	4.1	4.22	4.24	4.22	4.14	3.97	4.06	4.16	4.31
Mn (ppm)	1	613	600	641	642	667	640	681	683	754	947
Ti (%)	0.001	0.514	0.539	0.516	0.525	0.555	0.533	0.529	0.563	0.599	0.788
P (%)	0.001	0.1	0.092	0.078	0.073	0.072	0.074	0.068	0.066	0.059	0.049
S (%)	0.04	0.3	0.27	0.39	0.35	0.33	0.3	0.24	0.37	0.35	0.4
Ni (ppm)	0.1	35.6	37.1	35	35.3	36.1	34.5	31.5	32.2	31.7	27.4
Cu (ppm)	0.1	24.8	25.1	23.8	24.4	22.8	22.6	20.4	19.4	21.4	15.5
Pb (ppm)	0.02	16.23	16.07	17.78	18.43	18.57	18.14	17.15	16.72	17.91	16.74
Zn (ppm)	0.2	114.3	113.2	109.3	109.1	104.7	107	97.5	93.8	99.8	75.7
Cr (ppm)	1	64	63	60	62	66	62	63	61	62	80
Co (ppm)	0.2	16.4	16.4	16.2	17.3	16.5	16.6	15.7	15.9	17.4	15.8
Cd (ppm)	0.02	0.09	0.08	0.09	0.11	0.17	0.17	0.06	0.06	0.12	0.11
As (ppm)	0.2	9.9	10.6	11.5	11	11.6	10.4	9.7	11.6	12.1	10.6
Ag (ppb)	20	115	117	120	118	115	113	126	89	175	91
Li (ppm)	0.1	47.5	47.7	46.7	47.1	46.8	48.9	44.9	40.9	41	32.8
Be (ppm)	1	1	2	2	2	2	1	1	1	1	1
Rb (ppm)	0.1	35.3	28.4	38.5	32.2	41.5	34.7	27.7	30	24.5	16.1
Sr (ppm)	1	301	290	312	321	337	324	329	335	380	436
Cs (ppm)	0.1	2.5	2.2	2.9	2.7	2.8	2.7	2.3	2.3	2.2	1.4
Ba (ppm)	1	319	297	328	339	329	326	316	307	326	317
Mo (ppm)	0.05	1.23	1.54	1.87	1.81	2.1	1.76	1.51	1.53	1.65	1.21
W (ppm)	0.1	1	0.9	1	0.9	1	0.9	0.8	0.9	0.8	0.6
Re (ppm)	0.002	<0.002	<0.002	<0.002	<0.002	<0.002	<0.002	<0.002	<0.002	<0.002	<0.002
Ga (ppm)	0.02	18.56	16.95	17.1	17.69	18.23	17.88	16.37	17.72	17.16	16.9
In (ppm)	0.01	0.05	0.05	0.07	0.07	0.07	0.07	0.05	0.05	0.04	0.08
Sn (ppm)	0.1	1.8	1.6	1.9	2	1.9	2.1	2	1.9	1.9	2.1
Sb (ppm)	0.02	0.37	0.43	0.45	0.43	0.45	0.41	0.44	0.4	0.42	0.35
Bi (ppm)	0.04	0.2	0.22	0.24	0.24	0.23	0.23	0.21	0.21	0.23	0.22
Se (ppm)	0.3	<0.3	0.3	<0.3	<0.3	<0.3	<0.3	<0.3	<0.3	<0.3	<0.3
Te (ppm)	0.05	0.05	<0.05	<0.05	<0.05	<0.05	<0.05	<0.05	<0.05	<0.05	0.06
U (ppm)	0.1	2	2.1	2.3	2.5	2.4	2.3	2.1	2.2	2.2	2.6
Th (ppm)	0.1	5.8	5.6	6.9	7	7.6	7.6	6.5	7.4	7	8.5
Tl (ppm)	0.05	0.36	0.38	0.37	0.4	0.38	0.37	0.56	0.37	0.85	0.58
Zr (ppm)	0.2	42.1	55.5	38.7	38.6	39.4	39.6	34.8	35.2	35.4	28.1
Hf (ppm)	0.02	1.46	1.61	1.38	1.31	1.29	1.43	1.38	1.23	1.23	1.07
V (ppm)	1	134	141	143	146	146	143	142	144	149	158
Nb (ppm)	0.04	6.31	6.12	6.23	6.67	6.45	6.26	7.38	6.3	6.84	8.58
Ta (ppm)	0.1	0.4	0.4	0.5	0.6	0.5	0.5	0.5	0.5	0.5	0.7
Sc (ppm)	0.1	14.7	15.5	16.2	15.2	15.9	15.7	15	15.7	15	15.1
La (ppm)	0.1	19.1	17.7	22.4	21.3	26.1	24.2	21.2	21.5	25	31.6
Ce (ppm)	0.02	44.03	42.55	52.04	50.42	59.14	54.28	50.01	52.05	55.96	71.59
Pr (ppm)	0.1	6	5.6	6.8	6.6	7.9	7.5	6.5	7	7.1	9.1
Nd (ppm)	0.1	22.7	21.9	25.7	26.6	28	28.4	24.7	26.3	26.7	33.4
Sm (ppm)	0.1	4.9	4.6	5.2	5.8	5.7	5.4	4.7	5.4	5.1	6.1
Eu (ppm)	0.1	1.3	1.2	1.2	1.2	1.4	1.3	1.2	1.2	1.2	1.4
Gd (ppm)	0.1	4.3	4.5	4.6	4.8	5	4.8	4.5	4.9	4.6	5.4
Tb (ppm)	0.1	0.7	0.7	0.7	0.7	0.8	0.8	0.7	0.7	0.7	0.8
Dy (ppm)	0.1	3.7	3.9	4.6	4	4.2	4.4	3.7	3.8	4.5	4.5
Y (ppm)	0.1	18.3	18.7	19.1	18.8	20.9	19.5	18.2	18.9	20.5	22.2
Ho (ppm)	0.1	0.8	0.9	1	0.9	0.9	0.9	0.9	0.8	0.9	1
Er (ppm)	0.1	1.9	2.1	2.2	2.4	2.2	2.5	2.1	2.2	2.4	2.5
Tm (ppm)	0.1	0.3	0.3	0.4	0.4	0.4	0.4	0.3	0.3	0.4	0.4
Yb (ppm)	0.1	1.9	1.7	2.2	2.2	2.1	2.2	2.1	2	2.2	2.5
Lu (ppm)	0.1	0.3	0.3	0.3	0.3	0.3	0.3	0.3	0.3	0.3	0.4

Lower Waihopai Arm (LW)		Maximum Sampled Depth (cm)				
Element	Detection Limit	22	24	26	28	30
Al (%)	0.01	6.31	6.44	6.59	5.6	5.96
Na (%)	0.001	2.377	2.269	2.483	2.4	2.335
K (%)	0.01	1.21	1.23	1.29	1.15	1.14
Ca (%)	0.01	2.97	2.78	2.54	3.9	4.04
Mg (%)	0.02	1	0.96	1.02	0.8	0.85
Fe (%)	0.01	4.51	4.59	4.07	3.86	4.1
Mn (ppm)	1	1114	1132	876	909	1079
Ti (%)	0.001	0.867	0.892	0.616	0.62	0.72
P (%)	0.001	0.046	0.038	0.042	0.031	0.035
S (%)	0.04	0.35	0.38	0.34	0.69	0.59
Ni (ppm)	0.1	27.1	24.3	28.2	20.9	19.6
Cu (ppm)	0.1	14	10.9	14.1	10.1	9.4
Pb (ppm)	0.02	15.44	13.26	13.73	12.45	12.95
Zn (ppm)	0.2	67.8	58.3	58.5	48.9	46.1
Cr (ppm)	1	82	88	67	60	64
Co (ppm)	0.2	15.6	13.9	13.3	12.7	12.7
Cd (ppm)	0.02	0.12	0.08	0.03	0.07	0.08
As (ppm)	0.2	11.2	10.2	10.9	10.3	11.6
Ag (ppb)	20	78	41	49	32	38
Li (ppm)	0.1	31.9	28.5	31.5	25.4	22.1
Be (ppm)	1	2	<1	1	1	1
Rb (ppm)	0.1	21.9	39	32.7	11.5	13.4
Sr (ppm)	1	430	451	442	470	515
Cs (ppm)	0.1	1.7	1.9	1.9	0.9	0.9
Ba (ppm)	1	339	353	364	265	332
Mo (ppm)	0.05	1.24	1.35	1.35	1.46	1.71
W (ppm)	0.1	0.6	0.6	0.6	0.5	0.4
Re (ppm)	0.002	<0.002	<0.002	<0.002	<0.002	0.004
Ga (ppm)	0.02	16.85	16.09	16.5	15.36	14.78
In (ppm)	0.01	0.11	0.07	0.07	0.05	0.08
Sn (ppm)	0.1	1.9	1.8	1.7	1.6	1.5
Sb (ppm)	0.02	0.33	0.31	0.33	0.26	0.35
Bi (ppm)	0.04	0.18	0.16	0.16	0.13	0.14
Se (ppm)	0.3	<0.3	0.4	<0.3	<0.3	<0.3
Te (ppm)	0.05	<0.05	0.06	<0.05	0.1	0.11
U (ppm)	0.1	3.6	4	2	1.7	3.2
Th (ppm)	0.1	9.8	11.2	9.1	5.3	8
Tl (ppm)	0.05	0.81	0.34	0.36	0.28	0.31
Zr (ppm)	0.2	26.9	25.7	26	23.2	20.6
Hf (ppm)	0.02	1.05	1.06	0.92	0.85	0.73
V (ppm)	1	164	165	141	135	147
Nb (ppm)	0.04	9.89	9.9	7.05	6.11	7.47
Ta (ppm)	0.1	0.8	1	0.5	0.4	0.6
Sc (ppm)	0.1	15.6	16.4	14.8	12.5	13.8
La (ppm)	0.1	36.6	43.3	33.3	22.5	30.8
Ce (ppm)	0.02	78.35	89.98	72.21	51.59	68.91
Pr (ppm)	0.1	10.2	11.3	8.9	6.3	9
Nd (ppm)	0.1	36.1	40.9	32.5	25.8	32.2
Sm (ppm)	0.1	7.1	7.3	5.9	4.9	5.9
Eu (ppm)	0.1	1.6	1.6	1.5	1.2	1.4
Gd (ppm)	0.1	5.5	5.9	5	3.8	5
Tb (ppm)	0.1	0.9	0.8	0.8	0.6	0.8
Dy (ppm)	0.1	4.8	4.7	4.2	3.9	4
Y (ppm)	0.1	23.9	24.8	21	17.6	20.8
Ho (ppm)	0.1	1	1	0.9	0.8	0.9
Er (ppm)	0.1	2.7	2.8	2.5	2.1	2.4
Tm (ppm)	0.1	0.4	0.5	0.4	0.3	0.4
Yb (ppm)	0.1	2.6	2.7	2.2	2	2.4
Lu (ppm)	0.1	0.4	0.4	0.4	0.4	0.4

Table B-3. Total elemental concentrations by ICP-MS after a multi-acid digestion in the East Daffodil Bay (DE) deep core.

East Daffodil Bay (DE)		Maximum Sampled Depth (cm)									
Element	Detection Limint	2	4	6	8	10	12	14	16	18	20
Al (%)	0.01	6.2	4.94	5.61	5.72	5.89	5.76	5.69	5.62	5.71	5.32
Na (%)	0.001	2.517	2.702	2.748	2.775	2.744	2.633	2.711	2.686	2.654	2.598
K (%)	0.01	1.41	1.33	1.37	1.34	1.43	1.32	1.34	1.3	1.34	1.26
Ca (%)	0.01	1.58	2	2.07	1.99	2.12	2.19	2.2	2.19	2.14	2.16
Mg (%)	0.02	1.13	0.99	0.94	0.97	0.97	0.95	0.92	0.89	0.9	0.88
Fe (%)	0.01	4.29	3.61	3.68	3.77	3.77	3.67	3.65	3.49	3.52	3.57
Mn (ppm)	1	565	594	611	609	606	627	623	598	624	638
Ti (%)	0.001	0.482	0.439	0.473	0.481	0.485	0.478	0.494	0.461	0.468	0.486
P (%)	0.001	0.072	0.058	0.054	0.054	0.052	0.052	0.051	0.048	0.054	0.052
S (%)	0.04	0.61	0.33	0.31	0.39	0.33	0.38	0.3	0.28	0.36	0.28
Ni (ppm)	0.1	34.3	28.4	25.2	27	26.1	25.3	24.9	24.6	23.6	24.3
Cu (ppm)	0.1	24.7	18.5	16.1	17.2	16.5	16.5	15.4	15.1	14.9	14.4
Pb (ppm)	0.02	16.21	14.05	13.55	13.63	13.17	12.78	13.25	13.47	12.74	12.85
Zn (ppm)	0.2	81.2	73.5	70.8	76.2	69.2	69.4	68.8	63.1	65.9	63.1
Cr (ppm)	1	58	54	61	56	58	63	62	66	55	58
Co (ppm)	0.2	14	13.2	12.8	13.2	14.2	13.1	12.8	13.3	13.4	12.8
Cd (ppm)	0.02	0.1	0.11	0.11	0.08	0.1	0.07	0.1	0.08	0.07	0.09
As (ppm)	0.2	13.4	9.5	9.4	10.2	10.1	9.1	10.2	9.9	9.8	9.8
Ag (ppb)	20	95	55	60	61	59	61	66	35	47	62
Li (ppm)	0.1	49.1	34.6	31.4	36	33.1	32.8	30.1	29.3	30.3	30
Be (ppm)	1	1	2	1	1	1	1	1	1	1	1
Rb (ppm)	0.1	35	21.3	19.2	24	21.4	18.5	18.8	18.1	17.6	14.6
Sr (ppm)	1	289	310	356	358	363	350	382	364	371	357
Cs (ppm)	0.1	2.6	1.5	1.6	1.9	1.6	1.5	1.5	1.3	1.3	1.3
Ba (ppm)	1	311	323	342	357	336	337	350	355	333	327
Mo (ppm)	0.05	3.12	2.49	2.57	3.07	2.72	2.79	2.36	2.48	2.01	1.7
W (ppm)	0.1	0.8	0.7	0.7	0.7	0.6	0.6	0.6	0.6	0.6	0.5
Re (ppm)	0.002	<0.002	<0.002	<0.002	0.004	<0.002	0.002	<0.002	<0.002	<0.002	<0.002
Ga (ppm)	0.02	16.31	16.26	16.24	15.95	15.41	15.57	16.12	16.07	15.82	14.85
In (ppm)	0.01	0.05	0.06	0.05	0.06	0.06	0.05	0.05	0.04	0.04	0.04
Sn (ppm)	0.1	1.6	1.5	1.7	1.5	1.6	1.6	1.6	1.4	1.5	1.5
Sb (ppm)	0.02	0.41	0.33	0.31	0.34	0.3	0.31	0.31	0.3	0.29	0.3
Bi (ppm)	0.04	0.22	0.15	0.14	0.15	0.15	0.14	0.13	0.13	0.14	0.14
Se (ppm)	0.3	<0.3	<0.3	<0.3	0.4	<0.3	<0.3	<0.3	<0.3	<0.3	<0.3
Te (ppm)	0.05	<0.05	0.1	<0.05	0.06	<0.05	<0.05	<0.05	<0.05	<0.05	0.12
U (ppm)	0.1	2.6	1.6	2.2	2.3	2	2	1.8	1.8	1.8	1.5
Th (ppm)	0.1	5.6	4.1	4.9	4.8	4.7	4.3	4.6	4	4.6	3.8
Tl (ppm)	0.05	0.44	0.38	0.39	0.37	0.36	0.36	0.32	0.36	0.33	0.35
Zr (ppm)	0.2	37.1	28.1	28.4	30.4	29.7	27.1	27.6	25.8	26.2	27
Hf (ppm)	0.02	1.29	1	1.02	1.11	0.94	1.04	1.03	0.93	0.96	1.05
V (ppm)	1	141	127	129	132	132	130	129	124	125	127
Nb (ppm)	0.04	6	5.86	5.85	5.58	5.79	5.84	5.79	5.62	5.6	5.67
Ta (ppm)	0.1	0.4	0.4	0.5	0.4	0.4	0.4	0.4	0.4	0.4	0.4
Sc (ppm)	0.1	15.4	12.3	13.1	13.3	12.5	12.8	12.2	11.5	12.1	11
La (ppm)	0.1	16.8	11.7	14.6	16.9	15.9	14.3	15.8	13.7	15.8	12.6
Ce (ppm)	0.02	39.45	27.92	35.73	38.55	37.1	34.49	37.51	32.36	37.18	30.61
Pr (ppm)	0.1	5.5	3.6	4.7	5	4.9	4.5	4.8	4.1	4.8	4.1
Nd (ppm)	0.1	21.4	14.1	18.7	19.9	20.1	16.3	18.4	16.2	19.6	16.3
Sm (ppm)	0.1	4.4	3.2	4.1	4.1	3.7	3.5	3.9	3.5	4.2	3.3
Eu (ppm)	0.1	1.1	0.8	1	1.1	0.9	0.9	1.1	0.8	1	0.9
Gd (ppm)	0.1	4	2.9	3.8	3.8	3.5	3.4	3.5	3.3	3.7	3.3
Tb (ppm)	0.1	0.6	0.5	0.5	0.5	0.6	0.5	0.6	0.5	0.6	0.5
Dy (ppm)	0.1	3.6	2.8	3.1	3.3	3.2	3.3	2.9	2.9	3.5	2.8
Y (ppm)	0.1	17.3	12.7	13.8	15.8	14.6	13.9	14.5	13.5	14.6	12.9
Ho (ppm)	0.1	0.8	0.7	0.7	0.7	0.7	0.7	0.7	0.6	0.7	0.6
Er (ppm)	0.1	2	1.6	1.7	1.9	1.7	1.8	1.7	1.7	1.6	1.5
Tm (ppm)	0.1	0.3	0.3	0.3	0.3	0.3	0.3	0.3	0.3	0.2	0.3
Yb (ppm)	0.1	1.7	1.4	1.5	1.7	1.5	1.6	1.5	1.6	1.6	1.5
Lu (ppm)	0.1	0.2	0.2	0.2	0.2	0.3	0.2	0.3	0.2	0.2	0.2

East Daffodil Bay (DE)		Maximum Sampled Depth (cm)									
Element	Detection Limint	22	24	26	28	30	32	34	36	38	40
Al (%)	0.01	5.59	5.7	5.4	5.92	5.62	5.39	5.07	5.21	4.66	5.47
Na (%)	0.001	2.644	2.62	2.608	2.642	2.6	2.718	2.526	2.693	2.569	2.484
K (%)	0.01	1.29	1.29	1.26	1.3	1.26	1.34	1.25	1.3	1.11	1.26
Ca (%)	0.01	2.14	2.28	2.26	2.33	2.34	2.22	2.19	2.39	2.44	2.51
Mg (%)	0.02	0.91	0.91	0.85	0.94	0.87	0.85	0.85	0.8	0.76	0.84
Fe (%)	0.01	3.58	3.66	3.55	3.67	3.55	3.58	3.44	3.4	3.41	3.41
Mn (ppm)	1	609	626	642	648	655	629	596	648	708	637
Ti (%)	0.001	0.47	0.478	0.474	0.498	0.468	0.493	0.458	0.475	0.49	0.459
P (%)	0.001	0.049	0.053	0.05	0.049	0.049	0.049	0.048	0.047	0.042	0.042
S (%)	0.04	0.26	0.24	0.25	0.27	0.23	0.26	0.25	0.18	0.17	0.18
Ni (ppm)	0.1	24.5	25	21.8	23.7	21.3	23.8	22.2	20.8	20.8	20.2
Cu (ppm)	0.1	14.5	14.4	13	14.8	12.4	14.3	12.8	11.1	10.2	10.1
Pb (ppm)	0.02	13.06	13.89	12.79	14.35	12.35	13.11	12.6	12.5	11.61	11.75
Zn (ppm)	0.2	65.1	65.6	59.5	64.3	54.6	63.2	54.9	52.6	50.7	45.9
Cr (ppm)	1	64	63	59	64	61	60	59	57	66	60
Co (ppm)	0.2	13	13.6	12.4	13.5	11.7	12.8	11.9	11.5	12.7	10.8
Cd (ppm)	0.02	0.07	0.14	0.05	0.09	0.08	0.06	0.05	0.04	0.06	0.09
As (ppm)	0.2	9.7	11.1	10.3	11.3	10.6	10.4	9.6	10.1	8.8	9.4
Ag (ppb)	20	57	57	39	40	49	56	47	21	36	21
Li (ppm)	0.1	30.6	30.4	27.9	30.2	26.1	28.3	26.7	24.9	23.6	23
Be (ppm)	1	1	1	1	2	1	1	1	1	1	2
Rb (ppm)	0.1	15.9	18	14.6	18.5	16.2	14	14.1	12.2	8.6	15
Sr (ppm)	1	353	386	368	383	357	368	368	374	365	388
Cs (ppm)	0.1	1.3	1.4	1.1	1.4	1.2	1.1	1.1	0.9	0.7	1
Ba (ppm)	1	333	331	331	364	339	333	323	338	323	360
Mo (ppm)	0.05	1.77	1.8	1.47	1.55	1.43	1.44	1.12	1.19	1.08	1.1
W (ppm)	0.1	0.6	0.6	0.5	0.5	0.5	0.6	0.5	0.5	0.5	0.3
Re (ppm)	0.002	<0.002	0.003	<0.002	<0.002	<0.002	<0.002	<0.002	0.002	<0.002	<0.002
Ga (ppm)	0.02	15.07	15.45	14.04	16.06	14.31	16.47	14.92	15.31	14.5	15.05
In (ppm)	0.01	0.05	0.04	0.06	0.05	0.04	0.04	0.03	0.04	0.06	0.05
Sn (ppm)	0.1	1.6	1.8	1.4	1.7	1.4	1.5	1.5	1.4	1.5	1.2
Sb (ppm)	0.02	0.29	0.29	0.28	0.31	0.26	0.28	0.26	0.31	0.26	0.23
Bi (ppm)	0.04	0.14	0.14	0.14	0.16	0.12	0.15	0.14	0.13	0.13	0.12
Se (ppm)	0.3	<0.3	0.3	<0.3	<0.3	<0.3	<0.3	<0.3	<0.3	<0.3	0.4
Te (ppm)	0.05	0.06	0.07	0.08	<0.05	0.08	0.07	0.1	0.1	0.11	0.1
U (ppm)	0.1	1.7	1.6	1.5	1.8	1.5	1.5	1.3	1.3	1.3	1.3
Th (ppm)	0.1	3.7	4.8	4.2	4.6	4.5	4	3.5	3.6	3.4	4.4
Tl (ppm)	0.05	0.35	0.34	0.33	0.33	0.33	0.39	0.34	0.35	0.3	0.3
Zr (ppm)	0.2	26.8	27.6	26.5	27.2	24.6	26.7	26.6	24.5	23.9	22.8
Hf (ppm)	0.02	0.86	0.94	0.95	1.06	0.9	0.9	0.87	0.88	0.84	0.83
V (ppm)	1	127	130	126	129	124	126	121	122	124	118
Nb (ppm)	0.04	5.25	5.97	6.66	6.62	5.35	6.11	5.32	5.39	5.82	5.08
Ta (ppm)	0.1	0.4	0.4	0.6	0.5	0.4	0.4	0.4	0.4	0.5	0.4
Sc (ppm)	0.1	11.3	11.2	11.9	13	11.8	11.7	11.3	11	9.8	11.9
La (ppm)	0.1	13.1	16.2	14.5	17.9	16.2	13.8	12.9	12.9	12	15.4
Ce (ppm)	0.02	31.34	38.13	33.99	42.1	37.92	33.94	30.35	30.43	29.75	35.24
Pr (ppm)	0.1	4.3	4.5	4.6	5.4	4.9	4.5	3.8	4.1	3.9	4.5
Nd (ppm)	0.1	17.6	18.5	17.4	19.8	19.4	17.4	16.5	16.6	15.5	18.7
Sm (ppm)	0.1	3.7	3.8	3.5	4.3	3.8	3.6	3.4	3.3	3.1	3.5
Eu (ppm)	0.1	0.9	0.9	0.9	1	0.9	0.9	0.8	1	0.8	0.9
Gd (ppm)	0.1	3.5	3.2	3.5	3.4	3.5	3.8	3.1	3	2.8	3.5
Tb (ppm)	0.1	0.5	0.5	0.5	0.5	0.5	0.5	0.4	0.4	0.5	0.5
Dy (ppm)	0.1	3	3.1	2.8	3.2	2.9	2.8	2.7	2.6	2.9	3.3
Y (ppm)	0.1	13.6	13.6	13.8	14.6	13.7	13.5	12.4	12.2	12.2	13.5
Ho (ppm)	0.1	0.7	0.6	0.7	0.7	0.7	0.6	0.6	0.6	0.6	0.7
Er (ppm)	0.1	1.5	1.7	1.5	1.9	1.7	1.6	1.6	1.5	1.5	1.5
Tm (ppm)	0.1	0.3	0.3	0.3	0.3	0.3	0.3	0.3	0.2	0.2	0.2
Yb (ppm)	0.1	1.5	1.8	1.6	1.7	1.5	1.5	1.6	1.5	1.5	1.5
Lu (ppm)	0.1	0.2	0.2	0.2	0.3	0.2	0.2	0.2	0.2	0.2	0.2

East Daffodil Bay (DE)		Maximum Sampled Depth (cm)									
Element	Detection Limint	42	44	46	48	50	52	54	56	58	60
Al (%)	0.01	5.09	5.08	5.21	4.79	4.86	4.9	4.95	5.21	5.14	5.57
Na (%)	0.001	2.681	2.644	2.642	2.797	2.949	2.734	2.723	2.616	2.635	2.683
K (%)	0.01	1.27	1.3	1.19	1.19	1.28	1.27	1.18	1.19	1.13	1.12
Ca (%)	0.01	2.46	2.58	2.57	2.42	2.52	2.66	2.68	2.73	2.86	3.15
Mg (%)	0.02	0.78	0.78	0.77	0.75	0.65	0.65	0.73	0.75	0.74	0.83
Fe (%)	0.01	3.23	3.44	3.26	3.11	2.55	2.7	3.06	2.96	3.03	3.44
Mn (ppm)	1	607	660	650	658	533	606	672	690	689	906
Ti (%)	0.001	0.436	0.468	0.457	0.462	0.336	0.402	0.488	0.48	0.488	0.61
P (%)	0.001	0.04	0.041	0.039	0.044	0.037	0.037	0.04	0.04	0.035	0.039
S (%)	0.04	0.16	0.18	0.15	0.18	0.22	0.13	0.16	0.14	0.17	0.12
Ni (ppm)	0.1	18.5	18.6	16.7	19.8	16.1	14.8	15.7	14.8	14.9	16.1
Cu (ppm)	0.1	9.5	9.7	8.4	9.6	9.3	7	8.1	7.1	6.6	7
Pb (ppm)	0.02	11.68	11.35	11.14	13.23	12.06	11.86	12.2	11.99	11.82	11.94
Zn (ppm)	0.2	43.5	45.1	40.3	45.8	42.2	36.5	43.2	40.1	36.3	42.6
Cr (ppm)	1	59	62	61	57	44	45	61	53	57	65
Co (ppm)	0.2	10.4	10.3	10.3	11	9.2	9.2	10.8	9.8	10.6	12.2
Cd (ppm)	0.02	0.08	0.02	0.03	0.08	0.07	0.04	0.04	0.05	0.05	0.1
As (ppm)	0.2	8.5	8.1	7	8.1	7.2	6	7.4	6.5	5.7	6
Ag (ppb)	20	24	25	27	26	35	27	27	844	24	140
Li (ppm)	0.1	22.4	20.9	18.8	22.9	20	16.8	18.2	16.6	16	13.6
Be (ppm)	1	1	1	<1	1	2	1	1	<1	1	1
Rb (ppm)	0.1	13.3	10.4	11.4	8.5	10.8	9.2	7.3	8.8	7.7	7.1
Sr (ppm)	1	398	385	409	381	394	405	400	419	419	463
Cs (ppm)	0.1	0.9	0.8	0.7	0.7	0.7	0.6	0.5	0.7	0.5	0.5
Ba (ppm)	1	363	352	359	369	399	389	366	371	339	371
Mo (ppm)	0.05	1.09	1.11	0.82	1.06	0.73	0.52	0.78	0.99	0.81	0.72
W (ppm)	0.1	0.5	0.4	0.3	0.5	0.4	0.3	0.4	0.3	0.3	0.5
Re (ppm)	0.002	<0.002	0.002	<0.002	<0.002	<0.002	<0.002	<0.002	<0.002	<0.002	<0.002
Ga (ppm)	0.02	14.99	14.93	14.03	14.53	13.81	13.82	15.22	14.28	13.81	15.57
In (ppm)	0.01	0.04	0.06	0.03	0.05	0.03	0.03	0.03	0.06	0.05	0.07
Sn (ppm)	0.1	1.4	1.4	1.2	1.4	1	1.1	1.4	1.2	1.4	1.4
Sb (ppm)	0.02	0.22	0.22	0.26	0.29	0.25	0.24	0.23	0.2	0.23	0.25
Bi (ppm)	0.04	0.1	0.1	0.1	0.13	0.11	0.08	0.09	0.1	0.09	0.1
Se (ppm)	0.3	<0.3	<0.3	<0.3	<0.3	<0.3	<0.3	<0.3	<0.3	<0.3	<0.3
Te (ppm)	0.05	<0.05	0.12	0.11	0.23	0.11	0.11	0.14	0.1	0.14	0.06
U (ppm)	0.1	1.3	1.1	1.1	1.2	1	1.1	1.1	1.3	1.3	1.4
Th (ppm)	0.1	3.7	3.7	3.6	2.9	2.1	2.9	3	4.3	4	4.3
Tl (ppm)	0.05	0.29	0.28	0.33	0.31	0.33	0.3	0.31	0.3	0.29	0.36
Zr (ppm)	0.2	20.2	20.2	19.5	20.4	17	16	18.2	18.1	16.9	17.4
Hf (ppm)	0.02	0.67	0.74	0.73	0.85	0.64	0.66	0.72	0.73	0.65	0.73
V (ppm)	1	113	120	114	109	90	96	107	107	108	124
Nb (ppm)	0.04	5.6	5.02	5.2	5.67	3.94	4.77	5.56	5.66	5.7	7.04
Ta (ppm)	0.1	0.5	0.4	0.4	0.4	0.3	0.4	0.4	0.4	0.4	0.5
Sc (ppm)	0.1	11.2	10.9	10.8	8.7	6.8	7.5	8.7	10.1	9.1	10.7
La (ppm)	0.1	14.1	13.2	14	9.4	6.3	9.1	10.4	13.6	11.9	17.4
Ce (ppm)	0.02	33.35	32.06	33.4	24.16	16.36	22.67	26.06	32.96	29.21	41.73
Pr (ppm)	0.1	4.3	4.1	4.5	3.2	2.1	3	3.3	4.4	3.8	5.6
Nd (ppm)	0.1	16.5	16.6	16.6	12.3	9.1	11.4	13.1	15.7	14.6	20.2
Sm (ppm)	0.1	3.4	3.2	3.7	2.5	1.7	2.6	2.7	3.5	3.5	4.1
Eu (ppm)	0.1	0.9	0.9	1	0.7	0.5	0.6	0.7	0.9	0.9	1
Gd (ppm)	0.1	3.4	3.1	3.4	2.5	1.8	2.4	2.9	2.8	2.9	3.6
Tb (ppm)	0.1	0.5	0.5	0.5	0.5	0.3	0.3	0.4	0.4	0.4	0.6
Dy (ppm)	0.1	2.6	2.8	2.6	2.4	1.8	2	2.5	2.7	3	2.9
Y (ppm)	0.1	12.6	11.9	12.5	10.1	7.4	9.5	10.5	11.3	11.8	15.3
Ho (ppm)	0.1	0.6	0.6	0.6	0.5	0.4	0.5	0.6	0.6	0.6	0.7
Er (ppm)	0.1	1.4	1.4	1.4	1.6	1	1.2	1.6	1.4	1.6	1.7
Tm (ppm)	0.1	0.3	0.3	0.2	0.2	0.2	0.2	0.3	0.2	0.3	0.3
Yb (ppm)	0.1	1.6	1.5	1.4	1.5	1	1.2	1.4	1.5	1.4	2
Lu (ppm)	0.1	0.2	0.2	0.2	0.2	0.2	0.2	0.2	0.3	0.2	0.3

East Daffodil Bay (DE)		Maximum Sampled Depth (cm)										
Element	Detection Limint	62	64	66	70	72	74	76	78	80	87	95
Al (%)	0.01	5.69	5.69	5.57	4.86	5.01	5.08	4.98	4.69	4.64	4.96	4.64
Na (%)	0.001	2.631	2.648	2.535	2.591	2.768	2.755	2.789	2.834	2.833	2.942	2.859
K (%)	0.01	1.16	1.16	1.1	1.29	1.41	1.43	1.45	1.38	1.44	1.55	1.4
Ca (%)	0.01	2.98	3.2	3.57	3.14	3.23	3.25	2.93	2.77	2.96	2.78	2.87
Mg (%)	0.02	0.84	0.85	0.88	0.72	0.7	0.72	0.64	0.61	0.61	0.62	0.59
Fe (%)	0.01	3.34	3.46	3.71	2.97	2.9	2.81	2.5	2.52	2.41	2.29	2.23
Mn (ppm)	1	833	876	974	684	645	617	568	549	528	469	456
Ti (%)	0.001	0.582	0.635	0.724	0.475	0.463	0.438	0.357	0.363	0.331	0.296	0.274
P (%)	0.001	0.04	0.039	0.041	0.038	0.039	0.043	0.037	0.037	0.035	0.034	0.034
S (%)	0.04	0.11	0.15	0.16	0.14	0.12	0.11	0.11	0.12	0.13	0.09	0.14
Ni (ppm)	0.1	15.3	15.7	16.4	16.1	16.2	15.6	14.1	13	13.6	12.9	14.1
Cu (ppm)	0.1	6.3	6.5	8.4	7.9	8.8	8.4	7.9	7.7	7.6	7.4	7.7
Pb (ppm)	0.02	11.3	11.92	12.18	11.85	12.33	12.26	11.59	11.5	11.44	11.63	11.77
Zn (ppm)	0.2	38	43.1	41.7	38.9	40.8	40.1	36.5	38.1	36	32.2	37.1
Cr (ppm)	1	77	73	61	50	61	45	48	48	41	34	34
Co (ppm)	0.2	11	12.1	11.9	10.7	10.4	10.1	9	8.9	8.5	8.3	8.8
Cd (ppm)	0.02	0.07	0.07	0.1	0.08	0.04	0.03	0.04	0.03	0.03	0.07	0.03
As (ppm)	0.2	5.8	6.1	6.6	7.7	8.3	7.7	7.3	7.8	7.5	7.7	8
Ag (ppb)	20	<20	164	190	33	<20	<20	<20	46	23	27	<20
Li (ppm)	0.1	15	15.5	15.3	18.4	21.1	21.1	18.3	18.1	18.7	17.9	18.8
Be (ppm)	1	1	1	1	1	1	1	1	1	1	1	1
Rb (ppm)	0.1	8.8	8.8	8	9.8	10.9	11.9	12.6	11.4	12.1	14.1	12
Sr (ppm)	1	444	464	468	412	439	439	409	390	388	406	394
Cs (ppm)	0.1	0.5	0.5	0.5	0.7	0.8	0.8	0.8	0.7	0.8	0.8	0.8
Ba (ppm)	1	359	384	350	402	437	459	447	444	443	471	458
Mo (ppm)	0.05	0.66	0.67	0.74	0.52	0.43	0.41	0.34	0.38	0.4	0.28	0.41
W (ppm)	0.1	0.5	0.5	0.4	0.3	0.4	0.3	0.3	0.3	0.3	0.2	0.3
Re (ppm)	0.002	<0.002	<0.002	<0.002	<0.002	<0.002	0.004	<0.002	<0.002	<0.002	<0.002	<0.002
Ga (ppm)	0.02	14.92	15.26	14.64	13.73	14.78	14.35	14.29	13.71	12.98	12.82	13.12
In (ppm)	0.01	0.06	0.06	0.05	0.05	0.07	0.06	0.04	0.04	0.05	0.05	0.03
Sn (ppm)	0.1	1.4	1.6	1.7	1.4	1.2	1.1	1	1.3	0.9	1	0.8
Sb (ppm)	0.02	0.24	0.25	0.28	0.27	0.26	0.26	0.24	0.24	0.22	0.19	0.2
Bi (ppm)	0.04	0.09	0.1	0.1	0.08	0.07	0.07	0.06	0.06	0.06	0.05	0.06
Se (ppm)	0.3	<0.3	<0.3	<0.3	<0.3	<0.3	<0.3	<0.3	0.4	<0.3	<0.3	<0.3
Te (ppm)	0.05	0.15	0.14	0.15	0.19	0.13	0.16	0.14	0.17	0.19	0.26	0.11
U (ppm)	0.1	1.4	1.8	1.4	1.1	1.2	1.2	1.1	1.2	1.1	0.9	0.8
Th (ppm)	0.1	5	5.8	5.1	3.3	3.6	4.7	3.2	2.1	2.5	2.1	1.5
Tl (ppm)	0.05	0.38	0.33	0.28	0.32	0.34	0.38	0.32	0.31	0.32	0.32	0.32
Zr (ppm)	0.2	16.7	17.8	19.7	16.7	17.2	16.6	14.2	14.4	14	14.1	15.2
Hf (ppm)	0.02	0.66	0.73	0.68	0.65	0.64	0.64	0.56	0.58	0.56	0.49	0.54
V (ppm)	1	120	123	138	107	103	100	86	87	83	76	74
Nb (ppm)	0.04	7.41	7.27	7.7	5.42	5.91	4.9	4.14	4.37	3.91	3.4	3.42
Ta (ppm)	0.1	0.6	0.6	0.6	0.4	0.5	0.4	0.3	0.3	0.3	0.3	0.2
Sc (ppm)	0.1	11.3	11	12	8.3	7.9	8.2	6.4	6.2	6	6.3	5.4
La (ppm)	0.1	17.8	19.9	19	10.6	9.2	9.2	7.8	6.3	6.6	6.5	5.2
Ce (ppm)	0.02	41.67	45.3	46.16	26.46	22.27	23.63	20.12	16.75	16.95	15.82	13.26
Pr (ppm)	0.1	5.7	5.9	5.8	3.2	3	3	2.5	2.3	2.2	1.9	1.6
Nd (ppm)	0.1	20.8	21.6	23.4	14.2	12.2	11.7	9.7	8.9	9	7.8	7
Sm (ppm)	0.1	4.6	4.4	4.4	3	2.4	2.5	2.1	2	1.8	2	1.5
Eu (ppm)	0.1	1.1	1	1.1	0.7	0.7	0.6	0.6	0.5	0.6	0.5	0.4
Gd (ppm)	0.1	3.5	3.9	4	3.1	2.5	2.1	2.1	1.9	2.2	1.7	1.6
Tb (ppm)	0.1	0.6	0.6	0.6	0.4	0.3	0.3	0.3	0.3	0.3	0.3	0.2
Dy (ppm)	0.1	3.4	3.3	3.6	2.5	2.2	1.7	1.9	1.7	1.6	1.6	1.4
Y (ppm)	0.1	14.6	15.4	17.1	10.8	9.6	9.8	7.8	7.3	7.2	6.8	6.1
Ho (ppm)	0.1	0.7	0.7	0.8	0.6	0.5	0.5	0.4	0.4	0.4	0.4	0.3
Er (ppm)	0.1	1.8	1.8	2.1	1.4	1.2	1.2	1	1	1	0.8	0.7
Tm (ppm)	0.1	0.3	0.3	0.3	0.2	0.2	0.2	0.2	0.2	0.2	0.1	0.1
Yb (ppm)	0.1	1.6	1.8	2	1.5	1.4	1.3	1	1.1	1	1	0.8
Lu (ppm)	0.1	0.3	0.3	0.3	0.2	0.2	0.2	0.1	0.2	0.1	0.1	0.1

Table B-4. Total elemental concentrations by ICP-MS after a multi-acid digestions of duplicate sample horizons.

		Sample Duplicates		
Element	Detection Limit	DE (80 cm)	UNA (56 cm)	DE (24 cm)
Al (%)	0.01	4.91	6.31	5.75
Na (%)	0.001	2.841	2.631	2.601
K (%)	0.01	1.46	1.51	1.29
Ca (%)	0.01	2.95	1.81	2.27
Mg (%)	0.02	0.64	1	0.92
Fe (%)	0.01	2.38	3.6	3.63
Mn (ppm)	1	498	595	623
Ti (%)	0.001	0.317	0.406	0.49
P (%)	0.001	0.036	0.053	0.05
S (%)	0.04	0.13	0.46	0.27
Ni (ppm)	0.1	14.3	30.3	24.6
Cu (ppm)	0.1	7.7	17.9	13.3
Pb (ppm)	0.02	11.67	14.1	13.14
Zn (ppm)	0.2	38.1	74.5	63.3
Cr (ppm)	1	39	54	65
Co (ppm)	0.2	9.2	13	14.7
Cd (ppm)	0.02	0.04	0.09	0.1
As (ppm)	0.2	7.8	11.5	11.2
Ag (ppb)	20	27	58	51
Li (ppm)	0.1	19.2	43.1	30
Be (ppm)	1	2	1	1
Rb (ppm)	0.1	13.7	25.6	18.9
Sr (ppm)	1	401	327	373
Cs (ppm)	0.1	0.9	1.8	1.5
Ba (ppm)	1	458	379	340
Mo (ppm)	0.05	0.36	1.16	1.64
W (ppm)	0.1	0.3	0.7	0.5
Re (ppm)	0.002	<0.002	<0.002	<0.002
Ga (ppm)	0.02	12.96	15.92	14.83
In (ppm)	0.01	0.03	0.06	0.06
Sn (ppm)	0.1	1.1	1.7	1.7
Sb (ppm)	0.02	0.22	0.31	0.33
Bi (ppm)	0.04	0.05	0.15	0.14
Se (ppm)	0.3	0.4	<0.3	<0.3
Te (ppm)	0.05	0.17	0.06	0.06
U (ppm)	0.1	1	1.4	1.7
Th (ppm)	0.1	2	3.6	5.3
Tl (ppm)	0.05	0.31	0.36	0.32
Zr (ppm)	0.2	14	30.9	27.2
Hf (ppm)	0.02	0.5	1.03	1.02
V (ppm)	1	81	112	128
Nb (ppm)	0.04	3.59	5.04	5.67
Ta (ppm)	0.1	0.3	0.4	0.4
Sc (ppm)	0.1	6.3	11.5	12.4
La (ppm)	0.1	6.2	10.8	16
Ce (ppm)	0.02	16.37	26.73	37.84
Pr (ppm)	0.1	2.1	3.5	4.9
Nd (ppm)	0.1	8.4	15.4	19.6
Sm (ppm)	0.1	1.9	3.5	3.7
Eu (ppm)	0.1	0.5	0.9	1
Gd (ppm)	0.1	1.8	3.1	3.2
Tb (ppm)	0.1	0.3	0.5	0.5
Dy (ppm)	0.1	1.8	2.8	3.5
Y (ppm)	0.1	7	12.5	13.8
Ho (ppm)	0.1	0.4	0.6	0.6
Er (ppm)	0.1	0.9	1.5	1.6
Tm (ppm)	0.1	0.1	0.2	0.3
Yb (ppm)	0.1	0.8	1.2	1.6
Lu (ppm)	0.1	0.1	0.2	0.2

Table B-5. Total elemental concentrations by ICP-MS after a multi-acid digestion of standard reference material.

		Standard Reference Material					
Element	Detection Limit	OREAS45E_IG	OREAS45E_IG	OREAS45E_IG	OREAS45E_IG	OREAS45E_IG	OREAS45E_IG
Al (%)	0.01	5.81	5.84	5.64	5.52	5.75	5.39
Na (%)	0.001	0.056	0.054	0.056	0.06	0.057	0.059
K (%)	0.01	0.31	0.31	0.34	0.33	0.34	0.35
Ca (%)	0.01	0.04	0.05	0.05	0.05	0.05	0.05
Mg (%)	0.02	0.14	0.14	0.16	0.16	0.16	0.17
Fe (%)	0.01	24.43	23.73	24.17	24.31	23.89	22.73
Mn (ppm)	1	586	561	568	576	581	546
Ti (%)	0.001	0.469	0.416	0.367	0.406	0.353	0.355
P (%)	0.001	0.034	0.032	0.036	0.036	0.034	0.033
S (%)	0.04	0.04	0.04	0.04	0.05	0.11	0.2
Ni (ppm)	0.1	456.2	452.1	455.1	454.4	504.3	494.4
Cu (ppm)	0.1	786.2	773.9	781.8	786	799.8	778.6
Pb (ppm)	0.02	18.73	18.62	19.05	18.53	20.23	20.3
Zn (ppm)	0.2	44.2	44.4	42	43.4	45.8	44.8
Cr (ppm)	1	881	888	927	917	957	914
Co (ppm)	0.2	61.8	60	59.6	60.6	64.1	61.1
Cd (ppm)	0.02	<0.02	<0.02	<0.02	<0.02	<0.02	0.02
As (ppm)	0.2	15.8	15.1	16.9	16.3	16.3	15.8
Ag (ppb)	20	290	295	321	314	321	344
Li (ppm)	0.1	7.4	7.1	7	7.1	7.1	7.1
Be (ppm)	1	<1	<1	<1	<1	<1	<1
Rb (ppm)	0.1	13.4	11.7	14.4	12	16.4	15.8
Sr (ppm)	1	13	13	14	13	16	15
Cs (ppm)	0.1	0.7	0.6	0.8	0.7	1	0.8
Ba (ppm)	1	215	219	244	216	247	233
Mo (ppm)	0.05	2.29	2.4	2.32	2.25	2.4	2.34
W (ppm)	0.1	1	0.9	1	0.9	1	0.9
Re (ppm)	0.002	<0.002	<0.002	<0.002	<0.002	<0.002	<0.002
Ga (ppm)	0.02	15.86	15.54	17.6	17.36	17.79	17.56
In (ppm)	0.01	0.08	0.1	0.08	0.12	0.07	0.08
Sn (ppm)	0.1	1.2	1.2	1.4	1.3	1.2	1.3
Sb (ppm)	0.02	1.07	1.07	1.13	1.09	1.11	1.13
Bi (ppm)	0.04	0.32	0.32	0.34	0.31	0.34	0.33
Se (ppm)	0.3	2.7	2.2	2.5	2.5	2.1	2.4
Te (ppm)	0.05	0.17	0.15	0.17	0.11	0.1	0.13
U (ppm)	0.1	2.6	2.4	2.5	2.5	2.7	2.6
Th (ppm)	0.1	5.6	5.9	7	6	8.8	8
Tl (ppm)	0.05	0.16	0.16	0.18	0.17	0.2	0.19
Zr (ppm)	0.2	86.6	82.6	80.1	82.6	77.7	77.4
Hf (ppm)	0.02	2.45	2.53	2.53	2.47	2.58	2.47
V (ppm)	1	327	323	325	324	333	322
Nb (ppm)	0.04	5.86	5.22	5.04	5.28	4.97	4.98
Ta (ppm)	0.1	0.5	0.5	0.4	0.5	0.4	0.4
Sc (ppm)	0.1	65.6	67.6	86.2	83.2	86	89.1
La (ppm)	0.1	2.1	2	2.2	1.6	3.3	2.8
Ce (ppm)	0.02	5.88	5.57	6.11	4.85	9.1	7.9
Pr (ppm)	0.1	0.7	0.7	0.8	0.6	1.1	1
Nd (ppm)	0.1	2.6	2.9	3.2	2.2	4.1	3.5
Sm (ppm)	0.1	0.8	0.6	0.8	0.5	0.9	1.1
Eu (ppm)	0.1	0.2	0.2	0.2	0.2	0.3	0.3
Gd (ppm)	0.1	0.7	0.8	1	0.6	1.3	1
Tb (ppm)	0.1	0.1	0.1	0.1	0.1	0.2	0.2
Dy (ppm)	0.1	0.8	1	1.1	1	1.4	1.3
Y (ppm)	0.1	2.6	2.3	2.6	2.2	3.8	3.2
Ho (ppm)	0.1	0.2	0.2	0.2	0.2	0.3	0.2
Er (ppm)	0.1	0.6	0.6	0.7	0.5	0.8	0.7
Tm (ppm)	0.1	0.1	<0.1	<0.1	0.1	0.1	0.1
Yb (ppm)	0.1	0.7	0.7	0.7	0.6	1	0.8
Lu (ppm)	0.1	0.1	0.1	0.1	<0.1	0.2	0.1

Table B-6. Total elemental concentrations by ICP-MS after a multi-acid digestion of reference blanks.

Element	Detection Limit	Blanks		
		Blank	Blank	Blank
Al (%)	0.01	<0.01	<0.01	<0.01
Na (%)	0.001	<0.001	0.002	0.002
K (%)	0.01	<0.01	<0.01	<0.01
Ca (%)	0.01	<0.01	<0.01	<0.01
Mg (%)	0.02	<0.02	<0.02	<0.02
Fe (%)	0.01	<0.01	<0.01	<0.01
Mn (ppm)	1	<1	<1	<1
Ti (%)	0.001	<0.001	<0.001	<0.001
P (%)	0.001	<0.001	<0.001	<0.001
S (%)	0.04	<0.04	<0.04	<0.04
Ni (ppm)	0.1	<0.1	<0.1	0.2
Cu (ppm)	0.1	<0.1	<0.1	<0.1
Pb (ppm)	0.02	<0.02	<0.02	<0.02
Zn (ppm)	0.2	<0.2	<0.2	<0.2
Cr (ppm)	1	<1	<1	<1
Co (ppm)	0.2	<0.2	<0.2	<0.2
Cd (ppm)	0.02	<0.02	<0.02	<0.02
As (ppm)	0.2	<0.2	<0.2	<0.2
Ag (ppb)	20	<20	<20	<20
Li (ppm)	0.1	<0.1	<0.1	<0.1
Be (ppm)	1	<1	<1	<1
Rb (ppm)	0.1	<0.1	<0.1	<0.1
Sr (ppm)	1	<1	<1	<1
Cs (ppm)	0.1	<0.1	<0.1	<0.1
Ba (ppm)	1	<1	<1	<1
Mo (ppm)	0.05	<0.05	<0.05	<0.05
W (ppm)	0.1	<0.1	<0.1	<0.1
Re (ppm)	0.002	<0.002	<0.002	<0.002
Ga (ppm)	0.02	<0.02	<0.02	<0.02
In (ppm)	0.01	<0.01	<0.01	<0.01
Sn (ppm)	0.1	<0.1	<0.1	<0.1
Sb (ppm)	0.02	<0.02	<0.02	<0.02
Bi (ppm)	0.04	<0.04	<0.04	<0.04
Se (ppm)	0.3	<0.3	<0.3	<0.3
Te (ppm)	0.05	<0.05	<0.05	<0.05
U (ppm)	0.1	<0.1	<0.1	<0.1
Th (ppm)	0.1	<0.1	<0.1	<0.1
Tl (ppm)	0.05	<0.05	<0.05	<0.05
Zr (ppm)	0.2	<0.2	<0.2	<0.2
Hf (ppm)	0.02	<0.02	<0.02	<0.02
V (ppm)	1	<1	<1	<1
Nb (ppm)	0.04	<0.04	<0.04	<0.04
Ta (ppm)	0.1	<0.1	<0.1	<0.1
Sc (ppm)	0.1	<0.1	<0.1	<0.1
La (ppm)	0.1	<0.1	<0.1	<0.1
Ce (ppm)	0.02	<0.02	<0.02	<0.02
Pr (ppm)	0.1	<0.1	<0.1	<0.1
Nd (ppm)	0.1	<0.1	<0.1	<0.1
Sm (ppm)	0.1	<0.1	<0.1	<0.1
Eu (ppm)	0.1	<0.1	<0.1	<0.1
Gd (ppm)	0.1	<0.1	<0.1	<0.1
Tb (ppm)	0.1	<0.1	<0.1	<0.1
Dy (ppm)	0.1	<0.1	<0.1	<0.1
Y (ppm)	0.1	<0.1	<0.1	<0.1
Ho (ppm)	0.1	<0.1	<0.1	<0.1
Er (ppm)	0.1	<0.1	<0.1	<0.1
Tm (ppm)	0.1	<0.1	<0.1	<0.1
Yb (ppm)	0.1	<0.1	<0.1	<0.1
Lu (ppm)	0.1	<0.1	<0.1	<0.1

Appendix C – Partial Geochemistry

Table C-1. Partial elemental concentrations by ICP-MS after a modified aqua regia digestion in the Upper North Arm (UNA) deep core.

Upper North Arm (UNA)		Maximum Sampled Depth (cm)									
Element	Detection Limit	2	4	6	8	10	12	14	16	18	20
Al (%)	0.01	2.44	2.52	2.53	2.47	2.48	2.44	2.37	2.36	2.26	2.4
Na (%)	0.001	0.821	0.757	0.693	0.767	0.76	0.653	0.606	0.648	0.668	0.617
K (%)	0.01	0.25	0.25	0.25	0.25	0.25	0.25	0.23	0.24	0.23	0.24
Ca (%)	0.01	0.71	0.69	0.7	0.7	0.7	0.66	0.66	0.64	0.62	0.68
Mg (%)	0.01	0.98	0.98	0.99	0.97	0.98	0.94	0.94	0.94	0.9	0.92
Fe (%)	0.01	3.53	3.59	3.53	3.55	3.52	3.38	3.28	3.35	3.3	3.39
Mn (ppm)	1	379	403	375	360	354	380	363	369	359	375
Ti (%)	0.001	0.149	0.157	0.159	0.159	0.163	0.167	0.151	0.156	0.152	0.168
P (%)	0.001	0.13	0.134	0.112	0.087	0.085	0.087	0.083	0.078	0.075	0.077
S (%)	0.02	0.35	0.42	0.48	0.69	0.7	0.53	0.48	0.53	0.55	0.6
Ni (ppm)	0.1	29.6	31.2	31.1	31.3	32.1	32.3	30.3	31.2	29.8	30.8
Cu (ppm)	0.01	24.21	25.66	25.12	25.3	25.58	26.14	24.55	24.85	24.22	24.77
Pb (ppm)	0.01	15.59	16.67	16.63	16.53	16.86	18.11	16.44	16.26	16.17	16.46
Zn (ppm)	0.1	132.7	138	139.6	139.9	144.2	148.3	138.2	138.8	135.3	136.4
Cr (ppm)	0.5	36	36.8	37.8	37.9	38	37.7	35.3	36.9	36	37.2
Co (ppm)	0.1	13.1	13.2	13.7	14.4	14.7	14.6	14	14.3	13.9	14.5
Cd (ppm)	0.01	0.14	0.16	0.16	0.15	0.14	0.14	0.14	0.12	0.13	0.14
Hg (ppb)	5	63	64	73	55	66	61	81	52	62	71
As (ppm)	0.1	8.9	9.3	8.8	9.5	9.4	8.8	7.6	8	8.5	9.1
Au (ppb)	0.2	2.2	2.4	1.3	3	2.8	2	1.4	1.8	1.6	1.8
Ag (ppb)	2	121	135	141	132	146	139	149	145	162	173
Pd (ppb)	10	<10	<10	<10	<10	<10	<10	<10	<10	<10	<10
Pt (ppb)	2	<2	<2	<2	<2	<2	<2	<2	<2	<2	<2
Li (ppm)	0.1	39.7	43.4	42.8	41.2	40.5	41.6	41.3	39.9	41.6	42.6
Be (ppm)	0.1	0.8	0.7	0.7	0.8	0.7	0.7	0.8	0.7	0.8	0.7
B (ppm)	20	<20	<20	<20	<20	<20	<20	<20	<20	<20	<20
Rb (ppm)	0.1	18	18.4	18.8	18.2	18.6	18.7	17.8	17.6	16.9	17.9
Sr (ppm)	0.5	66	63.6	62.9	60.7	59.6	59.8	54.4	56.1	55.8	58
Cs (ppm)	0.02	1.39	1.41	1.49	1.37	1.38	1.46	1.47	1.38	1.31	1.38
Ba (ppm)	0.5	34.5	36.8	35.9	33.3	33.1	34.9	33.3	33.1	31.9	33.2
Mo (ppm)	0.01	0.37	0.41	0.54	0.9	0.79	0.67	0.72	0.82	0.72	0.7
W (ppm)	0.1	<0.1	<0.1	<0.1	<0.1	<0.1	<0.1	<0.1	<0.1	<0.1	<0.1
Re (ppb)	1	<1	<1	<1	<1	<1	<1	<1	<1	1	<1
Ga (ppm)	0.1	7.5	8	7.8	7.5	7.5	7.8	7.2	7.5	7.2	7.3
Ge (ppm)	0.1	<0.1	<0.1	<0.1	<0.1	<0.1	<0.1	<0.1	<0.1	<0.1	<0.1
In (ppm)	0.02	0.04	0.04	0.04	0.03	0.04	0.04	0.04	0.03	0.03	0.04
Sn (ppm)	0.1	1.4	1.3	1.3	1.2	1.4	1.4	1.3	1.3	1.1	1.4
Sb (ppm)	0.02	0.15	0.14	0.16	0.16	0.17	0.21	0.18	0.17	0.17	0.16
Bi (ppm)	0.02	0.22	0.23	0.22	0.21	0.22	0.23	0.21	0.21	0.2	0.2
Se (ppm)	0.1	0.3	0.3	0.3	0.3	0.3	0.3	0.3	0.3	0.2	0.3
Te (ppm)	0.02	<0.02	<0.02	<0.02	0.03	<0.02	0.02	0.02	<0.02	<0.02	<0.02
U (ppm)	0.1	1.1	1.2	1.3	1.3	1.3	1.3	1.4	1.3	1.3	1.3
Th (ppm)	0.1	3.9	4.1	4.1	4.1	4.2	4.1	4	4.2	3.9	4.2
Tl (ppm)	0.02	0.11	0.11	0.11	0.1	0.1	0.11	0.1	0.1	0.09	0.1
Zr (ppm)	0.1	5.4	5.7	6.2	6.3	6.6	5.8	5.6	5.7	5.7	6.6
Hf (ppm)	0.02	0.15	0.18	0.17	0.18	0.2	0.18	0.15	0.16	0.17	0.2
V (ppm)	2	75	76	77	77	76	75	73	74	72	74
Nb (ppm)	0.02	0.8	0.84	0.87	0.76	0.73	0.79	0.62	0.7	0.78	0.78
Ta (ppm)	0.05	<0.05	<0.05	<0.05	<0.05	<0.05	<0.05	<0.05	<0.05	<0.05	<0.05
Sc (ppm)	0.1	7.8	8.2	8.1	8.3	8.1	8.4	7.8	8	7.6	8.5
La (ppm)	0.5	16.2	17	16.8	16.2	16.3	17.3	15.9	16.3	16.2	16.4
Ce (ppm)	0.1	33.5	35.3	35.4	34.1	34.9	36	33.9	34.3	33.5	34.6
Pr (ppm)	0.02	4.09	4.59	4.61	4.5	4.56	4.7	4.42	4.51	4.35	4.5
Nd (ppm)	0.02	17.04	18.5	18.24	18.05	17.45	18.44	17.37	17.73	17.48	17.93
Sm (ppm)	0.02	3.94	4.19	3.67	3.9	4	4.01	3.63	3.57	3.66	3.59
Eu (ppm)	0.02	0.9	1.03	0.91	0.91	0.91	0.93	0.9	0.98	0.97	0.91
Gd (ppm)	0.02	3.44	3.4	3.29	3.21	3.35	3.45	3.36	3.32	3.29	3.26
Tb (ppm)	0.02	0.5	0.54	0.53	0.53	0.54	0.53	0.51	0.53	0.5	0.51
Dy (ppm)	0.02	2.99	2.89	3.16	2.81	3.06	3.08	2.95	3.01	2.85	3
Y (ppm)	0.01	13.91	14.24	14.73	14.44	14.52	15.06	13.89	13.94	13.86	14.17
Ho (ppm)	0.02	0.56	0.6	0.59	0.55	0.6	0.59	0.55	0.56	0.56	0.63
Er (ppm)	0.02	1.38	1.63	1.48	1.48	1.62	1.47	1.49	1.46	1.43	1.51
Tm (ppm)	0.02	0.17	0.19	0.21	0.19	0.21	0.22	0.22	0.2	0.22	0.19
Yb (ppm)	0.02	1.12	1.22	1.28	1.23	1.28	1.29	1.17	1.1	1.18	1.22
Lu (ppm)	0.02	0.16	0.19	0.17	0.19	0.17	0.18	0.16	0.15	0.16	0.19

Upper North Arm (UNA)		Maximum Sampled Depth (cm)									
Element	Detection Limit	24	26	28	32	34	38	40	42	44	46
Al (%)	0.01	2.4	2.36	2.29	2.38	2.37	2.29	1.79	1.6	1.65	1.64
Na (%)	0.001	0.524	0.546	0.502	0.482	0.518	0.472	0.321	0.289	0.33	0.304
K (%)	0.01	0.22	0.23	0.23	0.22	0.22	0.22	0.18	0.16	0.17	0.17
Ca (%)	0.01	0.69	0.67	0.66	0.67	0.64	0.65	0.53	0.57	0.6	0.83
Mg (%)	0.01	0.91	0.9	0.88	0.88	0.88	0.86	0.69	0.63	0.66	0.65
Fe (%)	0.01	3.38	3.3	3.17	3.32	3.2	3.19	2.57	2.34	2.44	2.45
Mn (ppm)	1	383	371	348	367	347	362	301	270	286	303
Ti (%)	0.001	0.172	0.171	0.167	0.168	0.166	0.161	0.14	0.133	0.138	0.142
P (%)	0.001	0.067	0.063	0.062	0.068	0.064	0.063	0.053	0.048	0.053	0.05
S (%)	0.02	0.51	0.51	0.5	0.58	0.58	0.69	0.47	0.48	0.52	0.54
Ni (ppm)	0.1	31.5	31.5	29.1	28.7	29.7	27.8	23.2	21.3	22.6	22.7
Cu (ppm)	0.01	23.48	23.83	23.06	24.33	23.57	22.59	17.12	14.73	15.46	15.64
Pb (ppm)	0.01	16.35	17.1	17.12	20.7	19.69	17.17	12.2	9.71	10.54	10.51
Zn (ppm)	0.1	120.9	120.5	122.6	116.4	120.5	118.8	89.1	75.5	76	76.6
Cr (ppm)	0.5	36.8	37.7	35.5	36.2	35.2	35.7	27.9	26.1	27.2	28.4
Co (ppm)	0.1	13.7	13.3	13.1	13.3	13.6	14	11.6	10.1	10.7	10.4
Cd (ppm)	0.01	0.11	0.13	0.11	0.11	0.15	0.11	0.08	0.08	0.08	0.08
Hg (ppb)	5	66	46	62	53	77	62	57	43	46	44
As (ppm)	0.1	8.3	8.3	7.9	8.2	8.3	8.5	8.3	8.6	8.8	8.3
Au (ppb)	0.2	1.5	1.1	1.8	2.4	2.1	2.6	1.8	1.3	1.9	1.7
Ag (ppb)	2	197	216	219	241	199	226	155	115	136	150
Pd (ppb)	10	<10	<10	<10	<10	<10	<10	<10	<10	12	<10
Pt (ppb)	2	<2	<2	<2	<2	<2	<2	<2	<2	<2	2
Li (ppm)	0.1	43.2	37.9	39.4	41.4	41.1	39.4	30.6	27.5	30	31.1
Be (ppm)	0.1	0.7	0.6	0.7	0.8	0.7	0.7	0.5	0.5	0.6	0.6
B (ppm)	20	<20	<20	<20	<20	<20	<20	<20	<20	<20	<20
Rb (ppm)	0.1	16.2	16.4	17.3	16.3	15.5	15.4	12.9	12.1	12.8	13
Sr (ppm)	0.5	56.1	55.3	58.7	60.4	57.8	57.4	44.5	38.6	40.8	62
Cs (ppm)	0.02	1.26	1.27	1.3	1.27	1.29	1.24	1.05	0.96	0.99	1.01
Ba (ppm)	0.5	32.1	31.8	33.2	34	32.2	32.1	24.1	20.3	21.7	22.6
Mo (ppm)	0.01	0.55	0.55	0.63	0.69	0.78	0.69	0.55	0.69	0.74	0.67
W (ppm)	0.1	<0.1	<0.1	<0.1	<0.1	<0.1	<0.1	<0.1	<0.1	<0.1	<0.1
Re (ppb)	1	1	<1	1	1	<1	1	<1	1	<1	1
Ga (ppm)	0.1	7.7	7.4	7.3	7.5	7.6	7.2	5.7	4.8	5	5.3
Ge (ppm)	0.1	<0.1	<0.1	<0.1	<0.1	<0.1	<0.1	<0.1	<0.1	<0.1	<0.1
In (ppm)	0.02	0.03	0.03	0.04	0.03	0.03	0.03	0.02	0.02	<0.02	0.03
Sn (ppm)	0.1	1.2	1.2	1.2	1.3	1.3	1.5	1	0.9	1	1
Sb (ppm)	0.02	0.14	0.16	0.15	0.13	0.18	0.16	0.14	0.13	0.13	0.12
Bi (ppm)	0.02	0.19	0.19	0.18	0.21	0.21	0.23	0.23	0.2	0.22	0.2
Se (ppm)	0.1	0.2	0.3	0.2	0.2	0.2	0.2	0.2	0.1	0.1	0.1
Te (ppm)	0.02	<0.02	<0.02	<0.02	<0.02	0.02	0.03	<0.02	<0.02	<0.02	<0.02
U (ppm)	0.1	1.1	1.2	1.2	1.1	1.4	1	0.9	0.9	0.9	0.9
Th (ppm)	0.1	3.9	3.8	3.6	3.9	3.8	3.7	2.9	2.9	2.7	2.9
Tl (ppm)	0.02	0.09	0.08	0.09	0.08	0.1	0.08	0.08	0.08	0.08	0.09
Zr (ppm)	0.1	6.3	6.3	6.1	6.3	5.7	5.8	4.4	4.1	4.1	4.4
Hf (ppm)	0.02	0.22	0.19	0.17	0.2	0.16	0.14	0.13	0.14	0.12	0.16
V (ppm)	2	73	73	72	74	73	71	58	54	55	55
Nb (ppm)	0.02	0.64	0.56	0.6	0.58	0.57	0.58	0.42	0.41	0.37	0.4
Ta (ppm)	0.05	<0.05	<0.05	<0.05	<0.05	<0.05	<0.05	<0.05	<0.05	<0.05	<0.05
Sc (ppm)	0.1	8.2	7.8	7.7	7.9	7.8	7.7	6.1	5.1	5.9	5.8
La (ppm)	0.5	15.1	14.8	14.9	15.3	15.1	15	11.8	10.5	11.2	10.9
Ce (ppm)	0.1	32	31.1	30.6	32.3	32.7	32.4	24.9	22	23.6	22.6
Pr (ppm)	0.02	4.14	3.94	4.08	4.06	4.03	4.05	3.12	2.73	2.99	2.9
Nd (ppm)	0.02	16.37	15.4	15.55	15.73	15.78	16.39	12.51	10.7	11.66	12.05
Sm (ppm)	0.02	3.48	3.65	3.41	3.57	3.53	3.46	2.7	2.32	2.5	2.52
Eu (ppm)	0.02	0.89	0.87	0.88	0.89	0.92	0.85	0.65	0.58	0.59	0.62
Gd (ppm)	0.02	3.15	3	2.85	3.12	2.95	2.86	2.39	2.16	2.39	2.22
Tb (ppm)	0.02	0.5	0.49	0.47	0.46	0.5	0.48	0.38	0.32	0.36	0.35
Dy (ppm)	0.02	2.67	2.64	2.72	2.75	2.78	2.71	2.1	1.97	2.2	1.96
Y (ppm)	0.01	12.96	12.9	12.65	12.56	12.72	12.73	10.36	9.03	9.57	9.39
Ho (ppm)	0.02	0.53	0.54	0.53	0.56	0.54	0.49	0.45	0.37	0.38	0.37
Er (ppm)	0.02	1.22	1.4	1.31	1.28	1.24	1.29	1.1	0.94	0.99	0.97
Tm (ppm)	0.02	0.21	0.19	0.17	0.2	0.2	0.19	0.16	0.14	0.14	0.13
Yb (ppm)	0.02	1.12	1.15	1.03	1.16	1.18	1.07	0.89	0.74	0.78	0.8
Lu (ppm)	0.02	0.18	0.17	0.14	0.14	0.15	0.14	0.11	0.1	0.11	0.13

Upper North Arm (UNA)		Maximum Sampled Depth (cm)									
Element	Detection Limit	48	50	52	54	56	58	60	62	64	66
Al (%)	0.01	1.91	1.6	1.69	1.78	1.87	1.69	1.5	1.29	1.11	0.91
Na (%)	0.001	0.379	0.292	0.332	0.373	0.387	0.378	0.314	0.287	0.239	0.182
K (%)	0.01	0.2	0.18	0.19	0.21	0.22	0.2	0.19	0.16	0.14	0.11
Ca (%)	0.01	0.74	0.62	0.68	0.71	0.79	0.82	0.8	0.7	0.64	0.56
Mg (%)	0.01	0.77	0.68	0.73	0.78	0.82	0.77	0.69	0.63	0.55	0.46
Fe (%)	0.01	2.79	2.5	2.7	2.87	2.98	2.8	2.52	2.16	1.9	1.6
Mn (ppm)	1	343	324	372	392	408	389	339	295	266	224
Ti (%)	0.001	0.163	0.143	0.148	0.151	0.16	0.149	0.137	0.125	0.115	0.099
P (%)	0.001	0.053	0.044	0.048	0.048	0.047	0.044	0.043	0.04	0.037	0.038
S (%)	0.02	0.7	0.6	0.87	1.05	1.12	1.04	0.86	0.55	0.53	0.34
Ni (ppm)	0.1	25.6	21.1	22.5	24.1	25.1	23.1	19.5	16.3	13.8	10.6
Cu (ppm)	0.01	18.22	13.72	14.94	15.4	16.29	14.71	12.09	10.07	8.55	6.63
Pb (ppm)	0.01	11.25	7.91	8.01	8.3	9.27	7.94	6.12	4.9	3.98	2.72
Zn (ppm)	0.1	75.5	59.4	56	60.5	66.8	59.3	50.2	43.1	37.7	28.6
Cr (ppm)	0.5	31.8	26.7	29.4	29.8	32.6	30.4	26.3	21.7	19.4	16.4
Co (ppm)	0.1	10.9	9.6	9.5	9.9	10.5	9.7	8.6	7.3	6.7	5.3
Cd (ppm)	0.01	0.08	0.06	0.06	0.06	0.05	0.05	0.05	0.04	0.03	0.02
Hg (ppb)	5	41	39	27	28	43	34	36	22	10	11
As (ppm)	0.1	9	8.1	10.2	10.2	10.3	10.4	9.3	7	6.2	5.1
Au (ppb)	0.2	1.9	<0.2	1.4	0.7	0.9	0.5	17.9	0.3	<0.2	<0.2
Ag (ppb)	2	127	51	49	47	55	45	51	24	17	11
Pd (ppb)	10	<10	<10	<10	<10	<10	<10	<10	<10	<10	<10
Pt (ppb)	2	<2	<2	<2	<2	<2	<2	<2	4	<2	<2
Li (ppm)	0.1	37.9	30.6	32.3	35.1	34.8	33.4	29.7	24.7	21	15.9
Be (ppm)	0.1	0.6	0.5	0.4	0.5	0.4	0.5	0.5	0.4	0.4	0.2
B (ppm)	20	<20	<20	<20	<20	<20	<20	<20	<20	<20	<20
Rb (ppm)	0.1	15.5	14	14.9	16.4	17	16.9	15.2	13.2	11.8	8.3
Sr (ppm)	0.5	50.6	40.7	46.9	49.6	56.7	60.7	57.8	47	41.7	30.8
Cs (ppm)	0.02	1.12	1.07	1.11	1.13	1.19	1.14	1.11	0.9	0.85	0.6
Ba (ppm)	0.5	24	21.4	22.3	23.1	25	25.2	22.2	19.6	16.7	12.5
Mo (ppm)	0.01	0.73	0.65	0.9	1	1.02	0.72	0.52	0.3	0.28	0.25
W (ppm)	0.1	<0.1	<0.1	<0.1	<0.1	<0.1	<0.1	<0.1	<0.1	<0.1	<0.1
Re (ppb)	1	1	<1	<1	<1	<1	1	<1	<1	<1	<1
Ga (ppm)	0.1	5.9	5.2	5.5	5.6	5.7	5.4	4.9	4.2	3.9	3.2
Ge (ppm)	0.1	<0.1	<0.1	<0.1	<0.1	<0.1	<0.1	<0.1	<0.1	<0.1	<0.1
In (ppm)	0.02	0.03	0.02	<0.02	<0.02	0.02	0.02	<0.02	<0.02	<0.02	<0.02
Sn (ppm)	0.1	1	0.8	0.7	0.8	0.8	0.7	0.6	0.5	0.4	0.4
Sb (ppm)	0.02	0.14	0.11	0.13	0.13	0.16	0.12	0.1	0.08	0.08	0.05
Bi (ppm)	0.02	0.16	0.17	0.13	0.13	0.14	0.12	0.09	0.06	0.05	0.04
Se (ppm)	0.1	0.2	0.3	0.3	0.3	0.3	0.3	<0.1	<0.1	<0.1	<0.1
Te (ppm)	0.02	<0.02	<0.02	<0.02	<0.02	<0.02	<0.02	<0.02	<0.02	<0.02	<0.02
U (ppm)	0.1	1.1	0.9	0.9	0.9	1	0.8	0.6	0.6	0.4	0.5
Th (ppm)	0.1	3.4	2.7	2.9	3	3.2	3	3	3.1	2.2	1.9
Tl (ppm)	0.02	0.08	0.07	0.09	0.09	0.09	0.09	0.1	0.08	0.08	0.07
Zr (ppm)	0.1	4.9	4	4.3	4.7	4.8	4.4	4.2	4.2	3.6	3.3
Hf (ppm)	0.02	0.15	0.12	0.12	0.12	0.14	0.14	0.12	0.13	0.11	0.11
V (ppm)	2	63	55	58	61	62	57	52	47	41	37
Nb (ppm)	0.02	0.41	0.33	0.35	0.39	0.47	0.42	0.36	0.3	0.25	0.22
Ta (ppm)	0.05	<0.05	<0.05	<0.05	<0.05	<0.05	<0.05	<0.05	<0.05	<0.05	<0.05
Sc (ppm)	0.1	6.5	5.5	5.7	5.9	6.4	5.7	5.3	4.5	4	3.2
La (ppm)	0.5	11.9	9.8	10.3	10.5	11.1	10.6	9.9	8.3	7	6.3
Ce (ppm)	0.1	26.3	21	22.4	22.5	24	22.6	20.5	17.6	14.6	12.9
Pr (ppm)	0.02	3.48	2.69	2.83	2.84	3.12	3.04	2.59	2.24	1.93	1.67
Nd (ppm)	0.02	13.11	10.65	10.77	11.22	12.18	11.51	10.01	8.82	7.19	6.39
Sm (ppm)	0.02	2.69	2.28	2.5	2.76	2.87	2.46	2.09	1.94	1.66	1.58
Eu (ppm)	0.02	0.66	0.57	0.52	0.62	0.65	0.58	0.55	0.44	0.38	0.33
Gd (ppm)	0.02	2.65	2.14	2.03	2.11	2.47	2.16	1.93	1.67	1.53	1.16
Tb (ppm)	0.02	0.4	0.33	0.36	0.35	0.38	0.35	0.32	0.27	0.22	0.19
Dy (ppm)	0.02	2.34	1.84	1.82	2.07	2.12	1.91	1.81	1.43	1.3	1.14
Y (ppm)	0.01	10.23	8.45	8.75	9.22	9.71	9.02	7.94	6.94	6.04	5.03
Ho (ppm)	0.02	0.47	0.36	0.36	0.39	0.41	0.35	0.36	0.3	0.25	0.21
Er (ppm)	0.02	1.13	0.87	0.89	0.97	1.09	0.96	0.88	0.77	0.63	0.54
Tm (ppm)	0.02	0.16	0.12	0.13	0.14	0.17	0.13	0.12	0.1	0.08	0.07
Yb (ppm)	0.02	0.9	0.81	0.83	0.81	0.82	0.8	0.76	0.65	0.55	0.44
Lu (ppm)	0.02	0.12	0.11	0.11	0.11	0.11	0.11	0.1	0.1	0.09	0.05

Upper North Arm (UNA)		Maximum Sampled Depth (cm)			
Element	Detection Limit	68	70	78	85
Al (%)	0.01	0.82	0.85	0.88	0.95
Na (%)	0.001	0.16	0.148	0.16	0.171
K (%)	0.01	0.1	0.1	0.1	0.12
Ca (%)	0.01	0.49	0.46	0.49	0.56
Mg (%)	0.01	0.42	0.42	0.43	0.46
Fe (%)	0.01	1.44	1.47	1.56	1.68
Mn (ppm)	1	208	196	194	205
Ti (%)	0.001	0.097	0.093	0.097	0.1
P (%)	0.001	0.039	0.033	0.035	0.037
S (%)	0.02	0.27	0.3	0.33	0.38
Ni (ppm)	0.1	10.5	10.1	11	11.8
Cu (ppm)	0.01	7.73	6.3	6.69	7.73
Pb (ppm)	0.01	2.74	2.75	2.99	3.3
Zn (ppm)	0.1	28.6	27.5	27.4	29.7
Cr (ppm)	0.5	14.9	14.3	15.8	17
Co (ppm)	0.1	5.3	5.2	5.4	5.4
Cd (ppm)	0.01	0.02	0.02	0.03	0.03
Hg (ppb)	5	6	7	7	7
As (ppm)	0.1	5	5.2	5.8	6.4
Au (ppb)	0.2	0.3	<0.2	<0.2	<0.2
Ag (ppb)	2	9	11	13	10
Pd (ppb)	10	<10	<10	<10	<10
Pt (ppb)	2	<2	<2	<2	<2
Li (ppm)	0.1	14.9	15	16	18.5
Be (ppm)	0.1	0.2	0.3	0.3	0.3
B (ppm)	20	<20	<20	<20	<20
Rb (ppm)	0.1	7.3	7.8	8	9.1
Sr (ppm)	0.5	27.5	25	29	36.5
Cs (ppm)	0.02	0.56	0.57	0.59	0.67
Ba (ppm)	0.5	11.5	11.4	11.1	13.1
Mo (ppm)	0.01	0.24	0.34	0.48	0.43
W (ppm)	0.1	<0.1	<0.1	<0.1	<0.1
Re (ppb)	1	<1	<1	<1	<1
Ga (ppm)	0.1	2.9	2.9	3	3.3
Ge (ppm)	0.1	<0.1	<0.1	<0.1	<0.1
In (ppm)	0.02	<0.02	<0.02	<0.02	<0.02
Sn (ppm)	0.1	0.3	0.3	0.4	0.4
Sb (ppm)	0.02	0.06	0.06	0.07	0.08
Bi (ppm)	0.02	0.03	0.03	0.04	0.04
Se (ppm)	0.1	<0.1	<0.1	<0.1	0.1
Te (ppm)	0.02	<0.02	<0.02	<0.02	<0.02
U (ppm)	0.1	0.4	0.4	0.4	0.5
Th (ppm)	0.1	2.4	1.8	1.7	2.5
Tl (ppm)	0.02	0.06	0.06	0.06	0.06
Zr (ppm)	0.1	3.6	3.2	3.3	3.2
Hf (ppm)	0.02	0.1	0.08	0.08	0.08
V (ppm)	2	34	34	36	38
Nb (ppm)	0.02	0.22	0.22	0.25	0.24
Ta (ppm)	0.05	<0.05	<0.05	<0.05	<0.05
Sc (ppm)	0.1	3.3	3.1	3.3	3.6
La (ppm)	0.5	6.4	6.1	5.9	6.1
Ce (ppm)	0.1	12.5	12.3	12.1	12.9
Pr (ppm)	0.02	1.68	1.59	1.56	1.75
Nd (ppm)	0.02	6.04	6.19	6.01	6.17
Sm (ppm)	0.02	1.35	1.32	1.49	1.34
Eu (ppm)	0.02	0.38	0.31	0.33	0.31
Gd (ppm)	0.02	1.1	1.16	1	1.17
Tb (ppm)	0.02	0.18	0.18	0.19	0.19
Dy (ppm)	0.02	1	1.06	1.07	1.05
Y (ppm)	0.01	4.9	4.77	5.12	5.33
Ho (ppm)	0.02	0.21	0.2	0.21	0.22
Er (ppm)	0.02	0.52	0.51	0.57	0.61
Tm (ppm)	0.02	0.07	0.07	0.08	0.1
Yb (ppm)	0.02	0.45	0.49	0.44	0.51
Lu (ppm)	0.02	0.06	0.06	0.06	0.07

Table C-2. Partial elemental concentrations by ICP-MS after a modified aqua regia digestion in the Lower Waihopai Arm (LW) deep core.

Lower Waihopai Arm (LW)		Maximum Sampled Depth (cm)									
Element	Detection Limit	2	4	6	8	10	12	14	16	18	20
Al (%)	0.01	2.12	2.18	2.15	2.26	2.25	2.22	2.07	2.02	1.94	1.5
Na (%)	0.001	0.588	0.661	0.628	0.634	0.639	0.64	0.568	0.45	0.493	0.348
K (%)	0.01	0.21	0.22	0.21	0.22	0.22	0.22	0.2	0.19	0.18	0.14
Ca (%)	0.01	0.62	0.63	0.63	0.66	0.65	0.66	0.66	0.62	0.84	1.02
Mg (%)	0.01	0.83	0.85	0.82	0.86	0.85	0.85	0.79	0.74	0.71	0.57
Fe (%)	0.01	2.99	3.07	3.08	3.14	3.14	3.06	2.84	2.82	2.73	2.32
Mn (ppm)	1	329	335	323	335	329	341	309	296	301	264
Ti (%)	0.001	0.146	0.148	0.155	0.161	0.162	0.159	0.157	0.15	0.154	0.138
P (%)	0.001	0.09	0.078	0.073	0.065	0.064	0.065	0.061	0.062	0.053	0.047
S (%)	0.02	0.5	0.62	0.74	0.75	0.76	0.7	0.56	0.53	0.63	0.61
Ni (ppm)	0.1	27.4	28.4	28.2	29.1	29.6	29.1	27	25.7	25.3	20
Cu (ppm)	0.01	21.87	23.28	22.88	23.41	22.56	22.48	20.63	19.08	20.17	14.4
Pb (ppm)	0.01	12.47	13.36	12.76	13.54	13.52	13.65	12.9	12.09	12.98	9.36
Zn (ppm)	0.1	95.8	101	99.9	105.1	105.3	100.2	99.2	90.7	92.9	69.8
Cr (ppm)	0.5	33.7	34.2	32.9	36.4	35.9	35.2	33.1	31.4	32.6	27.6
Co (ppm)	0.1	12.2	13.3	13.3	13.7	13	13.8	13.1	12.9	13.4	10.9
Cd (ppm)	0.01	0.11	0.14	0.12	0.13	0.13	0.11	0.1	0.1	0.11	0.08
Hg (ppb)	5	58	57	48	51	55	63	64	45	43	40
As (ppm)	0.1	8.1	8.8	9.4	9	9.9	9.2	8.5	10	10.5	9.7
Au (ppb)	0.2	1.4	0.8	2.3	1.6	1.1	1.3	0.8	2.3	1.7	1.3
Ag (ppb)	2	97	102	94	102	98	115	102	107	170	106
Pd (ppb)	10	<10	<10	<10	<10	<10	<10	<10	<10	<10	<10
Pt (ppb)	2	<2	<2	<2	4	<2	<2	<2	<2	2	<2
Li (ppm)	0.1	37	40.1	36.8	38.8	39.8	38.2	35.8	34.5	32.8	27.9
Be (ppm)	0.1	0.7	0.6	0.6	0.7	0.7	0.6	0.7	0.6	0.6	0.4
B (ppm)	20	<20	<20	<20	<20	<20	<20	<20	<20	<20	<20
Rb (ppm)	0.1	15.7	15.7	15.7	16.1	16.4	15.8	15.1	14.1	13.9	11
Sr (ppm)	0.5	52	53	53.1	55.7	55.5	54.2	52.1	48.2	61.2	67.1
Cs (ppm)	0.02	1.33	1.27	1.25	1.32	1.36	1.27	1.2	1.14	1.13	0.88
Ba (ppm)	0.5	27.9	27.2	25.2	27	26.5	27	25	23.8	23.2	18
Mo (ppm)	0.01	0.81	1.08	1.32	1.44	1.6	1.28	1.19	1.14	1.12	0.89
W (ppm)	0.1	<0.1	<0.1	<0.1	<0.1	<0.1	<0.1	<0.1	<0.1	<0.1	<0.1
Re (ppb)	1	1	1	1	2	<1	2	3	<1	2	1
Ga (ppm)	0.1	6.6	6.8	7	7.2	7.2	7.1	6.6	6.3	6.2	4.8
Ge (ppm)	0.1	<0.1	<0.1	<0.1	<0.1	<0.1	<0.1	<0.1	<0.1	<0.1	<0.1
In (ppm)	0.02	0.03	0.03	0.03	0.02	0.03	0.03	0.03	0.03	0.02	<0.02
Sn (ppm)	0.1	1.1	1	1	1.1	1.1	1	1	1	1	0.8
Sb (ppm)	0.02	0.15	0.14	0.17	0.17	0.17	0.15	0.14	0.14	0.15	0.16
Bi (ppm)	0.02	0.19	0.19	0.21	0.21	0.22	0.2	0.19	0.17	0.18	0.15
Se (ppm)	0.1	0.3	0.4	0.3	0.3	0.3	0.3	0.2	0.2	0.3	0.1
Te (ppm)	0.02	<0.02	<0.02	0.03	<0.02	<0.02	<0.02	0.03	<0.02	<0.02	<0.02
U (ppm)	0.1	1.4	1.4	1.5	1.6	1.7	1.5	1.4	1.4	1.5	1.3
Th (ppm)	0.1	5.6	3.7	3.6	3.9	3.9	4	3.8	3.6	4.7	4.7
Tl (ppm)	0.02	0.12	0.11	0.11	0.12	0.12	0.12	0.12	0.12	0.12	0.12
Zr (ppm)	0.1	4.7	5.8	6	6.5	6.7	6.6	6.4	5.3	6	4.9
Hf (ppm)	0.02	0.14	0.17	0.19	0.17	0.22	0.21	0.18	0.17	0.16	0.16
V (ppm)	2	66	68	68	71	70	70	68	66	65	57
Nb (ppm)	0.02	0.67	0.88	0.79	0.72	0.76	0.84	0.82	0.71	0.7	0.52
Ta (ppm)	0.05	<0.05	<0.05	<0.05	<0.05	<0.05	<0.05	<0.05	<0.05	<0.05	<0.05
Sc (ppm)	0.1	7.7	7.7	8.1	8.1	8	7.9	7.5	7.1	7.1	5.7
La (ppm)	0.5	14.6	14.7	14	15	15.1	15.3	14.6	13.7	14.2	12.6
Ce (ppm)	0.1	30.8	31.4	29.6	31.9	31.6	31.8	31	28.1	29.9	25.5
Pr (ppm)	0.02	3.96	4.22	3.82	4.16	4.14	4.21	3.75	3.68	3.8	3.37
Nd (ppm)	0.02	14.85	15.83	15.58	16.08	16.42	16.32	15.23	14.7	14.93	12.26
Sm (ppm)	0.02	3.29	3.43	3.36	3.46	3.52	3.46	3.16	3.18	3.03	2.36
Eu (ppm)	0.02	0.85	0.87	0.74	0.82	0.95	0.88	0.85	0.77	0.85	0.64
Gd (ppm)	0.02	3.12	3	2.99	3.25	3.1	3.17	3.29	2.73	2.93	2.28
Tb (ppm)	0.02	0.47	0.47	0.46	0.51	0.49	0.49	0.47	0.44	0.43	0.34
Dy (ppm)	0.02	2.55	2.51	2.75	2.74	2.85	2.74	2.55	2.48	2.38	1.99
Y (ppm)	0.01	12.1	12.14	11.99	12.91	12.72	12.6	11.89	10.99	11.41	9.08
Ho (ppm)	0.02	0.53	0.5	0.52	0.55	0.55	0.57	0.5	0.46	0.47	0.38
Er (ppm)	0.02	1.29	1.35	1.25	1.45	1.35	1.34	1.36	1.17	1.27	1.06
Tm (ppm)	0.02	0.18	0.2	0.19	0.22	0.18	0.18	0.16	0.17	0.19	0.15
Yb (ppm)	0.02	1.12	1.09	1.14	1.23	1.19	1.09	1.09	0.99	0.98	0.8
Lu (ppm)	0.02	0.14	0.14	0.14	0.17	0.15	0.17	0.15	0.15	0.16	0.12

Lower Waihopai Arm (LW)		Maximum Sampled Depth (cm)				
Element	Detection Limit	22	24	26	28	30
Al (%)	0.01	1.39	1.18	1.43	1.16	1.16
Na (%)	0.001	0.339	0.259	0.336	0.292	0.249
K (%)	0.01	0.14	0.12	0.14	0.12	0.11
Ca (%)	0.01	0.79	0.53	0.62	1.78	1.6
Mg (%)	0.01	0.56	0.48	0.59	0.47	0.45
Fe (%)	0.01	2.29	2.1	2.38	2.03	2.11
Mn (ppm)	1	267	254	299	248	253
Ti (%)	0.001	0.136	0.126	0.137	0.122	0.123
P (%)	0.001	0.043	0.033	0.036	0.034	0.036
S (%)	0.02	0.74	0.81	1.02	0.89	0.95
Ni (ppm)	0.1	20.6	16.4	21.7	14.9	14.4
Cu (ppm)	0.01	13.19	10.09	12.46	8.97	8.71
Pb (ppm)	0.01	7.86	5.58	6.94	5	5.17
Zn (ppm)	0.1	55.3	40.1	47.2	36	35.6
Cr (ppm)	0.5	28.4	25.4	30.3	22.5	21.1
Co (ppm)	0.1	9.7	7.3	8.7	6.9	7
Cd (ppm)	0.01	0.06	0.05	0.05	0.04	0.05
Hg (ppb)	5	35	19	27	16	23
As (ppm)	0.1	9.5	9	10.2	10.2	12.4
Au (ppb)	0.2	0.7	0.6	0.8	0.7	1.7
Ag (ppb)	2	95	50	44	25	24
Pd (ppb)	10	<10	<10	<10	<10	<10
Pt (ppb)	2	<2	<2	<2	<2	<2
Li (ppm)	0.1	27.3	21.6	27.8	22.7	21.9
Be (ppm)	0.1	0.4	0.4	0.4	0.4	0.3
B (ppm)	20	<20	<20	<20	<20	<20
Rb (ppm)	0.1	10.3	9.4	11.4	8.9	8.5
Sr (ppm)	0.5	53.1	35.6	43.7	113.9	105.8
Cs (ppm)	0.02	0.82	0.73	0.91	0.72	0.69
Ba (ppm)	0.5	16.4	14.1	17	13.8	13.9
Mo (ppm)	0.01	0.95	0.95	1.11	1.2	1.48
W (ppm)	0.1	<0.1	<0.1	<0.1	<0.1	<0.1
Re (ppb)	1	<1	<1	2	<1	6
Ga (ppm)	0.1	4.5	4.1	4.8	4	3.8
Ge (ppm)	0.1	<0.1	<0.1	<0.1	<0.1	<0.1
In (ppm)	0.02	0.03	<0.02	<0.02	<0.02	<0.02
Sn (ppm)	0.1	0.7	0.6	0.7	0.4	0.5
Sb (ppm)	0.02	0.15	0.12	0.15	0.12	0.22
Bi (ppm)	0.02	0.13	0.1	0.11	0.08	0.08
Se (ppm)	0.1	0.2	0.1	0.2	0.2	0.2
Te (ppm)	0.02	<0.02	<0.02	<0.02	<0.02	<0.02
U (ppm)	0.1	1.4	1.1	1.2	1.2	2.4
Th (ppm)	0.1	3.7	4.5	3.6	2.8	4.7
Tl (ppm)	0.02	0.12	0.12	0.13	0.13	0.11
Zr (ppm)	0.1	4.2	4.1	5.1	4.4	4.4
Hf (ppm)	0.02	0.09	0.11	0.13	0.13	0.13
V (ppm)	2	54	50	52	47	49
Nb (ppm)	0.02	0.38	0.35	0.3	0.31	0.31
Ta (ppm)	0.05	<0.05	<0.05	<0.05	<0.05	<0.05
Sc (ppm)	0.1	5.4	4.5	5.4	4.4	4.5
La (ppm)	0.5	11.6	10.8	11.5	11.1	12.6
Ce (ppm)	0.1	23.9	21.6	23.3	21.3	23.8
Pr (ppm)	0.02	2.98	2.72	2.98	2.77	3.11
Nd (ppm)	0.02	11.24	10.37	11.5	10.53	11.84
Sm (ppm)	0.02	2.47	2.06	2.41	2.26	2.06
Eu (ppm)	0.02	0.56	0.54	0.61	0.54	0.54
Gd (ppm)	0.02	2.1	1.9	2.22	2.14	2.02
Tb (ppm)	0.02	0.35	0.28	0.34	0.28	0.29
Dy (ppm)	0.02	1.72	1.59	1.82	1.58	1.6
Y (ppm)	0.01	8.45	7.29	8.59	7.21	7.31
Ho (ppm)	0.02	0.38	0.32	0.38	0.32	0.31
Er (ppm)	0.02	0.82	0.82	0.99	0.84	0.82
Tm (ppm)	0.02	0.13	0.11	0.13	0.1	0.11
Yb (ppm)	0.02	0.78	0.63	0.79	0.64	0.73
Lu (ppm)	0.02	0.11	0.09	0.12	0.11	0.1

Table C-3. Partial elemental concentrations by ICP-MS after a modified aqua regia digestion in the East Daffodil Bay (DE) deep core.

East Daffodil Bay (DE)		Maximum Sampled Depth (cm)									
Element	Detection Limit	2	4	6	8	10	12	14	16	18	20
Al (%)	0.01	2.34	1.68	1.58	1.69	1.7	1.57	1.53	1.52	1.47	1.48
Na (%)	0.001	0.789	0.675	0.633	0.678	0.667	0.52	0.562	0.514	0.52	0.54
K (%)	0.01	0.28	0.2	0.19	0.2	0.2	0.18	0.18	0.17	0.17	0.17
Ca (%)	0.01	0.71	0.66	0.6	0.62	0.63	0.62	0.61	0.61	0.61	0.62
Mg (%)	0.01	0.94	0.71	0.68	0.71	0.71	0.65	0.65	0.64	0.63	0.64
Fe (%)	0.01	3.45	2.54	2.46	2.56	2.56	2.4	2.38	2.35	2.29	2.33
Mn (ppm)	1	343	267	271	275	279	263	263	252	236	254
Ti (%)	0.001	0.165	0.138	0.135	0.135	0.14	0.13	0.131	0.127	0.127	0.126
P (%)	0.001	0.067	0.05	0.053	0.051	0.051	0.049	0.051	0.049	0.046	0.046
S (%)	0.02	1.15	0.8	0.81	0.87	0.83	0.77	0.76	0.72	0.7	0.69
Ni (ppm)	0.1	29.2	20.8	19.9	20.9	20.4	18.3	18.8	18.7	17.7	18.8
Cu (ppm)	0.01	23.52	16.36	15.78	16.76	16.36	14.9	14.64	13.91	13.39	13.44
Pb (ppm)	0.01	12.68	8.47	8.43	8.89	8.58	7.56	7.5	7.36	6.85	7.47
Zn (ppm)	0.1	84.1	64.2	65.7	67.2	67	58.7	60.8	58.1	54.7	57.1
Cr (ppm)	0.5	35.6	25.9	26.1	27.1	26.8	24.8	25.2	24.5	22.8	24.3
Co (ppm)	0.1	11.7	9.5	9.3	9.4	9.6	9	8.8	8.6	8.5	9
Cd (ppm)	0.01	0.11	0.1	0.09	0.09	0.1	0.07	0.07	0.05	0.09	0.07
Hg (ppb)	5	57	42	31	37	40	38	40	36	34	26
As (ppm)	0.1	11.4	8.2	8.5	8.6	8.4	8.1	9	8.6	8.6	8.9
Au (ppb)	0.2	0.2	0.4	2.5	1.1	0.6	0.9	<0.2	0.5	<0.2	<0.2
Ag (ppb)	2	75	48	51	50	45	43	50	46	43	48
Pd (ppb)	10	<10	<10	<10	<10	<10	<10	<10	<10	<10	<10
Pt (ppb)	2	2	<2	<2	<2	<2	<2	<2	<2	<2	<2
Li (ppm)	0.1	45.2	30.4	30.1	33	30.3	28.6	28	27.8	27.9	27.1
Be (ppm)	0.1	0.9	0.6	0.4	0.5	0.5	0.6	0.4	0.5	0.4	0.4
B (ppm)	20	<20	<20	<20	<20	<20	<20	<20	<20	<20	<20
Rb (ppm)	0.1	18.4	13.4	13.2	13.6	13.7	12.5	12.4	11.7	11.6	11.7
Sr (ppm)	0.5	59.5	47	41.9	43.4	44.4	40.7	41.4	39.5	39.5	39.9
Cs (ppm)	0.02	1.43	1.14	1.12	1.15	1.21	1.06	1.05	1.03	0.97	1
Ba (ppm)	0.5	27.1	18.9	19	21	20.3	18.2	18.3	16.7	16.6	17.2
Mo (ppm)	0.01	2.37	2	2.29	2.6	2.23	2.38	1.96	2.21	1.73	1.49
W (ppm)	0.1	<0.1	<0.1	<0.1	<0.1	<0.1	<0.1	<0.1	<0.1	<0.1	<0.1
Re (ppb)	1	1	3	2	2	<1	3	3	<1	3	2
Ga (ppm)	0.1	7.4	5.4	5.1	5.4	5.3	5.1	5	4.9	4.8	5
Ge (ppm)	0.1	<0.1	<0.1	<0.1	<0.1	<0.1	<0.1	<0.1	<0.1	<0.1	<0.1
In (ppm)	0.02	0.03	0.02	0.02	0.02	0.02	0.02	0.03	0.03	0.03	<0.02
Sn (ppm)	0.1	1	0.7	0.7	0.7	0.7	0.6	0.7	0.6	0.6	0.7
Sb (ppm)	0.02	0.13	0.11	0.12	0.14	0.13	0.12	0.13	0.14	0.13	0.11
Bi (ppm)	0.02	0.27	0.13	0.12	0.13	0.12	0.11	0.11	0.11	0.1	0.11
Se (ppm)	0.1	0.4	0.3	0.2	0.3	0.2	0.3	0.2	0.3	0.1	0.2
Te (ppm)	0.02	<0.02	<0.02	<0.02	<0.02	<0.02	<0.02	<0.02	<0.02	0.02	<0.02
U (ppm)	0.1	2.2	1.6	1.6	1.8	1.7	1.6	1.3	1.6	1.2	1.1
Th (ppm)	0.1	4.2	3.4	3.4	3.2	3.6	4.2	3.1	4.1	3.1	3.1
Tl (ppm)	0.02	0.19	0.18	0.17	0.16	0.16	0.15	0.15	0.14	0.13	0.15
Zr (ppm)	0.1	6.6	5.6	4.9	5	5.4	4.9	4.9	4.5	4.7	4.7
Hf (ppm)	0.02	0.22	0.17	0.13	0.17	0.15	0.15	0.15	0.12	0.14	0.14
V (ppm)	2	77	60	59	60	61	59	58	58	56	57
Nb (ppm)	0.02	0.73	0.73	0.53	0.52	0.59	0.49	0.4	0.34	0.4	0.38
Ta (ppm)	0.05	<0.05	<0.05	<0.05	<0.05	<0.05	<0.05	<0.05	<0.05	<0.05	<0.05
Sc (ppm)	0.1	8	6	5.8	5.9	5.8	5.3	5.5	5.3	5.1	5
La (ppm)	0.5	13.9	11	11	11.1	11.1	10.6	10.4	10	10.3	10.1
Ce (ppm)	0.1	29.7	22.7	23.4	23.2	23.6	21.9	21.8	21.6	21	20.9
Pr (ppm)	0.02	3.8	3.06	2.94	2.93	3.03	2.71	2.91	2.87	2.74	2.64
Nd (ppm)	0.02	15.35	11.7	11.91	12.17	11.91	11.15	11	10.72	11.35	10.65
Sm (ppm)	0.02	3.12	2.54	2.38	2.59	2.67	2.64	2.27	2.29	2.42	2.4
Eu (ppm)	0.02	0.83	0.65	0.57	0.62	0.62	0.59	0.57	0.6	0.54	0.62
Gd (ppm)	0.02	3.08	2.12	2.29	2.36	2.37	2.2	1.98	1.96	2.17	2.07
Tb (ppm)	0.02	0.47	0.36	0.36	0.36	0.37	0.36	0.34	0.33	0.29	0.33
Dy (ppm)	0.02	2.69	2.06	2.03	2	2.11	2.04	1.92	1.77	1.69	1.84
Y (ppm)	0.01	11.55	8.75	8.8	9.03	9.14	8.56	8.46	8.33	7.94	8.11
Ho (ppm)	0.02	0.49	0.39	0.4	0.42	0.41	0.38	0.37	0.33	0.35	0.34
Er (ppm)	0.02	1.4	0.97	1.03	1.05	1.03	0.88	0.95	0.97	0.91	0.89
Tm (ppm)	0.02	0.18	0.14	0.14	0.15	0.15	0.14	0.12	0.12	0.11	0.12
Yb (ppm)	0.02	1.08	0.91	0.84	0.87	0.9	0.76	0.77	0.72	0.8	0.73
Lu (ppm)	0.02	0.14	0.12	0.12	0.12	0.13	0.11	0.1	0.12	0.1	0.11

East Daffodil Bay (DE)		Maximum Sampled Depth (cm)									
Element	Detection Limit	22	24	26	28	30	32	34	36	38	40
Al (%)	0.01	1.47	1.37	1.36	1.37	1.32	1.34	1.37	1.22	1.18	1.15
Na (%)	0.001	0.555	0.463	0.459	0.445	0.468	0.426	0.492	0.386	0.344	0.354
K (%)	0.01	0.17	0.15	0.15	0.15	0.14	0.14	0.15	0.13	0.12	0.12
Ca (%)	0.01	0.6	0.56	0.55	0.58	0.56	0.57	0.6	0.59	0.59	0.6
Mg (%)	0.01	0.63	0.59	0.59	0.58	0.56	0.56	0.59	0.53	0.51	0.52
Fe (%)	0.01	2.3	2.26	2.24	2.24	2.18	2.19	2.26	2.07	2	2.01
Mn (ppm)	1	248	230	232	231	224	223	236	221	208	202
Ti (%)	0.001	0.132	0.122	0.123	0.126	0.12	0.123	0.124	0.118	0.118	0.118
P (%)	0.001	0.051	0.049	0.049	0.045	0.045	0.045	0.045	0.046	0.043	0.043
S (%)	0.02	0.67	0.62	0.6	0.61	0.63	0.61	0.62	0.5	0.44	0.48
Ni (ppm)	0.1	19.2	16.8	16.6	16.5	15.8	16.2	16.8	14.8	13.8	14
Cu (ppm)	0.01	14.1	12.78	13.07	12.7	11.82	11.53	12.2	10.15	9.69	9.77
Pb (ppm)	0.01	7.87	7.05	7.24	6.79	6.35	6.45	6.72	5.41	5.18	4.71
Zn (ppm)	0.1	57.6	52.9	53.2	52.3	49.6	49.9	48.4	42	41.5	36.1
Cr (ppm)	0.5	23.8	22.5	22	22.1	20.9	22	23.4	21.6	20.4	19.9
Co (ppm)	0.1	8.7	8.3	8.6	8.2	7.9	7.6	7.9	6.9	6.8	6.2
Cd (ppm)	0.01	0.08	0.06	0.08	0.06	0.07	0.07	0.06	0.05	0.04	0.03
Hg (ppb)	5	25	29	27	30	26	30	32	32	27	18
As (ppm)	0.1	9.3	10	9.6	9.5	9.6	8.9	9	8.8	8.3	8.6
Au (ppb)	0.2	<0.2	0.8	0.4	1.1	0.5	0.5	<0.2	<0.2	0.7	0.3
Ag (ppb)	2	50	48	54	47	45	49	44	30	30	22
Pd (ppb)	10	<10	<10	<10	<10	<10	<10	<10	<10	<10	<10
Pt (ppb)	2	<2	<2	<2	<2	<2	<2	<2	3	<2	<2
Li (ppm)	0.1	25.8	25.1	25.3	24.3	23.4	25.6	25.6	22.3	23.2	21.7
Be (ppm)	0.1	0.6	0.3	0.4	0.4	0.4	0.4	0.4	0.5	0.4	0.3
B (ppm)	20	<20	<20	<20	<20	<20	<20	<20	<20	<20	<20
Rb (ppm)	0.1	12	10.3	10.5	10.7	9.9	9.9	10.3	9.1	8.8	8.8
Sr (ppm)	0.5	41	37	36.8	38.8	36	36.7	38.8	35.1	34.2	34.7
Cs (ppm)	0.02	0.99	0.88	0.92	0.88	0.84	0.85	0.87	0.73	0.69	0.71
Ba (ppm)	0.5	17.1	15	16	15	14	14.2	15.2	14.2	13	13
Mo (ppm)	0.01	1.47	1.39	1.31	1.24	1.14	0.99	1.05	0.96	0.84	0.85
W (ppm)	0.1	<0.1	<0.1	<0.1	<0.1	<0.1	<0.1	<0.1	<0.1	<0.1	<0.1
Re (ppb)	1	3	<1	<1	<1	<1	<1	5	1	2	<1
Ga (ppm)	0.1	5	4.7	4.5	4.7	4.3	4.4	4.4	4	3.9	3.9
Ge (ppm)	0.1	<0.1	<0.1	<0.1	<0.1	<0.1	<0.1	<0.1	<0.1	<0.1	<0.1
In (ppm)	0.02	0.02	0.02	0.02	0.03	<0.02	0.02	<0.02	<0.02	<0.02	<0.02
Sn (ppm)	0.1	0.7	0.6	0.7	0.6	0.5	0.6	0.6	0.5	0.5	0.4
Sb (ppm)	0.02	0.11	0.13	0.13	0.13	0.12	0.12	0.12	0.12	0.1	0.1
Bi (ppm)	0.02	0.11	0.1	0.1	0.09	0.09	0.1	0.1	0.09	0.09	0.07
Se (ppm)	0.1	0.1	0.2	0.1	0.2	<0.1	0.2	<0.1	0.1	0.1	<0.1
Te (ppm)	0.02	<0.02	<0.02	<0.02	<0.02	<0.02	<0.02	<0.02	<0.02	<0.02	<0.02
U (ppm)	0.1	1.2	1	1.1	1.1	1	1	0.9	0.8	0.9	0.9
Th (ppm)	0.1	4.1	2.9	3.1	2.9	3.7	2.8	2.9	2.7	4.4	3.2
Tl (ppm)	0.02	0.15	0.13	0.13	0.13	0.13	0.13	0.12	0.11	0.11	0.1
Zr (ppm)	0.1	5.1	4.2	4.3	4.9	4.5	4.8	4.6	4.3	4.5	4.1
Hf (ppm)	0.02	0.15	0.12	0.11	0.15	0.11	0.11	0.1	0.11	0.14	0.11
V (ppm)	2	56	54	54	55	53	53	54	51	50	49
Nb (ppm)	0.02	0.5	0.33	0.37	0.37	0.32	0.3	0.31	0.28	0.27	0.25
Ta (ppm)	0.05	<0.05	<0.05	<0.05	<0.05	<0.05	<0.05	<0.05	<0.05	<0.05	<0.05
Sc (ppm)	0.1	5.5	4.9	5	4.9	4.8	4.7	5	4.3	4.5	4.2
La (ppm)	0.5	11.4	9.5	9.6	9.4	9.3	9.5	9.4	8.7	8.6	7.3
Ce (ppm)	0.1	23.6	19.5	19.5	20.2	19.3	19.3	19.4	18.1	17.2	15.7
Pr (ppm)	0.02	2.87	2.55	2.5	2.52	2.44	2.42	2.43	2.18	2.18	1.94
Nd (ppm)	0.02	11.26	9.84	11	10.14	9.44	9.37	9.88	9.24	9.38	8.07
Sm (ppm)	0.02	2.55	2.2	2.28	2.16	2.31	2.04	1.92	1.82	1.84	1.69
Eu (ppm)	0.02	0.56	0.52	0.6	0.52	0.51	0.48	0.53	0.48	0.44	0.43
Gd (ppm)	0.02	2.16	1.92	1.82	2.01	1.97	1.96	1.83	1.59	1.77	1.41
Tb (ppm)	0.02	0.33	0.3	0.31	0.3	0.28	0.28	0.29	0.27	0.27	0.25
Dy (ppm)	0.02	1.91	1.64	1.68	1.66	1.77	1.5	1.79	1.47	1.42	1.42
Y (ppm)	0.01	8.5	7.7	7.66	7.8	7.36	7.24	7.62	6.79	6.73	6.3
Ho (ppm)	0.02	0.37	0.34	0.35	0.36	0.34	0.33	0.33	0.28	0.29	0.29
Er (ppm)	0.02	0.94	0.83	0.71	0.87	0.81	0.76	0.77	0.75	0.72	0.66
Tm (ppm)	0.02	0.12	0.13	0.11	0.12	0.12	0.13	0.11	0.1	0.11	0.09
Yb (ppm)	0.02	0.8	0.68	0.75	0.7	0.64	0.62	0.63	0.53	0.56	0.55
Lu (ppm)	0.02	0.11	0.09	0.09	0.09	0.11	0.1	0.1	0.08	0.1	0.1

East Daffodil Bay (DE)		Maximum Sampled Depth (cm)									
Element	Detection Limit	42	44	46	48	50	52	54	56	58	60
Al (%)	0.01	1.1	1	0.93	0.96	0.91	0.77	0.83	0.8	0.79	0.69
Na (%)	0.001	0.342	0.293	0.291	0.321	0.35	0.211	0.247	0.216	0.222	0.221
K (%)	0.01	0.12	0.11	0.1	0.13	0.13	0.09	0.09	0.08	0.08	0.06
Ca (%)	0.01	0.58	0.62	0.56	0.62	0.92	0.79	0.67	0.68	0.7	0.55
Mg (%)	0.01	0.5	0.47	0.44	0.47	0.49	0.41	0.41	0.39	0.39	0.35
Fe (%)	0.01	1.97	1.92	1.75	1.75	1.62	1.38	1.57	1.51	1.55	1.44
Mn (ppm)	1	204	193	181	199	199	168	180	181	175	167
Ti (%)	0.001	0.117	0.106	0.1	0.117	0.111	0.101	0.107	0.109	0.104	0.104
P (%)	0.001	0.041	0.041	0.039	0.042	0.036	0.035	0.038	0.038	0.035	0.036
S (%)	0.02	0.47	0.45	0.38	0.4	0.3	0.17	0.3	0.23	0.28	0.16
Ni (ppm)	0.1	13.8	11.9	10.6	12.8	11.1	8.8	9.6	9.1	9.1	8.3
Cu (ppm)	0.01	8.94	8.18	6.85	8.5	7.66	5.62	6.4	5.93	5.85	5.1
Pb (ppm)	0.01	4.39	3.94	3.43	4.21	3.34	2.32	2.84	2.79	2.72	2.24
Zn (ppm)	0.1	34.1	32.9	28.9	33.3	31.5	25.2	26.2	25.6	24	20.8
Cr (ppm)	0.5	19.4	18.4	17.2	18.5	16.4	13.6	15.9	15.7	14.9	14.8
Co (ppm)	0.1	6.4	5.7	5.3	6	5.7	4.9	5	4.9	4.6	4.3
Cd (ppm)	0.01	0.03	0.03	0.03	0.06	0.06	0.02	0.02	0.03	0.03	0.03
Hg (ppb)	5	13	8	10	6	14	9	13	10	10	5
As (ppm)	0.1	7.9	7.2	6.3	6.4	6.3	5.2	5.6	5.2	5.4	4.7
Au (ppb)	0.2	0.3	0.7	0.4	2.5	0.2	<0.2	<0.2	<0.2	<0.2	<0.2
Ag (ppb)	2	20	17	15	24	17	10	17	10	10	6
Pd (ppb)	10	<10	<10	<10	<10	<10	<10	<10	<10	<10	<10
Pt (ppb)	2	<2	2	<2	2	<2	<2	<2	<2	<2	<2
Li (ppm)	0.1	21	19.6	16.7	18.7	18.2	14	14.6	14.3	14.7	13
Be (ppm)	0.1	0.3	0.3	0.2	0.2	0.1	0.2	0.2	0.2	0.2	0.3
B (ppm)	20	<20	<20	<20	<20	<20	<20	<20	<20	<20	<20
Rb (ppm)	0.1	8.6	7.9	7.1	7.9	9.9	7	6.3	5.9	5.5	4.5
Sr (ppm)	0.5	33.9	37.3	30.6	39.8	61.9	49.3	39.6	41.2	40.1	34.1
Cs (ppm)	0.02	0.67	0.65	0.57	0.64	0.73	0.53	0.52	0.48	0.47	0.39
Ba (ppm)	0.5	13.1	12.1	11.4	12.5	14.9	11.2	10.8	11.6	9.5	8.3
Mo (ppm)	0.01	0.78	0.88	0.68	0.79	0.57	0.35	0.54	0.51	0.58	0.4
W (ppm)	0.1	<0.1	<0.1	<0.1	<0.1	<0.1	<0.1	<0.1	<0.1	<0.1	<0.1
Re (ppb)	1	<1	<1	<1	1	1	1	<1	2	<1	<1
Ga (ppm)	0.1	3.7	3.4	2.9	3.3	3.1	2.6	2.7	2.9	2.6	2.5
Ge (ppm)	0.1	<0.1	<0.1	<0.1	<0.1	<0.1	<0.1	0.1	<0.1	0.1	<0.1
In (ppm)	0.02	<0.02	<0.02	<0.02	0.02	<0.02	<0.02	<0.02	<0.02	<0.02	<0.02
Sn (ppm)	0.1	0.4	0.4	0.3	0.4	0.4	0.3	0.3	0.4	0.3	0.3
Sb (ppm)	0.02	0.09	0.08	0.07	0.1	0.09	0.07	0.08	0.08	0.09	0.1
Bi (ppm)	0.02	0.07	0.06	0.06	0.07	0.05	0.03	0.04	0.04	0.04	0.03
Se (ppm)	0.1	0.1	0.1	0.1	<0.1	0.1	<0.1	<0.1	<0.1	0.2	0.1
Te (ppm)	0.02	<0.02	<0.02	<0.02	0.03	0.02	0.04	0.04	0.03	<0.02	<0.02
U (ppm)	0.1	0.7	0.6	0.6	0.8	0.8	0.7	0.7	0.8	0.7	0.9
Th (ppm)	0.1	2.5	3.5	2.8	3.2	2.1	1.8	2.2	2.9	2.1	4
Tl (ppm)	0.02	0.1	0.1	0.09	0.1	0.11	0.09	0.08	0.09	0.08	0.09
Zr (ppm)	0.1	4.3	3.6	3.4	3.9	3.9	3.8	3.6	3.8	3.7	3.9
Hf (ppm)	0.02	0.12	0.09	0.1	0.11	0.12	0.12	0.1	0.11	0.1	0.1
V (ppm)	2	48	45	42	42	39	36	40	40	39	38
Nb (ppm)	0.02	0.28	0.24	0.24	0.34	0.33	0.3	0.23	0.31	0.26	0.26
Ta (ppm)	0.05	<0.05	<0.05	<0.05	<0.05	<0.05	<0.05	<0.05	<0.05	<0.05	<0.05
Sc (ppm)	0.1	4.2	3.8	3.4	3.6	3.4	3	3.1	3	3.1	2.8
La (ppm)	0.5	7.7	7.9	6.5	7.6	6.2	5.8	6.6	7.4	6	6.5
Ce (ppm)	0.1	15.9	15.8	13.2	15.3	12.5	11.4	13.5	14.2	11.6	12.4
Pr (ppm)	0.02	1.97	1.97	1.69	2	1.59	1.48	1.76	1.76	1.55	1.57
Nd (ppm)	0.02	8.15	7.73	6.54	7.2	6.15	5.51	6.04	6.22	6.01	5.94
Sm (ppm)	0.02	1.86	1.73	1.41	1.36	1.34	1.1	1.48	1.4	1.24	1.13
Eu (ppm)	0.02	0.42	0.36	0.38	0.39	0.38	0.29	0.32	0.35	0.32	0.34
Gd (ppm)	0.02	1.52	1.49	1.2	1.58	1.16	1.02	1.32	1.31	1.14	1.16
Tb (ppm)	0.02	0.24	0.22	0.19	0.23	0.18	0.18	0.19	0.18	0.17	0.17
Dy (ppm)	0.02	1.25	1.36	1.17	1.19	1	0.9	1.01	1.05	1.01	1.02
Y (ppm)	0.01	6.27	5.93	5.26	5.61	5	4.28	4.84	4.98	4.64	4.66
Ho (ppm)	0.02	0.25	0.26	0.21	0.24	0.2	0.17	0.21	0.2	0.19	0.22
Er (ppm)	0.02	0.71	0.62	0.61	0.57	0.57	0.47	0.54	0.57	0.54	0.51
Tm (ppm)	0.02	0.1	0.11	0.08	0.09	0.08	0.06	0.07	0.07	0.09	0.08
Yb (ppm)	0.02	0.55	0.54	0.49	0.51	0.43	0.37	0.46	0.46	0.48	0.42
Lu (ppm)	0.02	0.07	0.05	0.05	0.08	0.07	0.06	0.07	0.06	0.06	0.06

East Daffodil Bay (DE)		Maximum Sampled Depth (cm)										
Element	Detection Limit	62	64	66	70	72	74	76	78	80	87	95
Al (%)	0.01	0.7	0.73	0.77	0.93	0.92	0.95	0.81	0.82	0.87	0.81	0.88
Na (%)	0.001	0.199	0.198	0.195	0.201	0.231	0.193	0.198	0.212	0.27	0.221	0.204
K (%)	0.01	0.07	0.07	0.07	0.12	0.12	0.14	0.12	0.12	0.14	0.11	0.12
Ca (%)	0.01	0.55	0.65	1.02	1.41	1.47	1.6	1.27	1.3	1.53	1.3	1.62
Mg (%)	0.01	0.35	0.35	0.37	0.5	0.49	0.54	0.46	0.47	0.52	0.47	0.51
Fe (%)	0.01	1.45	1.44	1.51	1.6	1.62	1.7	1.46	1.54	1.58	1.46	1.59
Mn (ppm)	1	159	168	171	189	199	217	185	192	201	183	192
Ti (%)	0.001	0.101	0.106	0.111	0.108	0.125	0.122	0.103	0.108	0.111	0.103	0.105
P (%)	0.001	0.037	0.035	0.037	0.037	0.039	0.04	0.034	0.035	0.035	0.036	0.034
S (%)	0.02	0.16	0.13	0.17	0.16	0.13	0.12	0.11	0.13	0.15	0.1	0.15
Ni (ppm)	0.1	8.1	8.3	8.7	9.5	11.7	11.3	9.2	9.7	10.7	8.9	10.1
Cu (ppm)	0.01	5.07	4.99	5.3	6.26	7.44	7.28	6.22	6.54	7.44	6.14	6.9
Pb (ppm)	0.01	2.25	2.25	2.46	2.5	2.88	2.68	2.36	2.43	2.64	2.37	2.6
Zn (ppm)	0.1	20.2	21.6	21.7	26.7	29.7	32	27	26.7	29.9	24.7	28.4
Cr (ppm)	0.5	14.2	15	15.9	15.6	17.3	16.9	14.4	14.4	15.6	14.1	14.7
Co (ppm)	0.1	4.3	4.4	4.6	5.2	5.6	5.7	5.1	5.3	5.7	5.2	5.2
Cd (ppm)	0.01	0.01	0.03	0.02	0.02	0.02	0.02	0.01	0.02	0.02	<0.01	0.02
Hg (ppb)	5	6	7	<5	<5	<5	9	<5	<5	6	6	<5
As (ppm)	0.1	4.7	5.1	5.3	6.4	6.7	7.1	6.4	7	7.5	6.1	7.4
Au (ppb)	0.2	<0.2	0.5	<0.2	0.4	1.4	<0.2	0.3	0.9	<0.2	<0.2	0.2
Ag (ppb)	2	6	5	9	8	12	6	8	4	5	4	5
Pd (ppb)	10	<10	<10	<10	<10	<10	<10	<10	<10	<10	<10	<10
Pt (ppb)	2	<2	<2	2	<2	<2	<2	<2	<2	<2	<2	<2
Li (ppm)	0.1	11.7	13	13.7	16.1	19	20.5	16.6	16.6	19.1	16.1	16.3
Be (ppm)	0.1	0.2	0.2	0.2	0.1	0.2	0.3	0.2	0.3	0.3	0.2	0.3
B (ppm)	20	<20	<20	<20	<20	<20	<20	<20	<20	<20	<20	<20
Rb (ppm)	0.1	4.6	4.4	5.4	9.4	10.5	13.1	10.3	10.8	13.9	8.7	10.3
Sr (ppm)	0.5	33.5	40.5	58.7	85.6	100.9	111.4	88.6	91.2	110.6	86.1	108.6
Cs (ppm)	0.02	0.38	0.36	0.43	0.65	0.77	0.88	0.71	0.74	0.9	0.61	0.71
Ba (ppm)	0.5	8	8.8	10.3	14.8	17.3	20.1	16	16.6	20.9	14.5	16.1
Mo (ppm)	0.01	0.39	0.37	0.43	0.27	0.27	0.21	0.23	0.25	0.27	0.19	0.3
W (ppm)	0.1	0.4	<0.1	<0.1	0.3	<0.1	<0.1	<0.1	<0.1	<0.1	<0.1	0.2
Re (ppb)	1	3	<1	<1	3	4	3	4	2	3	2	4
Ga (ppm)	0.1	2.5	2.6	2.6	2.9	3.3	3.4	2.9	3	3.2	2.8	3
Ge (ppm)	0.1	<0.1	<0.1	0.1	<0.1	<0.1	<0.1	0.1	<0.1	<0.1	<0.1	<0.1
In (ppm)	0.02	<0.02	<0.02	<0.02	<0.02	<0.02	<0.02	<0.02	<0.02	<0.02	<0.02	<0.02
Sn (ppm)	0.1	0.3	0.3	0.3	0.3	0.3	0.4	0.4	0.3	0.3	0.3	0.3
Sb (ppm)	0.02	0.1	0.08	0.12	0.11	0.12	0.13	0.11	0.11	0.1	0.09	0.08
Bi (ppm)	0.02	0.03	0.03	0.03	0.03	0.03	0.03	0.02	0.03	0.03	0.02	0.03
Se (ppm)	0.1	<0.1	0.1	<0.1	<0.1	<0.1	0.3	<0.1	<0.1	0.2	<0.1	0.2
Te (ppm)	0.02	<0.02	<0.02	0.03	<0.02	<0.02	<0.02	0.04	0.02	<0.02	<0.02	<0.02
U (ppm)	0.1	0.8	0.7	0.7	0.9	0.9	1	1	1.3	1.1	0.9	0.9
Th (ppm)	0.1	5.1	2.3	2.1	3.3	2.2	2.6	2	2.1	1.8	2.4	2.5
Tl (ppm)	0.02	0.08	0.08	0.09	0.08	0.08	0.09	0.07	0.07	0.07	0.05	0.06
Zr (ppm)	0.1	3.8	4	3.7	3.7	4.4	4.1	3.7	3.7	3.9	3.9	4.2
Hf (ppm)	0.02	0.1	0.12	0.13	0.1	0.14	0.13	0.12	0.14	0.11	0.11	0.13
V (ppm)	2	39	39	40	44	42	44	37	39	38	37	39
Nb (ppm)	0.02	0.24	0.24	0.25	0.22	0.24	0.24	0.2	0.24	0.26	0.2	0.21
Ta (ppm)	0.05	<0.05	<0.05	<0.05	<0.05	<0.05	<0.05	<0.05	<0.05	<0.05	<0.05	<0.05
Sc (ppm)	0.1	2.7	2.8	3	2.9	3.5	3.2	2.9	2.8	3	2.8	3
La (ppm)	0.5	7.6	7	6.8	6.6	7	7.2	5.8	6.2	6	6.4	6.3
Ce (ppm)	0.1	12	12.8	13.4	13.2	13.8	13.9	11.3	12.3	11.9	12.9	13.1
Pr (ppm)	0.02	1.54	1.64	1.74	1.7	1.78	1.83	1.43	1.52	1.57	1.6	1.69
Nd (ppm)	0.02	5.62	5.83	6.43	5.76	6.8	6.64	5.43	5.6	5.65	5.89	6.01
Sm (ppm)	0.02	1.3	1.24	1.29	1.18	1.48	1.33	1.03	1.27	1.25	1.17	1.43
Eu (ppm)	0.02	0.31	0.31	0.28	0.3	0.38	0.31	0.26	0.28	0.31	0.3	0.31
Gd (ppm)	0.02	0.91	1.11	1.3	1.19	1.35	1.04	1.05	1.14	1.12	1.12	1.18
Tb (ppm)	0.02	0.17	0.15	0.16	0.18	0.2	0.19	0.16	0.17	0.17	0.15	0.15
Dy (ppm)	0.02	0.9	0.86	1.02	0.97	1.02	1.01	0.81	0.88	1.06	1.03	0.9
Y (ppm)	0.01	4.84	4.69	4.71	4.91	5.15	5.16	4.31	4.4	4.43	4.47	4.88
Ho (ppm)	0.02	0.21	0.18	0.18	0.21	0.21	0.21	0.19	0.19	0.18	0.18	0.19
Er (ppm)	0.02	0.49	0.56	0.52	0.58	0.58	0.58	0.58	0.46	0.48	0.51	0.51
Tm (ppm)	0.02	0.08	0.06	0.08	0.09	0.08	0.08	0.07	0.06	0.06	0.07	0.07
Yb (ppm)	0.02	0.44	0.41	0.43	0.49	0.54	0.5	0.42	0.42	0.43	0.43	0.42
Lu (ppm)	0.02	0.06	0.06	0.07	0.06	0.07	0.06	0.05	0.07	0.07	0.07	0.07

Table C-4. Partial elemental concentrations by ICP-MS after a modified aqua regia digestion of duplicate sample horizons.

Element	Detection Limit	Sample Duplicates		
		DE (2 cm)	UNA (32 cm)	DE (62 cm)
Al (%)	0.01	2.39	2.38	0.7
Na (%)	0.001	0.803	0.474	0.199
K (%)	0.01	0.28	0.22	0.06
Ca (%)	0.01	0.7	0.65	0.56
Mg (%)	0.01	0.96	0.88	0.35
Fe (%)	0.01	3.5	3.33	1.39
Mn (ppm)	1	350	348	158
Ti (%)	0.001	0.165	0.162	0.096
P (%)	0.001	0.063	0.07	0.032
S (%)	0.02	1.17	0.58	0.16
Ni (ppm)	0.1	29.9	28.6	7.6
Cu (ppm)	0.01	24.19	23.22	5.01
Pb (ppm)	0.01	12.76	20.72	2.14
Zn (ppm)	0.1	85.7	115.4	19.1
Cr (ppm)	0.5	36.2	34.6	13.5
Co (ppm)	0.1	12.1	13.2	4.1
Cd (ppm)	0.01	0.13	0.1	0.01
Hg (ppb)	5	66	61	<5
As (ppm)	0.1	11.6	8.1	4.9
Au (ppb)	0.2	1	2.5	<0.2
Ag (ppb)	2	75	249	8
Pd (ppb)	10	<10	<10	<10
Pt (ppb)	2	<2	<2	2
Li (ppm)	0.1	44.8	41.5	11.4
Be (ppm)	0.1	0.6	0.7	0.1
B (ppm)	20	<20	<20	<20
Rb (ppm)	0.1	18.4	15.9	4.4
Sr (ppm)	0.5	58	59.7	31.2
Cs (ppm)	0.02	1.45	1.24	0.38
Ba (ppm)	0.5	27.4	33	7.6
Mo (ppm)	0.01	2.43	0.66	0.38
W (ppm)	0.1	<0.1	<0.1	0.3
Re (ppb)	1	2	<1	1
Ga (ppm)	0.1	7.3	7	2.4
Ge (ppm)	0.1	<0.1	<0.1	<0.1
In (ppm)	0.02	0.03	0.04	<0.02
Sn (ppm)	0.1	1	1.4	0.3
Sb (ppm)	0.02	0.13	0.13	0.08
Bi (ppm)	0.02	0.23	0.2	0.02
Se (ppm)	0.1	0.3	0.1	<0.1
Te (ppm)	0.02	<0.02	0.02	<0.02
U (ppm)	0.1	2.2	1.1	1
Th (ppm)	0.1	4.3	3.8	4.3
Tl (ppm)	0.02	0.21	0.09	0.08
Zr (ppm)	0.1	6.7	6.2	3.9
Hf (ppm)	0.02	0.21	0.17	0.13
V (ppm)	2	78	73	37
Nb (ppm)	0.02	0.76	0.54	0.24
Ta (ppm)	0.05	<0.05	<0.05	<0.05
Sc (ppm)	0.1	8	7.7	2.6
La (ppm)	0.5	14	14.7	5.8
Ce (ppm)	0.1	30.8	31.8	11.9
Pr (ppm)	0.02	3.92	4.02	1.53
Nd (ppm)	0.02	15.79	16.05	5.6
Sm (ppm)	0.02	3.45	3.39	1.17
Eu (ppm)	0.02	0.89	0.84	0.26
Gd (ppm)	0.02	2.99	3.06	0.8
Tb (ppm)	0.02	0.47	0.48	0.14
Dy (ppm)	0.02	2.75	2.79	0.91
Y (ppm)	0.01	11.92	12.46	4.39
Ho (ppm)	0.02	0.51	0.5	0.17
Er (ppm)	0.02	1.25	1.33	0.46
Tm (ppm)	0.02	0.17	0.18	0.08
Yb (ppm)	0.02	1.17	1.07	0.4
Lu (ppm)	0.02	0.15	0.15	0.04

Table C-5. Partial elemental concentrations by ICP-MS after a modified aqua regia digestion of standard reference material.

		Standard Reference Material					
Element	Detection Limit	OREAS45EA	DS11	OREAS45EA	DS11	OREAS45EA	DS11
Al (%)	0.01	3.59	1.21	3.46	1.17	3.52	1.17
Na (%)	0.001	0.026	0.078	0.025	0.075	0.022	0.076
K (%)	0.01	0.06	0.42	0.06	0.41	0.06	0.42
Ca (%)	0.01	0.03	1.11	0.03	1.07	0.03	1.13
Mg (%)	0.01	0.11	0.88	0.11	0.85	0.1	0.86
Fe (%)	0.01	24.05	3.22	23.39	3.13	24.08	3.1
Mn (ppm)	1	442	1078	431	1043	439	1058
Ti (%)	0.001	0.106	0.095	0.102	0.092	0.114	0.101
P (%)	0.001	0.032	0.074	0.032	0.072	0.031	0.074
S (%)	0.02	0.04	0.29	0.04	0.28	0.04	0.31
Ni (ppm)	0.1	419.2	80.1	406.8	77.5	393	80
Cu (ppm)	0.01	717.57	156.79	707.93	153.41	734.65	152.15
Pb (ppm)	0.01	16.02	154.33	15.7	140.63	16.38	137.4
Zn (ppm)	0.1	34.4	353.1	33.3	358.2	36.1	348.8
Cr (ppm)	0.5	913.3	60.3	879.4	58.3	878	60.6
Co (ppm)	0.1	53.9	14	51.3	13.5	57.7	14.1
Cd (ppm)	0.01	0.04	2.39	0.01	2.39	0.02	2.37
Hg (ppb)	5	8	266	12	260	10	244
As (ppm)	0.1	12.3	44.1	12	42.4	12.5	44.7
Au (ppb)	0.2	57.3	56	58	67.3	60.9	57.8
Ag (ppb)	2	253	1635	252	1874	294	1746
Pd (ppb)	10	75	100	81	100	93	111
Pt (ppb)	2	118	189	116	196	119	174
Li (ppm)	0.1	2.9	23.1	2.9	23.3	3.1	23.4
Be (ppm)	0.1	0.4	0.5	0.4	0.6	0.4	0.5
B (ppm)	20	<20	<20	<20	<20	<20	<20
Rb (ppm)	0.1	8.3	35	8.3	34.8	8.5	34.8
Sr (ppm)	0.5	4.1	71.4	4.1	68.9	4.5	75.4
Cs (ppm)	0.02	0.79	3.1	0.79	2.95	0.8	2.86
Ba (ppm)	0.5	153.8	446.6	152.1	437.3	164.9	420.8
Mo (ppm)	0.01	1.74	14.43	1.55	13.05	1.82	14.07
W (ppm)	0.1	<0.1	3.2	<0.1	2.7	<0.1	2.8
Re (ppb)	1	<1	51	<1	48	<1	50
Ga (ppm)	0.1	14	5.3	13.4	5	13.3	4.9
Ge (ppm)	0.1	0.3	<0.1	0.3	<0.1	0.3	<0.1
In (ppm)	0.02	0.1	0.25	0.11	0.25	0.11	0.21
Sn (ppm)	0.1	1	1.9	1	1.9	1	1.8
Sb (ppm)	0.02	0.35	7.33	0.3	7.34	0.34	7.72
Bi (ppm)	0.02	0.3	13.56	0.29	12.73	0.31	12.81
Se (ppm)	0.1	1.6	2.3	1.5	2.3	1.7	2.5
Te (ppm)	0.02	0.09	4.93	0.09	4.75	0.13	4.83
U (ppm)	0.1	2	2.8	2	2.6	2.1	2.9
Th (ppm)	0.1	11.5	8.1	10.9	7.5	11.8	8.5
Tl (ppm)	0.02	0.07	5.34	0.07	5.08	0.07	5.01
Zr (ppm)	0.1	20.6	2.5	20.6	2.3	23.6	2.5
Hf (ppm)	0.02	0.54	0.07	0.61	0.07	0.68	0.03
V (ppm)	2	323	52	317	50	323	50
Nb (ppm)	0.02	0.06	1.2	0.05	1.24	0.08	1.22
Ta (ppm)	0.05	<0.05	<0.05	<0.05	<0.05	<0.05	<0.05
Sc (ppm)	0.1	85.9	3.5	81.5	3.3	80.3	3.3
La (ppm)	0.5	7.7	19.7	7.5	18.7	8	18.6
Ce (ppm)	0.1	19.2	40	19.1	37.7	20.1	37.5
Pr (ppm)	0.02	2.09	4.17	2.11	4.04	2.32	4.07
Nd (ppm)	0.02	8.22	15.55	7.68	14.7	8.1	14.6
Sm (ppm)	0.02	1.86	3.21	1.83	2.53	2.01	2.74
Eu (ppm)	0.02	0.58	0.61	0.47	0.52	0.52	0.61
Gd (ppm)	0.02	1.53	2.37	1.83	2.18	1.75	2.07
Tb (ppm)	0.02	0.27	0.31	0.31	0.28	0.3	0.31
Dy (ppm)	0.02	1.77	1.79	1.66	1.64	1.67	1.58
Y (ppm)	0.01	5.88	7.98	5.52	7.87	5.83	7.91
Ho (ppm)	0.02	0.31	0.32	0.31	0.29	0.35	0.28
Er (ppm)	0.02	0.85	0.83	0.79	0.76	0.94	0.89
Tm (ppm)	0.02	0.14	0.13	0.12	0.12	0.15	0.13
Yb (ppm)	0.02	0.8	0.81	0.87	0.67	0.9	0.79
Lu (ppm)	0.02	0.11	0.1	0.11	0.12	0.14	0.12

Table C-6. Partial elemental concentrations by ICP-MS after a modified aqua regia digestion of reference blanks.

		Blanks		
Element	Detection Limit	Blank	Blank	Blank
Al (%)	0.01	<0.01	<0.01	<0.01
Na (%)	0.001	<0.001	<0.001	<0.001
K (%)	0.01	<0.01	<0.01	<0.01
Ca (%)	0.01	<0.01	<0.01	<0.01
Mg (%)	0.01	<0.01	<0.01	<0.01
Fe (%)	0.01	<0.01	<0.01	<0.01
Mn (ppm)	1	<1	<1	<1
Ti (%)	0.001	<0.001	<0.001	<0.001
P (%)	0.001	<0.001	<0.001	<0.001
S (%)	0.02	<0.02	<0.02	<0.02
Ni (ppm)	0.1	<0.1	<0.1	<0.1
Cu (ppm)	0.01	<0.01	0.04	<0.01
Pb (ppm)	0.01	<0.01	<0.01	<0.01
Zn (ppm)	0.1	<0.1	<0.1	<0.1
Cr (ppm)	0.5	<0.5	<0.5	<0.5
Co (ppm)	0.1	<0.1	<0.1	<0.1
Cd (ppm)	0.01	<0.01	<0.01	<0.01
Hg (ppb)	5	<5	<5	<5
As (ppm)	0.1	<0.1	<0.1	<0.1
Au (ppb)	0.2	<0.2	0.4	<0.2
Ag (ppb)	2	<2	<2	<2
Pd (ppb)	10	<10	<10	<10
Pt (ppb)	2	<2	<2	<2
Li (ppm)	0.1	<0.1	<0.1	<0.1
Be (ppm)	0.1	<0.1	<0.1	<0.1
B (ppm)	20	<20	<20	<20
Rb (ppm)	0.1	<0.1	<0.1	<0.1
Sr (ppm)	0.5	<0.5	<0.5	<0.5
Cs (ppm)	0.02	<0.02	<0.02	<0.02
Ba (ppm)	0.5	<0.5	<0.5	<0.5
Mo (ppm)	0.01	<0.01	<0.01	<0.01
W (ppm)	0.1	<0.1	<0.1	<0.1
Re (ppb)	1	<1	<1	<1
Ga (ppm)	0.1	<0.1	<0.1	<0.1
Ge (ppm)	0.1	<0.1	<0.1	<0.1
In (ppm)	0.02	<0.02	<0.02	<0.02
Sn (ppm)	0.1	<0.1	<0.1	<0.1
Sb (ppm)	0.02	<0.02	<0.02	<0.02
Bi (ppm)	0.02	<0.02	<0.02	<0.02
Se (ppm)	0.1	<0.1	<0.1	<0.1
Te (ppm)	0.02	<0.02	<0.02	0.02
U (ppm)	0.1	<0.1	<0.1	<0.1
Th (ppm)	0.1	<0.1	<0.1	<0.1
Tl (ppm)	0.02	<0.02	<0.02	<0.02
Zr (ppm)	0.1	<0.1	<0.1	<0.1
Hf (ppm)	0.02	<0.02	<0.02	<0.02
V (ppm)	2	<2	<2	<2
Nb (ppm)	0.02	<0.02	<0.02	<0.02
Ta (ppm)	0.05	<0.05	<0.05	<0.05
Sc (ppm)	0.1	<0.1	<0.1	<0.1
La (ppm)	0.5	<0.5	<0.5	<0.5
Ce (ppm)	0.1	<0.1	<0.1	<0.1
Pr (ppm)	0.02	<0.02	<0.02	<0.02
Nd (ppm)	0.02	<0.02	<0.02	<0.02
Sm (ppm)	0.02	<0.02	<0.02	<0.02
Eu (ppm)	0.02	<0.02	<0.02	<0.02
Gd (ppm)	0.02	<0.02	<0.02	<0.02
Tb (ppm)	0.02	<0.02	<0.02	<0.02
Dy (ppm)	0.02	<0.02	<0.02	<0.02
Y (ppm)	0.01	<0.01	<0.01	<0.01
Ho (ppm)	0.02	<0.02	<0.02	<0.02
Er (ppm)	0.02	<0.02	<0.02	<0.02
Tm (ppm)	0.02	<0.02	<0.02	<0.02
Yb (ppm)	0.02	<0.02	<0.02	<0.02
Lu (ppm)	0.02	<0.02	<0.02	<0.02

Appendix D – Stable Isotopes

Table D-1. Stable nitrogen, carbon, and sulfur isotopic signatures normalized to their respective international standard reference material in the Upper North Arm (UNA) deep core, with corresponding elemental concentrations.

Core	Maximum Depth (cm)	$\delta^{15}N$ (‰) vs. AIR	TN (%)	$\delta^{13}C$ (‰) vs. VPDB	Organic-C (%)	$\delta^{34}S$ (‰) vs. VCDT	S (%)
UNA	2	7.0	0.22	-27.6	2.24	-13.8	0.35
UNA	4	6.9	0.25	-27.1	2.28	-13.7	0.42
UNA	6	6.8	0.24	-27.1	2.24	-14.7	0.48
UNA	8	7.3	0.24	-26.8	2.11	-13.5	0.69
UNA	10	5.4	0.13	-26.7	2.15	-23.9	0.7
UNA	12	7.0	0.23	-26.8	1.99	-13.2	0.53
UNA	14	6.8	0.21	-26.9	1.92	-18.3	0.48
UNA	16	6.7	0.22	-26.8	2.03	-19.4	0.53
UNA	18	6.5	0.19	-27.0	2.00	-19.4	0.55
UNA	20	6.2	0.19	-27.0	1.72	-19.8	0.6
UNA	22	6.0	0.20	-27.1	1.62	-19.9	
UNA	24	5.6	0.17	-27.2	1.80	-22.5	0.51
UNA	26	5.8	0.18	-27.0	1.43	-22.2	0.51
UNA	28	5.7	0.15	-27.0	1.35	-23.1	0.5
UNA	30	7.4	0.15	-26.9	1.35	-23.3	
UNA	32	5.5	0.26	-26.9	1.26	-21.7	0.58
UNA	34	5.4	0.14	-27.0	1.51	-23.7	0.58
UNA	36	5.7	0.16	-27.0	1.59	-19.6	
UNA	38	insuff. %N		-26.2	1.28	-20.7	0.69
UNA	40	5.4	0.00	-26.3	0.90	-14.9	0.47
UNA	42	5.5	0.10	-26.0	0.71	-20.6	0.48
UNA	44	insuff. %N		-24.5	0.68	-21.1	0.52
UNA	46	5.4	0.00	-25.7	0.77	-20.1	0.54
UNA	48	5.4	0.02	-25.3	0.92	-24.6	0.7
UNA	50	5.4	0.09	-16.5	0.89	-23.5	0.6
UNA	52	5.8	0.10	-24.3	1.01	-19.0	0.87
UNA	54	5.4	0.07	-24.4	1.23	-14.7	1.05
UNA	56	5.7	0.11	-25.0	1.03	-18.5	1.12
UNA	58	5.7	0.13	-22.2	1.00	-14.7	1.04
UNA	60	5.5	0.11	-24.2	0.80	-8.4	0.86
UNA	62	4.9	0.11	-23.9	0.47	-6.8	0.55
UNA	64	5.2	0.11	-22.9	0.40	-7.7	0.53
UNA	66	5.0	0.11	-22.2	0.30	-7.8	0.34
UNA	68	4.5	0.04	-23.3	0.21	-8.5	0.27
UNA	70	insuff. %N		-23.0	0.17	-8.3	0.3
UNA	78	4.4	0.03	-23.1	0.33	-14.2	0.33
UNA	85	4.6	0.03	-23.6	0.34	-23.6	0.38

Table D-2. Stable nitrogen, carbon, and sulfur isotopic signatures normalized to their respective international standard reference material in the Lower Waihopai Arm (LW) deep core, with corresponding elemental concentrations.

Core	Maximum Depth (cm)	$\delta^{15}N$ (‰) vs. AIR	TN (%)	$\delta^{13}C$ (‰) vs. VPDB	Organic-C (%)	$\delta^{34}S$ (‰) vs. VCDT	S (%)
LW	2	7.6	0.43	-27.1	2.10	-17.3	25.048
LW	4	7.9	0.52	-26.6	2.21	-19.5	23.424
LW	6	8.3	0.54	-26.3	2.26	-20.5	25.662
LW	8	8.0	0.41	-26.4	2.23	-20.6	28.846
LW	10	8.3	0.42	-26.4	1.75	-19.8	25.109
LW	12	8.0	0.40	-26.4	1.67	-21.7	23.330
LW	14	8.3	0.30	-26.3	1.61	-20.1	25.153
LW	16	6.9	0.29	-26.2	1.39	-25.2	23.880
LW	18	6.9	0.19	-25.8	1.18	-24.7	24.183
LW	20	6.6	0.15	-26.1	0.88	-29.4	28.391
LW	22	5.8	0.20	-25.3	0.93	-29.8	25.440
LW	24	4.9	0.09	-25.0	0.57	-29.8	25.264
LW	26	5.6	0.08	-24.6	0.46	-30.4	24.453
LW	28	5.0	0.10	-24.4	0.49	-31.1	26.584
LW	30	5.4	0.10	-25.0	0.54	-31.9	27.172

Table D-3. Stable nitrogen, carbon, and sulfur isotopic signatures normalized to their respective international standard reference material in the East Daffodil Bay (DE) deep core, with corresponding elemental concentrations.

Core	Maximum Depth (cm)	$\delta^{15}N$ (‰) vs. AIR	TN (%)	$\delta^{13}C$ (‰) vs. VPDB	Organic-C (%)	$\delta^{34}S$ (‰) vs. VCDT	S (%)
DE	2	6.6	0.67	-25.1	2.42	-31.7	26.194
DE	4	7.2	0.40	-24.7	1.47	-23.2	26.336
DE	6	7.0	0.27	-24.7	1.26	-23.7	24.276
DE	8	6.7	0.27	-25.1	1.39	-23.7	27.982
DE	10	6.8	0.25	-24.9	1.26	-25.3	25.141
DE	12	7.1	0.33	-25.1	1.23	-22.7	26.718
DE	14	6.5	0.21	-25.4	1.10	-23.8	25.165
DE	16	6.5	0.23	-25.7	0.93	-23.0	24.254
DE	18	6.5	0.21	-25.6	1.06	-23.9	29.586
DE	20	6.2	0.28	-26.7	1.23	-25.9	24.198
DE	22	5.6	0.23	-25.6	1.15	-24.4	25.117
DE	24	6.2	0.16	-25.7	0.90	-26.9	25.443
DE	26	6.0	0.15	-25.9	0.63	-29.3	26.989
DE	28	6.0	0.15	-25.7	0.82	-26.4	25.750
DE	30	5.9	0.20	-25.8	0.85	-27.7	25.349
DE	32	5.5	0.14	-25.6	0.77	-29.5	25.809
DE	34	5.3	0.17	-25.7	0.74	-30.1	24.906
DE	36	5.4	0.18	-25.9	0.78	-29.5	25.661
DE	38	4.8	0.10	-25.6	0.45	-32.4	23.349
DE	40	4.7	0.07	-25.4	0.39	-32.7	24.605
DE	42	4.7	0.11	-25.2	0.49	-34.3	24.292
DE	44	4.8	0.07	-25.0	0.37	-33.7	27.904
DE	46	4.8	0.05	-23.8	0.27	-33.6	24.643
DE	48	8.5	0.13	-22.7	0.61	-28.6	26.782
DE	50	5.5	0.11	-22.7	0.50	-29.5	28.326
DE	52	3.0	0.04	-14.9	0.33	-24.2	27.750
DE	54	3.9	0.03	-23.9	0.18	-32.9	24.776
DE	56	4.1	0.03	-22.2	0.20	-30.9	25.528
DE	58	4.1	0.03	-22.2	0.14	-31.0	25.212
DE	60	0.8	0.02	-23.4	0.10	insuff. %S	
DE	62	-0.8	0.02	-22.7	0.10	-30.7	28.645
DE	64	2.6	0.04	-22.1	0.14	insuff. %S	
DE	66	4.4	0.04	-16.0	0.37	-32.8	25.359
DE	68	4.8	0.04	-19.0	0.30	-31.8	26.398
DE	70	5.1	0.05	-14.1	0.57	-28.0	26.865
DE	72	3.1	0.04	-14.9	0.41	-25.6	26.736
DE	74	3.0	0.03	-12.7	0.51	insuff. %S	
DE	76	0.9	0.02	-12.9	0.27	insuff. %S	
DE	78	2.0	0.05	-12.9	0.46	insuff. %S	
DE	80	2.6	0.02	-12.3	0.35	-24.4	28.696

Appendix E – Radiogenic Isotopes

Table E-1. Radiogenic isotopic signatures (Be, Cs, Pb, Ra) of select sediment horizons from the Upper North Arm (UNA), Lower Waihopai Arm (LW), and East Daffodil Bay (DE) shallow and deep cores.

Core	Type	Sampled Depth (cm)	Be-7 (Bq/kg)	Cs-137 (Bq/kg)	Total Pb-210 (Bq/kg)	Ra-226 (Bq/kg)	Ra-228 (Bq/kg)
DE	Shallow	0-1	< 11	< 1.7	22.5±5.4	17.6±1.9	25.3±3.4
DE	Shallow	1-2	< 9.9	< 1.3	21±6	14.7±1.6	19.7±2.8
DE	Shallow	10-14	< 9.6	< 1.5	18.7±5.7	16.6±1.6	23.3±2.9
DE	Deep	0-1	5.8±3.7	0.94±0.6	47.7±7.6	16.1±1.7	23.2±3
DE	Deep	12-14	< 11	0.86±0.57	39.2±7	22.3±2.2	25.7±3.8
DE	Deep	24-26	< 10	< 1.6	25.7±5.6	19.5±2	28.7±3.9
DE	Deep	42-44	< 8.4	< 1.4	17.8±4.7	18.4±2.1	27.7±3.1
DE	Deep	50-52	< 9.8	< 1.5	19.8±4.8	18.8±1.9	27.2±3.2
DE	Deep	72-74	< 8.9	< 1.2	12.7±4.8	13.8±1.4	18.7±2.6
LW	Shallow	0-1	11.4±4.1	1.57±0.59	40.8±7.7	20±1.8	24.5±3
LW	Shallow	1-2	19.4±5.6	< 3.6	56.1±9	20.7±2.1	24.4±3.5
LW	Shallow	10-14	< 20	< 3.0	46±10	19.8±2.6	24.6±4.7
LW	Deep	0-2	< 9.1	< 1.3	31.1±15.9	25.2±2.1	40.1±3.8
LW	Deep	6-8	< 10	< 1.6	46.1±7.2	20.6±2	26.5±3.4
LW	Deep	22-24	< 9.5	< 1.3	30±17	26.2±2.2	41.7±3.9
UNA	Shallow	0-1	12±7.1	< 2.9	68±12	23.1±2.8	22.2±4.9
UNA	Shallow	1-2	14±6.3	1.81±0.91	67±11	20.5±2.4	22.4±4.7
UNA	Shallow	14-16	< 12	1.1±0.69	53.9±8.7	19.2±2.5	26.1±3.7
UNA	Deep	0-2	10.1±4.7	< 3.3	57±8.8	18.3±1.9	23.7±3.2
UNA	Deep	10-12	< 9.8	1.53±0.6	46.6±7.4	16.4±1.7	24.2±3
UNA	Deep	46-48	< 8.9	< 1.3	13.2±5.1	13.3±1.5	22.4±2.9
UNA	Deep	60-62	< 9.4	< 1.5	16.4±4.5	16.8±0.8	17.7±2.8
UNA	Deep	76-78	< 9.0	< 1.4	12.8±5	14.4±1.5	17.7±2.5

Appendix F – Soil Classification Comparison

Table F-1. The nearest soil group equivalents of New Zealand Soil Classification (Hewitt, 2010) to the US Soil Taxonomy (Soil Survey Staff, 1999). Table modified after Table 1 in Hewitt (2010).

NZ Soil Classification	Soil Taxonomy
BROWN SOILS	
Allophanic Brown Soils	Dystrudepts
Sandy Brown Soils	Dystrustepts, Dystrudepts and Psamments
Oxidic Brown Soils	Dystrudepts
Mafic Brown Soils	Dystrudepts
Acid Brown Soils	Dystrudepts
Firm Brown Soils	Dystrudepts and Dystrustepts
Orthic Brown Soils	Dystrudepts and Dystrustepts
GLEY SOILS	
Sulphuric Gley Soils	Sulphaquepts
Sandy Gley Soils	Aquepts or Aquents
Acid Gley Soils	Aquepts
Oxidic Gley Soils	Aquox
Recent Gley Soils	Aquents
Orthic Gley Soils	Aquepts or Aquents
MELANIC SOILS	
Vertic Melanic Soils	Ustolls or Vertisols
Perch-gley Melanic Soils	Aquolls
Rendzic Melanic Soils	Rendolls
Mafic Melanic Soils	Haplustepts, Ustolls or Udolls
Orthic Melanic Soils	Ustolls, Udolls, Haplustepts or Calciustepts
ORGANIC SOILS	
Litter Organic Soils	Folists or unrecognised
Fibric Organic Soils	Fibrists
Mesic Organic Soils	Hemists
Humic Organic Soils	Saprists

NZ Soil Classification	Soil Taxonomy
PALLIC SOILS	
Perch-gley Pallic Soils	Aquepts, Aqualfs
Duric Pallic Soils	Duraqualfs
Fragic Pallic Soils	Fragiudalfs, Fragiochrepts
Laminar Pallic Soils	Haplustalfs, Hapludalfs
Argillic Pallic Soils	Haplustalfs, Hapludalfs
Immature Pallic Soils	Haplustepts
PODZOLS	
Densipan Podzols	Aquods, Orthods
Perch-gley Podzols	Aquods
Groundwater-gley Podzols	Aquods
Pan Podzols	Orthods
Orthic Podzols	Orthods
RECENT SOILS	
Hydrothermal Recent Soils	Aquents, Orthents
Rocky Recent Soils	Orthents
Sandy Recent Soils	Psamments
Fluvial Recent Soils	Fluvents, Udepts, Ustepts
Tephric Recent Soils	Orthents, Cryands, Udands
Orthic Recent Soils	Orthents, Udepts, Ustepts
ULTIC SOILS	
Densipan Ultic Soils	Aquults
Albic Ultic Soils	Aquults, Humults or Udults
Perch-gley Ultic Soils	Aquults
Sandy Ultic Soils	Hapludults
Yellow Ultic Soils	Hapludults